THE UNIVERSITY
of EDINBURGH

Dynamic Epigenetic Modifications during Human Fetal Germ Cell Development

Jieqian Zhou

BSc, Southern Medical University, China
MSc, University of Edinburgh
Centre for Reproductive Health, Queen's Medical Research Institute,
47 Little France Crescent,
Edinburgh EH16 4TJ

Thesis submitted to the University of Edinburgh for the Degree of Master of Philosophy
February, 2017

DECLARATION

The studies undertaken in the thesis were the sole work of the author, except where acknowledgement is made by reference. The work described in this thesis has not been previously accepted for, or is currently being submitted for another degree or qualification at the University of Edinburgh or any other institution.

Jieqian Zhou

February, 2017

ACHNOWLEDGEMENT

I AM DEEPLY INDEBTED to my supervisor Professor Richard Anderson and Dr Paul De Sousa for their kind interest, generous support and inspiring supervision throughout the past six years. I have benefitted tremendously from their rare insight, ample intuition, boundless patience and profound knowledge. Also, I am extremely thankful to Dr. Andrew Childs for providing me with valuable comments on my thesis as well as my experiments. This thesis would never have been written without their tireless and patient mentoring. It is my very great privilege to have been one of their research students.

I would like to thank the University of Edinburgh, as well as the Centre of Reproductive Health, for providing outstanding training and facilities to research students. I am very grateful to the China Scholarship Council (CSC) for the financial support of this work.

I would like to express my appreciations to many members from the Centre of Reproductive Health, who have generously helped me to develop my knowledge through wide-ranging discussions. I would like to extend my appreciations to my friends for making my stay at Edinburgh pleasant.

I wish to take this opportunity to thank my parents Xihui Zhou and Yinshan Zhou for their moral support throughout my studies.

Last, but most importantly, I wish to express my deepest gratitude and love to my beloved husband, Jie Tang, for his endless love and support. He is the reason for my blissful life at United Kingdom. I would like to dedicate this thesis to my parents and husband.

ABSTRACT

Germ cells are responsible for transferring genetic information from parents to offspring, highlighting the significance of normal germ cell development. Epigenetic modifications, which modify gene expression without changing the underlying DNA sequence, can affect the fate of germ cells. Abnormal epigenetic reprogramming will facilitate abnormal germ cell development; therefore, understanding of epigenetic reprogramming mechanisms can contribute to the discovery of medical interventions for reproductive disease. DNA methylation and histone modification are two main components of epigenetic modifications. Both of them play important roles in mammalian germ cells development. In human germ cells, very few observations about these epigenetic modifications have been reported. Therefore, this report aims to form the major epigenetic reprogramming study conducted in human fetal germ cells, establishing an accurate timeline of events pertaining to this process in human fetal germ cells. Specifically, this research is divided into understanding (1) the process of histone modifications in human fetal germ cells; (2) the reprogramming of DNA methylation and its related modifiers in human germ cell development; (3) the impact of chemical DNA demethylation in the expression of germ cell-specific genes and the meiotic genes in human *in vitro* and *ex vivo*.

Studies in human fetal gonads indicated that histone modifications changed dynamically during human fetal germ cell development. Experiments addressing DNA methylation reprogramming in human fetal germ cells collectively reveal a trend towards DNA demethylation and reductions in 5-methylcytosine (5mC), in the instance of both fetal ovarian and testicular germ cells alike. Furthermore, 5mC was re-detected in human fetal testicular germ cells at fetal stage, but in human fetal ovarian germ cells after birth. The studies in human germ cells here demonstrated that the existence of 5mC and 5-hydroxymethylcytosine (5hmC) were synchronous rather than alternate. Determination of the levels of TET (ten-eleven translocation) proteins (*TET 1, 2* and *3*) reveal higher levels during the 1st trimester, with subsequent reductions in levels with gestations. Additional findings, from the studies in a human testicular germ cell tumor cell line, TCam-2 cells, and human fetal gonads, showed that treatments with DNA demethylating agents are linked to the activation and increase of post-migratory germ cell-specific genes along with meiotic genes in human.

To conclude, the results from this study demonstrate that epigenetic changes, such as histone modification and DNA methylation, are dynamic in human germ cells, the precise nature of which necessitates further research.

LAY ABSTRACT

Normal germ cells development is important, as it will affect the normal development of next gestation. The fate of germ cells can be affected by epigenetic modification. Epigenetic modification refers to external modifications to chromatin that turn genes "on" or "off" without changing the underlying DNA sequence. Abnormal epigenetic modification will facilitate abnormal germ cell development. Therefore, understanding of epigenetic reprogramming mechanisms can contribute to understanding the mechanisms of germ cell disease. In mammalian germ cells, epigenetic modifications changed dynamically and have been found to play important roles in germ cell development. However, very few observations about these epigenetic modifications have been reported. Hence, this study attempts to carry out epigenetic reprogramming research on human fetal germ cells. The research findings here showed that epigenetic changes are dynamic in human germ cells. However, the biological significances of these dynamic epigenetic modifications in human germ cells need further study.

List of Contents

Chapter 1. Literature Review

1.1 *General introduction*

For the vast majority of multicellular organisms, germ cells are unique among a variety of cell types. Germ cells represent the mechanism by which parental organisms transmit their genetic material to the next generation. Therefore, normal germ cell development is very important for the health of their offspring (Allegrucci et al., 2005; Morgan et al., 2005; Surani et al., 2007).

In mammals, germ cell lineage is cast apart from somatic lineages in very early embryonic development. Relying on genetic and epigenetic mechanisms (the definition of epigenetic is showed in Section 1.4), germ cells express their specific genome to prepare for totipotency and germ cell fate (Allegrucci et al., 2005; Morgan et al., 2005; Surani et al., 2007). Furthermore, germ cells can facilitate the continuation of genetic and epigenetic information to offspring through fertilization (Allegrucci et al., 2005; Morgan et al., 2005; Surani et al., 2007). Any inappropriate epigenetic reprogramming during germ cell development may lead to abnormal epigenotypes in germ cells, which may undergo aberrant development and apoptosis (Stringer et al., 2013). In addition, germ cells with epigenetic abnormalities may pass down the abnormal epigenetic information to their next generation and influence the development of their offspring (Allegrucci et al., 2005; Morgan et al., 2005; Surani et al., 2007). To sum up, understanding accurately the epigenetic reprogramming during human germ cell development is important for further investigation of germ cell tumors, infertility and reproductive disorders that may have an epigenetic origin in germ cells (Stringer et al., 2013).

However, due to lack of human fetal tissue, most germ cell studies were performed in murine models before being identified in human. Therefore, the key processes of fetal germ cell development and the epigenetic modifications in germ cells will be discussed mainly in mice, with some limited data in human.

1.2 *Specification and Differentiation of Mouse Fetal Germ cells*

The processes of fetal gonad development are similar in human and mouse, including germ cell specification and migration, gonadal formation, sex determination and meiotic initiation. The table below summarizes the time course of gonadal development in human and mouse (Table 1.1).

The length of gestation is 20 days in mouse (Lanman and Seidman, 1977) and 40 weeks in human (Guerrero and Florez, 1969). In the study presented here, the age of human pregnancy is measured by week of gestational age (wga), which is calculated from the last normal menstrual period (Lynch and Zhang, 2007).

EVENT	Mouse	Human
Germ Cell	E 5.5-7.5 (Saitou, 2009)	≤5wga (Falin, 1969)
Germ Cell Migration	E 7.75-9.5 (Anderson et al., 2000)	6-7wga (Fujimoto et al., 1977)
Gonadal Colonization	E 10.5 (Molyneaux et al., 2001)	7wga (Francavilla et al., 1990)
Sexual Differentiation	E 12.5 (Koopman et al., 1991)	8-10wga (Moore, 1967)
Meiotic Initiation	E 13.5 (Hilscher et al., 1974)	11wga (Gondos et al.,
Length of Gestation	20-21days (Lanman and Seidman, 1977)	40wga (Guerrero and Florez, 1969)

Table1.1.Gestational comparison of gonadal development between human and mouse

(Abbreviations: E, embryonic day; wga, week of gestation age)

1.2.1 Primordial Germ Cell Specification in Mouse

In mouse embryo, a small number of pluripotent proximal epiblast cells are induced by specific signals to become the founders of the germ cell lineage (Lawson and Hage, 1994). The figure below represents the processes of germ cell specification (Fig 1.1).

At around E5.5, visceral endoderm (VE) and extraembryonic ectoderm (ExE), which surround the epiblast, start to secrete Bone morphogenetic proteins (Bmp) 2, 4 and 8b (Lawson et al., 1999; Ying et al., 2000; Ying et al., 2001; Ying and Zhao, 2001) (Fig 1.1). These three Bmp proteins have been identified as key inductive signals for the generation of germ cell precursors in mice (Lawson et al., 1999; Ying et al., 2000; Ying et al., 2001; Ying and Zhao, 2001). Once exposed to these inductive signals, some proximal epiblast cells are instructed to develop towards specified primordial germ cells (PGCs).

Under the induction of Bmps, *Fragilis* is expressed in the proximal epiblast cells from E6.0 (Saitou et al., 2002; Tanaka and Matsui, 2002) (Fig 1.1). At around E6.25, small portions of these *Fragilis*-positive cells start to express *Blimp1* (*B-lymphocyte-induced maturation protein 1*), encoding a key transcriptional regulator for PGC specification (Ohinata et al., 2005; Vincent et al., 2005) (Fig 1.1). The expression of *Blimp1* marks the origin of germ cell lineage, and these *Blimp1*-positive cells have been proven to be PGC precursor cells by genetic lineage tracing studies (Yabuta et al., 2006). From E6.5, the *Blimp1*-positive cells start to express *Prdm14* (PR domain-containing protein 14), which encodes another transcriptional regulator (Yamaji et al., 2008). At around E7.25,

Stella, (a definitive marker of founder PGCs), is expressed specifically by the *Fragilis*-positive and *Blimp1*-positive cells (Saitou et al., 2002; Sato et al., 2002) (Fig 1.1). During germ cell specification, the somatic genes *Hoxb1* and *Hoxa1* are repressed in these *Fragilis*-positive and *Stella*-positive PGC precursor cells (Saitou et al., 2002) (Fig 1.1).

During the establishment of founder PGCs, some pluripotency-related genes are also upregulated in the *Blimp1*-positive cells (Yabuta et al., 2006). *Sox2* (*Sry Box protein 2*) and *Nanog* are re-activated in PGCs from E6.75 (Yabuta et al., 2006). After E7.75, another pluripotency-associated gene *Pou5f1* (*POU domain, class 5, transcription factor 1*), encoding Oct4 protein (octamer-binding transcription factor 4), is progressively restricted to the germ line cells and expressed throughout PGC development in mice (Pesce et al., 1998).

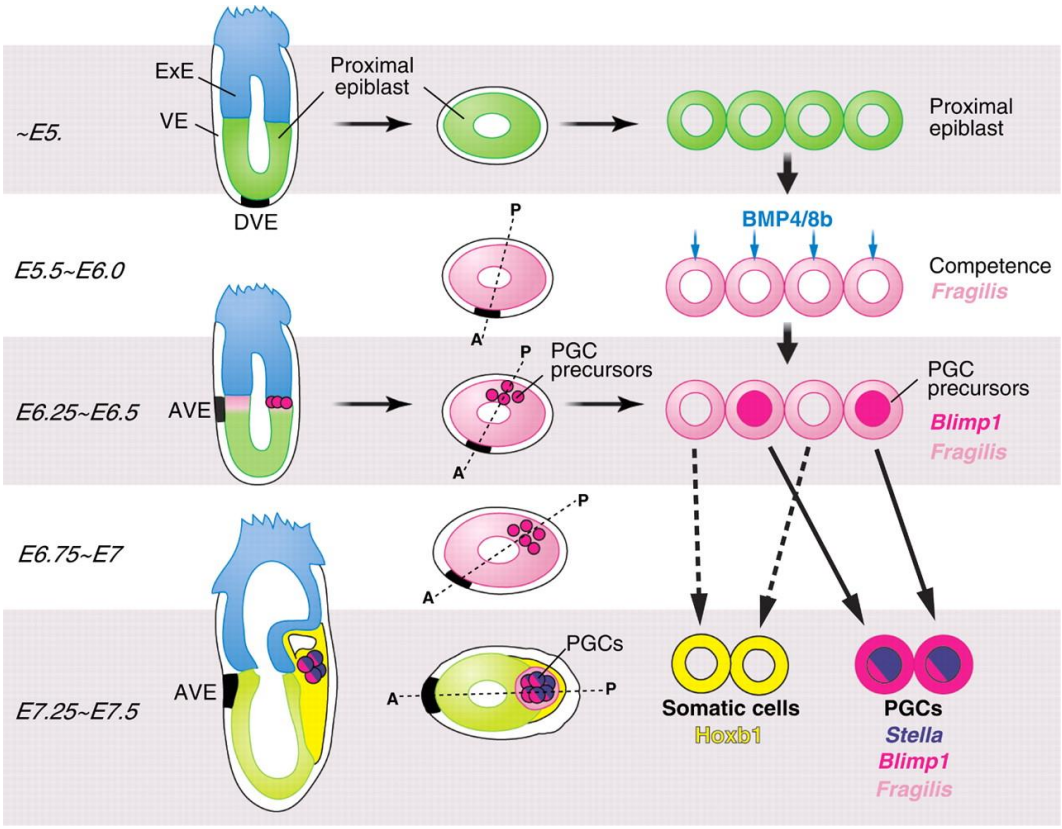

Figure 1.1 Formation of primordial germ cells in mice. During E5.5-6.0, some proximal posterior epiblast cells are inducted by Bmps signals and start to express *Fragilis*. At around E6.25, small portions of *Fragilis*-positive cells begin to express *Blimp1*. These *Blimp1*-positive cells start to generate the *Stella*-positive founder PGCs at around E7.25. Figure reproduced from (Hayashi et al., 2007). (Abbreviations: ExE, extraembryonic ectoderm; VE, visceral endoderm; DVE, distal visceral endoderm; AVE, anterior visceral endoderm; PGCs, primordial germ cells; A, anterior; P, posterior.)

1.2.2 Primordial Germ Cell Migration and Gonadal Colonization in Mouse

Once specified, PGCs begin to migrate towards the genital ridges to form the gonads in mice. At around E7.5, PGCs initially migrate from the posterior primitive streak into the adjacent posterior endoderm (future hindgut)(Anderson et al., 2000). Once the PGCs have arrived at the hindgut endoderm, they migrate along the hindgut between E8.0-9.5 (Anderson et al., 2000). Between E9.0 and 9.5, PGCs migrate from the hindgut toward the dorsal mesentery and finally enter into the genital ridges at around E10.5 (Anderson et al., 2000). Soon after PGCs arrive in the genital ridges, at around E10.5, they start to lose their motility and change their morphology to a larger and rounded profile with prominent nucleoli (Molyneaux et al., 2001).

Migrating PGCs start to proliferate on their way to genital ridges, and continue to proliferate upon arrival to the gonads. The number of PGCs rises from 10–100 at E9.5 to about 25,000 at E13.5 (De Felici et al., 1992; Molyneaux et al., 2001; Tam and Snow, 1981).

1.2.3 Sexual Determination and Differentiation in Mouse

The bipotential genital ridges are the primordia of testes and ovaries, there are no morphological or functional differences between male and female gonads before sex d*etermination (Wilhelm et al., 2007).*

The presence of Y chromosome gene *Sry* (Sex Determining Region Y) activates male sex determination and differentiation (Koopman et al., 1991). At the beginning of E10.5, the precursors of somatic supporting cells in the XY gonads start to express low levels of *Sry*. Afterwards, the expression of *Sry* increases and peaks at around E11.5; finally, it ceases at around E12.5 (Hacker et al., 1995; Jeske et al., 1995). *Sry* gene is necessary for male sexual differentiation, as XY gonads lacking *Sry* fail to activate the testis-determining pathway and form ovaries (Bullejos and Koopman, 2005). Soon after the expression of *Sry*, its direct downstream target *Sox9* (SRY box containing gene 9), is expressed by XY pre-Sertoli cells (Sekido et al., 2004; Wilhelm et al., 2005). Sox9 is necessary for male sexual differentiation, as loss of *Sox9* leads to XY sex reversal in XY transgenic mice (Barrionuevo et al., 2006).

In the absence of Y chromosome, no *Sry* expression occurs in XX gonadal ridges. Without the expression of *Sry*, female-specific genes such as *Wnt4* (*wingless-type MMTV integration site family, member 4*) and *Foxl2* (*forkhead box L2*) start to be expressed in XX genital ridges at around E11.5-12.5. The XX gonadal ridges differentiate into ovaries, with differentiation of the precursors of granulosa cells and theca cells, production of oocytes and formation of ovarian follicles (Koopman et al., 1991; Palmer and Burgoyne, 1991).

1.2.4 Regulation of Germ Cell Meiosis in Mouse

Before sex determination, PGCs are bipotential and can differentiate into either oogonia or spermatogonia (McLaren and Southee, 1997). The sexual fate of PGCs is not determined by their sex chromosome composition (XX or XY), but by the molecular signals from the surrounding gonadal environment (Adams and McLaren, 2002; Bowles et al., 2006). Exposure to an ovarian environment results in the differentiation of PGCs into oogonia (Adams and McLaren, 2002; McLaren and Southee, 1997), while exposure to a testicular environment leads to the differentiation of PGCs into spermatogonia (Adams and McLaren, 2002).

In mammals, the germ cells in ovary and testis enter into meiosis asynchronously. At around E12.5, the ovarian germ cells start to express *Stra8* (stimulated by retinoic acid 8), which encodes a protein required for pre-meiotic DNA replication and meiosis initiation (Baltus et al., 2006). Between E13.5 and E14.5 in mouse, ovarian germ cells stop proliferating and enter into meiotic prophase I (Hilscher et al., 1974; McLaren and Southee, 1997). The germ cells in mouse fetal ovary progress through leptotene (condensation of the chromosomes), zygotene (pairing of homologous chromosomes), pachytene (initiation of recombination) and arrest at the diplotene stage (paired homologous chromosomes start to separate but remain bound at chiasmata) at the time of birth (Borum, 1961; Speed, 1982). During this period, the expression of meiotic markers such as Sycp3 (Synaptonemal Complex Protein 3) and Dmc1 (the Dosage suppressor of mck1 homologue 1) are upregulated in the ovarian germ cells (Bullejos and Koopman, 2004; Menke et al., 2003; Yao et al., 2003). Soon after the initiation of meiosis, the levels of pluripotency genes, like *Pou5f1* and *Nanog*, are downregulated in the fetal ovaries (Bullejos and Koopman, 2004; Pesce et al., 1998). On the other hand, the germ cells in the testis do not enter into meiosis during fetal life. Instead, they enter mitotic arrest at around E13.5, stay in the G0/G1 phase of cell cycle for the remaining embryonic period and do not initiate meiosis until puberty (Hilscher et al., 1974; Western et al., 2008). During mitotic arrest, the fetal testicular germ cells do not express *Stra8* and express low levels of *Sycp3* and *Dmc1* (Chuma and Nakatsuji, 2001; Nakatsuji and Chuma, 2001).

1.2.4.1 *Molecular mechanisms of germ cell meiosis: retinoic acid synthesis and degradation*

Recent studies have revealed that retinoic acid (RA) is an essential extrinsic signal for the induction of meiosis in both male and female mouse germ cells (Bowles et al., 2006; Koubova et al., 2006; Li and Clagett-Dame, 2009) (Fig 1.2). The critical role of RA in meiotic initiation has been demonstrated by the studies using Vitamin A deficient (VAD) rodent models (Ghyselinck et al., 2006; Li and Clagett-Dame, 2009; Li et al., 2011). RA is a biologically active derivative of vitamin A; therefore the endogenous levels of RA are low in VAD rodents. With low levels of RA, the germ cells in the VAD rodents do not induce *Stra8*, fail to enter meiosis and remain in an undifferentiated state in both sexes (Ghyselinck et al., 2006; Li and Clagett-Dame,

2009; Li et al., 2011). *In vitro* culture experiments also showed that exogenous RA could induce meiosis in isolated XY germ cells (Ohta et al., 2010; Trautmann et al., 2008). All these studies suggest that RA is required for the initiation of meiosis in mice germ cells.

Between E11.5 and E13.5, the RA-synthesizing enzymes Aldh1a2 (retinaldehyde dehydrogenase 2) and Aldh1a3 (retinaldehyde dehydrogenase 3), which catalyze the oxidation of retinaldehyde into RA, are expressed in the mesonephros (Bowles et al., 2006; Mu et al., 2013). In mice, mesonephros-synthesized RA diffuses into the adjacent ovary in an anterior-to-posterior wave (Bullejos and Koopman, 2004; Menke et al., 2003). The ovarian germ cells in the anterior portion of the gonad, which connects to the mesonephric tubules directly, enter into meiosis earlier than those in the posterior end (Bullejos and Koopman, 2004; Menke et al., 2003). Consistent with this meiotic pattern, the increase of meiosis-specific genes and the decrease of pluripotency-associated genes occur in an anterior-to-posterior wave by germ cells (Bullejos and Koopman, 2004; Menke et al., 2003).

In fetal mouse testis, RA is mainly cleared by Cyp26b1 (cytochrome P450, family 26, subfamily b, polypeptide 1), a retinoid-degrading enzyme, which can catabolize RA into inactive oxidized metabolites (Bowles et al., 2006; Koubova et al., 2006; MacLean et al., 2001) (Fig 1.2). By E11.5, the levels of *Cyp26b1* are low in the gonads of both sexes. Afterwards, *Cyp26b1* expression decreases to an undetectable level in mouse ovary by E12.5 (Bowles et al., 2006; Koubova et al., 2006). Without Cyp26b1, ovarian germ cells are exposed to high levels of RA, which eventually induces the initiation of meiosis in mouse fetal ovarian germ cells. Conversely, after the onset of sex determination, the expression of *Cyp26b1* is upregulated in the mouse fetal testis. High expression of *Cyp26b1* prevents the entry of germ cells into meiosis in fetal mouse testis by degrading the endogenous RA (Bowles et al., 2006; Koubova et al., 2006).

Cyp26b1-knockout studies in mice have confirmed the importance of Cyp26b1 in meiosis inhibition (Bowles et al., 2006; MacLean et al., 2007; Yashiro et al., 2004). In *Cyp26b1*-null XY fetal gonads, endogenous RA is increased, indicating that Cyp26b1 is required for the repression of RA. With the presence of ectopic RA, meiosis-related genes *Stra8*, *Sycp3*, and *Dmc1* are greatly upregulated in *Cyp26b1*-null XY germ cells, which enter and progress through meiosis by E16.5 (Bowles et al., 2006; MacLean et al., 2007; Yashiro et al., 2004).

According to the studies above, the balance between retinoid synthesis and degradation determines the levels of RA, which will thus control the onset of meiosis in mice.

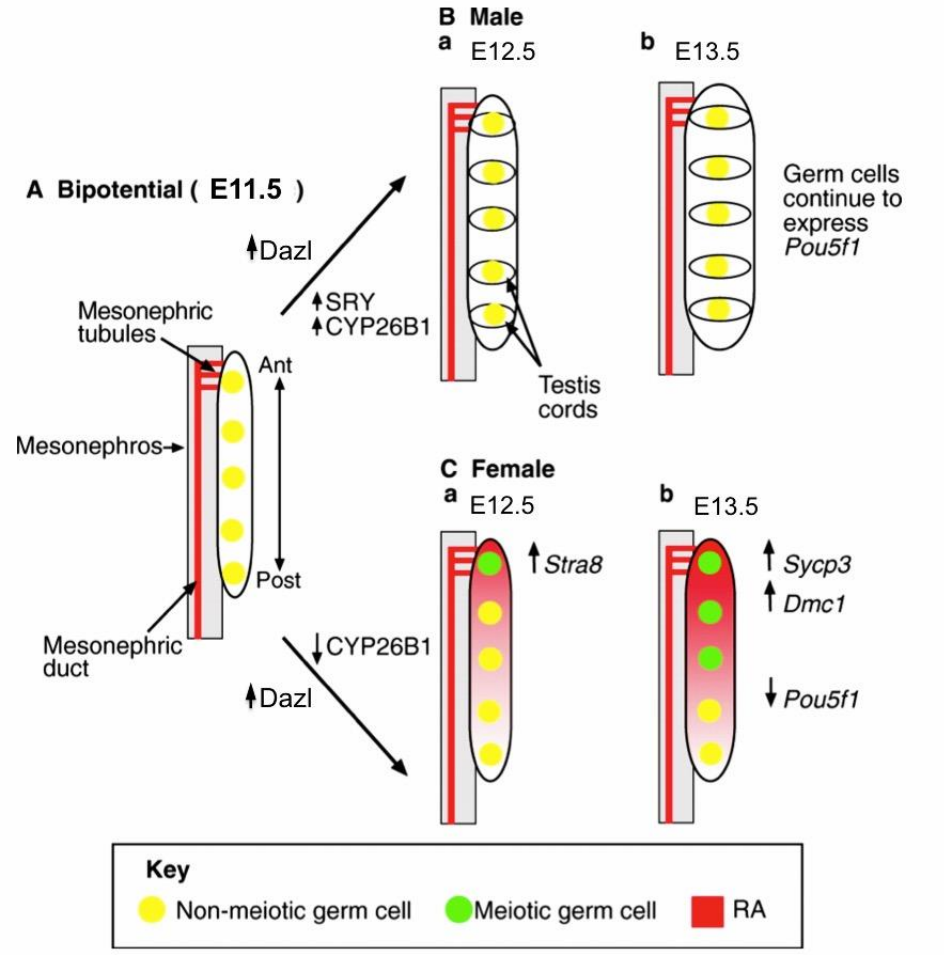

Figure 1.2 Regulation of meiotic initiation in mouse germ cells. A. At around E11.5, RA is synthesized in mesonephros, low levels of Cyp26b1 and *Dazl* are present in the bipotential gonad. **Ba.** Once *Sry* is expressed in the XY gonad, expression of Cyp26b1 is increased and protects testicular germ cells from the RA activity. **Bb.** At around E13.5, the testicular germ cells enter into mitotic arrest. **Ca.** In the female gonad, the expression of Cyp26b1 is decreased by E12.5. With the induction of RA, the ovarian germ cells enter into meiosis and start to express Stra8. **Cb.** The meiotic markers *Sycp3* and *Dmc1* increased in ovarian germ cells by E13.5. Figure reproduced from (Bowles and Koopman, 2007).

1.2.4.2 *The Meiotic Gatekeeper Gene Stra8*

Stra8 was first identified as a RA-responsive gene in mouse P19 embryonic carcinoma cells (Bouillet et al., 1995; Oulad-Abdelghani et al., 1996). RA induces the expression of *Stra8* by binding to RAR (retinoic acid receptors) and RXR (retinoid-X receptors), which bind to RAREs (retinoic acid response elements) in the *Stra8* promoter (Duester, 2008). *In vitro* culture experiments have shown that these RA receptors are necessary for the induction of *Stra8* and the initiation of meiosis in both sexes (Boulogne et al., 1999; Bowles et al., 2006; Dufour and Kim, 1999; Koubova et al., 2006). When treated with RAR antagonists, fetal ovarian germ cells fail to induce *Stra8* and fail to enter the meiotic cell cycle (Bowles et al., 2006; Koubova et al., 2006). Conversely, in

testis culture experiments, the presence of RAR agonists activates the expression of *Stra8* in fetal testicular germ cells (Boulogne et al., 1999; Dufour and Kim, 1999).

The key role of Stra8 as meiotic gatekeeper has been confirmed in both spermatogenesis and oogenesis by gene knockout studies (Anderson et al., 2008; Baltus et al., 2006; Mark et al., 2008). In *Stra8*-deficient female mouse embryos, ovarian germ cells retain pre-meiotic morphology and do not undergo any of the meiotic chromosomal events. There is no pre-meiotic DNA replication, and no meiotic chromosome condensation, cohesion, synapsis and recombination in *Stra8*-deficient ovarian germ cells (Anderson et al., 2008; Baltus et al., 2006). In the presence of exogenous RA, germ cells in *Stra8*-null fetal ovaries fail to initiate the subsequent meiotic process, indicating that the Stra8 is the trigger for meiotic initiation (Anderson et al., 2008; Baltus et al., 2006). In *Stra8*-deficient testis, impaired meiosis also has been observed (Anderson et al., 2008; Mark et al., 2008). However, whether meiotic disruption occurs before or after meiotic initiation in the *Stra8*-deficient testis is not consistent between the studies of Anderson *et al*. (Anderson et al., 2008) and Mark *et al.* (Mark et al., 2008).

Molecular hallmarks of meiotic chromosome cohesion, synapsis and recombination have been investigated in *Stra8*-deficient ovaries and testes (Anderson et al., 2008; Baltus et al., 2006). Normally, the meiosis-specific cohesion protein Rec8 (Meiotic recombination protein) (Eijpe et al., 2003; Lee et al., 2003) and the synaptonemal complex protein Sycp3 (Moens and Spyropoulos, 1995) are localized along the lengths of chromosomes in meiotic germ cells (Prieto et al., 2004). However, in *Stra8*-null ovarian germ cells, Rec8 and Sycp3 are not properly localized along chromosomes (Anderson et al., 2008; Baltus et al., 2006), suggesting that Stra8 is required for the formation of meiotic cohesion and synaptonemal complex in mice germ cells (Anderson et al., 2008; Baltus et al., 2006). During prophase I of meiosis, homologous recombination is initiated by DNA double-strand breaks (DSBs), which are formed by protein Spo11 (Baudat et al., 2000; Romanienko and Camerini-Otero, 2000) and repaired by Dmc1 (Pittman et al., 1998; Yoshida et al., 1998). In response to DNA DSBs, γ-H2AX is deposited at the sites of DNA damage generated during meiotic recombination (Rogakou et al., 1998). In *Stra8*-deficient ovaries and testes, the staining of γ-H2AX, and mRNA levels of *Spo11* and *Dmc1* were all undetectable, suggesting that germ cells lacking *Stra8* fail to form or repair meiotic DSBs, and thus fail to initiate meiotic recombination (Anderson et al., 2008; Baltus et al., 2006).

Recently, Saba and colleagues (Saba et al., 2014) generated mouse embryos with the double knockout of *Cyp26b1* and *Stra8*. Meiosis in XY germ cells, which was induced in the *Cyp26b1*-null mice (Bowles et al., 2006; MacLean et al., 2007; Yashiro et al., 2004), was inhibited in the *Cyp26b1−/−/Stra8−/−* XY germ cells (Saba et al., 2014). In this double knockout study, the meiotic markers Sycp3 and γH2AX were up-regulated in the *Cyp26b1−/−/Stra8+/+* male gonads, but not observed in the

Cyp26b1−/−/Stra8−/− male gonads and *Cyp26b1+/+/Stra8+/+* control (Saba et al., 2014). All these experiments indicate the indispensable role of Stra8 for meiotic initiation in mice (Anderson et al., 2008; Baltus et al., 2006; Mark et al., 2008; Saba et al., 2014).

1.2.4.3 *Intrinsic Factor involved in meiotic entry*

In addition to extrinsic signals, an intrinsic meiotic competence factor is also necessary for meiosis initiation (Lin et al., 2008). Dazl (Deleted in azoospermia-like), a germline-specific RNA-binding protein, is required for germ cells to respond to RA signals (Lin et al., 2008; Lin and Page, 2005). In the post-migratory mouse germ cells, *Dazl* mRNA is first detected at around E11.5 (Seligman and Page, 1998); the Dazl protein is localized to the cytoplasm of mouse fetal germ cells (Ruggiu et al., 1997).

In both male and female mice, targeted deletion of *Dazl* results in germ cell loss (Lin et al., 2008; Lin and Page, 2005; Ruggiu et al., 1997; Saunders et al., 2003). In *Dazl*-knockout mice, the expression of pluripotency-related genes is not downregulated in the germ cells, and they remain in an undifferentiated PGC-like state (Lin et al., 2008; Lin and Page, 2005). Deficiency of *Dazl* leads to failure to enter meiosis in these PGC-like ovarian germ cells (Lin et al., 2008; Saunders et al., 2003). The mRNA levels of *Stra8* are drastically decreased in surviving *Dazl*-deficient ovarian germ cells, suggesting that Dazl is responsible for the initiation of meiosis in the fetal mouse ovary (Lin et al., 2008). Germ cells in *Dazl*-deficient ovaries do not form DNA DSBs, and fail to initiate homologous recombination, as the surviving *Dazl*-null ovarian germ cells do not express *Spo11* and *Dmc1*, and are negative for γ-H2AX staining (Lin et al., 2008). In the *Dazl*-null mouse ovarian germ cells, Sycp3, the translation of which is regulated by Dazl (Reynolds et al., 2007), is markedly downregulated at mRNA and protein levels (Lin et al., 2008). Similarly, *Rec8* mRNA is undetectable in *Dazl*-deficient ovaries (Lin et al., 2008). Therefore, Dazl is also essential for the formation of meiotic cohesion and synaptonemal complex in mice fetal ovarian germ cell (Lin et al., 2008). When *Dazl*-deficient testes were exposed to exogenous RA, the germ cells were unable to induce *Stra8* and failed to enter meiosis (Lin et al., 2008).

The studies detailed above identify Dazl as an essential intrinsic competence factor for meiotic initiation in mice (Lin et al., 2008).

1.2.4.4 *Challenging the retinoic acid theory*

In 2011, the theory that meiotic induction is dependent on RA has been challenged. In the study by Kumar *et al*. (Kumar et al., 2011), meiotic induction was investigated in the *Aldh1a2*-single knockout (*Aldh1a2−/−)* and *Aldh1a2/Aldh1a3*-double knockout (*Aldh1a2−/−/Aldh1a3−/−*) mouse embryos. Despite the absence of these two major RA-synthesizing enzymes, the expression of *Stra8* was still induced in ovarian germ cells, which also entered into meiosis (Kumar et al., 2011). In these *Aldh1a2−/−* and

Aldh1a2-/-/Aldh1a3−/− mouse ovaries, RA was undetectable by transgenic *RARE-LacZ* reporter mouse line, which is sensitive to 25nM RA and above (Kumar et al., 2011). The data in this study led Kumar *et al.* to conclude that meiotic initiation is completely independent of RA (Kumar et al., 2011).

However, Griswold *et al.* (Griswold et al., 2012) has alternative explanations for this study. He argued that another RA-producing enzyme Aldh1a1, which is expressed in the ovary, might contribute to the RA synthesis in these *Aldh1a2−/−* and *Aldh1a2-/-/Aldh1a3−/−* embryos (Griswold et al., 2012). It also has been proven that very small amounts of RA (around 1nM) are sufficient to induce *Stra8* expression and subsequent meiosis (Ohta et al., 2010; Zhou et al., 2008). Recently, an *in-vitro* study in cultured mouse fetal ovaries has indicated that the Aldh1a1-synthesized RA can initiate meiosis (Mu et al., 2013). Therefore, within *Aldh1a2−/−* and *Aldh1a2-/-/Aldh1a3−/−* ovaries, Aldh1a1 may locally produce low levels of RA, which is sufficient to induce the expression of *Stra8*, but not high enough to be detected by the *RARE-LacZ* reporter mouse line (Griswold et al., 2012; Mu et al., 2013).

1.3 *Germ cell specification and differentiation in human*

1.3.1 **Generation of Primordial Germ Cells in Human**

In human embryos, some PGC precursor cells have been identified in the dorsal wall of the yolk sac at around 5wga (Falin, 1969; Fuss, 1912; Witschi, 1948). PGCs can be distinguished from other cells by their large size, spherical shape, round nucleus with prominent nucleoli, and pale cytoplasm (Falin, 1969; Fuss, 1912; Witschi, 1948).

Due to lack of accessibility to early human tissues, the process of human PGC specification is not clear. In order to investigate the molecular mechanisms controlling PGC formation in humans, human embryonic stem cells (hESCs) have been used as an important *in vitro* system (Clark et al., 2004; Tilgner et al., 2008). The *in vitro* studies in hESCs have shown that human BMPs may be involved in the formation of human PGCs (Kee et al., 2009; Kee et al., 2006), as they were in mice (Lawson et al., 1999; Ying et al., 2000; Ying et al., 2001; Ying and Zhao, 2001). In hESCs, the transcriptional repressor BLIMP1 has been found to induce the PGC formation by switching off the pluripotency-related gene *SOX2* (Lin et al., 2014). The studies in hESCs (Lin et al., 2014) and 16-22wga human fetal gonads (Eckert et al., 2008) have indicated that BLIMP1 might be associated with early PGC development in humans, as it was in mice (Yabuta et al., 2006). The findings mentioned above suggest that the mechanisms involved in PGC formation may be evolutionarily conserved between human and mouse; however, this need further investigation.

1.3.2 Differentiation of Human Fetal Germ Cells

At around 6wga, human PGCs migrate from the yolk sac to the hindgut endoderm (Fujimoto et al., 1977). The migrating PGCs reach the dorsal mesentery early in 7wga, and continue to move and pass beyond the primitive mesonephros (Fujimoto et al., 1977). At around the end of 7wga, most of the human PGCs have reached the genital ridges and the gonadal primordia are colonized by 8wga (Francavilla et al., 1990; Fujimoto et al., 1977).

In the early migration stage, human germ cells proliferate by mitotic division, and continue to increase in number after they reach the genital ridges. From 7wga to 11wga, the number of germ cells increases from around 1000 to about 250,000 in females and around 75,000 in males (Baker, 1963; Bendsen et al., 2006; Mamsen et al., 2011). At the end of the proliferative phase at around 20wga, the number of human ovarian and testicular germ cell number rises to approximately 5,000,000 and 1,500,000, respectively (Baker, 1963; Bendsen et al., 2006; Mamsen et al., 2011).

Before sexual differentiation in humans, the newly colonized genital ridges are indistinguishable between males and females. From 8wga, with the activation of SRY on the Y chromosome, human XY gonads undergo testis-specific differentiation and form testicular cords (Hanley et al., 2000). The expression of human SRY is maintained in the testicular cords throughout the embryonic period and beyond (Hanley et al., 2000), which is different from the expression observed in mouse (Hacker et al., 1995; Jeske et al., 1995). As the first morphological sign of male sex differentiation, the testicular cords are gradually formed during 8 and 10wga (Pelliniemi, 1993). At around 9wga, the mesonephric origin pre-Sertoli cells migrate into the central regions of the testis and surround the testicular PGCs (Heyn et al., 2001) (Fig 1.3). With the differentiation of Sertoli cells, the differentiated peritubular myoid cells, which migrate from the mesonephros, enclose the mix of Sertoli cells and PGCs to form the testicular cords (Pelliniemi, 1993; Wartenberg, 1981) (Fig 1.3). During these periods, the testicular androgen-producing Leydig cells undergo proliferation and occupy the spaces between the testicular cords (DeFalco et al., 2011; Murray et al., 2000) (Fig 1.3). The testicular PGCs are referred to as gonocytes after they are enclosed in testis cords (Gaskell et al., 2004; Wartenberg, 1981). The human gonocytes are inhibited from meiosis; without any apparent arrest, some of them undergo several rounds of mitosis and further differentiate into more mature prespermatogonia (Bendsen et al., 2003; Gaskell et al., 2004). During 13-20wga (2nd trimester), both gonocytes and prespermatogonia are visible in the same human testes cords (Gaskell et al., 2004). The smaller, round gonocytes are usually present in the center of a cord, while the larger, irregular prespermatogonia are usually observed in groups at the periphery of a cord (Gaskell et al., 2004) (Fig 1.3).

Conversely, without the expression of SRY, human XX gonads differentiate into ovaries (Hanley et al., 2000). Following sex determination in humans, germ cells in

the nascent ovaries continue to proliferate for several weeks and differentiate into oogonia (Wartenberg, 1982). At 8-9wga, the ovaries contain only undifferentiated PGCs, which distribute throughout the ovary and integrate with somatic cells in an unorganized pattern (Byskov, 1986) (Fig 1.3). During rapid mitotic proliferation, clusters of human oogonia undergo incomplete division of cell body and form clusters of interconnected germ cell nests (Gondos et al., 1986; Gondos and Zamboni, 1969; Wartenberg, 1982) (Fig 1.3). Groups of oogonia in the germ cell nests are joined via intercellular bridges (Gondos and Zamboni, 1969). At roughly 12wga, the somatic pre-granulosa cells integrate with germ cells and become part of the germ nests; meanwhile, streams of mesenchymal somatic cells run amongst the nests (Wartenberg, 1982) (Fig 1.3). Around 11-12wga, some clustered oogonia located in the inner cortex of the ovary begin to enter meiotic prophase I (Gondos et al., 1986), while the smaller germ cells in the periphery of ovary continue to proliferate via mitosis (Gondos et al., 1986; Le Bouffant et al., 2010). With the development of human fetal ovary, meiosis spreads radially towards the periphery of the ovary in human (Gondos et al., 1986; Le Bouffant et al., 2010), which is different from the anterior-to-posterior meiotic entry in mouse ovarian germ cells (Bullejos and Koopman, 2004; Menke et al., 2003). By the time of birth, nearly all of oocytes have progressed through meiotic prophase I and arrested at the diplotene stage before birth (Gondos et al., 1986). Following the initiation of meiosis, breakdown of the germ-cell nests occurs, accompanied with apoptotic death of about two-thirds of the oocytes (De Pol et al., 1997; Fulton et al., 2005; Vaskivuo et al., 2001). The surviving oocytes interact with the surrounding pre-granulosa cells to initiate the formation of primordial follicles (Stoop et al., 2005; Tingen et al., 2009). From around 17wga onwards (the late 2nd trimester), primordial follicle is formed with one oocyte surrounded by a single layer of pre-granulosa cells (Stoop et al., 2005; Tingen et al., 2009) (Fig 1.3).

During 13-20wga, the ovarian germ cells at different developmental stages are distributed radially in human ovaries. During this period, the undifferentiated PGC-like cells are located in the outer cortex of human fetal ovary; while the mature ovarian germ cells settle in the central cortex and medulla of fetal ovary (Anderson et al., 2007; Stoop et al., 2005). During 17-20wga, the proliferative PGC-like cells, pre-meiotic oogonia, meiotic oocytes and primordial follicles can be simultaneously detected in the same human ovary (Fulton et al., 2005; Stoop et al., 2005). These observations suggest that differentiation of human fetal germ cells occurs in an asynchronous way, which is different from the more synchronous differentiation of mouse germ cells (Bullejos and Koopman, 2004; Menke et al., 2003).

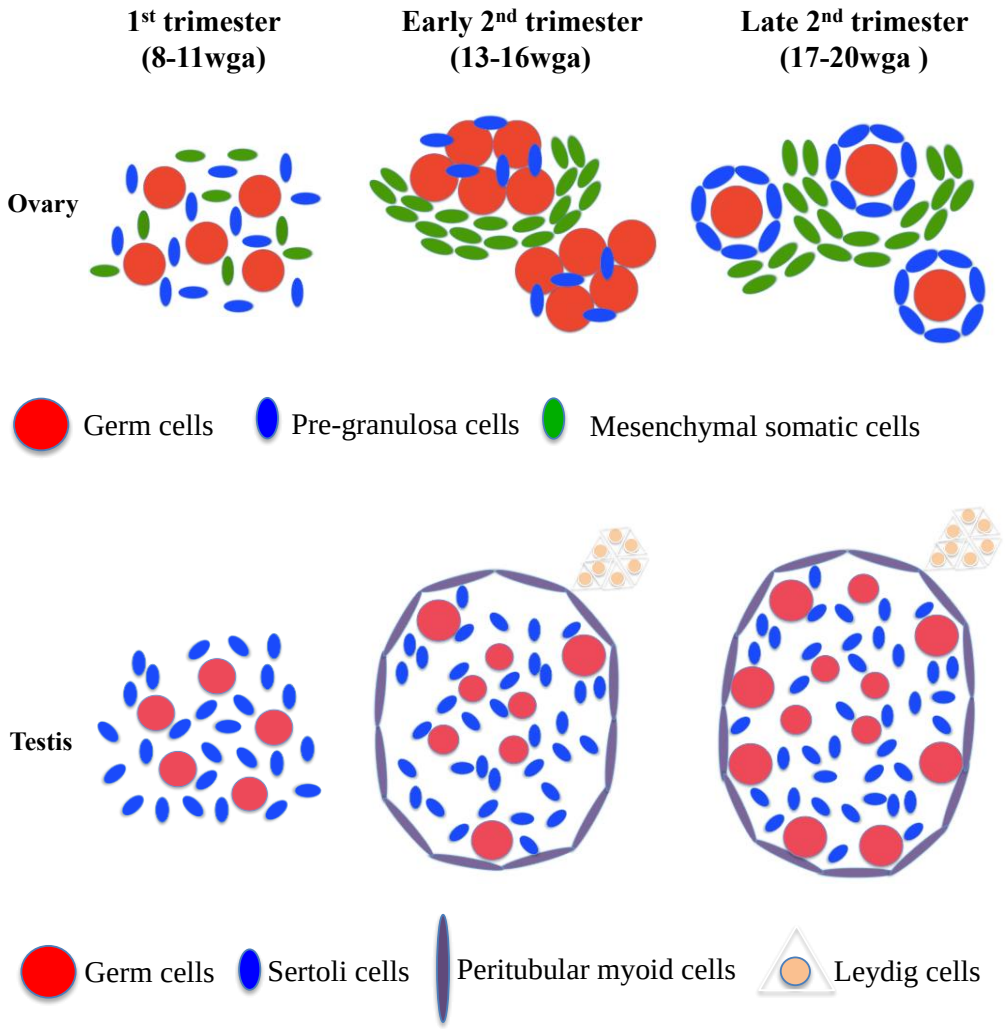

Figure 1.3 Schematic of fetal human ovarian and testicular development. Ovaries: In 1st trimester, PGCs distribute throughout the ovary and integrate with mesenchymal somatic cells and pre-granulosa cells in an unorganized pattern. In early 2nd trimester, clusters of oogonia form the germ cell nests with pre-granulosa cells. Streams of mesenchymal somatic cells run amongst the nests. In late 2nd trimester, the nests break down, and oocytes become surrounded by a single layer of pre-granulosa cells to form primordial follicles. **Testes:** In 1st trimester, PGCs are distributed throughout the testis and integrate with Sertoli cells in an unorganized pattern; the testicular cords start to be formed at this stage. In early 2nd trimester, testicular cords are distinct. A layer of peritubular myoid cells encloses the Sertoli cells and gonocytes into the cords. The Leydig cells are located between the cords. The centrally located gonocytes gradually move to the periphery of the cords as they differentiate into prespermatogonia. This pattern becomes more obvious in the late 2nd trimester. Figures are partly adapted from (Eddie, 2011).

1.3.3 Expression of Pluripotent Marker OCT4 and Germ Cell-specific Marker VASA in Human Fetal Ovary and Testis

In humans, the pluripotency-associated gene *POU5F1* (also known as *OCT4*), which encodes the OCT4 protein, is detectable in both male and female fetal gonads (Anderson et al., 2007). In human fetal ovary, the expression of *POU5F1* is in a high level at 1st trimester; and slightly declines at 2nd trimester. In human fetal testis, no significant difference has been observed between different gestations (Anderson et al., 2007).

During 1st trimester, the PGCs in the human fetal ovary and testis all express this pluripotency-associated marker OCT4. At this stage, OCT4-positive PGCs are evenly distributed throughout the male and female gonads. With the maturation of germ cells, OCT4 expression progressively decreases in ovaries and testes (Anderson et al., 2007; Kerr et al., 2008a; Kerr et al., 2008b). During 2nd trimester, OCT4 is repressed asynchronously in human fetal ovary, in which the ovarian germ cells are differentiated asynchronously (Anderson et al., 2007; Stoop et al., 2005). During this period, a subpopulation of PGC-like cells in the periphery of fetal ovary still maintain the OCT4 expression; while the central located oocytes, which have already entered meiotic prophase I, have lost the expression of OCT4. The mature oocytes in primordial follicles are OCT4-negative as well. The asynchronous down-regulation of OCT4 has also been observed in human 2nd trimester fetal testes, in which a mixture of OCT4-positive and OCT4-negative germ cells has been observed in the same testicular cords (Anderson et al., 2007; Kerr et al., 2008b). This observation in human testis is different to that in mouse, in which the expression of OCT4 is reduced synchronously in all testicular germ cells (Pesce et al., 1998; Zayed et al., 2007).

VASA, a member of the DEAD-box family, was first identified in Drosophila (Lasko and Ashburner, 1988). Study in 2000 indicated that VASA was expressed in migratory PGCs in the region of the gonadal ridge (Castrillon et al., 2000), earlier than occurred in mouse (Toyooka et al., 2000). However, in later studies, VASA has been identified as a mature germ cell-specific marker in human gonads (Anderson et al., 2007; Kerr et al., 2008a; Kerr et al., 2008b). During 1st trimester, *VASA* is present at very low levels or barely detectable in human fetal gonads. At 2nd trimester, the expression of *VASA* is significantly upregulated in both ovary and testis, although the increase in testis is less substantial than that in ovary. During 1st trimester, the VASA protein is undetectable in human ovary and testis (Anderson et al., 2007). From the early 2nd trimester, an asynchronous increase in VASA also has been observed in both ovarian and testicular germ cells (Anderson et al., 2007; Kerr et al., 2008a; Kerr et al., 2008b). In 2nd trimester human fetal ovaries, the mature oocytes, which are negative for OCT4, display intense cytoplasmic VASA staining. Meanwhile, the PGC-like cells, which are positive for OCT4, do not display VASA staining. This observation indicates that the expression of VASA is restricted to the maturing oocytes rather than PGC-like cells. In 2nd trimester human fetal testes, a mixture of VASA-positive and OCT4-positive germ

cells has been observed at the same testicular cords. Similar to the ovarian germ cells, the more differentiated OCT4-negative testicular germ cells are VASA-positive; while the OCT4-positive gonocytes are VASA-negative (Anderson et al., 2007; Kerr et al., 2008b).

The asynchronous decrease of OCT4 and increase of VASA in human fetal ovary and testis further demonstrates that the human fetal germ cells differentiate in an asynchronous way (Anderson et al., 2007; Fulton et al., 2005; Kerr et al., 2008a; Kerr et al., 2008b; Stoop et al., 2005). The mutually exclusive expression of OCT4 and VASA in human 2nd trimester gonads further supports that VASA is a specific marker of germ cell maturation (Anderson et al., 2007; Kerr et al., 2008a; Kerr et al., 2008b).

1.3.4 Meiotic Regulators in Human Fetal Gonads

Following the initiation of meiosis, human oocytes undergo chromosome condensation, homologous chromosome synapsis, homologous recombination and finally arrest at the diplotene stage of meiotic prophase I before birth (Hunt and Hassold, 2008).

During these periods, multiple meiosis-related genes are upregulated in human fetal ovary (Childs et al., 2011; Houmard et al., 2009; Le Bouffant et al., 2010). At around the onset of meiosis, the pre-meiotic gene *STRA8*, which is present at low levels in early human fetal ovaries (8-9wga), is markedly increased (Childs et al., 2011; Houmard et al., 2009; Le Bouffant et al., 2010). In addition to *STRA8*, the expression *SPO11*, which is required for meiotic recombination; *SYCP1* and *SYCP3*, which encode essential structural components of synaptonemal complex; are all sharply increased in human fetal ovaries from 12wga onwards (Childs et al., 2011; Houmard et al., 2009; Le Bouffant et al., 2010). Another meiotic gene *DMC1*, which encodes a meiotic homologous recombination protein, is elevated later at 17wga in human fetal ovaries (Le Bouffant et al., 2010). Between 12-20wga, SYCP3 protein has been observed in the human fetal ovaries (Childs et al., 2012; Jorgensen et al., 2012), which corroborates the observation on *SYCP3* gene expression (Childs et al., 2011; Houmard et al., 2009; Le Bouffant et al., 2010). During these stages, the meiotic oocytes display intense nuclear SYCP3-staining; while the oogonia, which do not enter into meiosis, are negative for SYCP3 (Childs et al., 2012; Jorgensen et al., 2012).

During the process of meiotic prophase I, any errors occurred can alter the expression of these meiotic genes, and further affect the formation of haploid gametes causing fertility problems, miscarriage and birth defects in human (Zheng et al., 2010). Therefore, it is important to understand the mechanisms that regulate meiotic initiation and meiotic prophase in human fetal ovary. However, due to the difficulty in obtaining human fetal ovarian samples, knowledge about human female meiosis is limited.
The critical role of RA in meiotic initiation has been demonstrated in human fetal ovaries by Childs *et al* and Le Bouffant *et al*'s studies (Childs et al., 2011; Le Bouffant et al., 2010). Unlike the mouse (Bowles et al., 2006; Koubova et al., 2006), the local gonadal RA synthesis rather than diffusion of RA from the mesonephros may drive the

initiation of meiosis in human fetal ovary; as the gonadal produced RA-producing enzyme ALDH1A can synthesize RA locally (Childs et al., 2011; Le Bouffant et al., 2010). At around 2nd trimester, nuclear-localized RA receptors RARα, RARβ and RXRα are all detectable in human ovarian germ cells (Childs et al., 2011). RA receptors have been found to be essential for retinoid signals transduction (Kastner et al., 1997). The nuclear localization of these receptors in human fetal ovarian germ cells suggests that higher local RA concentration is existed in these cells.

Conversely, meiosis is inhibited in human fetal testis (Bendsen et al., 2003; Gaskell et al., 2004). The expression of *STRA8* is barely detectable in human fetal testes. In addition to *STRA8*, the mRNA levels of other meiotic genes *SPO11, SYCP1, SYCP3 and DMC1* are all expressed at very levels across all the detected gestations in human fetal testes (Childs et al., 2011; Houmard et al., 2009; Le Bouffant et al., 2010). The knowledge about the mechanism of meiotic inhibition in human fetal testis remains limited. Cyp26b1-mediated RA degradation has been proposed to be involved in the prevention of meiosis in mouse fetal testis (Bowles et al., 2006; Koubova et al., 2006). However, in human fetal testis, there is no any really evidence to support that CYP26B1 play an important role in the inhibition of meiosis (Childs et al., 2011; Jorgensen et al., 2012; Le Bouffant et al., 2010). In male, the nuclear-localization of RA receptors has been detected in human fetal testicular germ cells (Childs et al., 2011). This observation indicates that these human fetal testicular germ cells are receiving RA signals and the RA-degrading enzyme CYP26B1 does not effectively block the RA signals in these cells (Childs et al., 2011). Different from the observation in mice (Bowles et al., 2006; Koubova et al., 2006), *CYP26B1* does not specifically increase in human fetal testis (Childs et al., 2011). The expression of *CYP26B1*, which is relatively similar in the early human fetal testes and ovaries, is unexpectedly higher in the human fetal ovary during 14-16wga. CYP26B1 protein is also detectable in both human fetal ovary and testis (Childs et al., 2011). All these observations suggest that CYP26B1 may not be the main meiotic inhibition factor in human fetal testes. Some other mechanisms of meiotic inhibition may be involved in human fetal testis, which need to be further investigated.

In addition to RA and its RA-degrading enzyme Cyp26b1, Dazl also has been identified as an essential intrinsic meiotic competence factor for RA response in mice (Lin et al., 2008). In humans, DAZL is a candidate fertility factor, as mutations of *DAZL* may be linked to infertility in males and females (Dorfman et al., 1999; Seboun et al., 1997; Tung et al., 2006; Yen et al., 1996). *In vitro* studies in human germ cells differentiated from hESCs and human iPSCs (Induced Pluripotent Stem Cells) have demonstrated that overexpression of *DAZL* and/or its closely-related gene *BOLL* can enhance the entry into and progression through meiosis (Kee et al., 2009; Medrano et al., 2012; Panula et al., 2011).

The mRNA expression of *DAZL* is present at a very low level in both human fetal ovary and testis during the 1st trimester. Following the onset of meiosis, ovary-specific *DAZL* upregulation has been observed (Anderson et al., 2007). DAZL protein is initially localized in the nucleus of human ovarian PGCs. With the development of human ovary, the DAZL protein is re-located from nucleus to cytoplasm in the more differentiated oocytes (Anderson et al., 2007). The expression and distribution of DAZL has been further investigated in human fetal ovary (He et al., 2013). In meiotic human oocytes, DAZL was expressed in the early stages of meiotic prophase I, after that, DAZL was downregulated, and then replaced by another DAZ-family protein BOLL. Finally, at the end of meiotic prophase I, the expression of BOLL was erased and DAZL re-expressed. DAZL protein also has been found to co-localize with the meiotic markers SYCP3 in some human fetal oocytes (He et al., 2013). According to the observations mentioned above, the role for DAZL in regulating the meiotic entry is conserved in humans and mice (Lin et al., 2008).

1.4 *Epigenetics and Inheritance*

The growth process of multicellular organisms demands the close regulation of gene expression. If unregulated, gene expression can have significant adverse effects on the phenotypes, leading to the development of various diseases in humans, including cancer (Alberts, 2008).

Changes in gene expression can be inherited without altering the underlying DNA sequence. This phenomenon has been identified as epigenetic modification, which can be transferred to daughter cells or next generation by mitosis and meiosis (Bird, 2007; Goldberg et al., 2007). The development of a multicellular organism from a totipotent zygote is the most compelling case of epigenetic modification. The main feature of a totipotent zygote is its capacity for differentiation into any cell type, including neural, muscle, epithelium and germ cells (Reik, 2007). Although all of the cells in a multicellular organism contain identical DNA sequences, different types of cells only express the genes required for their particular functions. These tissue and cell specific gene expression patterns are not dependent upon intracellular DNA sequence, but on epigenetic modifications, which can either trigger gene expression or inhibit it (Reik, 2007).

Epigenetic modifications are relatively stable in the mammalian somatic cells. The epigenetic state can be transmitted to the daughter cells by cell division in order to recall active or repressive transcriptional states (Reik, 2007). In general, the majority of epigenetic modifications in somatic cells only take place within the course of one individual organism's lifetime and can’t be transmitted to the following generation (Reik, 2007). However, in mammalian germ cells, epigenetic modifications are subject to reprogramming throughout the genome (Seki et al., 2005). Epigenetic changes can be passed on to the following generation if they take place in a germ cell that is involved in fertilisation (Reik, 2007). Thus, the next generation may exhibit incorrect

epi-genotypes due to disruption of the epigenetic status in germ cells, and as a result, the embryo may develop abnormally (Reik, 2007; Seki et al., 2005). This underscores the importance of having comprehensive knowledge of the epigenetic modifications during the development process of germ cells.

Of the known epigenetic mechanisms, the most significant epigenetic modifications are caused by DNA methylation and histone modifications (Berger et al., 2009). During the complex biological process, DNA methylation and histone modifications affect the specific epigenetic phenomenon independently; they also interact with each other and jointly determine gene transcriptional status during this process.

1.5 *Histone modification*

1.5.1 Chromatin Structure and Modification of Histone Proteins

In eukaryotes, chromatin, which consists of complexes of DNA and proteins, can compress the DNA to fit in the cell nucleus (Kornberg, 1974; Kornberg, 1977).

Heterochromatin and euchromatin are the two distinct geographically regions of chromatin, the former being largely transcriptionally inactive, while the latter is largely active (Dillon, 2004; Nicholson and Wood, 2006). The genes in eukaryotes are not activated unless RNA polymerase and transcription factors can access them. The initiation of gene transcription depends on the interaction between the transcription factors and gene segments known as promoter regions (Alberts, 2008). In the compressed heterochromatin, transcription factors cannot access the promoter regions and therefore cannot activate gene expression (Dillon, 2004; Grewal and Jia, 2007). Thus, heterochromatin is usually associated with gene silencing. In order to activate gene expression, the heterochromatin structure has to be loosened up in a specific and regulated way. This loose chromatin structure has been identified as euchromatin (Nicholson and Wood, 2006). Usually, but not always, euchromatin undergoes active transcription because it is not as compressed as heterochromatin, thus permitting access of gene regulatory proteins to the DNA (Nicholson and Wood, 2006).

The fundamental subunit of chromatin in eukaryotes is nucleosome, which consists of the nucleosome core particle, linker DNA, and linker histone (Kornberg, 1974; Kornberg, 1977). In every nucleosome core particle, around 147 base pairs of DNA envelope a histone octamer in 1.65 left-handed superhelix turns (Luger et al., 1997). The histone octamer core in the nucleosome is formed by eight subunits, two molecules of each histone proteins (H2A, H2B, H3 and H4). Each histone protein has a structured basic domain, known as the histone fold, which consists of three α-helices linked by two unstructured loops (Arents and Moudrianakis, 1993; Arents and Moudrianakis, 1995). During the process of nucleosome assembly, the histone folds undergo the so-called handshake interaction, in which they attach to each other to create two sets of H3-H4 and H2A-H2B dimers. Subsequently, tetramers are formed from the combination of the H3-H4 dimers and they in turn combine with two

H2A-H2B dimers to create the compact octamer core, thus accomplishing the assembling process (Arents and Moudrianakis, 1993; Arents and Moudrianakis, 1995). All core histones display an conserved amino (N)-terminal amino acid tail that projects from the globular section of the DNA-histone core and make contact with adjacent nucleosomes (Luger and Richmond, 1998). Within a single nucleosome, such histone tails are unstructured and highly flexible. Furthermore, they are subject to a variety of posttranslational modifications (e.g. acetylation, methylation, phosphorylation and biotinylation) in a number of areas, especially at lysine and arginine residues (Berger, 2001; Luger and Richmond, 1998). In 2001, a hypothesis known as the 'histone code' was been proposed (Jenuwein and Allis, 2001). According to this theory, single or combined histone modifications build a code that affects the gene transcriptional status (Jenuwein and Allis, 2001). Two categories of biochemical activities are outlined by this histone code hypothesis (Jenuwein and Allis, 2001; Strahl and Allis, 2000). In the first category, the code is written by specific enzymes, which can add or remove particular modifications (e.g. acetylation, methylation, phosphorylation and biotinylation) in certain histone areas. In the second category, specific effector proteins can read the histone code and translate them into biological functions. These proteins can recognize the modified histones via special protein domains. Through interaction with the appropriate histone modifications, these specific effector proteins can alter chromatin structure, and hence change the transcriptional activity (Jenuwein and Allis, 2001; Strahl and Allis, 2000).

Modifications in histone tails can influence the DNA accessibility and protein/protein interactions, and thus affect transcription levels (Berger, 2001; Luger and Richmond, 1998). Histone modifications can have two effects - they make chromatin either more relaxed and accessible or more condensed and less accessible for replication and transcription (Kouzarides, 2007). Due to this, a number of fundamental biological processes, such as gene transcription, DNA replication, repair, and chromosome condensation, are affected by histone modifications (Kouzarides, 2007; Wolffe and Hayes, 1999; Wu and Grunstein, 2000).

Several factors have been identified to affect the outcome of histone modifications, including the modified organism, modification type, the modified residue, the level of modification, and the chromatin context (Kouzarides, 2007). Sections 1.5.2 and 1.5.3 discuss two histone modifications that have been extensively studied.

1.5.2 Histone Acetylation and Deacetylation

In eukaryotic cells, the conserved lysine (K) residues at the N-terminal tail of histone proteins can be acetylated and deacetylated by histone acetyltransferases (HATs) and histone deacetylases (HDACs), respectively (Kuzmichev and Reinberg, 2001; Roth et al., 2001). Histone acetylation and deacetylation are essential for gene regulation (Kuo and Allis, 1998; Struhl, 1998).

In the process of histone acetylation, HATs utilize Acetyl Coenzyme-A (Acetyl-CoA) as cofactor and catalyse the transfer of an acetyl functional group to the histone lysine residues (Struhl, 1998). Notably, acetylation occurs on numerous histone lysine residues on histone 3 and 4 (H3 and H4) (Kouzarides, 2007). Modification of histone tails by acetylation has been found to promote transcriptional activity and be associated with euchromatin (activated genomic regions) (Hebbes et al., 1988; Mikkelsen et al., 2007; Roh et al., 2005). Mechanistically, histone octamers derive their positive charge primarily from lysine, which thus plays a key role in the binding of the negatively-charged DNA phosphate-sugar backbone (Allfrey and Mirsky, 1964; Van Holde, 1989). Through neutralizing the positive charge of lysine residues on histone tails, histone acetylation weakens the affinity between DNA and histones (Allfrey and Mirsky, 1964; Turner, 2000). By loosening the chromatin structure, histone acetylation makes the DNA promoter areas more accessible to transcription factors and RNA polymerases, and thus enhances the activation of transcription process (Mikkelsen et al., 2007; Roh et al., 2005). Furthermore, as a posttranslational modification, histone acetylation also provides a binding site for protein binding (Cheung et al., 2000). The acetylated histone tails can act as protein recognition sites where bromodomain-containing transcription factors interact with the acetylated histone tails via bromodomain, an acetyl-lysine binding domain (Yang, 2004). After recognizing the acetylated histone tails, the transcription initiation factors help recruit extra nucleosomal remodelling complexes that contribute to chromatin relaxation (Hassan et al., 2002).

On the other hand, HDACs can reverse histone acetylation by removing the acetyl group from the acetylated lysine residues (Kuo and Allis, 1998; Kuzmichev and Reinberg, 2001). By deacetylating the histone tails, the lysine's positive charge is restored, and hence DNA becomes more tightly wrapped around the histone cores. This makes the transcription factors harder to bind to the DNA and leads to transcriptional repression and finally silences gene expression (de Ruijter et al., 2003; Gallinari et al., 2007; Struhl, 1998).

1.5.3 **Histone Methylation**

In eukaryotes, both lysine (K) and arginine (R) residues located in the N-terminal tails of Histone H3 (H3) and Histone H4 (H4) can be dynamically modified by histone methyltransferases (HMTs) and histone demethylases (HDMs), the former adding methyl groups to the histone tails, while the latter removes them (Aletta et al., 1998). Multiple methyl groups can be added to a single amino acid residue. Every K residue can take up to three methyl groups (giving mono-(me), di-(me2) or tri-(me3) methylated forms), whereas R residues can be mono- or di-methylated (Bannister et al., 2002; Zhang and Reinberg, 2001). In accordance with the location of the methylated residue and the degree of methylation, the outcome of histone methylation can be either gene activation or suppression (Bannister et al., 2002; Lachner and Jenuwein, 2002).

Histone lysine methylation is not likely to affect the chromatin structure directly, as it does not change the charge of the histone tails as it is by acetylation. Instead, histone methylation creates binding sites for the recruitment of regulatory proteins, which recognize methylated residues through chromo-domains (Kouzarides, 2007).

So far, methylation within the lysine 4, 9 and 27 of histones H3 has been functionally characterized. In general, H3K9 and H3K27 methylation has been implicated in transcriptional silencing; whereas, H3K4 methylation is associated with transcriptionally active regions (Hublitz et al., 2009).

1.5.3.1 *Methylation of H3 on lysine 9*

Methylation of H3 on lysine 9 (H3K9) is largely associated with silencing and repression in many species. The pervasive assumption is that H3K9 is involved in euchromatic gene silencing, as well as in heterochromatin formation (Nielsen et al., 2001).

H3K9 mono- and di-methylation are facilitated by a heteromeric complex consisting of H3K9 methyltransferases G9a and Glp (G9a-related protein) (Tachibana et al., 2005). Mutation of either G9a or Glp leads to significant reduction of mono- and di methylated H3K9 (H3K9me1 and H3K9me2) levels in mouse ESCs (Peters et al., 2003; Tachibana et al., 2005). In mammals, H3K9me2, acts as a repressive histone mark, and is associated with silent domains within euchromatic regions (Peters et al., 2003; Rice et al., 2003); while H3K9me1 is closely related to active transcriptional start sites (Barski et al., 2007). In differentiating mouse ESCs, the promoter region of *Oct3/4* is enriched in H3K9me2, suggesting that the presence of H3K9me2 is essential for the suppression of this pluripotency gene (Feldman et al., 2006).

Methylated by H3K9 tri-methyltransferases Suv39h1 and Suv39h2, tri-methylated H3K9 (H3K9me3) is specifically enriched in heterochromatin (Kouzarides, 2007; Lachner et al., 2001; Lehnertz et al., 2003). H3K9me3 can be bound by Heterochromatin protein 1 (HP1) via its N-terminal chromodomain, and this leads to the formation of compacted chromatin that physically inhibits the access of the transcriptional machinery to the underlying DNA (Bannister et al., 2001; Lachner et al., 2001). In turn, HP1 serves as a docking site for the recruitment of additional repressive factors to heterochromatin, such as Suv39 (Lachner et al., 2001; Smallwood et al., 2007). During DNA replication, HP1, through the recruitment of Suv39, can also promote the deposition of the me3 mark onto H3K9 residues in the newly synthesized histones of the replicated chromatin, thus ensuring the inheritance of the mark. Therefore, the binding of HP1 to H3K9me3 is important for the establishment and maintenance of heterochromatin (Bannister et al., 2001; Lachner et al., 2001).

1.5.3.2 *Methylation of H3 on lysine 27 and lysine4*

Methylation on lysine 27 of histone H3 (H3K27) is largely associated with silenced genes (Boyer et al., 2006; Cao et al., 2002; Lee et al., 2006; Zhang et al., 2004). Three states of methylation, mono-, di-, and tri-, are observed on H3K27 (Schwartz and Pirrotta, 2007). Polycomb repressive complex 2 (PRC2), a chromatin-remodelling complex, is primarily responsible for catalysing H3K27 trimethylation (H3K27me3) through its catalytic subunits enhancer of zeste homologue 2 (Ezh2) (Cao et al., 2002; Kuzmichev et al., 2002; Muller et al., 2002). A close correlation between H3K27me3 and inactive gene promoters has been confirmed in ESCs by chromatin immunoprecipitation with DNA microarray technology (ChIP-chip). In ESCs, numerous genes essential for development and differentiation are suppressed by H3K27me3 mark (Boyer et al., 2006; Bracken et al., 2006; Cao et al., 2002; Kuzmichev et al., 2002; Lee et al., 2006; Muller et al., 2002; Shen et al., 2008; Vire et al., 2006). It also has been shown that removal of PRC2 results in a loss of H3K27me3 and loss of pluripotency in ESCs (Boyer et al., 2006; Chamberlain et al., 2008; Shen et al., 2008). Therefore, it is believed that H3K27me3-mediated repression is essential for maintenance of ESC pluripotency (Boyer et al., 2006; Lee et al., 2006).

Generally, methylation of histone 3 on lysine 4 (H3K4) is most often associated with transcription activation or permissive chromatin regions, and is thus considered as an activating mark (Berger, 2007; Bernstein et al., 2005; Chi et al., 2010; Turner, 2007). The association of H3K4 mono-, di- and tri- methylations (H3K4me, H3K4me2 and H3K4me3) with transcription activation has been validated by ChIP-chip and ChIP-sequencing (ChIP-Seq) (Barski et al., 2007; Schneider et al., 2004). H3K4me3, which is catalysed by SET1 complexes or the MLL (mixed lineage leukemia protein) complexes (Santos-Rosa et al., 2002; Vermeulen and Timmers, 2010; Yokoyama et al., 2004), is enriched in promoter regions of active genes (Barski et al., 2007; Bernstein et al., 2005; Heintzman et al., 2007; Santos-Rosa et al., 2002).

Interestingly, a unique chromatin domain known as “bivalent domain” is found in mouse ESCs (Bernstein et al., 2006). In pluripotent mouse ESCs, many genes involved in differentiation are enriched in activating mark H3K4me3 as well as repressive mark H3K27me3 (Bernstein et al., 2006). During the stage of pluripotency, repressive mark H3K27me3 silences the genes related to development and differentiation. Though silent, the genes present in these bivalent domains can become activated rapidly in response to downstream developmental signals, and do not require epigenetic reprogramming at the loci (Bernstein et al., 2006). Upon differentiation, PRC2 occupancy is lost and H3K27me3 is removed while H3K4me3 is maintained, permitting expression of differentiation genes (Boyer et al., 2006). The bivalent domains that exist in undifferentiated ESCs are therefore assumed to dictate a ‘poised state’ for rapid gene activation during differentiation, with H3K4me3 serving for rapid activation upon removal of H3K27me3 (Bernstein et al., 2006; Mikkelsen et al., 2007). Co-modification of development-associated genes by the bivalent histone marks

H3K27me3 and H3K4me3 has also been observed in undifferentiated human ESCs (Pan et al., 2007). In addition, during human ESC differentiation, the expression of pluripotency-associated genes is repressed by the transition from H3K4me3 modification to the bivalent modifications with both H3K27me3 and H3K4me3 (Pan et al., 2007).

1.5.3.3 *Crosstalk between histone modifications*

For the establishment of gene expression states, intense crosstalk occurs between different histone modifications. Cross-regulation of histone modifications can occur on the same histone residue (*in situ* crosstalk), on the same histone tail (*in cis* crosstalk), between different histones within the same nucleosome (*in trans* crosstalk) or across different nucleosomes (nucleosome crosstalk) (Briggs et al., 2002; Wang et al., 2001).

In situ cross-regulation is the first level of posttranslational crosstalk. Several different types of covalent modifications (e.g. acetylated, methylated or ubiquitylated) can target the same residues, such as lysine residues. If more than one modification pathway is targeting the same site, different marks on the same amino acid cannot co-exist; and therefore, they antagonize each other (Kouzarides, 2007; Wang et al., 2008). In eukaryotes, H3K9 methylation normally opposes the functions of H3K9 acetylation in gene regulation (Nakayama et al., 2001; Rea et al., 2000). The mutually exclusive methylation or acetylation of H3K9 is a well-studied example of *in situ* crosstalk (Turner, 2005). An acetyl group must be removed before a methyl group can be added, and vice versa. Furthermore, a coupling of H3K9 methylation and histone deacetylation has been identified (Czermin et al., 2001; Vaute et al., 2002; Zhang et al., 2002). Deacetylation of H3K9 and other sites in the H3 tail facilitates H3K9 methylation, which in turn promotes HP1 binding and recruits HDACs and HMTs to promote heterochromatin formation (Czermin et al., 2001; Vaute et al., 2002; Zhang et al., 2002).

Antagonism between different modifications also exists on the same histone tail. For example, methylation of H3K4 can inhibit the recruitment of repressive factors (e.g. HP1) to methylated H3K9 (Beisel et al., 2002; Nishioka et al., 2002; Zegerman et al., 2002). On the other hand, one histone modification may promote the deposition of another modification (Kouzarides, 2007; Wang et al., 2008). Methylation on H3K4 can promote the subsequent acetylation of H3 by P300 (Wang et al., 2001), and acetylation of H3K9 and H3K14 can stimulate the methylation of H3K4 by MLL (Milne et al., 2002; Nakanishi et al., 2008).

According to the observations above, each histone modification ought to be considered as a component of a complex interconnected mechanism, rather than as an independent regulatory mark (Suganuma and Workman, 2008).

1.6 *Histone modifications and Germ cell development*

A range of dynamic changes in the type and level of epigenetic modifications takes place during the development of germ cells. It is thought that these changes act as reprogramming processes that the germ cells need to confer totipotency to the zygote following fertilization.

1.6.1 Histone modifications in the migratory PGCs

Upon establishment of the germ-cell fate, the newly formed germ cells and the adjacent somatic cells have an identical epigenetic status. The germ cells are subject to dynamic global histone modifications following the specification process (Seki et al., 2005; Seki et al., 2007). Not long after the germ cell fate is established, there is an initial wave of global histone modification, characterized by H3K9me2 down-regulation and H3K27me3 up-regulation (Seki et al., 2005; Seki et al., 2007) (Fig 1.4). PGCs are located in the allantois around E7.75, as they start to migrate there is a non-uniform, gradual loss of H3K9me2 (Seki et al., 2005; Seki et al., 2007). As a result, by E8.75, the PGCs display less H3K9me2 than the adjacent somatic cells (Seki et al., 2005; Seki et al., 2007) (Fig 1.4). H3K9me2 was reported to serve as an epigenetic barrier, suppressing the expression of germ cell-specific genes in pluripotent ESCs (Maeda et al., 2013). In the case of ESCs, germ cell-specific genes are inhibited by the transcription factor Max, which also exhibits interaction with the H3K9 di-methylating enzymes Glp and G9a. A reduction in Max expression in ESCs through RNA interference (RNAi) resulted in a decline in H3K9me2 levels at the promoter areas of PGC-related genes, ultimately leading to the selective activation of germ cell-related genes in undifferentiated ESCs due to repressor inhibition (Maeda et al., 2013). The findings above indicate that the removal of H3K9me2 may be important for germ cell-specific genes to enhance their expression in PGCs.

Significant and long-standing controversy surrounds the issue of the mechanism by which H3K9me2 is demethylated in mouse PGCs. Histone demethylase Jmjd1a, a JumonjiC (JmjC)-domain-containing protein, is responsible for direct H3K9me2 demethylation (Klose et al., 2006). Before H3K9me2 demethylation, the expression of *Jmjd1a* is not specifically upregulated in murine PGCs, as the level of *Jmjd1a* is similar in PGCs and their neighboring somatic cells (Seki et al., 2007). It can thus be inferred that the genome-wide removal of H3K9me2 in early mouse PGCs is not based on histone demethylase Jmjd1a. Formed by histone methyltransferases G9a and Glp, G9a-Glp complex mediates the maintenance and dimethylation of H3K9me2 (Tachibana et al., 2005). Lack of either G9a or Glp alone will lead to the loss of function of this enzyme complex and the downregulation of H3K9me2 (Tachibana et al., 2005). Therefore, the G9a-Glp complex might be another putative mechanism crucial for the genome-wide demethylation of H3K9me2 in PGCs. In order to prove this, the expression of G9a and Glp proteins in murine embryos was detected by immunofluorescence (Seki et al., 2007; Yabuta et al., 2006). As a candidate for this

putative mechanism, Glp is specifically downregulated in murine PGCs as early as E7.25 (Fig 1.4), immediately prior to the global demethylation of H3K9me2 in PGCs (Seki et al., 2007; Yabuta et al., 2006). By contrast, the expression of G9a was significantly reduced in PGCs at around E9.5 (Fig 1.4), following H3K9me2 demethylation (Seki et al., 2007). Therefore, Seki *et al.* (Seki et al., 2007) concluded that the suppression of Glp from the G9a-Glp complex was essential for the H3K9me2 removal during early murine germ cell development.

From a low level in the epiblast, H3K27me3 levels begin to increase after H3K9me2 downregulation and reach a maximum level by E9.5 in PGC nuclei, which is then maintained until E11.5 (Seki et al., 2005) (Fig 1.4). It is proposed that this upregulation of H3K27me3 may be due to the stable expression of H3K27 tri-methyltransferase Ezh2 in PGCs until E8.25 (Seki et al., 2007) (Fig 1.4). The stable expression of Ezh2 is important for the upregulatioof H3K27me3.

H3K27me3 upregulation and H3K9me2 removal are most likely reciprocal, contributing to the maintenance of a proper repressive mode in early PGCs, and therefore playing an essential role in the development processes of early PGCs (Hajkova et al., 2008). This is supported by the case of PGCs that lack Prdm14 (Yamaji et al., 2008). In this *Prdm14*-negative PGC research, increase in H3K27me3 and reduction of H3K9me2 are not observed, and it is notable that these PGCs undergo abnormal development and completely disappear by E12.5 (Yamaji et al., 2008). This research confirms that the decrease of H3K9me2 and increase of H3K27me3 may be crucial for appropriate PGC development.

Compared to adjacent somatic cells, early germ cells exhibit a lower level of heterochromatin mark H3K9me3, which remains consistent all through the early development of germ cells (Seki et al., 2005) (Fig 1.4). Suv39h HMTases, which are required to direct H3-K9 trimethylation, have been found to have a complex correlation with DNA methylation systems (Section 1.7) in mammals (Lehnertz et al., 2003). Both these methylation systems are important in maintaining and preserving the stability of heterochromatic subdomains subsequently owing to this action there is protection of the genome integrity (Lehnertz et al., 2003). Therefore, the low level of H3K9me3 in early mouse germ cells may be associated with the DNA methylation systems (Section 1.7) and the genome integrity (Lehnertz et al., 2003). Another explanation for the low level of H3K9me3 may be the pluripotency-related gene expression in early PGCs, since no connection was observed between undifferentiated ESCs and H3K9me3 methyltransferase Suv39h.

Migrating germ cells and neighboring somatic cells display similar levels of the transcriptional active marks H3K4me and H3K9ac until the arrival of the germ cells at the genital ridge (Seki et al., 2005) (Fig 1.4). Pluripotency-related gene expression in early PGCs may be due, to some extent, to the stable expression of H3K4me and H3K9ac. High levels of active histone modifications, like acetylated histones and

methylated H3K4me, are involved in the regulation of the flanking regions of *OCT4* and *NANOG*, just as in PGC-like cells derived from human ESCs (Pan et al., 2007; Tilgner et al., 2008).

The epigenetic modifications mentioned above occur only in the nascent PGCs before they enter the genital ridges and not in the adjacent somatic cells (Seki et al., 2005; Seki et al., 2007). Such significant epigenetic changes taking place in early germ cells may act as a prerequisite for subsequent specific epigenetic reprogramming and possibly related to the regain of underlying totipotency in PGCs (Seki et al., 2005; Seki et al., 2007; Surani et al., 2007).

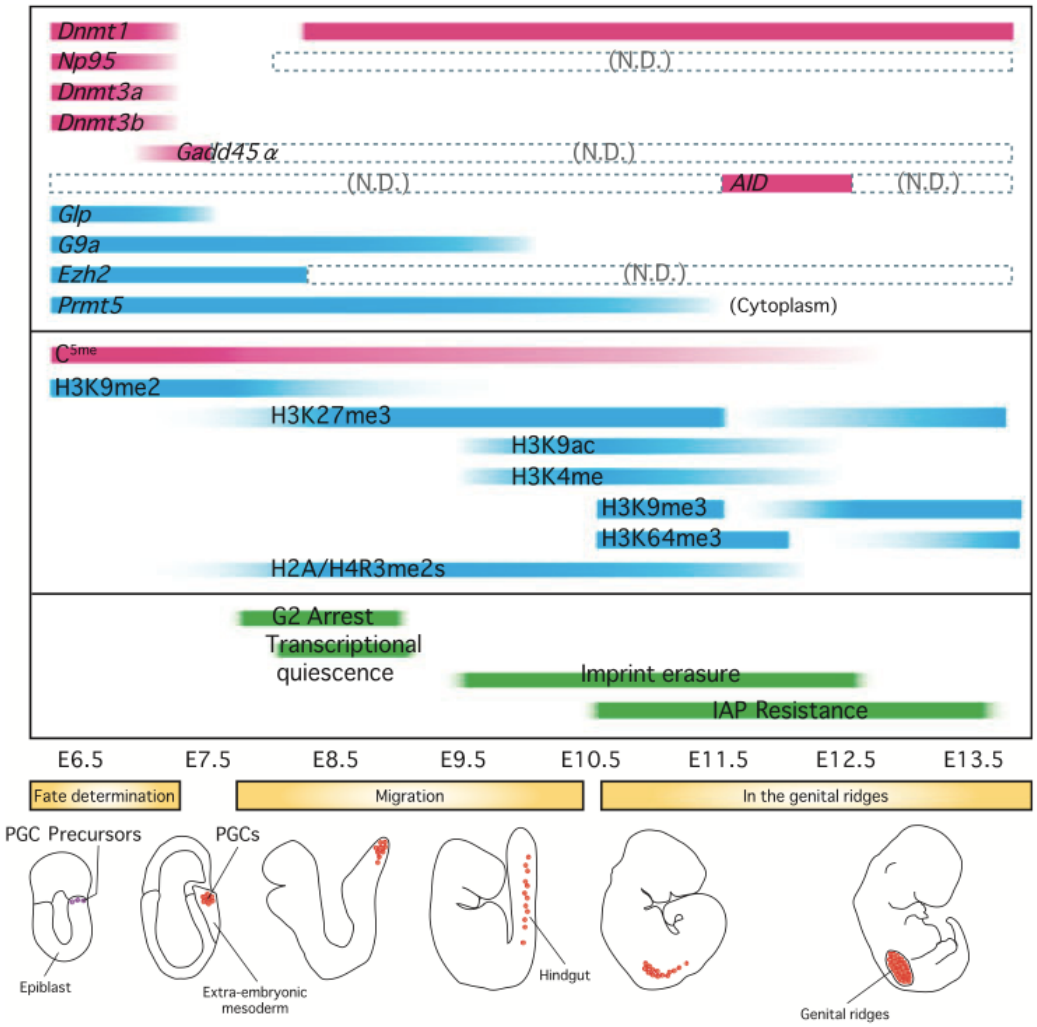

Figure 1.4 Dynamics epigenetic changes during PGC specification and differentiation. A number of changes in DNA methylation, histone modifications and expression of their epigenetic modifiers, and related cellular events occur during PGC development. Figure reproduced from (Mochizuki and Matsui, 2010).

1.6.2 Histone modification in the post-migratory PGCs

Subsequently, when the majority of PGCs arrive at the genital ridges, the levels of histone modifications undergo further fluctuation (Hajkova et al., 2008; Seki et al., 2005). Upon arrival at the genital ridge, levels of the permissive marks H3K9ac and H3K4me first increase significantly then diminish permanently by E12.5 (Hajkova et al., 2008; Seki et al., 2005) (Fig 1.4). Furthermore, at about E11.0-E12.0, there is a brief decrease in the repressive marks H3K9me3 and H3K27me3, whilst after E12.5; H3K9me3 displays a rapid increase (Hajkova et al., 2008; Seki et al., 2005) (Fig 1.4).

The decline of H3K27me3 levels at about E10.5-E11.0 is probably associated with the re-establishment in the expression of some pluripotency and PGC-specific genes. This decrease appears to be important for germ cell development, as deficiency of Utx, a H3K27 demethylase, causes abnormal histone modification and failure of germ cell development (Mansour et al., 2012). In PGCs that lack *Utx*, timely erasure of H3K27me3 does not occur at about E11.0; and there is reduced expression of the pluripotency markers *Nanog*, *Sal4*, *Oct4* and *SSEA-1*, as well as of of later germ cells-specific mark *Mvh* compared to wild-type PGCs. By E12.5, PGC development is interrupted by such aberrant expression of genes, resulting in abnormal germ cell development in mice lacking *Utx* (Mansour et al., 2012).

The functional implications of the histone modifications in germ cell development are yet to be clarified, but the significant repressive modifications in developing germ cells after E12.5 are likely not only to impede the transcriptional activation at genome level in the subsequent stages of germ cell development, but also to participate in the appropriate expression of genes related to differentiated germ cell (Hajkova et al., 2008; Seki et al., 2005).

1.6.3 Histone modifications in the germ cells after sex determination

Remarkable sexual dimorphism is observed in mouse germ cells after E13.5. The ovarian germ cells stop proliferating and enter prophase I meiosis while the testicular germ cells undergo meiotic arrest (Hilscher et al., 1974; McLaren and Southee, 1997). Meanwhile, the sex-specific epigenetic reprogramming is also observed in mouse germ cells after E13.5 (Abe et al., 2011).

Using immunocytochemistry, (Abe et al., 2011) reported that fetal germ cells of male and female mice displayed sex-related histone modifications after E13.5, , in contrast to the gonadal somatic cells used as a control. The dynamic changes in histone modifications were more pronounced in male than female fetal germ cells between E13.5 and E17.5 (Abe et al., 2011).Unlike somatic cells throughout the development stage, both male and female germ cells showed strong H3K9ac staining. Abe *et al.* (Abe et al., 2011) reported that, whereas female germ cells did not exhibit any noticeable change, male germ cells displayed an increase in H3K9ac levels, which peak at E15.5. There were close similarities between the levels of H3K4me3 in female

germ cells and in somatic cells. In male germ cells, H3K4me3 levels increased at E15.5 relative to E13.5 and subsequently was found to increase further by E17.5 in comparison to E15.5 and E13.5 (Abe et al., 2011).

During this interval, male and female germ cells showed comparable H3K9me2 changes. H3K9me2 staining was weak in fetal germ cells at all stages apart from E15.5, when staining was maximal in male as well as female germ cells (Abe et al., 2011). Through every detected stage of fetal development, male and female germ cells exhibited higher levels of H3K9me3 than somatic cells. At E15.5 and E17.5, male germ cells showed much higher levels of H3K9me3 when compared to E13.5, while the female germ cells did not (Abe et al., 2011). In male germ cells, H3K27me3 levels increased significantly at E15.5 when compared to the E13.5 germ cells. At the same time it was concomitantly decreasing in female germ cells (Abe et al., 2011).

Following sex determination, such global changes in histone modifications were present exclusively in male germ cells. Considering that, these chromatin modifications occur before or simultaneously with global DNA de novo methylation (Section 1.8.2) in fetal testicular germ cells, these dynamic male-specific histone modifications may provide a framework for the male-specific global DNA de novo methylation in fetal testicular germ cells.

1.6.4 **The role of histone methyltransferases in mouse germ cell meiosis**

Different epigenetic modifiers are involved in the strict regulation of meiotic prophase development, particularly during the pachytene stage. Mouse germ cell meiosis may depend to a significant degree on histone methyltransferases, the functions of which have been outlined in gene-knockout studies in mice (Hayashi et al., 2005; Peters et al., 2001; Tachibana et al., 2007). It has been found that the H3K9 tri-methylating enzymes Suv39h1/2 (Peters et al., 2001), H3K4 tri-methylating enzyme Meisetz (Hayashi et al., 2005), and H3K9 mono and di-methylating enzymes G9a (Tachibana et al., 2007) are the enzymes that actively participate in the meiotic prophase.

Empirical research has reported that pericentric H3K9me3 was absent in mutant spermatocytes due to double mutations of the H3K9 trimethyltransferase genes *Suv39h1* and *Suv39h2* in mouse testis. Impaired chromosome synapsis and pericentric heterochromatin modification were the result of *Suv39h* mutations. At the pachytene stage, the mutant testicular germ cells underwent arrest, followed by pronounced spermatocyte apoptosis. It can thus be inferred that proper meiotic development relies on Suv39h and its modified chromatin H3K9me3. Although the molecular characteristics of *Suv39h* deficiency have not been clarified in female germ cells, the meiotic aberrations were also observed in the double-mutant female mice (Peters et al., 2001).

A H3K4 tri-methyltransferase, was formerly known as *Meisetz* now known as PRDM9 (PR domain-containing protein 9) (Eram et al., 2014). PRDM9 has been found to be an essential enzyme that is involved in the progression of early meiotic prophase (Eram et al., 2014). Serious impairment of the DSB repair pathway, impaired sex body formation and incorrect pairing of homologous chromosomes have been observed in *Meisetz-/-* mice, which is sterile in males and females (Hayashi and Matsui, 2006; Hayashi et al., 2005). The DSB repair, which was normally to be accomplished by pachytene, was not completed in *Meisetz-/-* spermatocytes (Hayashi and Matsui, 2006; Hayashi et al., 2005). This impaired DSB repair was accompanied by inadequate recruitment of the meiosis-related DSB repair protein DMC1 to DSB sites in the nuclei of *Meisetz-/-* spermatocytes. In wild-type mice, γH2AX (which marks sites of DSBs) was absent from autosomal areas of synapsed chromosomes, concentrating around the sex chromosomes and contributing to the formation of the sex body (Mahadevaiah et al., 2001). However, it has been observed that in *Meisetz-/-* mice, each chromosome including autosome in the germ cells of both sexes inappropriately retained γH2AX. This subsequently points to the formation of an impaired sex body (Hayashi and Matsui, 2006; Hayashi et al., 2005). At the same time, *Meisetz-/-* mice displayed the pachytene chromosomes that were frequently branched and linked to other chromosomes, suggesting impairment of homologous chromosome pairing as well (Hayashi and Matsui, 2006; Hayashi et al., 2005).

Tachibana *et al.* (Tachibana et al., 2007) noted that the developmental impairment of germ cells lacking *G9a* occurs at the pachytene stage , and numbers of germ cells were severe reduced or absent after the pachytene stage . As a result of germ-lineage specific deletion of *G9a*, sperm or oocytes were significantly reduced or lost altogether, causing the mice to become infertile. Moreover, in the early pachytene stage and in meiotic prophase, *G9a* mutation in mouse germ cells resulted in a flawed chromosome synapsis. Additionally, during the meiotic prophase, the G9a deficiency in the germ-lineage was accompanied by the loss of H3K9me1 and H3K9me2 in male and female germ cells. *G9a*-deficient germ cells also exhibited upregulation of its target genes, which are suppressed in normal meiotic germ cells; this led Tachibana *et al.*(Tachibana et al., 2007) to conclude that meiotic prophase progression requires epigenetic gene inhibition facilitated by G9a.

The functional importance of histone methyltransferases in germ cell meiosis clearly is evident from the above information. Nonetheless, further research is required to determine the extent to which their modified chromatins H3K9me1, H3K9me2, H3K9me3 and H3K4me3 contribute to changes in germ cell meiosis.

1.7 *DNA Methylation*

1.7.1 **Methylation of DNA in mammals**

DNA methylation, an inactive epigenetic mark, is addition of a methyl group to the DNA (Holliday and Pugh, 1975; Riggs, 1975; Wolffe and Matzke, 1999). Bird (Bird,

1984) suggested that suppression of transcription and the heritable preservation of a silent chromatin state are the two key functions fulfilled by DNA methylation in mammalian organisms. In the case of multicellular eukaryotes, DNA methylation takes place at the fifth position of the cytosine pyrimidine ring and its outcome is 5-methylcytosine (5mC) (Su et al., 2011).

In mammals, DNA methylation occurs almost exclusively at cytosine-guanine dinucleotides (CpG) (Bird, 1980; Bird, 1986). High concentrations of CpGs are cluster into regions known as CpG islands, which are often found at promoters of genes (Branciamore et al., 2010; Ioshikhes and Zhang, 2000). Compared to the majority of CpG sites which are typically methylated, these CpG islands tend to retain unmethylated (Deaton and Bird, 2011). The patterns of CpG methylation found in the gene promoter areas are a significant source of epigenetic information related to gene expression. DNA methylation causes chromatin to condense, leading to promoter inactivation, which is marked by the presence of 5mC in a CpG island; on the other hand, gene expression is activated when the DNA of gene promoter regions areis non-methylated (Deaton and Bird, 2011; Meissner et al., 2008).

How does DNA methylation lead to gene silencing? There are probably several mechanisms by which this can happen. However, the primary mechanism is thought to involve the methylation of CpGs, as methylated CpGs can be bound by methylated CpG binding proteins (MBPs), which have a DNA binding domain and transcriptional repression domain, and can recruit other factors that condense the chromatin (Bird and Wolffe, 1999).

In mammals, DNA methylation has been found to play an essential role in numerous biological processes (Bird, 2002; Egger et al., 2004; Stringer et al., 2013). During the development of ESCs, DNA methylation acts as an important epigenetic control mechanism that restricts differentiation. During mitosis, DNA methylation acts as an epigenetic barrier to prevent differentiated cells from returning to an undifferentiated state (Messerschmidt et al., 2014). Since numerous vital cellular functions are underpinned by CpG methylation, abnormal DNA methylation patterns are associated with various pathologies, including development of cancer, vulnerability to disease, as well as aging (Bird, 2002; Egger et al., 2004).

1.7.2 Enzymes Inducing DNA Methylation in Mammalian Organisms

DNA methyltransferases represent the key enzymes of targeting and maintaining of global DNA methylation in all organisms (Chen and Li, 2006; Siedlecki and Zielenkiewicz, 2006). There are two types of DNA methylation: maintenance and de novo (Siedlecki and Zielenkiewicz, 2006).

During the process of DNA replication, DNA methylation is maintained by a chief maintenance methyltransferase Dnmt1 (Damelin and Bestor, 2007). Dnmt1 is

responsible for transmitting methylation signals from the parent DNA strand to the newly synthesised daughter DNA strand (Jones and Liang, 2009; Robert et al., 2003). When DNA is replicated, hemi-methylated DNA is generated, with the parent strand is methylated and the daughter strand is not. Dnmt1 has a preference for hemi-methylated DNA. Dnmt1 binds this hemi-methylated DNA, and Dnmt1 lays down methylation on the daughter strand to generate a fully methylated CpG dinucleotide (Jones and Liang, 2009; Robert et al., 2003).

Dnmt3a and Dnmt3b, control the de novo methylation of unmethylated DNA. Though closely similar, each of the two enzymes is characterized by different target specificities and patterns of expression (Okano et al., 1999). Expressed early in embryonic development, Dnmt3b performs DNA re-methylation during the implantation stage. By contrast, Dnmt3a is expressed in more developed embryos as well as in differentiated cells (Okano et al., 1999). Dnmt3a and Dnmt3b do not just function as de novo methyltransferases, but also interact with Dnmt1 for the maintenance of DNA methylation during the process of replication in areas that Dnmt1 has overlooked (Jones and Liang, 2009; Liang et al., 2002). In ESCs lacking Dnmt3a and Dnmt3b, hemimethylated CpGs occurred in a greater proportion and methylation is gradually lost during cell division (Liang et al., 2002). A cofactor of the Dnmt3 enzymes is Dnmt3L, which is responsible for promoting the catalytic action of de novo DNA methyltransferases (Chedin et al., 2002; Gowher et al., 2005; Jia et al., 2007; Ooi et al., 2007).

1.7.3 **The DNA Demethylation-related roles of Tets and 5hmC**

There are two types of mechanisms through which DNA demethylation can take place, namely, active and passive mechanisms, which are respectively DNA replication independent and dependent (Ohno et al., 2013; Ooi and Bestor, 2008). Passive demethylation occurs when insufficient expression, or lack of key cofactors, causes Dnmt1 to function improperly, leading to the progressive demethylation of methylated DNA following multiple cell divisions (Bostick et al., 2007; Ohno et al., 2013). Active DNA demethylation is an enzymatic process in which a carbon-carbon bond is broken and consequently a methyl group on a cytosine residue is removed (Ooi and Bestor, 2008).

Recently, a potential DNA demethylation mechanism, reliant on the ten-eleven translocation (Tet) proteins and 5-hydroxymethylcytosine (5hmC), has been identified (Ito et al., 2010; Tahiliani et al., 2009). 5hmC is considered to be an important epigenetic control mechanism for the DNA methylation process *(Kriaucionis and Heintz, 2009).* Tahiliani *et al. (2009)* has noted the existence of 5hmC, a novel epigenetic DNA modification, in Purkinje neurons and mouse ESCs.

The Tet (ten-eleven translocation) proteins are members of the 2-oxoglutarate and Fe (II)-dependent dioxygenases superfamily (Ito et al., 2010; Ko et al., 2010; Tahiliani et

al., 2009). The three Tet enzymes (Tet1, Tet2, and Tet3) in mammalian organisms can catalyze the conversion of 5mC to 5hmC *in vitro* (Ito et al., 2010) and *in vivo* (Ko et al., 2010). Tet proteins show tissue-specific differential expression, with Tet1 being highly expressed in ESCs, whereas are Tet2 and Tet3 are more ubiquitously expressed (Szwagierczak et al., 2010; Tahiliani et al., 2009). Tahiliani *et al*. (Tahiliani et al., 2009) reported that TET1 expression in human ESCs repressed the expression of 5mC and increased the expression of 5hmC. In differentiated ESCs, the expression of TET1 is repressed, and this results in reduction of 5hmC and upregulation of 5mC levels. Consistent with this, Tet1 over expression leads to a decline of 5mC in ESCs (Tahiliani et al., 2009). Wossidlo *et al.* (Wossidlo et al., 2011) suggested that Tet3 might be responsible for oxidation of 5mC to 5hmC in fertilized zygotes, since it is the only Tet protein with a high expression in the fertilized zygotes. A direct correlation was found between the decrease in 5mC levels in the paternal genome and the emergence of 5hmC in fertilized zygotes (Gu et al., 2011). By contrast, in zygotes without Tet3, the level of 5mC stays unchanged because the paternal genome is unable to convert 5mC into 5hmC (Gu et al., 2011).

As key regulators in the roles conversion of 5mC to 5hmC, Tet family proteins may participate in the DNA demethylation either passively or actively (Hackett et al., 2013; Ito et al., 2010; Vincent et al., 2013). When 5hmC is converted from 5mC, the majority of 5mC-binding proteins, including Dnmt1 (Valinluck and Sowers, 2007), do not recognize 5hmC, thus, 5hmC may be diluted from the DNA following its replication, since it is not recognized by Dnmt1(Valinluck and Sowers, 2007). Hence, Inoue *et al.*(Inoue and Zhang, 2011) proposed that the conversion of 5hmC to cytosine could be performed passively on the basis of DNA replication (Ohno et al., 2013).

Active demethylation may also be responsible for the conversion of 5hmC to cytosine. Through further oxidation by TET enzymes, 5hmC is converted to 5-formylcytosine (5fC) and 5-carboxylcytosine (5caC) (Ito et al., 2011) (Fig 1.5). Furthermore, 5hmC deamination, which is mediated by activation-induced cytidine deaminase (AID), results in the formation of 5-hydroxymethyluracil (5hmU) (Hashimoto et al., 2012; Nabel et al., 2012) (Fig 1.5). Thymine DNA glycosylase (TDG) then mediates the excision not only of 5hmU, but also 5fC and 5caC to abasic sites. The base excision repair (BER) mechanism subsequently repairs the formed abasic sites to unmodified cytosine (Cortellino et al., 2011; He et al., 2011; Inoue et al., 2011) (Fig 1.5). Since it can be converted to cytosine, 5hmC may serve as a temporary mediator in the process of DNA demethylation (Branco et al., 2012).

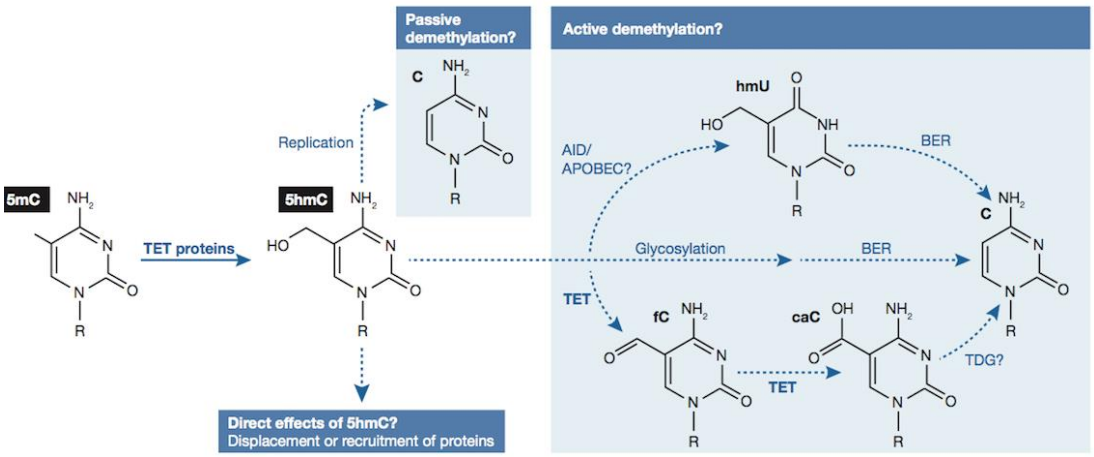

Figure 1.5 Possible biological roles of TET proteins and 5hmC in DNA demethylation. TET enzymes can oxidize 5mC to 5hmC, 5fC, and 5caC and facilitate DNA demethylation. 5hmC can be passively converted to cytosine and depleted from the DNA through its DNA replication. 5hmC, as well as 5fC, and 5caC, can be excised by TDG and further repaired to unmodified cytosine via BER machinery. Figure reproduced from (Williams et al., 2011).

1.8 *Genome-wide Reprogramming of DNA Methylation in Mouse Fetal Germ Cells*

1.8.1 Global erasure of DNA Methylation in Mouse PGCs

During the early life development of an organism, the genome is subjected to dynamic changes in DNA methylation (Smith et al., 2012). Genome-wide DNA demethylation occurs once fertilisation is completed, leading to the global hypomethylation of embryos in the blastocyst stage and even the inner cell mass. Near the time of implantation, the embryonic epiblast is formed as a result of the differentiation of cells within the inner cell mass. The epiblast is then subjected to de novo DNA methylation to promote embryo differentiation and lineage development before PGC generation (Smith et al., 2012).

By E8.0-E8.5, the parent epiblast cells pass on methylated DNA to PGCs, which in this regard are the same as other epiblast cells (Hajkova et al., 2002). To generate germ cell potency, the genome-wide erasure and reprogramming of epigenetic patterns are necessary, due to the fact that the PGCs developing from the pluripotent epiblast begin to assume a somatic course (Hajkova et al., 2002; Saitou et al., 2002).

Following PGC specification from epiblast precursors and after E8.5, PGCs begin to lose 5mC (Fig 1.6), which denotes that genome-wide DNA demethylation takes place during PGC migration (Hajkova et al., 2002). The DNA demethylation of PGC genome occurs at around E9.5 (Fig 1.6) has been demonstrated by immunostaining (Seki et al., 2005) and locus-targeted analysis (Mochizuki et al., 2012). The entrance of PGCs into the gonads between E10.5 and E13.5 represents the start of another phase

of reprogramming. PGCs are subject to further genome-wide DNA demethylation upon arrival at the genital ridges, and by E13.5, germ cells has lost over 90% of their methylated DNA (Hajkova et al., 2010; Seki et al., 2005) (Fig 1.6).

During these periods, genome-wide DNA demethylation is modified by Dnmts and their cofactors in mouse germ cells (Seki et al., 2005). Following the establishment of germ cell fate, Dnmt1 and its cofactor Np95 undergo a temporary decrease in a subset of PGCs (Fig 1.4), which may be associated with passive DNA demethylation (Popp et al., 2010; Seki et al., 2005). The de novo DNA methyltransferases Dnmt3a and Dnmt3b are poorly expressed in PGCs (Fig 1.4). As speculated by some researchers, the low Dnmt3 levels may be associated with the maintenance of the unmethylated DNA state (Kagiwada et al., 2013; Seki et al., 2005).

Since other cell types do not usually exhibit genome-wide DNA demethylation, an assumption arose that such significant removal of 5mC from PGC genomes is a requirement for the establishment of the germline ground state, including totipotency gain after gamete development and ensuing syngamy (Guibert et al., 2012; Saitou et al., 2012; Seki et al., 2005).

1.8.2 Re-Establishment of Sex Specific DNA Methylation Patterns in Mouse Fetal Germ Cells

After the gender has been determined, the re-establishment of DNA methylation occurs differently in male and female germ cells (Abe et al., 2011). In the case of male embryos, de novo methylation begins from E15.5 in the prospermatogonia that are arrested in the G1 mitotic phase, and is completed prior to birth. Therefore, the re-establishment of DNA methylation before the initiation of meiosis in male germ cells (Abe et al., 2011). In the case of female embryos, oocytes undergo meiosis and arrest in the prophase I of meiosis, while the levels of DNA methylation in female fetal germ cells remain constantly low and de novo DNA methylation begins following birth (Abe et al., 2011).

1.8.3 Dynamics of Tets and 5hmC during Mouse Germ Cell undergo Epigenetic Reprogramming

Three stages have been outlined in the genome-wide DNA demethylation in PGCs. During the first stage, between E8.5 and E9.5, 5mC declines considerably. Given the low levels of Tet proteins and 5hmC, this stage is not likely to be Tet-dependent (Yamaguchi et al., 2013) (Fig 1.6). Instead, replication-based dilution is the probable mediator in this stage, due to the downregulation of cofactor Np95 of Dnmt1 in E8.5 PGCs (Kurimoto et al., 2008). As massive loss of 5mC takes place about two days before the increase of 5hmC, the levels of 5mC and 5hmC are extremely low from E8.5 to E9.5. Therefore, PGCs undergo a hypomethylated and hypohydroxymethylated state during this stage (Yamaguchi et al., 2013) (Fig 1.6). In the second stage, at about E10.5, Tet proteins oxidise the rest of 5mC to 5hmC, Tet1

and 5hmC showing a particular increase in PGCs (Yamaguchi et al., 2013) (Fig 1.6). In the third stage, during E11.5-E12.5, there is a decline in 5hmC levels. Neither 5fC nor 5caC display dynamic transformations in this period, while between E8.5 and E12.5, TDG is poorly expressed in PGCs as well (Hackett et al., 2013; Seisenberger et al., 2012; Yamaguchi et al., 2013; Yamaguchi et al., 2012). Yamaguchi et al. (Yamaguchi et al., 2013) (Fig 1.6) concluded that the passive elimination of 5hmC in PGCs can be achieved based on replication, additional oxidation being unnecessary.

The regulatory mechanism responsible for Tet enzymatic activity is yet to be identified. Nonetheless, it seems that 5mC is removed during PGC reprogramming through TET-mediated oxidation and replication-based dilution (Kagiwada et al., 2013; Yamaguchi et al., 2013; Yamaguchi et al., 2012)

RT-qPCR analysis revealed that Tet1 has preferential expression in PGCs, Tet2 expression occurs in PGCs as well as in somatic cells, while Tet3 expression occurs primarily in somatic cells between E9.5 and E13.5 of PGC development (Yamaguchi et al., 2012). Although the presence of both Tet1 and Tet2 was confirmed in PGC during global epigenetic reprogramming, Tet1 is the only one undergoing upregulation during this process (Hackett et al., 2013; Yamaguchi et al., 2012).

However, as observed by Yamaguchi (Yamaguchi et al., 2012), genome-wide demethylation in PGCs is not greatly influenced by *Tet1* deficiency. Yet *Tet1* deficiency results in a considerable decrease in the number of female germ cells and results in abnormal synapse formation. Furthermore, the germ cells of mice female mice with *Tet1* deficiency display aberrant meiotic prophase. Tet1 may be crucially involved in meiosis control, since *Tet1* deficiency is associated with impaired DNA demethylation and reduced expression of a series of meiotic genes of female mouse germ cells (Yamaguchi et al., 2012).

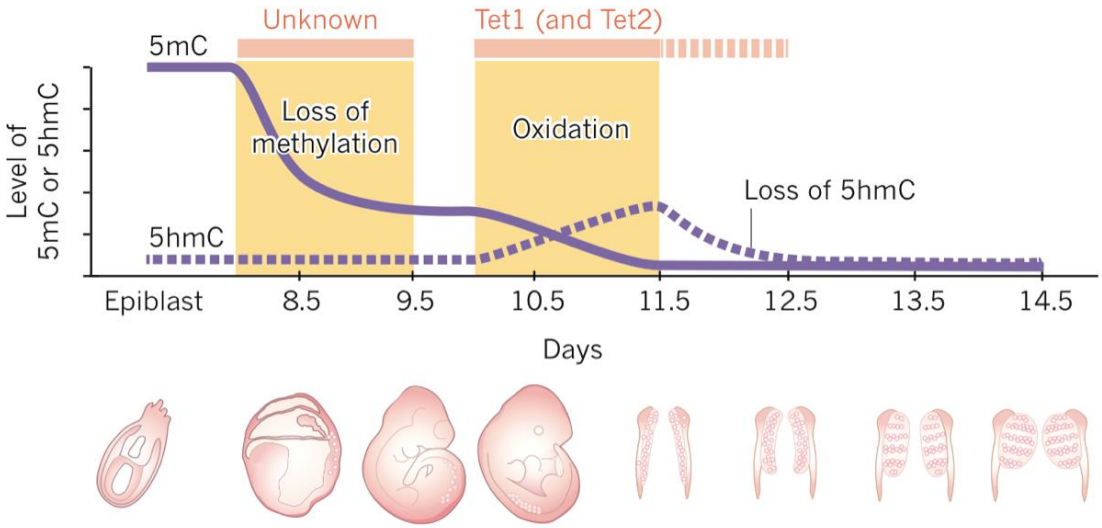

Firgure1.6. Dynamic changes of Tets and 5hmC in PGCs during their global DNA reprogramming The global DNA demethylation phases of PGC reprogramming are: loss of bulk DNA methylation independent of Tet; Tet1 and possibly Tet2 oxidation of the rest of 5mC to 5hmC; and 5hmC dilution based on replication. Figure adapted from (Kohli and Zhang, 2013).

1.8.4 DNA Methylation Involvement in Germ cell-related Gene Expression

It has been established that the Genome-wide DNA methylation reprogramming in PGCs is required to restore a novel epigenetic state, which is compatible with the expression of the germ cell-specific genes in PGCs.

The induction of *Blimp1*, *Fragilis* and *Stella* together with other PGC-related genes occurs at or immediately prior to the establishment of PGC fate (Saitou, 2009). Until E7.5, the presumed regulatory components of these genes undergo hypermethylation, followed by demethylation by E10.5, when the expression of these genes is further increased (Mochizuki et al., 2012). The importance of DNA demethylation for gene upregulation was clearly demonstrated by the fact that the genes were expressed more intensely when Dnmt1 was suppressed in PGC-like cells derived from ESCs (Mochizuki et al., 2012).

Post-migratory genes specific to germ cells are also regulated by DNA methylation. Once PGCs enter the genital ridge during E10.5-E11.5, the induction of genes such as *Mvh*, *Sycp3* and *Dazl* occurs. Maatouk *et al*. (Maatouk et al., 2006a) conducted an analysis of DNA methylation in PGCs and found that, after E8.0, DNA methylation declined at genome level, yet the methylation of these gene flanking regions was maintained at E10.5, undergoing hypomethylation by E13.5 due to high expression. In mice embryos with Dnmt1 deficiency, *Dazl* and *Mvh* are expressed at E9.5, before their usual expression at E10.5-E11.5, indicating that the activation timing of these genes is controlled by DNA methylation (Maatouk et al., 2006a). The regulation of *Dazl* expression is undertaken by DNA demethylation of a Sp1-binding site located in

the gene's flanking region, which is present in mouse, porcine and human PGCs. This means that *Dazl* is regulated by similar epigenetic modifications across different species of mammals (Linher et al., 2009).

Prior to E11.5, when genome-wide demethylation occurs, promoter CpG islands of genes associated with meiosis exhibit significantly higher methylation. Seisenberger *et al.* (Seisenberger et al., 2012) suggested that the activation of these meiotic genes at an appropriate developmental stage is a possible reason for this delayed DNA demethylation.

1.9 *Epigenetic modifications in human Primordial Germ Cells*

Similar to the epigenetic reprogramming in mouse PGCs, human PGCs may also undergo genome wide epigenetic reprogramming to the totipotency in PGCs and prepare for the subsequent germ cell-specific developmental process. There is limited literature about the exact mechanisms of epigenetic reprogramming in human cells.
Wermann *et al.* (Wermann et al., 2010) studied genome-wide DNA methylation patterns by 5mC immunostaining in human germ cells from 15wga to post-pubertal age, and found global reprogramming of DNA methylation to be different in human female and male gonads. At 15wga, staining of 5mC was absent in both human ovarian and testicular germ cells (Wermann et al., 2010). Afterwards, the female germ cells were remained unmethylated in the prenatal and postnatal human ovaries. However, the absolute numbers of demethylated testicular germ cells in seminiferous tubule decreased with increasing gestation. Finally, almost all the postnatal germ cells are hypermethylated in human testis (Wermann et al., 2010). According to this study, human germ cells have already undergone genome-wide DNA demethylation by 15wga and the gradual DNA de novo methylation has occurred prenatally in human testicular germ cells. But when DNA demethylation happens in human PGCs and when DNA de novo methylation happened in human ovarian germ cells are still unknown (Wermann et al., 2010).

Almstrup *et al* (Almstrup et al., 2010) studied H3K9me2, H3K27me3, H3K4me3 and H3K9ac by immunostaining in human fetal testicular germ cells from 21wga to 24wga. During this period, H3K9me2 and H3K27me3 were undetectable in the testicular germ cells. A small portion of testicular germ cells was H3K4me3 positive, while most of the testicular germ cells were stained with H3K9ac at this stage (Almstrup et al., 2010). Another study in 16-24wga human testes showed very low level of H3K9me3 in male germ cells (Bartkova et al., 2010). These two studies have identified 5 important modifications of histones in human male PGCs. However, the gestations they studied were quite limited, so the definitive trend of these histone modifications neither in human male or female PGCs is still unknown.

Sofia Gkountela and colleagues tried to identified the timing of major epigenetic events in human PGCs by analyzing human embryonic and fetal gonadal samples

from 6wga to 20wga (Gkountela et al., 2013). By immunofluorescence, they found 5mC to be nearly undetectable in human testicular and ovarian PGCs at all stages investigated, indicating that genome-wide DNA demethylation has occurred in human PGCs before 6wga (Gkountela et al., 2013). In contrast to 5mC, the level of 5hmC exhibited dynamic changes in human PGCs. Before 11wga, 5hmC showed punctate nuclear staining in human testicular PGCs. Afterwards, testicular PGCs in 13.5-16wga gonads were negative for 5hmC, but this was regained in some OCT4A-positive testicular PGCs by 17wga. In human fetal ovaries, the staining of 5hmC was variable;, it was positive in some but not all OCT4A-positive ovarian PGCs at all the gestations examined (Gkountela et al., 2013). The expression of *TET* genes was detected by RNA-Sequencing at 16–16.5wga human fetal gonads and H1 human ESCs (hESCs). During this period, all three *TETs* (*TET*1, 2 and 3) were expressed by human testicular and ovarian PGCs, with a significant enrichment of *TET*2 when compared to *TET*1 and *TET*3. Relative to H1 hESCs, the expression of *TET*1 was much lower in PGCs (Gkountela et al., 2013).

This study provided the first outline of major epigenetic reprogramming in human PGCs. DNA methylation has been identified being erased in human PGCs by 6wga. This study also showed the dynamic changes of 5hmC in human PGCs across different gestation, and the expression of *TET* genes at 16–16.5wga. The definitive trend of H3K27me3 during human PGCs development has also been characterized. But when the DNA methylation has been erased in human PGCs is still unknown. And the definitive trend of other important histone modifications has not been identified in human PGCs.

1.10 *Aim of Mphil*

The studies here aim to carry out significant epigenetic reprogramming research on human fetal germ cells, establishing an accurate timeline of events pertaining to this process in human fetal germ cells.

The objectives of this research was to

- Characterize the process of 5 important histone modifications (H3K9me2, H3K9me3, H3K27me3, H3K4me3, H3K9ac) in human fetal germ cells during development.

- Comprehend the reprogramming of DNA methylation and its related modifiers in human germ cells

- Understand whether the chemical DNA demethylation will affect the expression of germ cell-specific genes and the meiotic genes in human *in vitro* and *ex vivo*

Chapter 2. Materials and Methods

2.1 *Human Dissection and Tissue Collection*

Human fetuses (8-20wga) were obtained following both medical and surgical termination of pregnancy. Informed consent was obtained according to the national guidelines (John Polkinghorne, 1989), and the study was approved by the Lothian Research Ethics Committee (LRC08/S1101/1). Medical termination was induced by administration of oral mifepristone (200mg), 48h later, followed by vaginal misoprostol (800mcg) 3 hourly. Surgical termination was performed after administration of vaginal misoprostol (200mg). Prior to the termination, ultrasound scan was used to determine the gestation of fetuses. After the specimens were obtained, this gestation was subsequently confirmed by direct measurement of either crown-rump length in first trimester specimens or foot length in second trimester specimens. The appearances of all fetuses were grossly morphologically normal. Gonads were removed from the fetuses and then placed in small plastic petri dish with Dulbecco's Phosphate Buffered Saline (DPBS, Gibco，UK) for further dissection. Gonads were carefully separated from all extraneous material including the mesonephros using sterile 28G needle (BD) attached to 1ml syringe (BD). A small piece of non-gonadal tissue (e.g. limb) was taken for *SRY* polymerase chain reaction (PCR) as explained below (Section 2.2) to identify the gender of first trimester fetuses. Gonads were generally processed in 3 ways. Gonads were either snap frozen and stored at −80 °C for RNA analysis; fixed in Bouin's Fluid or 4% Neutral Buffered Formalin (NBF) solution followed by transferring to 70% ethanol for histology; or prepared for tissue culture as described below (Section 2.4).

2.2 *Determination of Fetal Gender by PCR for SRY*

The gender of first trimester human fetus was hard to determine by gonadal or gross morphology. In order to identify whether the dissected gonad was an ovary or testis, a small piece of non-gonadal tissue (e.g. the limb) was taken for DNA extraction. PCR amplification of the male-specific sex-determining gene *SRY* (Hanley et al., 2000) was performed (The primer sequences of *SRY* were showed in Table 2.11).

The non-gonadal tissue was digested in 100µl Extraction Buffer (containing 25mM Sodium Hydroxide (NaOH) /0.2mM Ethylenediaminetetraacetic acid (EDTA)). The solution mix was vigorously shaken at 95°C for 20min. Another 100µl Neutralization Buffer (containing 40mM Tris HCl) was added to the tissue. After vigorous vortex, 5µl of extracted DNA sample was added to the assembled PCR reaction mix (Table 2.1). Remaining DNA sample was stored at -20°C for further use. *SRY* PCR amplification was performed on a PTC-100 Thermal Cycler (MJ Research，UK) with the specific cycling program (Table2.2).

Table 2.1 *SRY* Assemble RT-PCR Reaction Mix

Reagent	Amount Used	Manufacturer
2X ImmoMix Red	12.5µl	Bioline
25µM SRY Forward Primer	0.5µl	Eurogentech
25µM SRY Reverse Primer	0.5µl	Eurogentech
Nuclease-Free Water	6.5µl	Ambion

ImmoMix Red included Pre-mixed DNA polymerase/dNTPs/PCR buffer/gel loading dye.

Table 2.2 *SRY* PCR Thermocycler Program

Program	Temperature	Time
1.Initial denaturation	95°C	10 min
2.Denaturation	95°C	30 sec
3.Annealing	58°C	30 sec
4.Elongation	72°C	45 sec
Repeat steps 2-4 for 35 cycles		
5.Final Elongation	72°C	10 min

After the amplification, 10µl of PCR products were run with 100 base pair (bp) ladder (Promega) on a 2% Tris-acetate-EDTA (TAE, diluted from 50X stock TAE, Table 2.3) agarose (Galileo Bioscience) gel containing 0.01% Gel Red (Biotium) for visualization.

Table 2.3 Compositions of Tris-acetate-EDTA (TAE) Buffer

1mL Compositions of 50X TAE buffer	Manufacturer	Final volume
Tris base	Sigma	242 g
Glacial Acetic Acid	Sigma	57.1 mL
500mM EDTA	Sigma	100mL

SRY gene expression was detected by UV transilluminator, the presence of a 300bp band determined the specimen to be male, and absence of the band indicates the specimen to be female specimen. Known positive and negative controls were loaded to ensure successful reaction (See Figure 2.1).

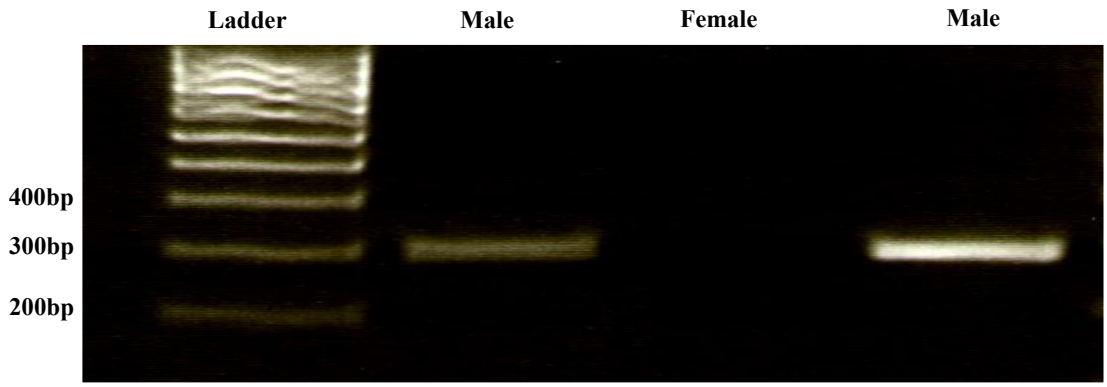

Figure2.1 *SRY* gene expression in different human specimens

2.3 *T-Cam2 cells: culture maintenance and Treatment*

The T-Cam2 cells were cultured in RPMI1640 (Gibco) medium, supplemented with 10% heat inactivated Fetal Bovine Serum (FBS, Gibco) and 2mM L-glutamine (L-Gln, Gibco，UK). The growth medium was stored in the fridge for up to 1 month and pre-warmed to 37°C before use.

The T-Cam2 cells were maintained in T75 flasks (Corning, UK) at 37°C with 5% CO_2 humidified incubator and passaged every 4-5 days using 0.5% Trypsin/EDTA (Gibco). Warm Trypsin/EDTA was added to the cells and incubated at 37°C for several minutes to accelerate the detachment. After all the cells came off the flask, the trypsin was inactivated by growth medium. For maintenance passage, cells were usually split 1:4.

In order to identify that whether the DNA demethylation reagent will affect the expression of germ cell-specific and the meiotic genes in human fetal germ cells, T-Cam2 cells were used as an *in vitro* model. T-Cam2 cells were divided into 2 main groups to optimize the optimum concentration and treatment duration, which has the lowest toxicity and highest demethylation efficiency. One of the groups was treated with different doses of 5-azacytidine for longer duration treatment; the other one was treated with higher concentration for different duration treatment (Table 2.4).

T-Cam2 cells were divided to a 6-well plate or a 10cm dishes (Corning) 24 hours before the treatment to ensure that the cells were actively dividing and reach the appropriate cell density at the time of treatment. 24 hours later, T-Cam2 cells were treated with different doses of 5-azacytidine (Sigma, UK) with different treatment duration (Table 2.4). 5-azacytidine powder (Sigma) was made up to 100mM in Dimethyl Sulfoxide (DMSO, Sigma) and the stored at -20°C as stock solution. 100mM stock 5-azacytidine was diluted in cultured medium to the final concentration of 1, 2, 3, 4, and 10μM for further treatment. A control was set up only with 0.05 or 0.1μl DMSO per mL culture medium which has the same DMSO volume as the 5μM or 10μM 5-azacytidine treatment has. As 5-azacytidine is very unstable in aqueous solutions and degraded with time, the cultured medium was changed every 24-hour with freshly made 5-azacytidine medium.

Table 2.4 Different 5-azacytidine treatments in T-Cam2 cells

Culture Group	Treatment	Final Concentration	Culture Duration
Group 1. Different doses treatment	DMSO (Control)	0.05µl DMSO /mL culture medium	72h
	5-Azacytidine	1,2,3,4 and 5µM	72h
Group 2. Different duration treatment	DMSO (Control)	0.1µl DMSO /mL culture medium	4h, 12h, 24h
	5-Azacytidine	10µM	4h, 12h, 24h

Demethylated T-Cam2 cells were treated with Retinoic Acid (Sigma, UK) to further study whether DNA demethylation reagent was associated with the regulation of retinoic acid responsiveness and the activation of germ cell-specific and meiotic genes. T-Cam2 cells were divided into 2 groups to to optimize the optimum concentration and treatment duration, which has the lowest toxicity and highest Retinoic Acid responsiveness. After treated with 5-azacytidine, the demethylated T-Cam2 cells were treated with Retinoic Acid; one groups was treated with different doses of retinoic acid for 24 hours; the other one was treated with different doses of retinoic acid for 48 hours (Table 2.5). Retinoic acid was made up to 100mM in DMSO and stored at -20°C as stock solution. 100mM stock Retinoic Acid was diluted in DMSO to the final concentration of 0.1 and 1nM for treatment. A control containing the same DMSO volume as the retinoic acid reagents was set up. Retinoic acid-containing medium was kept in the dark, and changed every 24 hours with freshly made medium. After the treatment, the cells were harvest for next analysis (see Section 2.5).

Table 2.5 Different Retinoic Acid treatments in T-Cam2 cells

Culture Group	Treatment	Final Concentration	Culture Time
Group 1. 24 hour Retinoic Acid treatment with different doses of Retinoic Acid	DMSO+DMSO	0.05µl DMSO / mL culture medium+1µl DMSO per mL culture medium	72h +24h
	DMSO +Retinoic Acid	0.05µl DMSO / mL culture medium+0.1nM/1nM RA	72h +24h
	5-Azacytidine+ DMSO	5µM aza +1µl DMSO/ mL culture medium	72h +24h
	5-Azacytidine+ Retinoic Acid	5µM aza +0.1nM/1nM RA	72h +24h
Group 2. 48 hours Retinoic Acid treatment with different doses of Retinoic Acid	DMSO+DMSO	0.05µl DMSO / mL culture medium+1µl DMSO per mL culture medium	72h +48h
	DMSO +Retinoic Acid	0.05µl DMSO /mL culture medium+0.1nM/1nM RA	72h +48h
	5-Azacytidine+ DMSO	5µM aza +1µl DMSO/ mL culture medium	72h +48h
	5-Azacytidine+ Retinoic Acid	5µM aza +0.1nM/1nM RA	72h +48h

2.4 ***Human Fetal Gonads Culture and Treatment***

Human fetal gonads were treated with 5µM 5-azacytidine (Table 2.6) to study the role of DNA demethylation reagent in the expression of germ cell-specific and meiotic genes *in vivo*. After DNA demethylation, the demethylated human fetal gonads were treated with 1nM Retinoic Acid (Table 2.7) to further study the relation between DNA demethylation reagent and the retinoic acid responsiveness *in vivo*.

Table 2.6 5-azacytidine treatment in human fetal gonads

Treatment	Final concentration	Culture Duration
DMSO (control)	0.05µl DMSO /mL culture medium	96h
5-Azacytidine	5µM	96h

Table 2.7 Retinoic Acid treatments in human fetal gonads

Treatment	Final concentration	Culture Time
DMSO+ DMSO	0.05µl DMSO / mL culture medium+ 1µl DMSO / mL culture medium	72h+48h
DMSO + RA	0.05µl DMSO /mL culture medium+1nM RA	72h+48h
5-Azacytidine+DMSO	5µM aza +1µl DMSO/mL culture medium	72h+48h
5-Azacytidine+ RA	5µM aza +1nM RA	72h+48h

MEM-alpha complete medium for human fetal gonads culture was made previously (Table 2.8). 1ml of culture medium supplemented with treatment reagent (5µM 5-azacytidine or 1nM Retinoic Acid) and another 1ml supplemented with control reagent (DMSO) were prepared freshly. 900µl of each supplemented medium was placed in adjacent wells of a 12 well tissue culture plate (Corning), and then a polyester capillary pore membrane (pore size 0.4µm, Greiner Bio-One) was placed into each well. A drop (approximately 50µl-100µl) of the corresponding medium was place onto the upper surface of each membrane. The remaining wells were filled with 1ml Dulbecco's Phosphate-Buffered Saline (DPBS, Gibco) to humidify the plate.

Table 2.8 Compositions of human fetal gonads culture medium

Compositions of 50mL Culture Medium	Manufacturer	Final volume
MEM-ALPHA	Gibco	43ml
KnockOut™ Serum Replacement (KOSR)	Gibco	5ml(10% final)
100mM Sodium Pyruvate	Gibco	0.5ml(2mM final)
100X MEM Non-Essential Amino Acids	Gibco	0.5ml(1X final)
200mM L-Glutamine	Gibco	0.5ml(2mM final)
100X Penicillin-Streptomycin	Gibco	0.5ml (1X final)
500X Insulin-Transferrin-Selenium (ITS)	Lonza	0.1ml(1X final)
Bovine Serum Albumin (BSA)	Sigma	150mg(3mg/ml final)

Fetal gonads tissues were micro-dissected into small pieces, which were randomly put into treatment group and control. Gonads were carefully transferred into the drop of medium on the upper surface of the membrane. The culture plate containing the fetal gonads was incubated at 37°C in a humidified atmosphere containing 95% air-5% CO2. A complete culture medium change was performed every 24h.
After culture, tissues were washed by DPBS carefully and harvest for further analysis.

2.5 *Gene expression analysis*

The Polymerase Chain Reaction (PCR) technique was used to qualify and quantify the mRNA expression level in cells and tissues. These steps involved total RNA extraction, RNA concentration measurement, cDNA synthesis, reverse transcription-PCR (RT-PCR) and quantitative real-time PCR (qRT- PCR).

2.5.1 **Total RNA Extraction**

RNA from snap frozen samples (-80º C) or cultured cells was extracted by utilizing the Nucleospin RNA II Kit (Macherey-Nagel), RNeasy Mini Kit or RNeasy Micro Kit (Qiagen) according to manufacturer's instructions.

When there were less than 5×10^6 cultured cells or less than 30mg human tissue, the Nucleospin RNA II Kit (Macherey-Nagel) was used. Some of the experiments were performed with RNeasy Mini Kit or RNeasy Micro Kit (Qiagen). When there were less than 5×10^6 cultured cells or less than 30mg human tissue, the RNeasy Mini Kit (Qiagen) was used. When there were fewer than 5×10^5 cultured cells or <5mg human tissue, the RNeasy Micro Kit was used.

Extracted RNA was immediately placed on ice. RNA was quantitated by NanoDrop ™ 1000 Spectrophotometer (Thermo Scientific) by measuring ultraviolet absorbance at 260nm and 280nm. The A260/A280 ratio is generally between 1.9 and 2.1, indicating purity of the RNA. Extracted RNA was frozen at -20℃ for short-term storage and -80℃ for long-term storage.

2.5.2 **First Strand cDNA Synthesis**

First strand cDNA synthesized from 200ng RNA using the Maxima First Strand complementary DNA (cDNA) Synthesis Kit (Thermo Scientific) or SuperScript® VILO™ cDNA Synthesis Kit (Invitrogen) according the manufacturer's instructions. The components of these two Kits are show in the table (Table 2.9). The first strand cDNA synthesis reaction mixes were performed as an individual reaction or as a series of parallel reactions with different RNA templates. Reverse transcription (RT) -negative samples were prepared similar to normal sample except adding reverse transcriptase enzymes. RT-negative samples were used to ensure the RNA used was free of DNA contaminants. No template control (NTC) lacking RNA template was prepared to assess reagent contamination (Table 2.9).

After the master mixtures were prepared, all the tubes were arranged in a PTC-100 Thermo cycler (MJ Research) and the program "Maxima" or "SurperScript" was run (Table 2.10). After the completion of the program, the first strand cDNA was used directly for PCR or stored at -20℃.

Table 2.9 Components of the cDNA Synthesis Kits

Maxima First Strand cDNA Synthesis Kit	**RT+**	**RT-**	**NTC**
Maxima Enzyme Mix	2µl	0µl	2µl
5X Reaction Mix	4µl	4µl	4µl
Nuclease-free Water	6µl	8µl	14µl
Template RNA	100ng-500ng	100ng-500ng	0ng
Total volume	20µl	20µl	20µl
SuperScript® VILO™ cDNA Synthesis Kit	**RT+**	**RT-**	**NTC**
10X SuperScript® Enzyme Mix	2µl	0µl	2µl
5X VILO™ Reaction Mix	4µl	4µl	4µl
Nuclease-free Water	6µl	8µl	14µl
Template RNA	100ng-500ng	100ng-500ng	0ng
Total volume	20µl	20µl	20µl

Table 2.10 Thermocycler Program for cDNA synthesis

Program in PTC-100 Thermo cycler	**Maxima program**	**SuperScript program**
Step 1. Anneal	25℃ for 10min	25℃ for 10min
Step 2. Extend	50℃ for 15min	50℃ for 30min
Step 3. Inactivate Reverse Transcriptase	85℃ for 5min	85℃ for 5min
Step4. Hold	4℃ to hold	4℃ to hold

2.5.3 **Primer Design**

Most of the primers that I used (Table 2.11) were designed and donated by the Richard Anderson's lab (University of Edinburgh, UK).

Among the primers used here, TET1, 2, and 3 were designed by myself using Primer3 input software, version 0.4.0. Primers were designed to: I) be between 18 and 28 nucleotides in length; II) have a GC content within the range of 20-80 %; III) have a Tm of 58-60℃; and IV) amplify 50-150bp of DNA. During RNA extraction, DNase

has already digested the DNA in cells and tissues. Meanwhile, in the later PCR experiments, the mRNA levels rather than the DNA levels were detected, so the intron spanning was not performed during the primer design.

Table 2.11 Primers used for RT-PCR or qRT-PCR

Genes	Forward Primer	Reverse Primer	Size
TET1	AAATGTTGCCCGAGAATGT	TTGATCTTGGCTTCCATTCC	264bp
TET2	GAGACGCTGAGGAAATACGG	TGGTGCCATAAGAGTGGACA	258bp
TET3	CAGAACGCTGTGATCGTCAT	AACTTGCGAGGTGTCTTGCT	263bp
NANOG	CAGCTGTGTGTACTCAATGATAGATTT	ACACCATTGCTATTCGGCCAGTTG	132bp
OCT4	ACATCAAAGCTCTGCAGAAAGAAC	CTGAATACCTTCCCAAATAGAACCC	126bp
DAZL	GAAGGCAAAATCATGCCAAACAC	CTTCTGCACATCCACGTCATTA	186bp
STRA8	CTCAAAGTGGCAGGTTCTGAA	TCCTCTAAGCTGCTTGCATGC	126bp
SYCP3	AGCCGTCTGTGGAAGATCAG	CAACTCCAACTCCTTCCAGC	198bp
SYCP1	GCAGCAGGTGTCTGCGGTG	CAACCTGCTCAAGCACGG	191bp
DMC1	AGCAGCAAAGTTCCATGAAG	TGAGCTCTCCTCTTCCCTTT	314bp
VASA	AAGAGAGGCGGCTATCGAGATGGA	CGTTCACTTCCACTGCCACTTCTG	238bp
B2M	ACTGAATTCACCCCCACTGA	CCTCCATGATGCTGCTTACA	114bp
BOLL	TATAAGGATAAGAAGCTGAACATTGGT	CGAAGTTACCTCTGGAGTATGAAAATA	171bp
REC8	TGAGGGTGAATGTGGTGAAA	CTGGGATTGCAGCCTCTAAG	393bp
CYP26B1	TCGAGCTTGATGGTTTCCAGA	TGCTATACATGACACTCCAGCCTT	51bp
RPL32	CATCTCCTTCTCGGCATCA	AACCCTGTTGTCAATGCCTC	100bp
AFP	TGCAGCCAAAGTGAAGAGGGAA	ATAGCGAGCAGCCCAAAGAAGA	216bp
mStra8	GGAGAAAAAGGCCAGACTCC	GACATATGCTGGGCCTCACT	228bp
SRY	ACAGTAAAGGCAACGTCCAG	ATCTGCGGGAAGCAAACTGC	300bp

2.5.4 **Reverse Transcription Polymerase Chain Reaction (RT-PCR)**

RT-PCR was used to qualitatively detect gene expression through creation of cDNA transcripts from RNA. The cDNA was diluted 1 in 5 and then used as a template for

exponential amplification using RT-PCR. The master mix (Table 2.12) containing appropriate primers (Table 2.11) was added to each PCR tube. 1µl of the RT+ or RT- cDNA reaction was added to each PCR tube with 19µl master mix. PCR tubes were put in a PTC-100 Thermo cycler (MJ Research) for the "Immo" amplification program (Table 2.13).

The RT-PCR products were analyzed with gel electrophoresis on a 2.5% agarose gels (Galileo Bioscience) containing 10% GelRed for visualization. PCR products were observed by UV light and images were captured using Gel-DOC programme (Bio-Rad). The 10µl of 100bp DNA ladder (New England Biolab) was used to determine size of PCR products.

Table 2.12 Compositions of RT-PCR master mix

Reagent	Amount Used	Manufacturer
ImmoMix Red	10µl	Bioline
25µM Forward Primer	0.5µl	Eurogentech
25µM Reverse Primer	0.5µl	Eurogentech
Nuclease-free water	8µl	Ambion

ImmoMix Red (Pre-mixed DNA polymerase/dNTPs/PCR buffer/gel loading dye)

Table 2.13 "Immo" RT-PCR amplification program

Program	Temperature	Duration of Cycle
1.Initial denaturation	95°C	10 min
2.Denaturation	95°C	30 sec
3.Annealing	58°C	30 sec
4.Elongation	72°C	45 sec
Repeat steps 2-4 for 35 cycles		
5.Final Elongation	72°C	10 min

2.5.5 Quantitative Real-time Polymerase Chain Reaction (qRT- PCR)

qRT-PCR was performed to analyze gene expression using 25µM each of the primer pairs (Table 2.11) and Brilliant III SYBR Green Master Mix (Agilent Technologies, Wokingham, UK) (Table 2.14). The reaction was place in the ABI7900HT Fast Real-Time PCR System with SDS2.4 software (Applied Biosystems, Warrington, UK), and the appropriate PCR program was run as the table below (Table 2.15), the instrument was set to detect and report fluorescence at each cycle during 60°C

annealing/extension step. For each gene of interest, each RT (+) sample was analyzed in triplicate and a single RT (−) reaction was performed as a negative control.
In order to determine amplification efficiency, standard curves for *B2M*, *TET1*, *2* and *3* were generated using a series of increasing dilutions (from 1/10 to 1/10,000) of 14wga human fetal ovarian cDNA. The resulting slope of the standard curves is a measure of the efficiency of the PCR reaction and was all close to −3.3 (equivalent to 100% PCR efficiency or two-fold amplification per cycle) (Hartley et al., 2002), allowing quantification using the $2^{-\Delta\Delta Ct}$ method (Bayne et al., 2009).

Melt curve analysis of each run confirmed expected product sizes. Signal acquisition was performed for 40 amplification cycles followed by continuous melt curve analysis to ensure product accuracy. For quantification, cDNAs were used at 1/20 dilutions with all amplification reactions performed in triplicate. In order to allow quantitative comparisons between cDNAs, *gene*-of-interest expression was normalized to that of the housekeeping gene *B2M*, which remained stable across gestation and between treatments.

Table 2.14 Compositions of qRT-PCR master mix

Reagent	Amount Used	Manufacturer
2x Brilliant III SYBR Green Mix	5µl	Agilent Technologies
25µM Forward Primer	0.2µl	Eurogentech
25µM Reverse Primer	0.2µl	Eurogentech
Diluted Reference DYE (Diluted 1/50 in H2O)	0.15µl	Agilent Technologies
Nuclease-free water	2.45µl	Ambion
Sample (diluted 1/20 in H2O)	2µl	--

Table 2.15 Program for qRT-PCR

Program	Temperature	Duration of Cycle
Step 1. Hot start	95°C	3 min
Step2. Denaturation	95°C	5 sec
Step3. Anneal/Extension	60°C	15 sec
Repeat steps 2-3 for 40 cycles		
Dissociation curve	95°C	15 sec
	60°C	15 sec
	95°C	15 sec

2.5.6 **Statistical analysis**

Statistical analysis was performed using ABI SDS2.4 software (Applied Biosystems, Warrington, UK), Microsoft Excel 2003 and GraphPad Prism 5 software (La Jolla, CA, USA). Data presented represent mean ± standard error of the mean (SEM) of at least three independent biological replicates. P values of less than 0.05 were considered statistically significant.

Gestational comparison data were analyzed using one-way ANOVA; data were analyzed as described for further analysis. Data were then analyzed utilizing the Newman-Keuls Multiple Comparison post-test to determine significant changes between gestational values. Some data was also analyzed using a post-test for linear trend; this test was performed when data were in a natural order (ie across gestation).

Data were analyzed using paired t-tests compared the treated cells/gonads to the control cells/ gonads

2.6 ***Tissue Fixation, Processing, and Sectioning***

Fixation is an important step before the immunostaining, as the right fixation way not only immobilizes antigens but also facilitate the access of antibodies. The fixation method is chose by the balance between morphological preservation and antigen accessibility to antibody. Bouin's fixation was usually used for fetal gonads as it usually gave both good morphological preservation and good antigenicity preservation. 4% Neutral Buffered Formaldehyde (NBF，Clintec, UK) also gave good antigen preservation, but the morphological preservation of human gonads in NBF was substantially inferior to preservation in Bouins.

In the experiments here, tissues were fixed in Bouins solution or 4% NBF and then transferred to 70% ethanol (VWR) for further processing (Table 2.16).

Table 2.16 Tissue fixation for human fetal gonads

Fixation method	First trimester human gonads	Second trimester human gonads
Bouins	Gonads was fixed 1-2 hours before being transferred to 70% ethanol	Gonads was fixed 2-3 hours before being transferred to 70% ethanol
4% NBF	Gonads was fixed overnight before being transferred to 70% ethanol	

The fixed tissues were paraffin processed to make the tissues firm enough to be cut on a microtome. Tissue processing was usually done on an automated tissue processor (Leica TP1050). Following processing, tissues were embedded in molten paraffin wax. Paraffin blocks were cut into 5μm thick sections via a paraffin microtome (Leica) and floated onto a heated water bath at 45°C to promote smooth tissue transfer. Sections were mounted on electrostatically charged glass slides (Thermo-scientific or Leica).

The slides were dried at 50°C overnight to ensure the tissue adhered to the slide surface.

2.7 *Haematoxylin and Eosin Staining*

Hematoxylin and Eosin staining (H&E) is the most common staining technique in histology laboratories. In order to determine tissue quality and orientation, every 10th slide was taken from each specimen for H&E staining. The staining of Haematoxylin is purplish blue and aimed at DNA in the nucleus and RNA in ribosomes; the staining of Eosin is pink and aimed at proteins in the cytoplasm.

Sections were deparaffinized in xylene (VWR) twice for 5 min each, and then rehydrated through graded alcohol (VWR) for 20 sec each (From absolute alcohol, 95% alcohol to 70% alcohol). Sections were rinse in tap water for further process. Sections were incubated in haematoxylin (Leica) for 30-60 sec to counterstain nuclei. A very quick incubation in acid alcohol was performed to remove non-specific cytoplasmic staining. Sections were further immersed in Scott's tap water for 30 sec to allow the haematoxylin to develop. Slides were immersed in Eosin (BD, UK) for 1 min to stain cytoplasm. Slides were then rinsed in the water to remove excess staining between every step. After counterstaining, slides were transferred through baths of progressively increasing concentrated alcohol to dehydrate the tissues. The slides were then immersed in the hydrophobic clearing agent xylene twice for 5 min. After dehydration, a glass coverslip (VWR, UK) was cover with a small amount of Pertex glue (Histolab, UK), and the slide was mounted on its section side down. The slides were left to dry and stored in dry storage at room temperature.

2.8 *Chromogenic Immunohistochemistry (IHC)*

Immunohistochemistry was used to identify the distribution of target proteins in tissues of interest.

2.8.1 **Deparaffinization and Rehydration**

Sections were deparaffinized and rehydrated as described above, and were transferred to antigen retrieval after rinsing in water.

2.8.2 **Antigen Retrieval**

Before immunohistochemistry, the masked antigenicity needs to be break by Antigen retrieval, through which some tissues was exposed to a heated buffer solution. Citrate buffer of pH6.0 was the most commonly used retrieval solution.
0.1M stock Citrate Buffer was prepared with 42.02g Citric Acid (Sigma) being dissolved in 1900mL distilled water, and the pH was adjusted to 6.0 with 1N NaOH.
Dewaxed slides were immersed in 0.01M Citrate Buffer, and heated to 125℃ for 30sec and then cooled down to 90℃ in a Decloaking Chamber (Biocare Medical, UK).

2.8.3 Non-Specific Blocking

When HRP conjugated antibody is used, non-specific background will be detected in some tissues, which contain endogenous peroxidase. In order to reduce this non-specific background, hydrogen peroxide (H_2O_2) blocking was used prior to HRP conjugated antibody. Sectioned tissues were incubated in 3% Hydrogen peroxide (H_2O_2, Fisher Scientific) diluted in methanol (VWR, UK) to block endogenous peroxidase activity.

After 30 min peroxidase blocking, sectioned tissues were washed in pH7.6 wash buffer Tris-buffered saline (TBS, 0.05M Trizma base, 0.9% Sodium Chloride, (Sigma)) twice for 5 min.

Normal serum was used as a common blocking reagent to block non-specific binding of immunoglobulin. The blocking serum must be taken from the species that secondary antibody was generated in rather than the species of the primary antibody. Slides were incubated in a blocking buffer for 30 min (including 1 part of normal serum (NS (Biosera, UK), 4 parts of TBS and 5% Bovine serum albumin (BSA, Sigma) (NS/TBS/BSA)).

Endogenous biotin results in non-specific background staining when an avidin-biotin detection system is used. This non-specific background can be significantly reduced by treating tissues with avidin/biotin blocking reagents prior to the incubation of biotinylated antibody. This blocking step was performed immediately after normal serum blocking and before primary antibody incubation.

Sections were incubated in strepavidin blocking solution (Vector, UK) for 15 min followed by a brief rinse in TBS, and then blocked in biotin blocking solution (Vector, UK) for 15 min. The sections were briefly rinsed in TBS and processed for primary antibody blocking.

2.8.4 Primary Antibody

The concentration, incubation time and incubation temperature of primary antibodies are all important impact factors for immunohistochemistry. In order to get specific staining and lowest background, optimization is needed for each antibody and tissue. Longer incubation periods (overnight) and lower temperatures (4 °C) were often employed to ensure penetration through tissue sections to promote specific staining. Primary antibody concentration optimization was achieved by varying dilution on standard tissue to find the maximum level of detection while minimizing non-specific background staining. The primary antibody was diluted in blocking serum (NS/TBS/BSA) with the optimum concentration. The sections were incubated in the primary antibody overnight at 4° C. The table below (Table 2.17) showed the antibodies used and the optimum concentrations for human fetal tissues.

Non-immunized blocking serum omitting primary antibody was used as negative control to test the specificity of the primary antibody involved.

Table 12.17 Antibodies used in Chromogenic Immunohistochemistry

Primary Antibody	Manufacturer	Species Raised	Blocking Serum	Dilution	Detection and Visualization
H3K9ac	Abcam Ab10812	Rabbit polyclonal	NGS/TBS/BSA	1:700	GARB+Streptavidin-HRP +DAB
			NGS/TBS/BSA	1:150	GARBfab + ABC Streptavidin-AP+ Fast Blue
H3K4me3	Cell Signaling Technology #9727	Rabbit polyclonal	NGS/TBS/BSA	1:2000	Anti-rabbit ImmPRESS kit +DAB
H3K27me3	Cell Signaling Technology #8112	Rabbit polyclonal	NGS/TBS/BSA	1:70	Anti-rabbit ImmPRESS kit +DAB
H3K9me2	Abcam Ab1220	Mouse monoclonal	NGS/TBS/BSA	1:150	Anti-rabbit ImmPRESS kit +DAB
5mC	Eurogentec BI-MECY-0100	Mouse monoclonal	NGS/TBS/BSA	1:150	Anti-rabbit ImmPRESS kit +DAB
5hmC	Active Motif 39769	Rabbit polyclonal	NGS/TBS/BSA	1:300	Anti-rabbit ImmPRESS kit +DAB
C-Kit	DAKO A4502	Rabbit polyclonal	NGS/TBS/BSA	1:50	Anti-rabbit ImmPRESS kit +DAB
VASA	Abcam Ab13840	Rabbit polyclonal	NGS/TBS/BSA	1:50	Anti-rabbit ImmPRESS kit +DAB

GARB: goat anti-rabbit biotinylated secondary antibody

CARBfab: goat anti-rabbit biotinylated conjugated FAB fragment secondary antibody

2.8.5 Streptavidin Detection Method

After overnight incubation, slides were washed twice in TBS for 5 min to remove primary antibody. A biotinylated secondary antibody was used to link primary antibodies to an avidin-biotin-peroxidase complex. A biotinylated secondary antibody

(diluted 1:200 in blocking serum), with specificity against the primary antibody (Table 2.17), was applied to the tissue samples and incubated at room temperature for 30 min. The secondary antibody was rinsed in the TBS twice for 5min.

A biotinylated enzyme, Streptavidin-horseradish peroxidase (HRP) (Vector), was diluted 1:1000 in TBS and applied to the slides for 30 min incubation. The avidin-biotin-peroxidase complex was bound to the biotinylated antibody that was already bound to the tissue and the visualization of antibody was developed as described below (Section 2.11.7).

2.8.6 ImmPress Polymer Detection Method

For antibodies that were not readily detectable with standard secondary antibodies, ImmPress Polymer Detection Reagents (Vector) was used. This ImmPress Polymer staining system uses novel conjugation and micropolymer chemistries to produce a highly sensitive, low background, non-biotin detection system. Avidin/Biotin blocking steps were eliminated by ImmPress detection system even in tissues containing endogenous biotin.
The staining procedure for ImmPress kit was simple. Following the normal horse serum-blocking step, primary antibody was diluted in normal horse serum and the section tissues were incubated with primary antibody as described above. After primary antibody incubation, the appropriate ImmPress reagent was added to the sections and incubated for 30 min. Section were rinsed with TBS and the visualization of antibody was developed as described below (Section 2.9.7).

2.8.7 Visualization of Antibody

3, 3′ -diaminobenzidine tetrahydrochloride (DAB; DAKO) was used to detect the bound antibodies. 1 drop (or 20µl) of the DAB Chromogen was added to 1mL of Substrate Buffer. Sections were then incubated with DAB until staining was optimally detected (determined via observation by light microscope). The sections were immersed in water to stop the reaction.

2.8.8 Counterstaining, Dehydration, and Slide Mounting

After antigen detection, the slides were counterstained using haematoxylin (no eosin) and mounted as described previously.

2.9 *Fluorescent Immunohistochemistry*

Fluorescent immunohistochemistry was used to detect the distribution of specific proteins within the cell or tissue. Fluorescent dyes are conjugated to secondary antibodies or probes to visualize the location of the primary antibodies to detect target antigens; this technique has the ability to generate high-resolution images for specific proteins localization studies and the capacity to quantitate the fluorescent signal.
The general protocol for fluorescent immunohistochemistry was similar to that of DAB Immunohistochemistry with minor changes for fluorescent detection.

2.9.1 Washes Buffer and Blocking Serum

All washes between each step were performed in phosphate-buffered saline (PBS, Sigma) instead of TBS for fluorescent immunohistochemistry. The blocking serum comprised of normal serum and BSA was diluted in PBS (NS/PBS/BSA) rather than in TBS.

2.9.2 Primary Antibody

Primary antibody was diluted in the blocking serum NS/PBS/BSA rather than NS/TBS/BSA. As fluorescent immunohistochemistry was more sensitive, the optimum concentration of primary antibody was adjusted (Table 2.18).

Table 12.18 Antibodies used in immunofluorescence

Primary Antibody	Manufacturer	Species Raised	Blocking Serum	Dilution	Detection and Visualization
H3K9me3	Abcam Ab8898	Rabbit polyclonal	NHS/PBS/BSA	1:800	Anti-rabbit ImmPRESS kit +Tyramide
			NDS/PBS/BSA	1:300	Donkey Anti-Rabbit Alexa Fluor® 555
5mC	Eurogentec BI-MECY-0100	Mouse monoclonal	NGS/PBS/BSA	1:800	GAMP+ Tyramide
5hmC	Active Motif 39769	Rabbit polyclonal	NGS/PBS/BSA	1:1000	GARP+ Tyramide
VASA	Abcam Ab13840	Rabbit polyclonal	NHS/PBS/BSA	1:800	Anti-rabbit ImmPRESS kit +Tyramide
OCT4	Santa Cruz Sc-5279	Mouse monoclonal	NHS/PBS/BSA	1:700	Anti-mouse ImmPRESS kit +Tyramide
DAZL	Cell Signalling #8042	Rabbit polyclonal	NGS/PBS/BSA	1:1000	GARP+ Tyramide
SYCP3	Abcam Ab15093	Rabbit polyclonal	NGS/PBS/BSA	1:30000	GARP+ Tyramide

GAMP: goat anti-mouse peroxidase secondary antibody

GARP: goat anti-rabbit peroxidase secondary antibody

2.9.3 Secondary Antibody and Visualization of Binding Antibody

There were several methods to detect and visualize the primary antibody. The bound primary antibody was detected by fluorophore-conjugated secondary antibody, or by Tyramide Signal Amplification (TSA, Perkin Elmer) Detection.

The fluorophore-conjugated secondary antibody detection approach was the simplest form of signal amplification. With this approach, multiple antigens can be labeled concurrently when the primary antibodies were raised from different species. A fluorophore-conjugated secondary antibody, with specificity against the primary antibody, was diluted 1:200 in blocking serum. The section tissues were incubated with this secondary antibody for 1 hour at room temperature to allow binding to the primary antibody. This incubation was performed in darkness, as the fluorophores degrade under light exposure.

TSA is a patented technology, which can significantly enhance the fluorescent signals. It is particularly useful for detection of relatively sparse antigens that other systems have difficulty detecting. The TSA system uses a HRP catalyzed reaction to covalently attach the tyramide portion of tyramine-protein conjugated to the area around the protein of interest. A peroxidase-conjugated secondary antibody, with specificity against the primary antibody, was diluted 1:200 in blocking serum. The section tissues were incubated with this secondary antibody for 30 min at room temperature to allow binding to the primary antibody. After rinsed in PBS twice for 5 min, a tyramide enhancer was diluted 1:50 in its own amplification buffer as described by the manufacturer. The slides were then incubated in darkness for 10 min. The TSA was removed with PBS in an opaque container to prevent any bleaching of the fluorescence.

2.9.4 Counterstain

Nuclear counterstaining was performed with 4', 6-diamidino-2-phenylindole (DAPI, Invitrogen) or Propidium Iodide (PI, Invitrogen). The counterstain used for fluorescence varied depending on the color of detection used for the primary antibodies. They were diluted 1:1000 in PBS and applied to the slides for 10 min incubation in darkness.

2.9.5 Mounting

Dehydration was not need for fluorophore-labeled tissue samples; the samples must be mounted with a solution containing an antifade compound to stabilize the fluorescence. A small amount of PermaFluor Mounting Medium (Thermo Scientific) was added to a glass coverslip (VWR) and the slide was mounted on its section side down. The mounted slides were stored at 4°C in the dark for weeks to months.

2.10 *Fluorescent immunocytochemistry (ICC)*

Immunocytochemistry (ICC) is a technique used to assess the presence of the target specific peptides or protein antigens in the cells by utilizing a specific antibody. Cells were cultured in 4-well chamber slides (Thermo Scientific), and attached to the slides to allow easy handling in subsequent procedures.

To ensure free access of the antibodies to all cells and subcellular compartments, the cells were fixed and permeabilized. After aspirating culture medium, the cells were washed with PBS twice, and fixed with 4% NBF for 10 min. After that, permeabilization was performed. The permeabilization method used depended on the epitopes and antibodies. 0.2% NP-40 (Sigma) was applied for intracellular epitopes when the antibody required access to the inside of the cell to detect the protein. When the epitope was in the cytoplasm or the cytoplasmic face of the plasma membrane, a milder membrane solubilizer was needed. 0.2% Tween 20 (Bio-rad) was suitable for the antigens in the cytoplasmic region. It gave large enough pores for antibodies to pass through without dissolving the plasma membrane. The cells were permeabilized and blocked in the blocking solvents which included 0.2% NP-40/0.2% Tween 20, 1% BSA, 10% Serum and PBS. Cells were incubated with the blocking solvents for 30 min at room temperature. The target specific peptides or protein antigens in the cells were detected by primary antibody, which was diluted in the normal blocking serum. After incubated at 4℃ overnight, both fluorochrome-conjugated secondary antibody and TSA were used to detect the binding primary antibody. Cells were incubated in PI or DAPI for 10 min. Chambers were removed and the slides were mounted with PermaFluor Mounting Medium (Thermo Scientific).

2.11 *IHC and ICC for 5-Methyl Cytosine (5mC) and 5-Hydroxymethyl Cytosine (5hmC)*

The protocol for 5mC and 5hmC detection was similar to the general protocol with minor changes.

For IHC, after peroxidase blocking, the detected tissues were permeabilised by 0.5% Triton 100 (Sigma) for 30 min. To further improve binding affinity of the antibodies, the DNA was denatured by incubating the tissues in 4N hydrochloric acid (HCl, VWR) for 15 min at room temperature. Following denaturation, the tissues were blocked in NS/TBS/BSA and then incubated with 5mC (Eurogentec) or 5hmC (Active Motif) antibody (Table 2.17).

For ICC, after permeabilization by 0.5% Triton X100 (Sigma), the cells were denatured by 4N HCl. The cells were incubated with NS/PBS/BSA following the 5mC or 5hmC antibody incubation (Table 2.18).

2.12 *Dual Immunohistochemistry and Co-localization by immunofluorescence*

For dual immunohistochemistry, detection using the first primary antibodies was performed as described above. After DAB detection, the slides were microwaved in 0.01M Citrate Buffer for 2.5 minutes for second time antigen retrieval. NGS/TBS/BSA was used to block the slides before adding second primary antibody (Table 2.17). Goat anti-rabbit biotinylated Fab fragments (Abcam) was used as secondary antibody diluted 1:200 in NGS/TBS/BSA. The Vectastain ABC alkaline phosphatase kit (Vector) was used to bind to the peroxidase antibody that was already bound to the tissue and the visualization of antibody was applied by fast blue (Sigma) following the manufacturer's instructions. Slides were then mounted in PermaFluor Mounting Medium (Thermo Scientific).

For dual immunofluorescence, the above protocol (Section 2.11) was followed by additional citrate retrieval by boiling in a microwave oven for 2.5 min. After the antigen retrieval, the above section was repeated starting from the serum blocking stage. Slides were kept in the dark as much as possible to preserve fluorescence, and the strongest primary antibody (one used at the highest dilution) was used first. The antibodies used in dual fluorescent immunohistochemistry are shown in Table 2.18.

2.13 *Light microscopy and Fluorescent microscopy*

For immunohistochemistry staining, the expression of target proteins were determined and photographed by utilizing a Provis AX70 (Olympus) microscope fitted with a camera (AxioCam HRc, Zeiss). Scale bars were generated and Adobe Photoshop CS5 was used to compile the photographic figures shown in the text.
For immunofluorescence staining, slides were visualized using a LSM710 confocal microscope (Zeiss). Scale bars were embedded using the Zeiss software and images compiled into figures using Photoshop CS5.

2.14 *Western blot analysis of protein expression*

2.14.1 **Protein Extraction and quantification**

Cells were cultured in a 10cm diameter culture dishes. Before harvesting, the cells were washed briefly in cold PBS. 500µl of RIPA buffer（containing 25mM Tris HCl pH 7.5, 150mM NaCl, 1%Triton X100, 0.1% SDS, 0.05 Sodium Deoxycholate）was added to lyse the cells for 5min on ice. The lysed cells were scraped down with a cell scraper and the entire lysate was transferred into a 1.5ml tube. Before processing the next step, the lysates were homogenized with an electronic pestle (Sigma) with disposable tips (Sigma) to ensure maximum protein extraction.

The concentration of protein extracts were measured by the Bradford protein assay which is a spectroscopic analytical procedure (Bradford et al, 1976)

Serial dilution of BSA standards (1.0, 0.5 0.25 and 0.125mg/ml) were diluted in 1/10 RIPA buffer. 1/10 diluted lysate proteins were prepared appropriately for further detection. The Protein Assay Components (Bio-Rad) were prepared according to manufacturer's instructions utilizing a 96-well microplate (Corning). All assays (standards and test lysates) were incubated with the Protein Assay Components for 15 min in triplicate. The plates were scanned on a Multiskan EX microplate reader (Labsystems) to measure absorbance at 590nm. The absorbance of test lysates was compared to a BSA standard curve run on the same microplate to determine the concentration of the lysate.

2.14.2 **Western Blot**

The Western Blot is an analytical technique used to qualitatively and semi-quantitatively identify specific proteins.

Protein samples were diluted in RIPA buffer to a final concentration of 20µg and then 1/3 volume of 4X SDS loading buffer (containing 625mM PH6.8 Tris, 5% Glycerol, 2% SDS, 0.0025% Bromophenol Bule and distilled water) with 10% reducing agent β-ME (Sigma Aldrich) was added. The samples were denatured at 99° C for 6 min on a Thermomixer (Eppendorf) and then cooled on ice.

Gel electrophoresis was used to separate proteins. The samples were loaded into a 12% tris-HEPES-SDS Precise Protein gel (Thermo Scientific) alongside PageRuler Plus Prestained Protein Ladder (Thermo Scientific). Gels were run in a protein electrophoresis system (Bio-Rad) with running buffer (1x Tris-HEPES SDS Buffer, Thermo Scientific) at 125V for 45-60 min until the loading dye had run to the bottom of the gel.
After electrophoresis, the separated molecules were transferred from the electrophoresis gel to a polyvinylidene difluoride (PVDF) membrane for further detection. The electrophoresis gels were washed in distilled water and then soaked in transfer buffer (fast semi-dry buffer, Thermo Scientific) for 10 min. PVDF membrane Immobilon-FL Transfer Membrane (Millipore) was cut to the appropriate size for the gel. The membrane was dehydrated by soaking in methanol for 30sec, 1min in distilled H_2O, and then soaked in Fast Transfer Buffer for 15min prior to blotting. Immobilon Blotting Filter Paper (Millipore) was prepared by soaking in transfer buffer. The protein-containing gel was placed directly onto the Immobilon-FL Transfer Membrane and loaded with two filter papers. The blot sandwich was loaded into a semi-dry blotter as per manufacturer's instructions and run at 25V for 7-9min depending on protein size to transfer proteins to the membrane.

The membranes used in western blotting have a high affinity for proteins. Therefore, after transferring, a blocking buffer was applied to block the remaining surface of the membrane to prevent nonspecific binding of the detection antibodies during subsequent steps. The membrane was washed in distilled water, and then blocked in blocking buffer (1:1 0.1% PBS tween: Millipore Block-FL) for at least 1 hour at room

temperature. Typically, the blocked membrane was probed with a primary antibody that recognized a specific protein or epitope on a group of proteins. A DAZL antibody raised from rabbit (1:150, 50kDa, Cell Signalling) was used to detect the target protein and a α-tubulin antibody raised from mouse (1:3000, 37kDa, Cell Signalling) was used as a loading control. Primary antibodies were diluted in blocking buffer and the membrane was left to incubate at 4 °C overnight.

Next day, the membrane was washed in 0.1% PBS tween x4 for 5 min. Anti-rabbit Alexa680 conjugated secondary antibody (red signal, life technologies) and anti-mouse IRDye800 conjugated antibody (green signal, life technologies) were applied to the detected the bound primary antibody. Fluorophore-conjugated secondary antibodies diluted in blocking buffer were applied to the membrane. After incubating with the secondary antibodies for 1h at room temperature in the dark, the membrane was washed in 0.1% PBS tween twice for 5 min and then in PBS twice for 5 min in the dark. The membrane was directly scanned with the aid of the Li-Cor Infrared Imaging System (Odyssey).

2.15 *Plasmid DNA Transfection*

2.15.1 **Bacteria Transformation**

A plasmid containing resistance to antibiotic was used as a vector to clone, transfer and manipulate genes. The gene of interest was inserted into a plasmid vector, creating a newly constructed plasmid. This plasmid was introduced into a bacterium by bacterial transformation. The bacterial used for transformation was sensitive to specific antibiotic. The bacteria were then spread over a plate that contained specific antibiotic. The antibiotic was used as a selective pressure as only bacteria that have acquired the plasmid can grow on the plate. Therefore, in order to survive in the plate, which contains antibiotic, the bacteria continually replicated the plasmid along with the gene of interest that has been inserted to the plasmid. This allows generation of large quantities of plasmid.

All procedures in bacteria transformation were performed under sterile conditions. NEB 5-alpha Competent E.Coli Cells (New England BioLabs) were thawed in ice for 10 min. 100ng plasmid DNA (pEGFP-C1-Stra8, provided by Dr. Andrew Childs) was added to the NEB 5-alpha Competent E.Coli Cells on ice as soon as the last ice crystals disappeared. In order to maximum the transformation efficiency, cells and DNA plasmid were incubated together on ice for 30 min. The cell mixtures were heat shocked at exactly 42℃ for 30 sec and then returned to ice another 5 min. 950µl S.O.C medium (Invitrogen) was added to the cell mixtures and shaken vigorously (250rpm) at 37℃ for 1 hour. Outgrowth at 37℃ for 1 hour was best for cell recovery and for expression of antibiotic resistance to obtain maximal transformation efficiency. The LB Agar plates (Bio-Red) with 100µg/ml Ampicillin or 30µg/ml Kanamycin were prepared in advanced and warmed up to 37℃. After 1-hour incubation, several 10-fold serial dilutions of the cell mixtures were made in S.O.C

medium (1ng, 10ng, 100ng). 100µl of each dilution was spread onto the antibiotic selection plates and incubated overnight at 37℃.

After 24 hours, the LB agar plates were removed from the incubator to check the number of bacterial colonies. A single colony was picked up and inoculated in a 5mL starter LB Broth (Fisher Scientific) with the appropriate selective antibiotic (100µg/ml ampicillin or 30µg/ml kanamycin). The starter culture LB medium was shaken vigorously (300rpm) at 37℃ for 8h. In order to get enough plasmid DNA for later DNA extraction, the starter culture medium with a single colony was diluted into 250mL LB Broth medium containing the appropriate selective antibiotic. This 250mL LB culture medium was shaken vigorously (300rpm) at 37℃ for 16h. The rest of the plates were wrapped in parafilm and kept in a refrigerator for later use.

2.15.2 **Plasmid DNA extraction and purification**

The bacterial cells were harvested by being centrifuged at 6000 g at 4℃ for 10min and the supernatant was discarded. Plasmid DNA Purification Kit (Macherey Nagel) was used to extract plasmid DNA. 12mL of buffer RES with RNase A was added to re-suspend the cell pellet completely. 12mL Lysis Buffer LYS was added and incubated at room temperature for 5 min. A NucleoBond Xtra Column together with the inserted column was equilibrated with 25mL Equilibration Buffer EQU. EQU buffer was applied onto the rim of the column filter and wet the entire filter. The lysate suspension was mixed with 12mL Neutralization Buffer NEU and inverted gently for several times. The lysate was immediately loaded onto the column. After the column was emptied by gravity flow, 15mL Buffer EQU was added to wash the column filter and column to wash away the remaining lysate in the filter. The column filter was discarded and the column was washed with 25mL Wash Buffer. 15mL Elution Buffer ELU was added to the column and the ELU buffer was collected in a 50mL centrifuge tube (Corning). 15mL room temperature isopropanol was added to the mixture to precipitate the eluted plasmid DNA. The precipitated DNA was loaded slowly with a 30mL syringe attached to a NucleoBond Finalizer. After discarding all the flow-through, the syringe was washed slowly with 5mL ethanol with the attachment with the Finalizer. After discarding the flow-through again, the NucleoBond Finalizer was dried by passing air through the Finalizer 6 times. Finally, the Finalizer was attached to a 1ml syringe, and 750µl re-dissolving Buffer TRIS was added to elute plasmid DNA drop by drop by inserting the plunger slowly. The first eluate was transferred back into the syringe and eluted into the same collection tube to get a high yield of plasmid DNA.

Plasmid DNA was quantitated by NanoDrop TM 1000 Spectrophotometer (Thermo Scientific) through measuring its ultraviolet light (UV) absorbance at 260nm. The A260/A280 ratio was generally between 1.9 and 2.1, indicating purity of the DNA. For long-term storage, plasmid DNA was frozen at -20℃.

2.15.3 **The Process of Transfection**

Cells were divided 24 hours before transfection to ensure that the cells were actively dividing and at the appropriate cell density at the time of transfection to maximize transfection efficiency. The volumes of culture medium and transfection reagent were varied according to culture plate used. When the cells were cultured in the 6-well plate, 2.5µg of DNA from each plasmid (pEGFP-C1-Stra8, pCDNA3-N2MYC-Stra8 vectors and empty vector pCMV6-Entry from (OriGene)) and10µl TransIT –LT1 transfection reagent (Mirus) were incubated in 250µl serum-free growth medium (Opti-MEM I Reduced-Serum Medium (Invitrogen)) for 20min. The solution containing the plasmid was then dropped onto the plates with 2.5 mL fresh medium and mixed by gentle rocking.

The cells were incubated overnight with the transfection solution. In order to determine the best post-transfection time, the cells were incubated for 24-72 hours. The transfections were performed in complete growth medium without a post-transfection medium change to yield high transfection efficiency. After transfection, the expression of transfected gene was detected by qRT-PCR.

Chapter3. Dynamic changes in histone modifications during human fetal germ cell development

3.1 *Introduction*

Among the modified histone marks, H3K9ac, H3K4me3, H3K27me3, H3K9me2 and H3K9me3 are the most studied.

The active histone mark H3K9ac has been identified to activate transcription by neutralisation the electrostatic interaction between DNA and histones (Nishida et al., 2006; Turner, 2000). In undifferentiated human ESCs, enrichment of H3K9ac contributes to the maintenance of pluripotency-related genes *POU5F1*, *NANOG* and *SOX2* (Pan et al., 2007). Once human ESCs enter into differentiation, the global level of H3K9ac is significantly reduced (Krejci et al., 2009).

Another histone mark H3K4me3 is also tightly associated with active genes (Barski et al., 2007; Bernstein et al., 2005). H3K4me3 regulates active transcription by recruiting chromatin-remodelling enzymes (Flanagan et al., 2005; Li et al., 2006). In undifferentiated human ESCs, high levels of H3K4me3 contribute to maintenance of the pluripotency-related genes *POU5F1*, *NANOG* and *SOX2* before differentiation (Pan et al., 2007).

H3K27me3, a hallmark of condensed heterochromatin, is tightly associated with transcriptional repressive genes (Boyer et al., 2006; Margueron and Reinberg, 2011). In undifferentiated human and murine ESCs, developmental genes are silenced by H3K27me3 and its methyltransferase PRC2 (Boyer et al., 2006; Lee et al., 2006).

In mammalian cells, H3K9me2, acting as a crucial histone mark for transcriptional repression, is enriched within the silent euchromatic regions (Peters et al., 2003; Rice et al., 2003). In differentiated murine ESCs, the expression of the pluripotency-associated gene *Pou5f1* is repressed by high levels of H3K9me2 (Feldman et al., 2006).

H3K9me3, which is greatly enriched in heterochromatin, is generally associated with transcriptional silence (Bannister et al., 2001; Lachner et al., 2001). In mouse ESCs, H3K9 trimethyltransferase Suv39h does not contribute to maintain the undifferentiated status (Lehnertz et al., 2003). In addition, Suv39h and its modified chromatin H3K9me3 have been found to be critical for germ cell meiosis in mice (Peters et al., 2001).

In the mouse embryo, these five histone marks have been identified to change dynamically during germ cell development, and may be associated with the normal development of mouse fetal germ cells (Abe et al., 2011; Hajkova et al., 2008; Seki et al., 2005; Seki et al., 2007; Yabuta et al., 2006). In line with the dynamic histone modifications in mouse fetal germ cells, human fetal germ cells may also undergo global histone modifications to prepare for the subsequent germ cell-specific developmental process. However, observations about histone modifications in human fetal germ cells are very limited. In order to identify whether the dynamic changes of

these histone marks are similar to those observed in mouse, expression of these five important histone modifications was here investigated in human fetal germ cells.
In order to identify the antibody's antigen-binding specificities, these five histone marks were first detected in the seminoma-derived TCam-2 cells, which is obtained from a primary testicular seminoma of a 35-year-old patient (Mizuno et al., 1993). Seminomatous testicular germ cell tumors are the result of abnormal development of early gonocytes during migration or on their arrival in the gonad (Kristensen et al., 2008). Testicular seminoma cells have similar morphology and maker expression patterns as PGCs (Kristensen et al., 2008). Therefore, TCam-2 cells can be used as a PGC model in human *in-vitro* studies (de Jong et al., 2008). Subsequently, these five histone marks were investigated in human gonad tissues *in vivo*.

3.2 *Results*

3.2.1 Distinct distributions of H3K9ac, H3K4me3, H3K9me2, H3K9me3 and H3K27me3 in NBF fixed TCam-2 cells

As a negative control, NBF fixed human TCam-2 cells were incubated with non-immune serum rather than primary histone antibodies (Fig 3.1F). In control TCam-2 cells, the interphase nuclei were stained by PI (Propidium iodide), which labeled the condensed chromocenters with stronger and heavier staining (Fig 3.1F, white arrow).

In TCam-2 cells, the active histone mark H3K9ac was evenly distributed across cell nuclei and was excluded from the chromocenters (Fig 3.1A). The endogenous levels of active histone mark H3K4me3 were also detected in TCam-2 cells. Being absent from the condensed chromocenters, H3K4me3 was present in the TCam-2 cell nuclei specifically, with a distinct punctuate pattern of staining (Fig 3.1B). The distribution of H3K9me2, a repressive histone mark in the silent euchromatic regions, distributed non-condensed throughout the TCam-2 cell nuclei and was also absent from the strongly stained chromocenters (Fig 3.1C, white arrow). In TCam-2 cells H3K9me3 was present in a speckled staining pattern (Fig 3.1D). H3K9me3 localized preferentially to PI-dense (DNA-dense) heterochromatin (Fig 3.1D) and part of the chromocenters (Fig 3.1D). Finally, H3K27me3 distributed diffusely throughout the TCam-2 cells nuclei (Fig 3.1E) and stained intensely in the chromocenters (Fig 3.1 E).

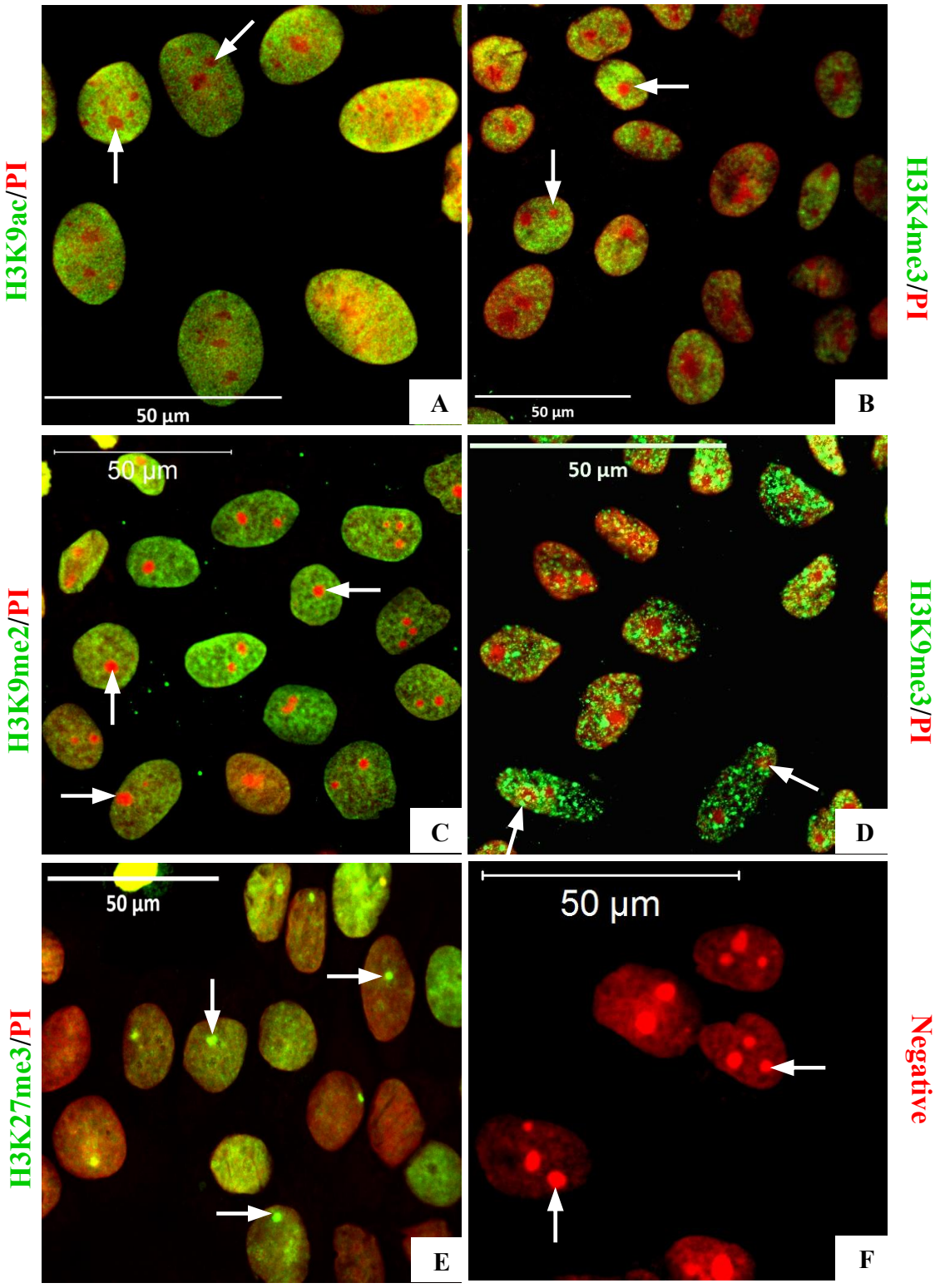

Figure3.1. Distribution of different histone marks in the nuclei of NBF fixed TCam-2 cells. **A**, H3K9ac; **B**, H3K4me3; **C**, H3K9me2; **D**, H3K9me3; **E**, H3K27me3; **F**, Negative control. The staining for the histone marks is shown in green; the PI nuclear counterstaining is shown in red. The white arrows represent the chromocenters in the TCam-2 cells. The scale bars in all panels are equal to 50µm.

3.2.2 Distributions of H3K4me3, H3K27me3 and H3K9me2 in Bouins and NBF fixed human ovaries

In order to determine whether the antigen-binding ability is affected by different fixation ways or not, the expression of H3K4me3, H3K27me3 and H3K9me2 was examined in both Bouins and NBF fixed 18wga human fetal ovaries (Fig 3.2).

At 18wga human ovary, which was fixed in either Bouins or NBF, the smaller and less differentiated ovarian germ cells located in the peripheral ovary displayed H3K4me3 staining (Black arrow, Fig 3.2 A and B); while the larger and more mature ovarian germ cells located in the central region were H3K4me3-negative (White arrow, Figure 3.2 A and B), including oocytes in primordial follicles (insert panels, Fig 3.2 A and B).

At 18wga, H3K27me3 was rarely detectable in both the Bouins and NBF fixed human ovarian germ cells (White arrow, Fig 3.2 C and D), involving oocytes in primordial follicles (insert panels, Fig 3.2 C and D).

The Bouins and NBF fixed 18wga human fetal ovaries displayed a similar H3K9me2 staining, with a mixture of H3K9me2-positive (Black arrow, Fig 3.2 E and F) and H3K9me2-negative ovarian germ cells (White arrow, Fig 3.2 E and F) towards the edge or the middle of the ovary.

Bouins and NBF fixed human gonadal sections incubated with non-immune serum instead of primary antibody were used as negative control (Fig 3.2 G and H).

In Bouins and NBF fixed human fetal ovaries, the distributions of H3K4me3, H3K27me3 and H3K9me2 were quite similar, suggesting that the antigen-binding specificities of these three histone antibodies were not greatly influenced by different fixation methods. Meanwhile, the morphological structure was preserved better in Bouins fixed gonads than NBF fixed ones. Therefore, these histone marks were investigated in Bouins fixed human fetal ovaries and testes across different gestations.

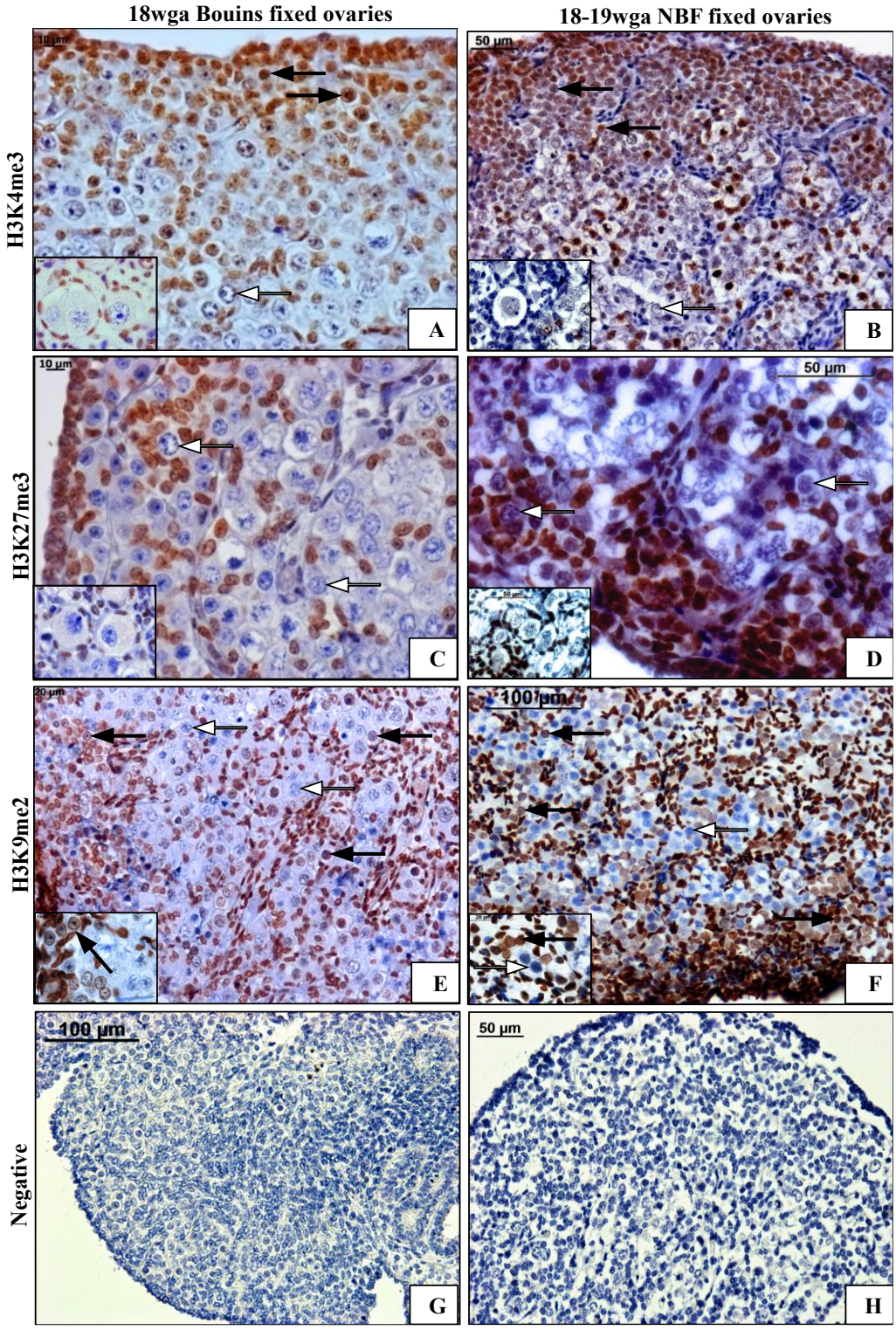

Figure 3.2 Distribution of different histone marks in Bouins or NBF fixed 18wga human fetal ovaries. A and **B**, H3K4me3; **insert panels** in **A** and **B**, primordial follicles; **C** and **D**, H3K27me3; **insert panels** in **C** and **D**, primordial follicles; **E** and **F**, H3K9me2; **insert panels** in **E** and **F**, middle of the ovary; **G**, Bouins fixed negative control; **H**, NBF fixed negative control. Black arrows represent positive staining ovarian germ cells, while white arrows represent negative staining ovarian germ cells. The scale bars equal to 10µm in panels A and C; 20µm in E; 50µm in B, D and H; 100µm in F and G.

3.2.3 Global changes of H3K4me3 during human fetal ovarian and testicular germ cell development

DAB immunohistochemical detection was performed to determine the distribution of the active histone mark H3K4me3 in Bouins fixed human fetal ovaries and testes across different gestations. Overall, the global levels of H3K4me3 in human fetal ovarian and testicular germ cells progressively declined as they differentiated (Fig 3.3 and 3.4). At 9wga, human fetal ovary only contains undifferentiated PGCs; all these PGCs displayed nuclear H3K4me3 staining (Black arrow, Fig 3.3 A and B). However by 15wga, following the onset of meiosis, most ovarian germ cells had lost this active mark and the staining was restricted to the smaller and undifferentiated germ cells at the periphery of ovary (Black arrow, Fig 3.3 D-F). The larger, more differentiated germ cells at the center of ovary were H3K4me3-negative (white arrow, Fig 3.3D-F). At later gestations, this pattern became more pronounced. At 19wga, most germ cells were H3K4me3-negative (white arrow, Fig 3.3 G-H)), including oocytes in primordial follicles (asterisk, Fig 3.3 I).

Most of the somatic cells in the ovaries, as well as the pre-granulosa cells in the primordial follicles, were H3K4me3-positive (black arrowhead, Figure 3.3). Only very few somatic cells in the 2nd trimester were H3K4me3-negative (white arrowhead, Figure 3.3). Ovarian sections incubated with non-immune serum rather than H3K4me3 primary antibody was used as a negative control (Figure 3.3C).

In Bouins fixed human fetal testes, parallel changes in H3K4me3 distribution were found in testicular germ cells across the same developmental window (Figure 3.4). At 9wga, all PGCs were H3K4me3-positive (Black arrow, Fig 3.4A). However, by 14wga, some large H3K4me3-negative testicular germ cells at the edge of seminiferous cords were clearly visible (White arrow, Fig 3.4B), although a sub-population of testicular germ cells still retained this modification (black arrow, Fig 3.4B). A similar pattern was observed at 18wga (Fig 3.4C).

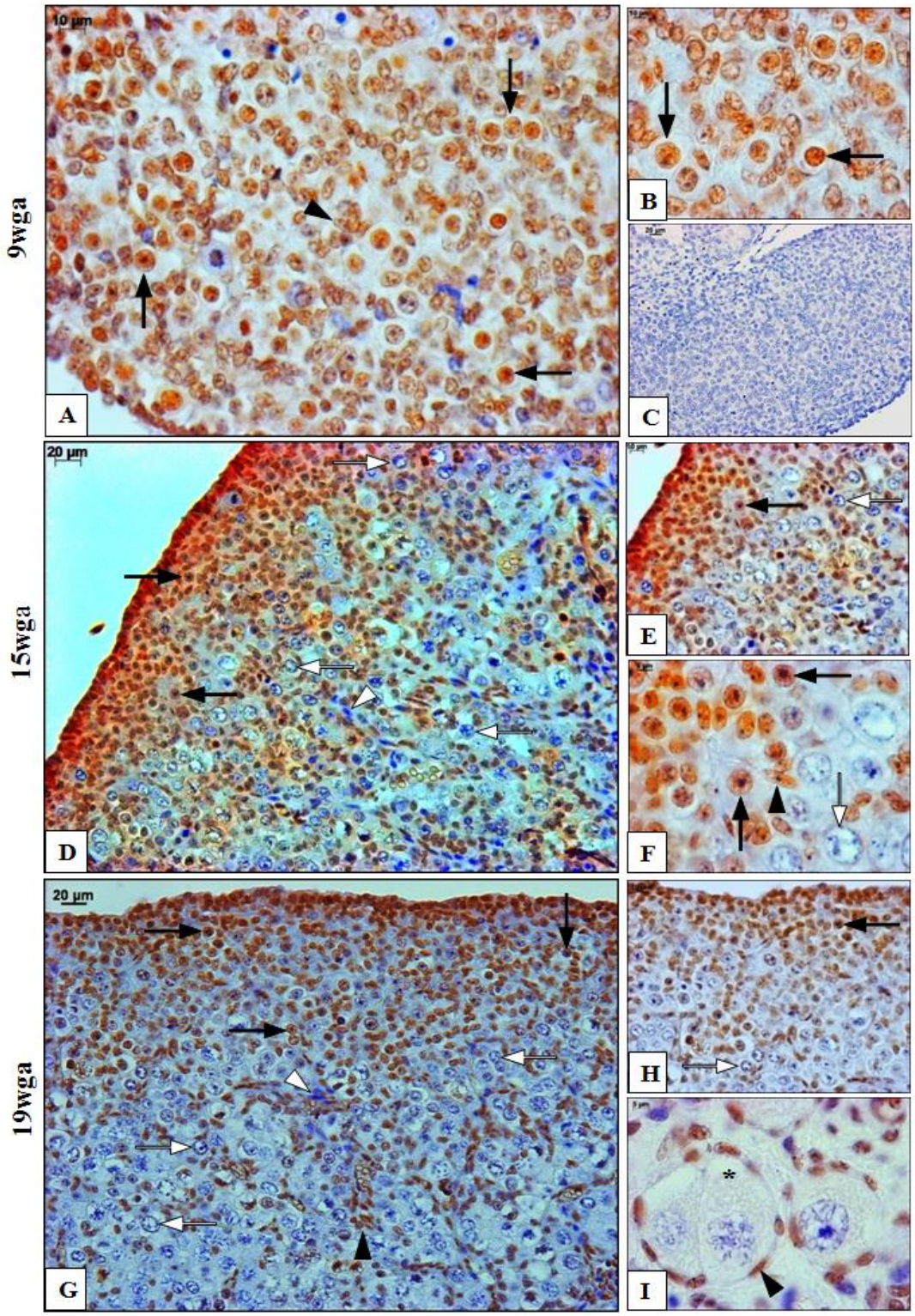

Figure 3.3 Distribution of H3K4me3 in Bouins fixed human fetal ovaries. A and **B**, 9wga human fetal ovarian sections; **C**, negative control; **D**, **E** and **F**, 15wga; **G**, **H** and **I**, 19wga. Black and white arrows represent H3K4me3-positive and negative germ cells, respectively. While black and white arrowheads represent H3K4me3-positive and negative somatic cells, respectively. The asterisk represents the primordial follicles. The scale bars equal to 5µm in F and I panels; 10µm in A, B, E and H panels; 20µm in the C, D and G panels.

Almost all the testicular somatic cells displayed H3K4me3 staining in the 1st trimester (black arrowhead, Fig 3.4A). In the 2nd trimester, Sertoli cells within testicular cords, and peritubular myoid cells surrounding cords, were H3K4me3-positive (black arrowhead, Fig 3.4B and C) while the Leydig cells located between the testicular cords were H3K4me3-negative (white arrowhead, Fig 3.4B and C). The negative control is shown in Figure 3.4 D.

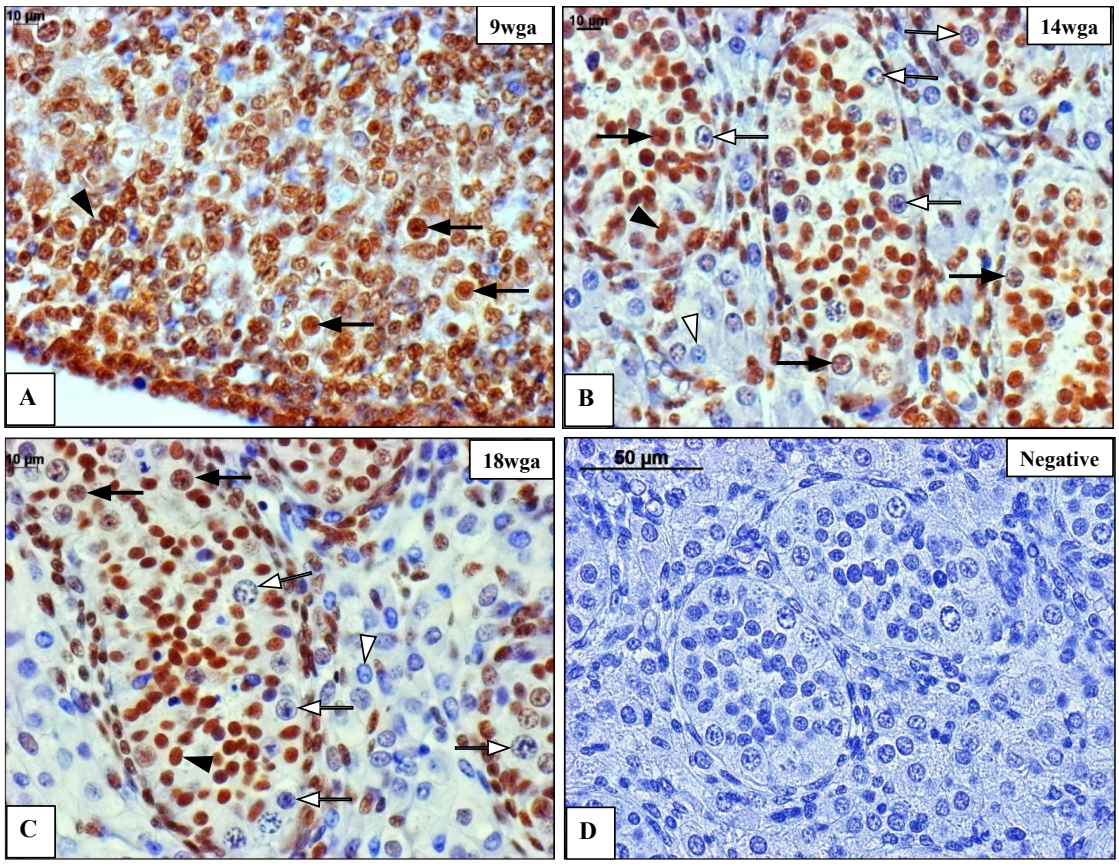

Figure 3.4 Distribution of H3K4me3 in Bouins fixed human fetal testes. **A**, 9wga human fetal testicular section; **B**, 14wga human fetal testicular section; **C**, 18wga human fetal testicular section; **D**, negative control. Black and white arrows represent H3K4me3-positive and negative germ cells, respectively. Black and white arrowheads represent H3K4me3-positive and negative somatic cells, respectively. The scale bar is equal to 10µm in A, B and C panels; 50µm in D panel.

3.2.4 Global changes of H3K27me3 during human fetal ovarian and testicular germ cell development

H3K27me3, which is associated with repressed genes, displayed a similar pattern to that of H3K4me3 in human fetal ovarian and testicular germ cells, but appeared to be erased at an earlier stage (Fig 3.5 and 3.6).

At 8wga, nearly all the ovarian germ cells displayed H3K27me3 staining (black arrow, Fig 3.5 A-C), however, some of the staining was weakly positive (black arrow, Fig 3.6 B). By 15wga, most of the ovarian germ cells had lost H3K27me3 (white arrow, Fig 3.5 D and E), with only very few smaller and undifferentiated germ cells at the periphery of the ovary displaying nuclear H3K27me3 staining (black arrow, Fig 3.5 D and E). By 19wga, all of the germ cells in the human fetal ovary, including undifferentiated germ cells located at the periphery of the ovary, did not show H3K27me3 staining (white arrow, Fig 3.5 G-H). Oocytes in primordial follicles were also completely H3K27me3-negative (asterisk, Fig 3.5 I).

At 8wga, most of the ovarian somatic cells were H3K27me3-negative or weakly positive (white arrowhead, Fig 3.5A-C); however, at later gestations, H3K27me3-positive somatic cells were abundant (black arrowhead, Fig 3.5D-E, G-H). Pre-granulosa cells in primordial follicles were also mostly H3K27me3-positive (black arrowhead, Fig 3.5I). The negative control is shown in Fig 3.5 F.

With increasing gestation, parallel changes in H3K27me3 distribution were detected in Bouins fixed human fetal testicular germ cells (Fig 3.6 A-C). At 9wga, most testicular germ cells were H3K27me3-positive, although some of them were only weakly H3K27me3-positive (black arrow, Fig 3.6 A). H3K27me3 was completely erased in testicular germ cells by 15wga (white arrow, Fig 3.6 B), and remained undetectable at 19wga (white arrow, Fig 3.6 C).

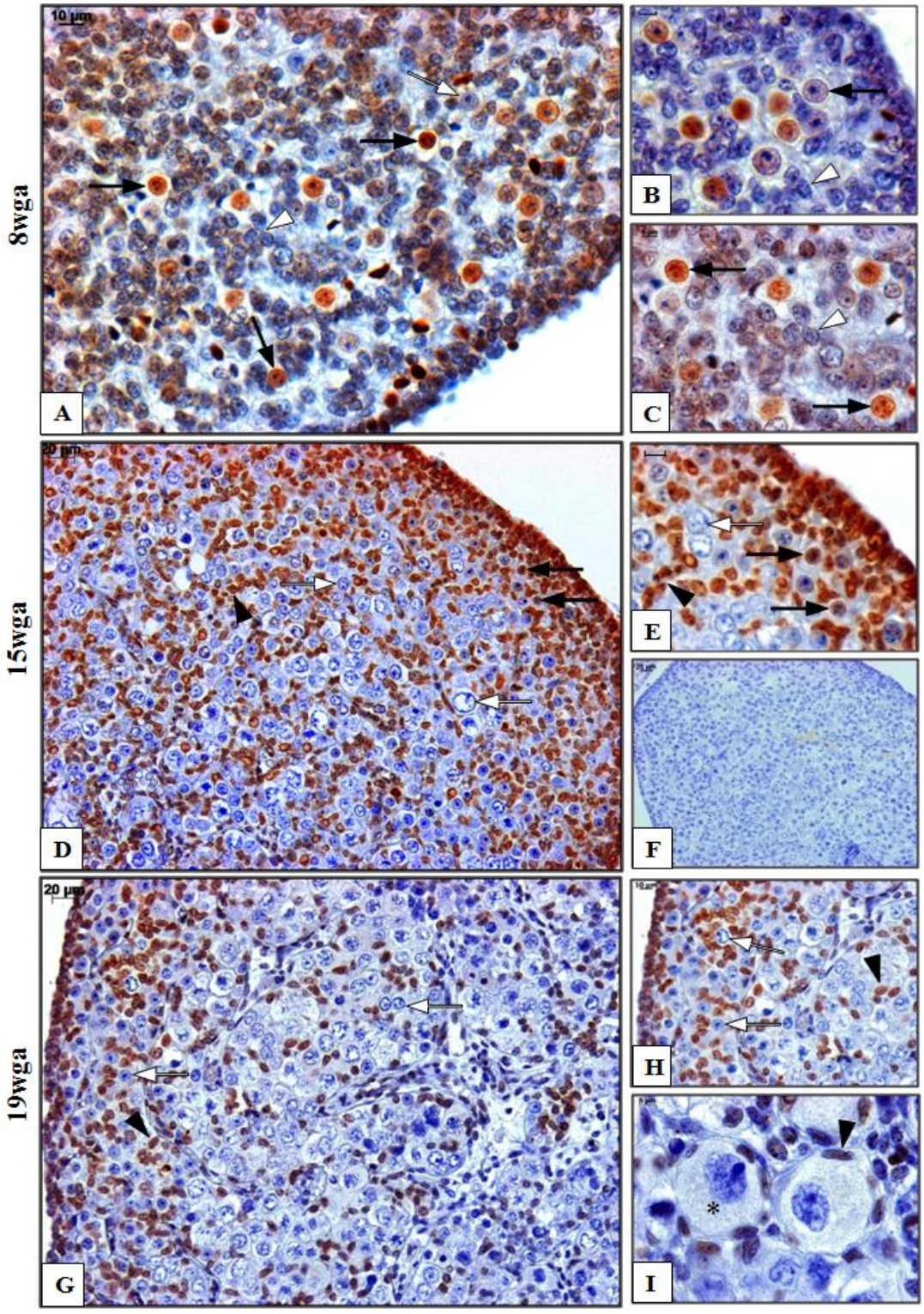

Figure 3.5 Distribution of H3K27me3 in Bouins fixed human fetal ovaries. A, **B** and **C**, 8wga human fetal ovarian sections; **D** and **E**, 15wga; **F,** negative control**; G**, **H** and **I**, 19wga. Black and white arrows represent H3K27me3-positive and negative germ cells, respectively. While black and white arrowheads represent H3K27me3-positive and negative somatic cells, respectively. The asterisk represents the primordial follicles. The scale bars equal to 5µm in B, C, E and I panels; 10µm in A and H panels; 20µm in the D, F and G panels.

Testicular somatic cells were largely H3K27me3-positive at 9wga (black arrowhead, Fig 3.6 A). At 15wga and 19wga, the Sertoli cells within testicular cords showed intense positive staining for H3K27me3 (black arrowhead, Fig 3.6 B), whilst peritubular myoid cells and Leydig cells were either weakly positive, or showed no H3K27me3 staining (White arrowhead, Fig 3.6 B). The negative control is shown in Fig 3.6 D.

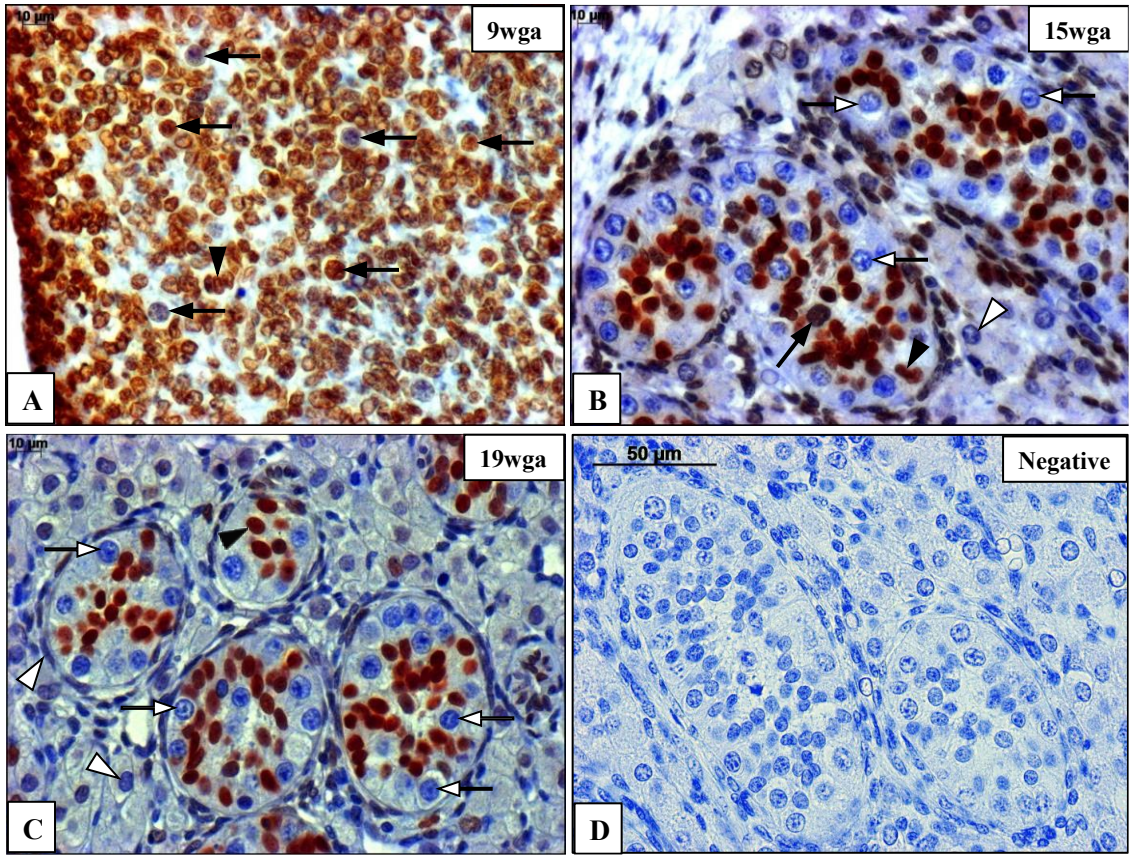

Figure 3.6 Distribution of H3K27me3 in Bouins fixed human fetal testes. **A**, 9wga human fetal testicular section; **B**, 15wga human fetal testicular section; **C**, 19wga human fetal testicular sections; **D**, negative control. Black and white arrows represent H3K27me3-positive and negative germ cells, respectively. While black and white arrowheads represent H3K27me3-positive and negative somatic cells, respectively. The scale bars equal to 10µm in the A, B and C panels, and 50µm in D panel.

3.2.5 Dynamic Changes of H3K9me2 during human fetal ovarian and testicular germ cell development

H3K9me2 displayed a distinct, sex-specific distribution in human fetal germ cells. H3K9me2 was undetectable in ovarian germ cells at 9 and 19wga, but was transiently detected at 15wga, which was coincident with the early stages of meiosis (Fig 3.7). At 9wga, the repressive histone mark H3K9me2 was undetectable in most human fetal ovarian germ cells (White arrow, Fig 3.7A-B), but some displayed low levels of this histone mark (Black arrow, Fig 3.7A-B). At 15wga, H3K9me2-positive ovarian germ cells were detected both at the edge (Black arrow, Fig 3.7D and E) and the middle of the ovary (Black arrow, Fig 3.7D and F). However, not all ovarian germ cells displayed H3K9me2 at this stage (White arrow, Fig 3.7D-F). At 19wga, H3K9me2 was nearly undetectable in the ovarian germ cells most showed no H3K9me2 staining (White arrow, Fig 3.7G-I). Oocytes in primordial follicles were also H3K9me2-negative at this stage (Asterisk, Fig 3.7I). In distinction to the dynamic changes in human ovarian fetal germ cells, the ovarian somatic cells were largely H3K9me2-positive at all gestation (Fig 3.7A-I). The primary antibody was omitted for negative controls (Fig 3.7C).

In contrast, H3K9me2 was undetectable in testicular germ cells at all stages examined (White arrow, Fig 3.8A-C). In the testicular somatic cells, the staining of H3K9me2 was highly dynamic across gestation (Fig 3.8). At around 9wga, almost all the testicular somatic cells showed strong H3K9me2-staining (Black arrowhead, Fig 3.8A). However, during 2nd trimester, the staining of H3K9me2 declined in different populations of testicular somatic cells (Fig 3.8 B and C). At 15wga, only some Sertoli cells, peritubular myoid cells displayed H3K9me2 staining (Black arrowhead, Fig 3.8B). Later at 19wga, the number of H3K9me2-positive Sertoli cells increased (Black arrowhead, Fig 3.8C), however, most of the Leydig cells remained negative for H3K9me2 (White arrowhead, Fig 3.8C). The negative control is shown in Figure 3.8 D.

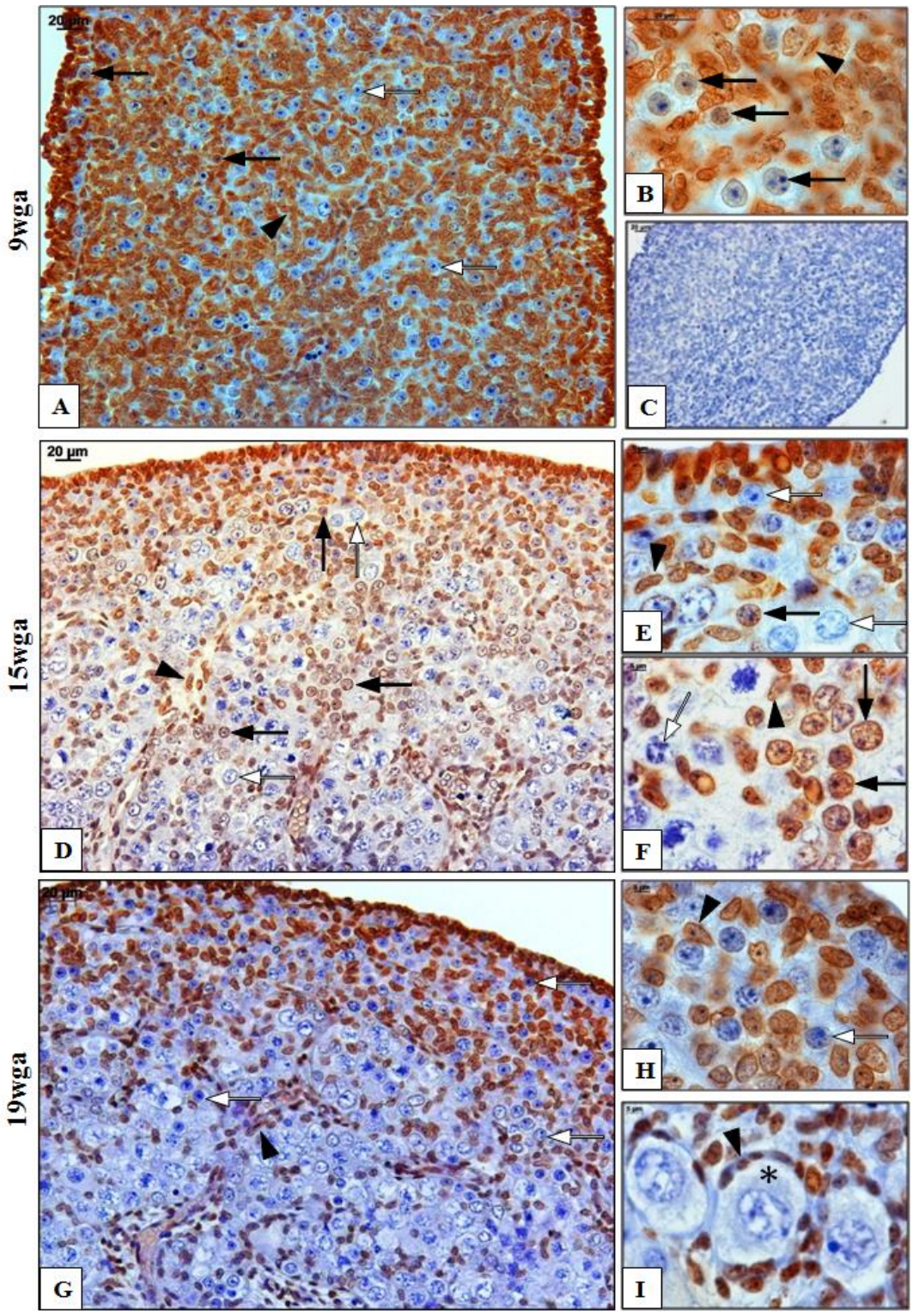

Figure 3.7 Distribution of H3K9me2 in Bouins fixed human fetal ovaries. A and **B**, 9wga ; **C**, negative control; **D**, 15wga; **E**, the edge of 15wga human fetal ovary; **F**, the middle of 15wga human fetal ovary; **G**, **H** and **I**, 19wga. The asterisk represents the primordial follicles. Black and white arrows represent H3K9me2-positive and negative germ cells, respectively. While black and white arrowheads represent H3K9me2-positive and negative somatic cells, respectively. The scale bars equal to 5µm in E, F, H and I; 20µm in A, B, C, D and G.

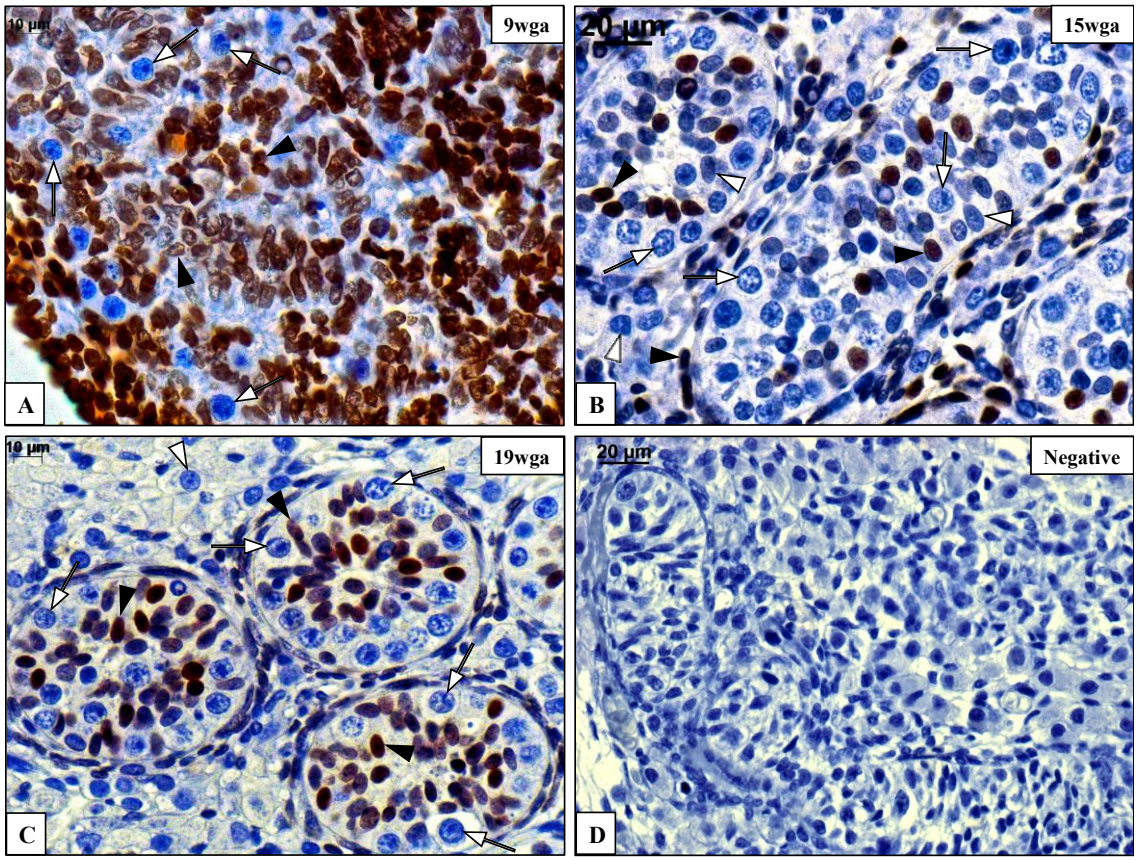

Figure 3.8 Distribution of H3K9me2 in Bouins fixed human fetal testes. A, 9wga human fetal testicular section; **B**, 15wga human fetal testicular section; **C**, 19wga human fetal testicular section; **D**, negative control. Black and white arrows represent H3K9me2-positive and negative germ cells, respectively. While black and white arrowheads represent H3K9me2-positive and negative somatic cells, respectively. The scale bars equal to 10µm in A and C panels, 20µm in B and D panels.

3.2.6 Global changes of H3K9me3 in human fetal and postnatal ovarian germ cells and human fetal testicular germ cells

Initial investigation of the expression of H3K9me3 in both Bouins and NBF fixed human fetal gonads via DAB immunohistochemical detection did not give clear results. Therefore, immunofluorescent detection, which has a higher level of sensitivity, was performed to identify the distribution of H3K9me3. Unfortunately, the Bouins fixed human fetal gonads displayed strong non-specific background immunostaining. NBF fixed human fetal gonads however displayed a clear pattern of H3K9me3 staining. Thereafter, by immunofluorescence, the distribution of H3K9me3 was detected in NBF fixed human gonads across different gestations.

A distinctly gender-specific distribution of H3K9me3 was observed in NBF fixed human fetal gonads (Fig 3.9 and 3.10). In human fetal ovary, the staining of H3K9me3 was restricted to the ovarian germ cells and progressively increased with developing gestations (Fig 3.9). On the other hand, H3K9me3 was present at low levels in testicular germ cells across all examined stages (Fig 3.10).

At 9wga, H3K9me3 was present at a low level in ovarian PGCs (White arrow, Fig 3.9A), and appeared as 2-3 punctate spots over the nucleus of H3K9me3-positive PGCs (Insert panel, Fig 3.9A). At 15wga, after the initiation of meiosis, the more mature ovarian germ cells located towards the middle of the ovary started to display intense H3K9me3 staining (White arrow, Fig 3.9C). At 17wga, this pattern became more noticeable, with most of the centrally-located ovarian germ cells being H3K9me3-positive, and only a thin band of cells at the very periphery of the ovary displaying no staining (White arrow, Fig 3.9D). During the later gestations, H3K9me3 was found to distribute evenly throughout the nucleus of the mature ovarian germ cells (Insert panel, Fig 3.9C and D). Notably, H3K9me3 was undetectable in ovarian somatic cells at all examined gestations (Figure 3.9A, C and D). The absence of primary antibody was used as negative control (Fig 3.9 B).

In human fetal testicular germ cells, levels of H3K9me3 were low across all examined gestations. This repressive histone mark was restricted to punctate spots within the germ cell nucleus through all detected gestations (White arrow, Fig 3.10A-C). At 9wga, H3K9me3 was more apparent in human fetal testicular germ cells than those in the ovary at the same developmental stage, but remained restricted to distinct foci within germ cell nucleus (White arrow, Fig 3.10A). In the 2nd trimester, H3K9me3-staining was restricted to 1-2 distinct foci (White arrow, Fig 3.10B and C). The H3K9me3-negative testicular germ cells were largely restricted to the periphery of the testicular cords (White arrow, Fig 3.10B and C). Dual immunostaining with the mature germ cell marker VASA confirmed the population of cells with little or punctate H3K9me3 staining to be germ cells (White arrow, Fig 3. 10D). The negative control, which was absence of primary antibody, is shown in Fig 3.10 C, inserted panel.

Different from the ovarian somatic cells, H3K9me3 was detectable in the testicular somatic cells. At 9wga, testicular somatic cells were initially H3K9me3-negative. From 16wga onwards, Sertoli cells were generally H3K9me3-positive (White arrowhead, Fig 3.10B and C), while the peritubular myoid cells were all H3K9me3-negative. Notably, Leydig cells displayed H3K9me3 staining at 16wga (Fig 3.10B white arrowhead), but were negative for H3K9me3 at 20wga (Fig 3.10C). The negative control was shown in the insert panel in Figure 3.10 C.

H3K9me3 was also detected in the postnatal ovaries (from 3-year-old to 32-year-old) to determine whether the H3K9me3 remained in mature oocytes even after birth (Fig 3.11). The mature germ cell marker VASA was used to visualize oocytes (Green, Fig 3.11). In these postnatal ovaries, follicles in different development stages were observed. Primordial follicles with an oocyte surrounded by a single layer of squamous granulosa cells were observed in the 3-year-old ovary (Fig 3.11 A and B). The oocytes became enlarged with the maturation of follicles. In Fig 3.11F, a primary follicle with enlarged and cuboidal granulosa cells is shown. Preantral follicles with more than one layer of granulosa cells are shown in Fig 3.11 C, D and E. In all these postnatal follicles, the oocytes displayed punctuate H3K9me3 staining (Red, Fig 3.11). Meanwhile, nearly all the granulosa cells around the oocytes were H3K9me3-positive in the postnatal ovaries (Red, Fig 3. 11).

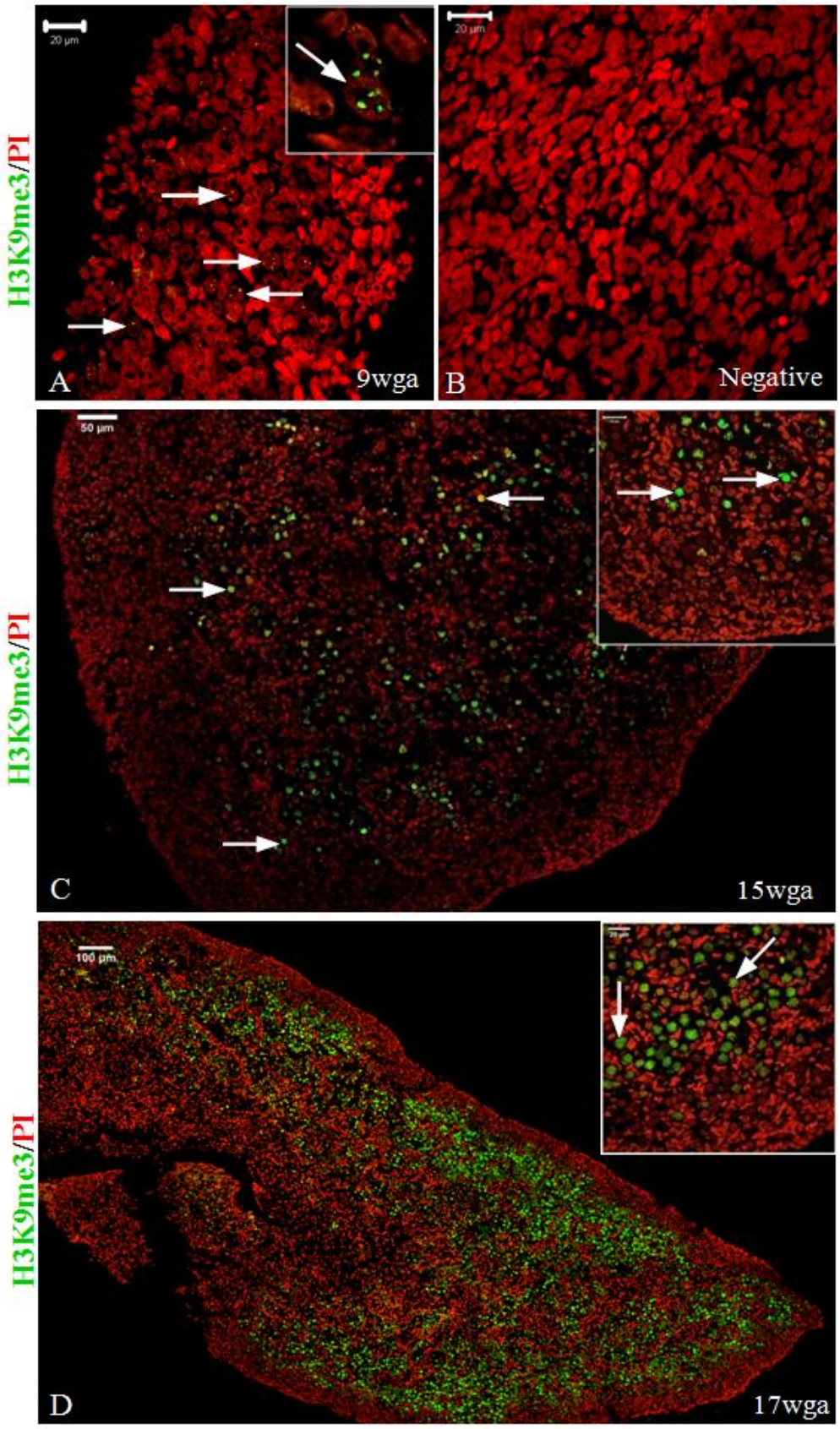

Figure 3.9 Distribution of H3K9me3 in NBF fixed human fetal ovaries. **A**, 9wga human fetal ovarian section; **insert panel** in **A**, higher power image of H3K9me3-positive PGCs; **B**,

negative control; **C**, 15wga; **insert panel** in **C**, higher power image of 15wga human fetal ovary; **D**, 17wga; **insert panel** in **D**, higher power image of 17wga human fetal ovary. The PI counterstaining is present in Red, while the H3K9me3 staining is present in Green. White arrow indicates H3K9me3-positive germ cells. The scale bars equal to 20μm in A and B; 50μm in C; 100μm in D.

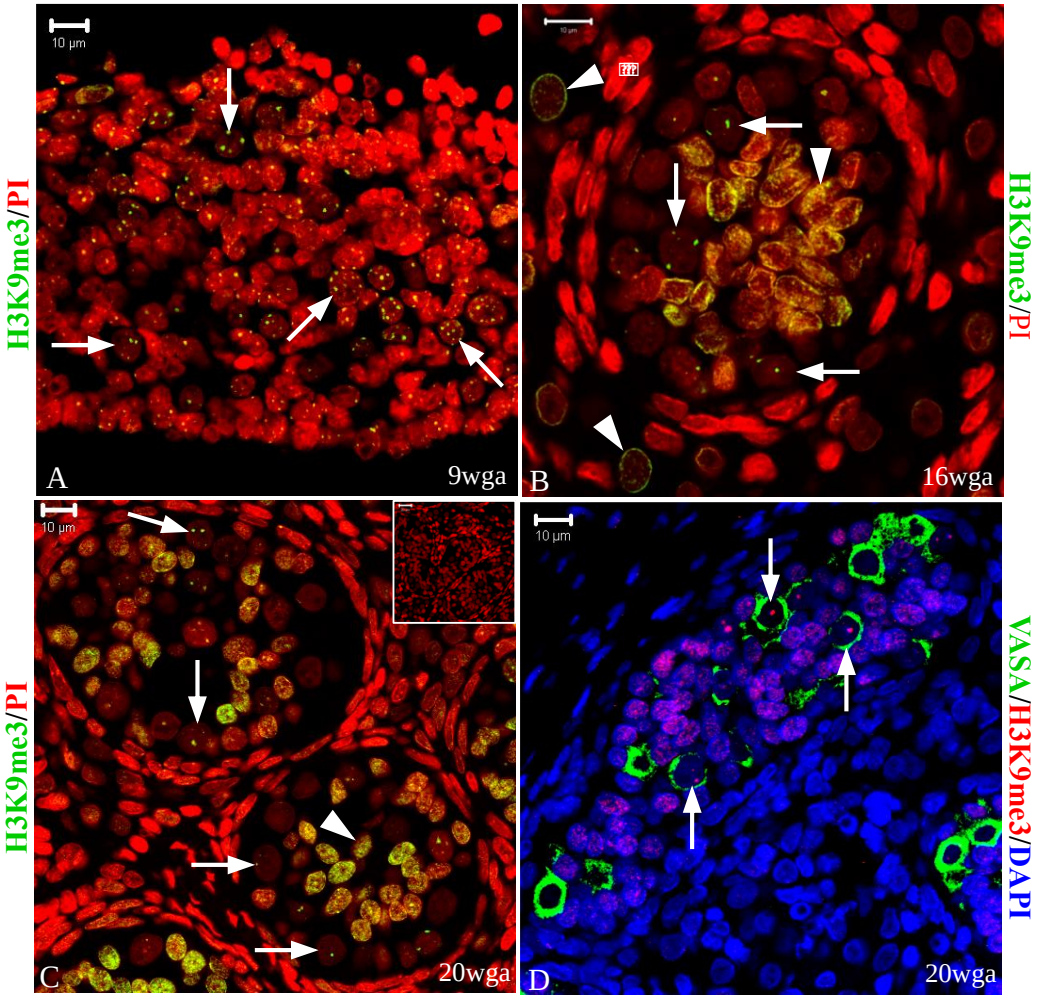

Figure 3.10 Distribution of H3K9me3 in NBF fixed human fetal testes. A, 9wga human fetal testicular section; **B**, 16wga human fetal testicular section; **C**, 20wga human fetal testicular section; insert panel in **C**, negative control; **D**, double-immunostaining of VASA and H3K9me3 in 20wga human fetal testicular sections. The PI counterstaining is shown in Red, while the H3K9me3 staining is shown in Green. White arrows represent H3K9me3-positive germ cells, while white arrowhead represents H3K9me3-positive somatic cells. The scale bars equal to 10μm in A, B, C and D panels.

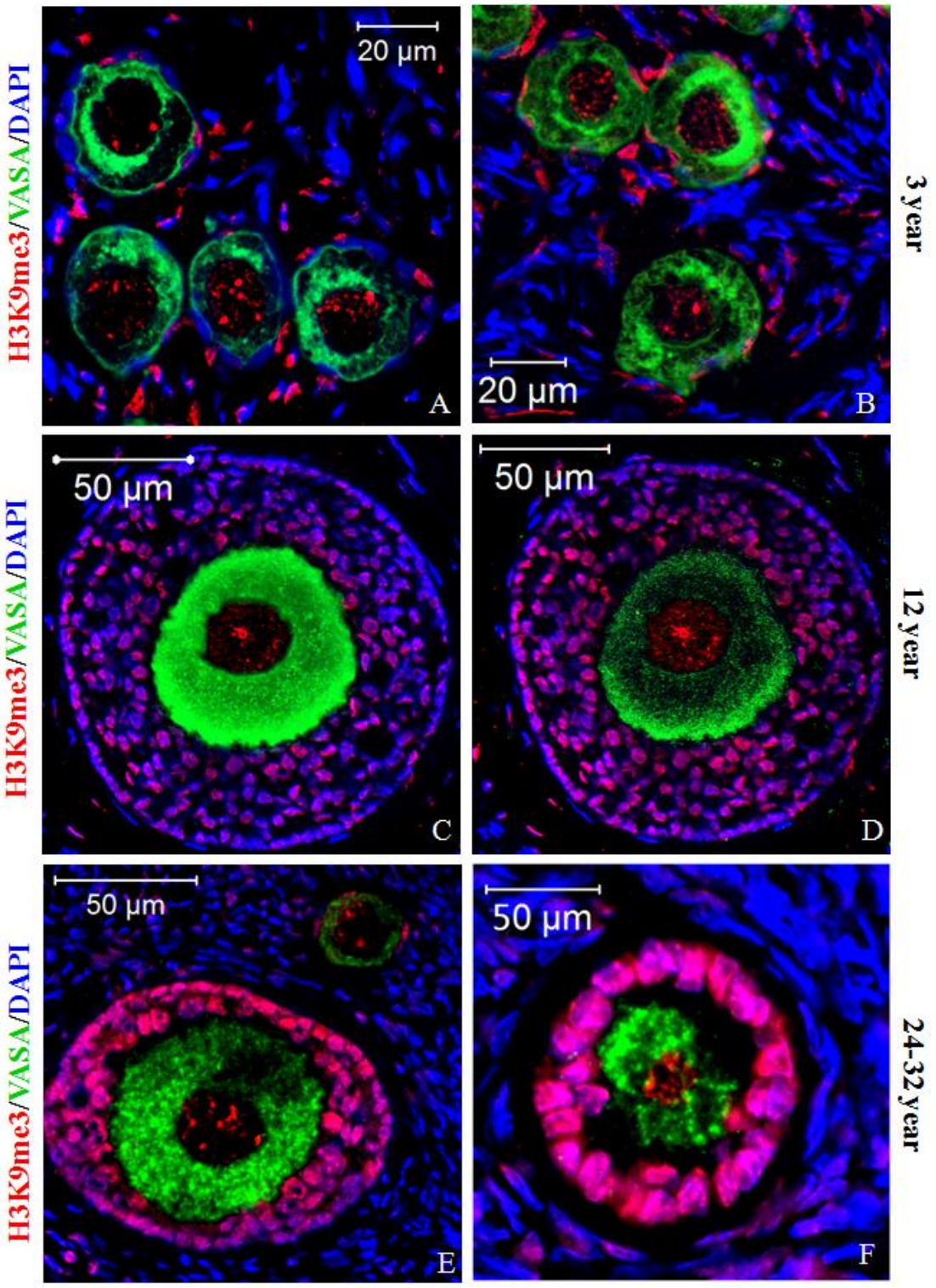

Figure3.11 Distribution of H3K9me3 in NBF fixed human postnatal ovaries. A and **B**, primordial follicles in 3-year-old human ovary; **C** and **D**, preantral follicles in 12-year-old human ovary; **E**, preantral follicle in 24-year-old human ovary; **F**, primary follicle in 32-year-old human ovary. The DAPI nuclear counterstaining was shown in Blue, H3K9me3 staining was shown in Red, and VASA staining was showed in Green. The scale bars equal to 20μm in A and B panels, 50μm in C, D, E and F panels.

3.2.7 Distribution of H3K9ac in Bouins fixed human fetal germ cells

Another active histone mark H3K9ac was also detected in Bouins fixed human fetal gonads across different gestations. In Bouins fixed human fetal ovarian and testicular germ cells, levels of H3K9ac were found to decrease with increasing gestations (Fig 3.12 and 3.13).

At 9wga, all the undifferentiated PGCs displayed nuclear H3K9ac staining (Black arrow, Fig 3.12A and B). By 14wga, the more differentiated germ cells located at the center of the ovary were negative for H3K9ac staining (White arrow, Fig 3.12D-F) whilst the smaller undifferentiated germ cells at the periphery of the ovary retained this modification (Black arrow, Fig 3.12D-F). At 18wga, there were only very few undifferentiated ovarian germ cells displaying H3K9ac staining (Black arrow, Fig 3.12G); all of the mature germ cells were H3K9ac-negative (White arrow, Fig 3.12G-I). Oocytes in primordial follicles also were H3K9ac-negative (Asterisk, Fig 3.12I).

At 9wga, most of the ovarian somatic cells were H3K9ac-negative (White arrowhead, Fig 3.12A and B). The numbers of H3K9ac-positive somatic cells increased as the development of fetal ovary; by 18wga, most of the ovarian somatic cells were H3K9ac-positive (Black arrowhead, Fig 3.12F-H). Pre-granulosa cells in primordial follicles were mostly H3K9ac-positive (Black arrowhead, Fig 3.12I) although some immuno-negative pre-granulosa cells could be detected (White arrowhead, Fig 3.12I). Human fetal ovarian sections cultured with non-immune serum were used as a negative control (Fig 3.12C).

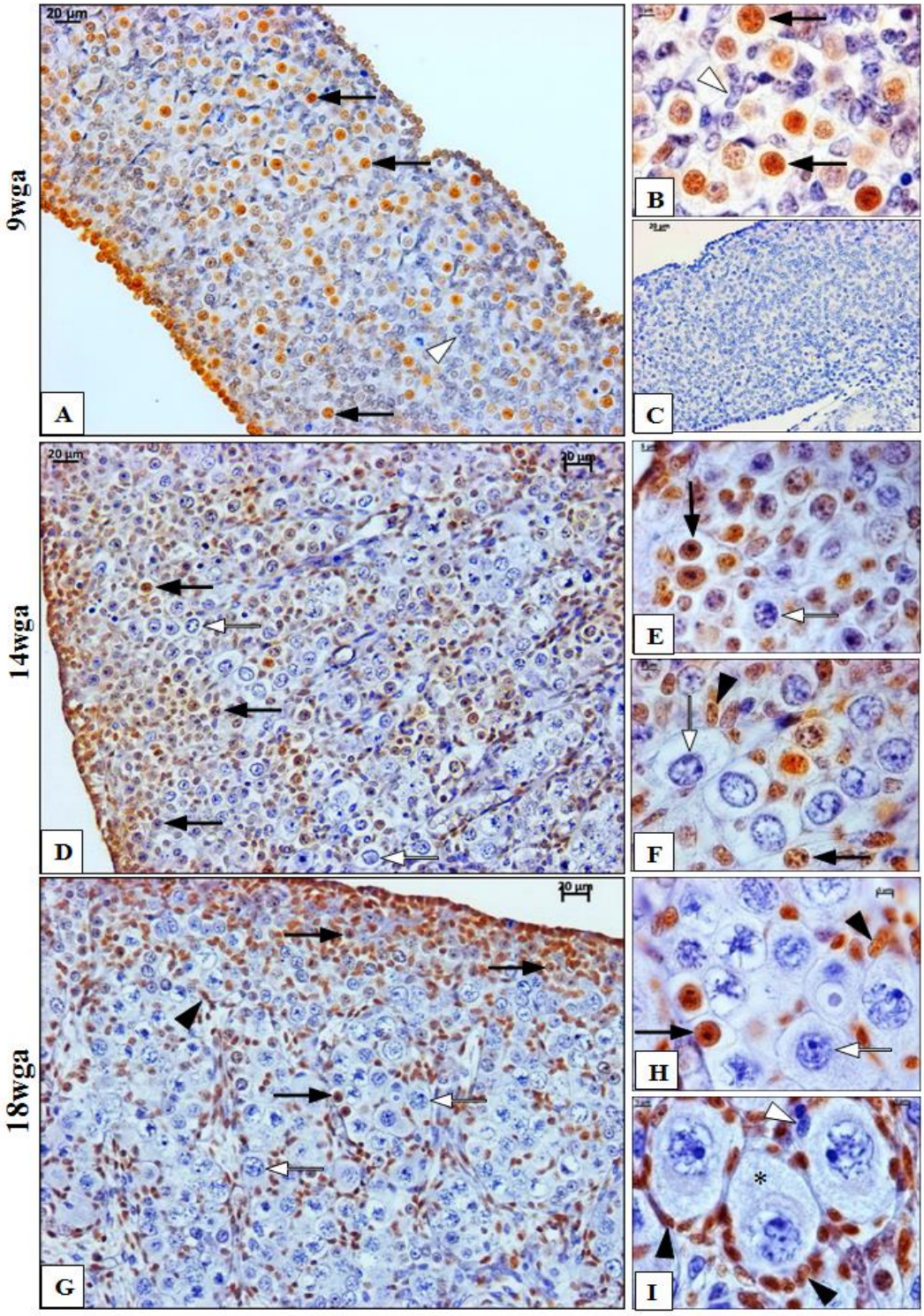

Figure 3.12 Distribution of H3K9ac in Bouins fixed human fetal ovaries. A and **B**, 9wga human fetal ovarian sections; **C**, negative control; **D**, 14wga human fetal ovarian sections; **E**, the edge part of ovary; **F**, the middle part of ovary; **G**,**H** and **I**, 18wga human fetal ovarian sections. Black and white arrows represent H3K9ac-positive and negative germ cells, respectively. Black and white arrowheads represent H3K9ac-positive and negative somatic cells, respectively. The asterisk represents the primordial follicle. The scale bars equal to 5µm in B, E, F, H and I; 20µm in A, C, D and G.

The changes of H3K9ac distribution were similar in Bouins fixed human fetal testes (Fig 3.13A-C). Almost all the testicular PGCs were H3K9ac-positive at 9wga (Black arrow, Fig 3.13A). However, during 2nd trimester most of the testicular germ cells at the periphery of cords had lost H3K9ac staining (White arrow, Fig 3.13B and C), while a sub-population of testicular germ cells at the center of cords retained this modification (Black arrow, Fig 3.13B and C).

The number of H3K9ac-positive somatic cells increased with increasing gestation (Black arrowhead, Fig 3.13). At the later gestations, most Sertoli cells were H3K9ac-positive (Black arrowhead, Fig 3.13B and C), although few of them displayed weak H3K9ac staining (White arrow head, Fig 3.13C). During these stages, the peritubular myoid cells and Leydig cells were also predominantly H3K9ac-positive. No staining was detected in the negative controls (Fig 3.13D).

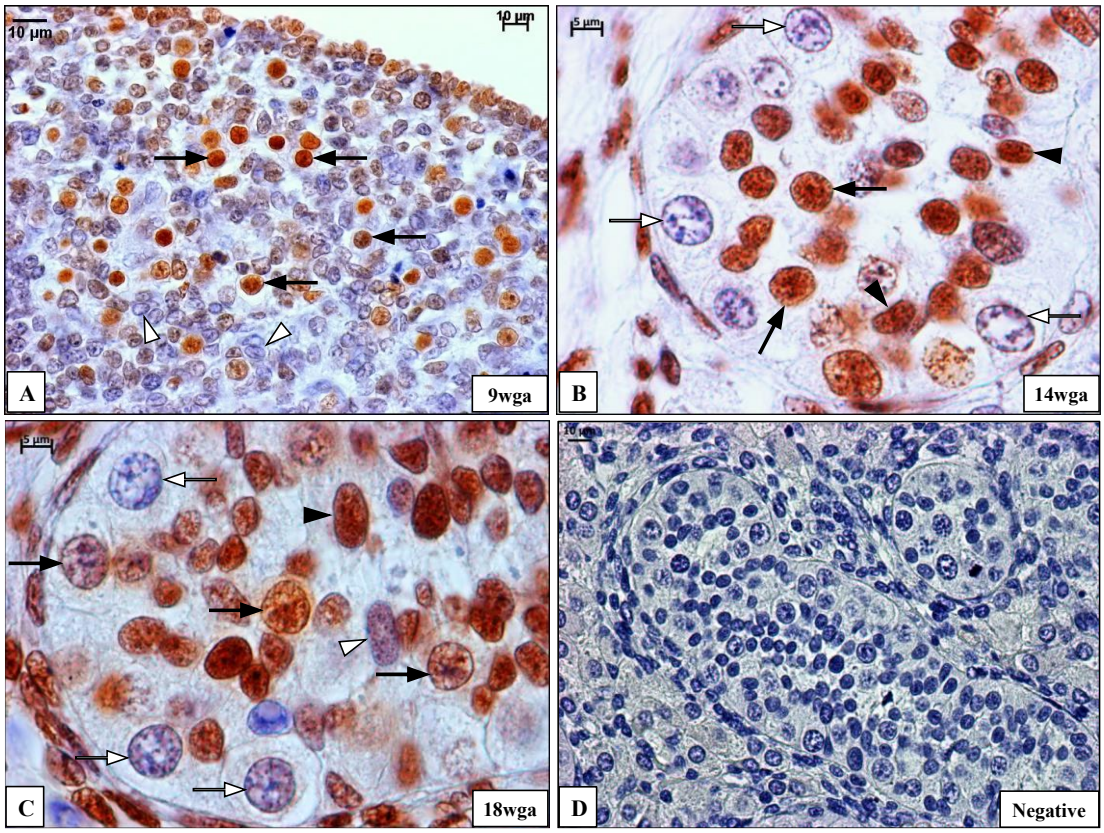

Figure3.13 Distribution of H3K9ac in Bouins fixed human fetal testes. A, 9wga human fetal testicular section; **B**, 14wga human fetal testicular section; **C**, 18wga human fetal testicular section; **D**, Negative control. Black and white arrows represent H3K9ac-positive and negative germ cells, respectively. While black and white arrowheads represent H3K9ac-positive and negative somatic cells, respectively. The scale bars equal to 5µm in B and C panels; 10µm in A and D panels.

In the Bouins fixed human fetal gonads, H3K9ac appeared to be restricted to the undifferentiated germ cells. In order to further confirmed this,

dual-immunohistochemistry with the immature germ cell (PGC) marker C-KIT was performed in Bouins fixed human fetal gonads, alongside co-localization with a mature germ cell marker VASA (Anderson et al., 2007; Castrillon et al., 2000; Kerr et al., 2008a; Kerr et al., 2008b). In Bouins fixed human fetal gonads, the immature germ cell (PGC) marker C-KIT located in the membrane of undifferentiated germ cells (Brown, Fig 3.14 A and B). The H3K9ac-positive ovarian and testicular germ cells in the Bouins fixed human fetal gonads displayed intense C-KIT staining (Black arrow, Fig 3.14 A and B). On the other hand, cytoplasmic staining of VASA was observed in the center of ovary or the edge of testicular cords (White arrow, Fig 3.14 C and D). H3K9ac, which was seen to stain the immature germ cells on the periphery of the ovary or in the center of the testicular cords, did not co-localized with VASA in Bouins fixed human fetal ovary or testis (White arrow, Fig 3.14 C and D).

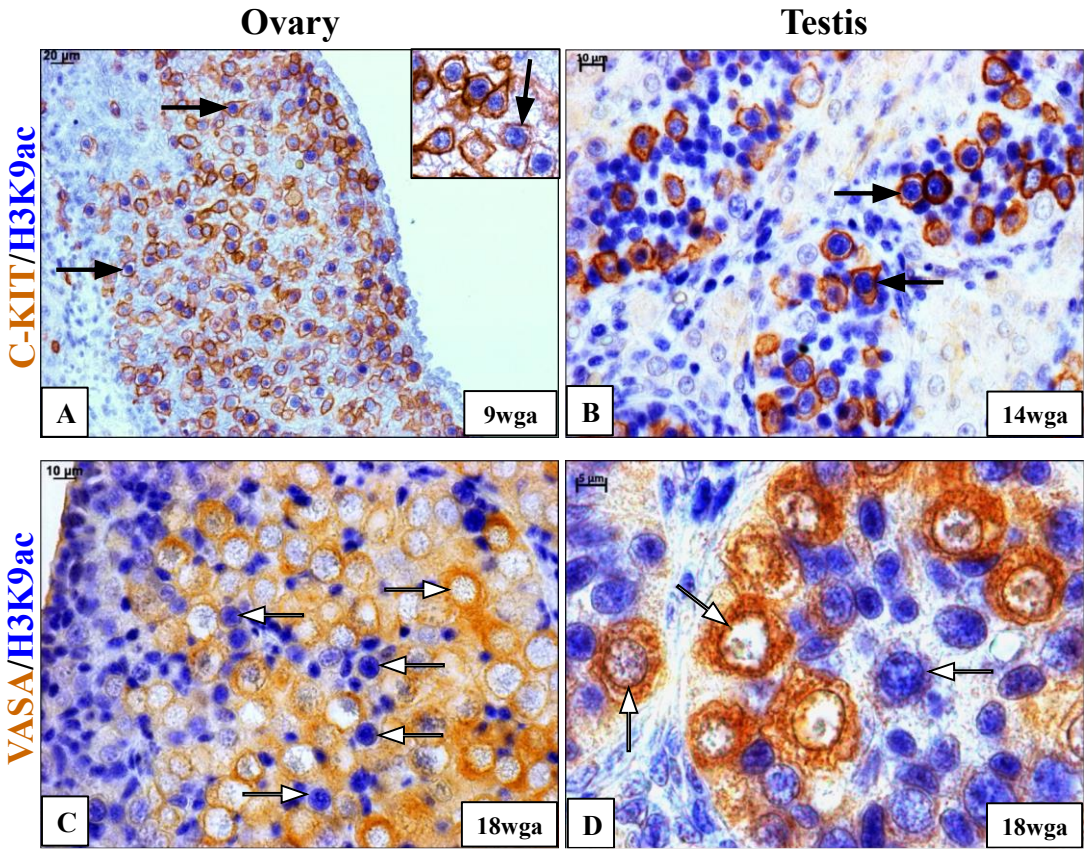

Figure 3.14 Dual-immunohistochemistry of H3K9ac with immature germ cell marker C-KIT and the mature germ cell marker VASA in Bouins fixed human fetal ovaries and testes. A, co-localization of H3K9ac and C-KIT at 9wga human fetal ovary; **B**, co-localization of H3K9ac and C-KIT at 14wga human fetal testis; **C**, double-immunostaining of H3K9ac and VASA at 18wga human fetal ovary; **D**, double-immunostaining of H3K9ac and VASA at 18wga human fetal testis. The staining of C-KIT and VASA were showed in brown, while the staining of H3K9ac was present in blue. Black arrows represent the co-localization of H3K9ac and C-KIT, while white arrows represent the non-co-localization of H3K9ac and VASA. The scale bars equal to 5µm in D panel; 10µm in B and C panels, 20µm in A panel.

3.2.8 The distribution of H3K9ac in NBF fixed human fetal and postnatal ovaries

The observations in Bouins fixed human fetal gonads showed that H3K9ac was restricted to the smaller and undifferentiated germ cells. In order to identify whether different fixatives affected the antigen-binding ability, the H3K9ac antibody was also used in NBF fixed human ovaries (Fig 3.15).

Surprisingly, the distribution of H3K9ac was different between Bouins fixed and NBF fixed human fetal ovaries at the same gestations. In bouins fixed human fetal ovaries, the H3K9ac staining was only observed in the smaller undifferentiated germ cells during 2nd trimester (14wga and 18wga) (Fig 3.12D-I). Contrarily, in the NBF fixed human fetal ovaries, nearly all the ovarian germ cells, including the smaller undifferentiated germ cells at the periphery of the ovary and the more differentiated germ cells located at the center of the ovary, were H3K9ac-positive during 2nd trimester (14wga and 18wga)(Black arrow, Fig 3.15A-F). The distribution of H3K9ac was also identified in the NBF fixed human postnatal ovaries (Fig 3.15 G-I). The mature oocytes in the NBF fixed postnatal ovaries displayed intense H3K9ac staining also (Fig 3.15 G-I). Two totally different distributions of H3K9ac were observed in Bouins and NBF fixed human fetal ovaries. The mature fetal ovarian germ cells in the bouins fixed human fetal ovaries were H3K9ac-negative; while the mature ovarian germ cells in the NBF fixed human fetal ovaries were H3K9ac-positive.

Difference of H3K9ac staining was also observed in the ovarian somatic cells. At the 2nd trimester, most of the mesenchymal somatic cells, which displayed H3K9ac staining in the bouins fixed human fetal ovaries (Fig 3.12), were negative for H3K9ac in NBF fixed human fetal ovaries (White arrowhead, Fig 3.15A-F). The pre-granulosa and granulosa cells in the NBF fixed human ovaries were H3K9ac-positive (Black arrowhead, Fig 3.15F-I).

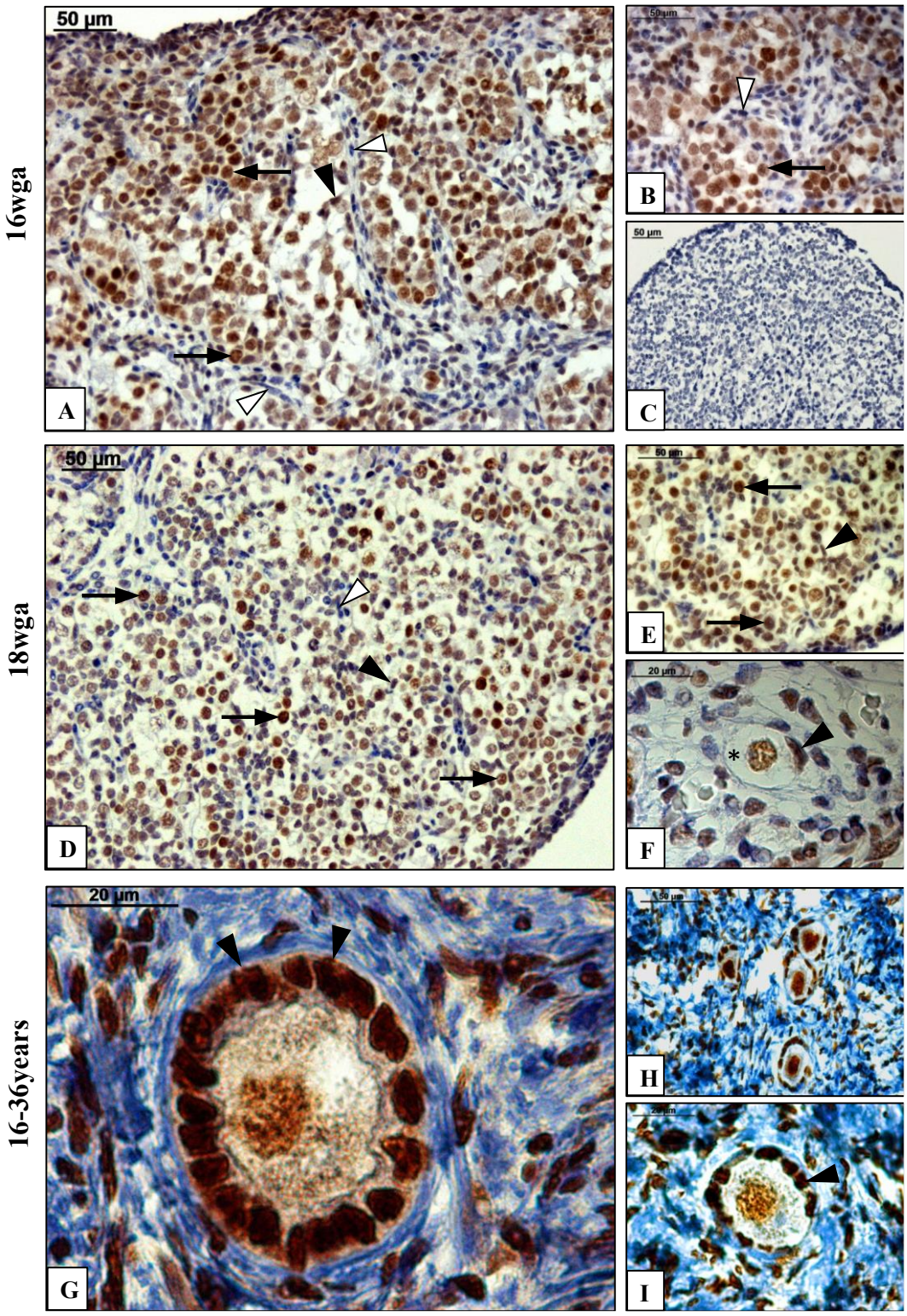

Figure 3.15 Distribution of H3K9ac in NBF fixed human ovaries. A and **B**, 16wga human fetal ovarian sections; **C**, negative control; **D**, **E** and **F**, 18wga human fetal ovarian sections; **G**, **H** and **I**, 16~36-year-old human postnatal ovarian sections. Black arrows represent H3K9ac-positive germ cells. While black and white arrowheads represent H3K9ac-positive and negative somatic cells, respectively. The asterisk represents the primordial follicle. The scale bars equal to 20µm in F, G and I panels; 50µm in A, B, C, D, E and H panels.

3.3 *Discussion*

3.3.1 Distinct localization of H3K9ac, H3K4me3, H3K9me2, H3K9me3 and H3K27me3 in human seminoma-derived TCam-2 cells

In TCam-2 cells, the distributions of H3K9ac, H3K4me3, H3K9me2, H3K9me3 and H3K27me3 were different from each other (Fig 3.1). However, the distribution of these five histone marks were consistent with what has been shown in the antibody datasheets (Abcam, H3K9ac; Abcam, H3K9me2; Abcam, H3K9me3; CellSignaling, H3K4me3; CellSignaling, H3K27me3); with the active H3K9ac and H3K4me3 (Barski et al., 2007; Nishida et al., 2006) being excluded from the condensed chromocenters; the silent euchromatic histone mark H3K9me2 preferentially localized to the euchromatin rather than the heterochromatin (Rice et al., 2003); the heterochromatic histone marks H3K9me3 and H3K27me3 (Boyer et al., 2006; Lachner et al., 2001) being accumulated preferentially in the inactive heterochromatin domains. All these observations in TCam-2 cells suggest that these five histone marks localized as expected, indicating their antigen-binding specificities.

3.3.2 Dynamic changes of H3K4me3, H3K27me3, H3K9me2, and H3K9me3 in human fetal gonads are different from the changes in mouse

The studies in human fetal gonads here showed that the global levels of H3K4me3, H3K27me3, H3K9me2, and H3K9me3 underwent dynamic changes in the post-migratory human fetal germ cells (Fig 3.16). The histone modifications mentioned above were strikingly different from those reported in mouse fetal germ cells (Hajkova et al., 2008; Seki et al., 2005). Compared to the progressive decrease of H3K4me3 and H3K27me3 in human fetal gonads, methylated H3K4 and H3K27me3 dynamically fluctuated in mouse PGCs (Hajkova et al., 2008; Seki et al., 2005). Methylated H3K4 significantly increased in mouse PGCs around the time of their arrival at the genital ridge, and subsequently decreased to the same levels found in the surrounding somatic cells by E12.5 (Hajkova et al., 2008; Seki et al., 2005). Levels of H3K27me3 in mouse germ cells increased after E8.0, reached a maximum level by E9.5, and briefly decreased between E11.0-E12.0, afterwards, increased again (Seki et al., 2005). Different to the peak expression of H3K9me2 in human fetal ovarian germ cells, H3K9me2 had already been erased in mouse nascent PGCs soon after germ cell specification (Hajkova et al., 2008; Seki et al., 2005). Unlike the increasing levels of H3K9me3 in human fetal ovarian germ cells, H3K9me3 transiently decreased in mouse germ cells around E11.5–E12.0, and were re-elevated afterwards (Hajkova et al., 2008; Seki et al., 2005). The findings above indicate that the extensive changes of histone modifications in fetal germ cells are strikingly different between human and mouse, suggesting that the species differences in histone modifications do exist between human and mouse, and hence, further emphasizing the importance of human study.

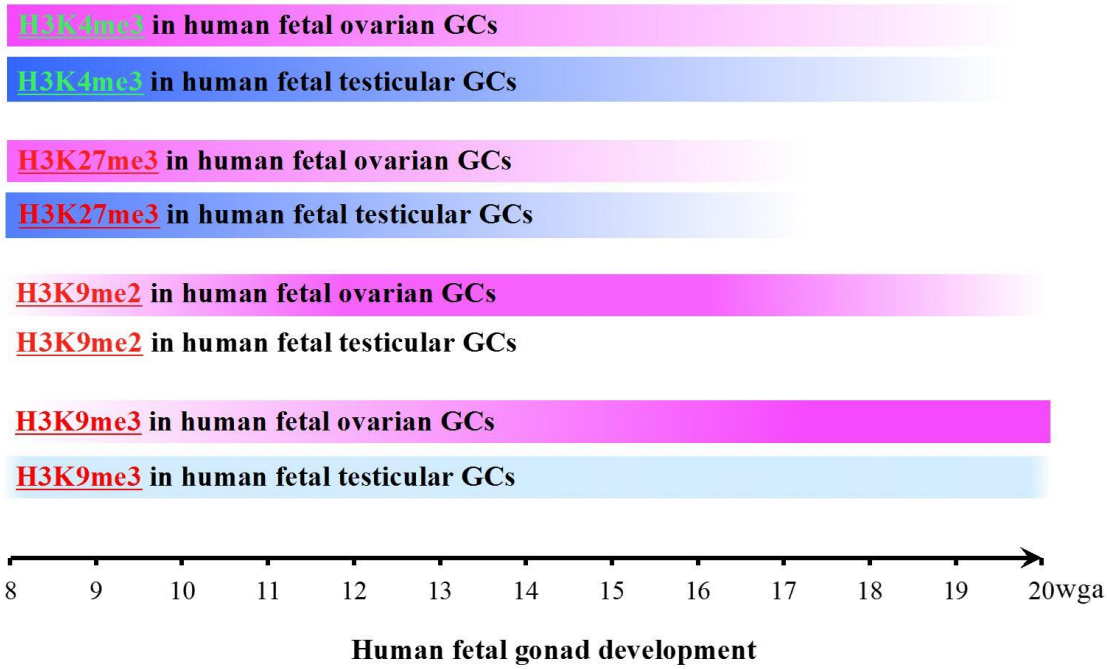

Figure 3.16. Dynamic changes of H3K4me3, H3K27me3, H3K9me2 and H3K9me3 in human fetal germ cells across the gestational period 8-20wga. Levels of H3K4me3 and H3K27me3 were progressively decreased in human fetal ovarian and testicular germ cells with maturation of germ cells. In human fetal ovarian germ cells, level of H3K9me2 was low at 9 and 19wga.Shortly after the onset of meiosis, the levels of H3K9me2 peaked in human ovarian germ cells at around 15wga. On the other hand, H3K9me2 was undetectable in human fetal testicular germ cells at all detected gestations. For the case of H3K9me3, level of H3K9me3 was progressively increased with germ cell maturation in human fetal ovarian germ cells. Contrarily, human fetal testicular germ cells displayed weak H3K9me3 expression at all detected stages. The pink bars represent the levels of histone marks in human fetal ovarian germ cells (GCs), while the blue bars represent the levels of histone marks in human fetal testicular germ cells (GCs).

3.3.3 The restriction of H3K4me3 and H3K27me3 in smaller and undifferentiating human fetal germ cells may be associated with the expression of pluripotency-associated genes and the repression of developmental genes in early stages of germ cell development

In previous studies, H3K4me2/3 was observed in a small proportion of human fetal testicular germ cells from 21wga onwards (Almstrup et al., 2010). In the studies here, the distribution of H3K4me3 was extended to different gestations in both human fetal ovary and testis. However, we did not investigate human fetal gonads from 20wga onwards due to lack of availability of samples.

The studies present here showed that H3K4me3 was restricted to the smaller fetal germ cells and declined in human fetal germ cells as ovary and testis differentiation. Previous study in undifferentiated human ESCs showed that high levels of H3K4me3

have been found to be involved in the maintenance of the pluripotency-related genes *POU5F1*, *NANOG* and *SOX2* (Pan et al., 2007). Thus the restriction of H3K4me3 in the smaller and undifferentiating human fetal germ cells may be associated with the expression of pluripotency-associated genes.

The study by Gkountela and colleagues showed that the repressive histone mark H3K27me3 was enriched in human early PGCs in both sexes (Gkountela et al., 2013). From 11wga onwards, H3K27me3 was globally erased from human fetal PGCs (Gkountela et al., 2013). Consistent with the previous findings, the study present here also showed high levels of H3K27me3 in early human PGCs. Similarly, in the study here, the reduction in H3K27me3 was initiated in human fetal germ cells by 14wga, which is in accordance with what has been observed by Gkountela *et al*. Gkountela *et al* also reported that the testicular PGCs regained H3K27me3 at around 17wga. However, in Almstrup et al's study, H3K27me3 was undetectable in testicular germ cells between 21wga and 24wga (Almstrup et al., 2010). In the study here, re-expression of H3K27me3 was also not detected in testicular germ cells at later gestations. These different findings in later fetal testicular germ cells may be associated with the different sensitivities in DAB immunohistochemistry used by Almstrup and here, versus the fluorescent detection used by Gkountela.

In undifferentiated ESCs, H3K27me3 has been found to play an important role in repressing developmental genes; the erasure of H3K27me3 led to de-repression of these developmental genes and initiated the differentiation of ESCs (Boyer et al., 2006; Lee et al., 2006). The restriction of H3K27me3 in the undifferentiated fetal germ cells in human may be associated with the repression of developmental genes in early stages of germ cell development.

The activating H3K4me3 and repressing H3K27me3 here displayed similar trends in human fetal germ cells, they both declined during germ cell development and were both restricted to the smaller, undifferentiated germ cells. In mouse ESCs, H3K4me3 and H3K27me3 have been found to co-exist at the same genomic domains, which are referred to as bivalent domains (Bernstein et al., 2006). The co-existence of H3K4me3 and H3K27me3 in the undifferentiated ESCs are considered to poise timely activation of developmental genes (Bernstein et al., 2006; Mikkelsen et al., 2007). In the absence of differentiation signals, developmental genes were maintained in a temporary silent state by the presence of both H3K27me3 and H3K4me3 in undifferentiated ESCs. Though silent, the genes present in these bivalent domains can become activated immediately in response to downstream developmental signals, and do not require epigenetic reprogramming (Bernstein et al., 2006; Mikkelsen et al., 2007). Upon differentiation, H3K27me3 was removed while H3K4me3 was retained, leading to the expression of these bivalent genes (Boyer et al., 2006; Lee et al., 2006). In contrast, other bivalent genes, in which H3K4me3 was erased and H3K27me3 was retained, remained silenced (Bernstein et al., 2006). Co-modification of the

development-associated genes by the bivalent histone marks H3K27me3 and H3K4me3 have also been observed in undifferentiated human ESCs (Pan et al., 2007). Inferring from the knowledge above, the similar trend of H3K4me3 and H3K27me3 in human fetal germ cells may be associated with the bivalent modifications of developmental genes in early germ cells, which need further inverstigation.

3.3.4 The sex-specific distribution of H3K9me2 and H3K9me3 in human fetal germ cells may be associated with the suppression of the pluripotency-associated genes and the onset of germ cell differentiation and /or meiosis

In Almstrup *et al*'s study, transcriptional repressive mark H3K9me2 was undetectable in human testicular germ cells between 21wga and 24wga (Almstrup et al., 2010). Due to lack of availability of samples, human fetal gonads from 20wga onwards were not investigated. In the present studies, the distribution of H3K9me2 was investigated in both human fetal ovary and testis across different gestations and showed a sex-specific distribution.

A previous study in differentiating murine ESCs indicated that H3K9me2 contributed to the suppression of pluripotency-associated gene *Pou5f1* (Feldman et al., 2006). In addition, another study in murine germ cells showed that G9a, a H3K9 mono- and dimethylatransferase, played an important role in meiotic prophase (Tachibana et al., 2007). According to the previous findings and the observation of H3K9me2 here, the specific increase of H3K9me2 in the early 2nd trimester human ovarian germ cell may be associated with the suppression of the pluripotency-associated genes and the initiation of meiosis.

In Bartkova *et al*'s study, the distribution of H3K9me3 was identified in human testicular germ cells, which displayed a very low level of H3K9me3 during 16-24wga (Bartkova et al., 2010). In the study here, the human testicular germ cells also displayed low levels of H3K9me3 at all examined stages. On the other hand, H3K9me3 was found to be restricted to the more mature ovarian germ cells.
Previous study in mice showed that H3K9 trimethyltransferase Suv39h and its modified chromatin H3K9me3 are critical for germ cell meiosis (Peters et al., 2001). Double deletions of *Suv39h1* and *Suv39h2* in mice cause the absence of H3K9me3 and abnormal meiosis in both male and female (Peters et al., 2001). On the basis of the previous findings in mice and the observation here, the accumulation of H3K9me3 in mature human fetal ovarian germ cells may be associated with the onset of germ cell differentiation and /or meiosis in humans.

3.3.5 The distribution of H3K9ac is different between Bouins and NBF fixed human fetal gonads at comparable gestations

In Bouins fixed human fetal testes, levels of H3K9ac were reduced in testicular germ cells as they differentiated. The observations here were different from the findings in Almstrup *et al*'s study, in which most of the NBF fixed gonocytes were positive for

H3K9ac at later gestations (Almstrup et al., 2010). H3K9ac was also decreased in Bouins fixed human fetal ovarian germ cells with differentiation. During 2nd trimester, most of Bouins fixed human fetal ovarian germ cells were negative for H3K9ac; only the smaller, undifferentiated PGC-like cells displayed this histone mark. Contrarily, nearly all of the NBF fixed human fetal ovarian germ cells displayed H3K9ac-staining at these later gestational ages.

When an immunostaining is performed, an ideal fixation can immobilize antigens and allow the antibodies to bind the antigens. The fixative is determined by the balance between morphological preservation and accessibility of antigen-antibody binding. Bouins was usually used for fetal gonads as it usually gave both good morphological and antigenicity preservation. NBF also gave good preservation of antigen, but usually had an inferior preservation of morphology. The different distributions of H3K9ac in Bouins and NBF fixed human fetal suggested that fixation may affect the cellular structure or accessibility of antigen-antibody binding. It cannot determine which fixation method gave accurate results for H3K9ac in human gonads on the basis of these studies. Thus, the results of H3K9ac here were unreliable and further investigation is required.

The distribution of H3K9ac in human fetal germ cells can be further detected in future work. In further studies, human fetal gonads could be disaggregated into a single-cell suspension by mechanical and enzymatic dispersion (Childs et al., 2010; Coutts et al., 2008). The cell suspension, which consists of both somatic and germ cells, can be fluorescently labeled with PGC marker OCT4 and mature germ cell marker VASA. The OCT4 or VASA-labeled human fetal germ cells can be sorted from the unlabeled somatic cells by Fluorescence-Activated Cell Sorting (FACS) (Mozdziak et al., 2005; Woods and Tilly, 2013). The isolated human fetal germ cells can be collected for protein extraction and western blotting can be performed to determine the levels of H3K9ac in these isolated fetal germ cells. These detections can be performed in human fetal gonads across different gestations, giving a further robust method for assessing dynamic changes of H3K9ac in human fetal germ cells.

Chapter4. Dynamic reprogramming of DNA methylation during human germ cell development

4.1 *Introduction*

DNA methylation is a heritable epigenetic mark which is associated with transcriptional silencing (Bird and Wolffe, 1999). In multicellular eukaryotes, DNA methylation takes place at the fifth carbon of the cytosine pyrimidine ring and its outcome is 5mC (Su et al., 2011). In mammals, DNA methylation has been found to play an essential role in numerous biological processes (Bird, 2002; Egger et al., 2004; Stringer et al., 2013). For sexual reproduction, mouse germ cells undergo dynamic changes of DNA methylation during development. (Borgel et al., 2010; Hajkova et al., 2002; Maatouk et al., 2006b; Seisenberger et al., 2012; Shen et al., 2007; Weber et al., 2007; Yamaguchi et al., 2013). At the early embryonic stage, PGC precursor cells display similar DNA methylation levels with the somatic epiblast cells. At this point, the pluripotency genes and CpG island-associated germline-specific genes are tightly repressed by DNA methylation in the PGC precursor cells (Borgel et al., 2010; Maatouk et al., 2006b; Seisenberger et al., 2012; Shen et al., 2007; Weber et al., 2007). In order to erase somatic cell fate, generate germ cell potency and activate key pluripotency markers, genome-wide DNA demethylation occurs in early mouse PGCs from E8.5 to E13.5 (Hajkova et al., 2002; Seisenberger et al., 2012; Yamaguchi et al., 2013). During the process of DNA demethylation in mouse germ cells, passive DNA demethylation, which is DNA replication-dependent, are identified to be an essential mechanism (Kagiwada et al., 2013); meanwhile, TETs and 5hmC are also believed to be involved (Hackett et al., 2013; Yamaguchi et al., 2013). After sex determination, DNA methylation is re-established in mouse germ cells in a sex-specific pattern (Abe et al., 2011; Saitou and Yamaji, 2012; Sasaki and Matsui, 2008). In mouse testicular germ cells, levels of 5mC increase from E15.5 onwards (Abe et al., 2011; Kota and Feil, 2010). DNA de novo methylation in mouse testicular germ cells is completed at birth and then maintained throughout many cycles of mitotic divisions before the cells enter into meiosis (Davis et al., 2000). In contrast, DNA de novo methylation is not initiated until after birth in mouse ovarian germ cells, which are arrested in prophase of meiosis I (Abe et al., 2011; Kota and Feil, 2010).

According to the observation in mouse germ cells, the human germ cells may also undergo genome wide reprogramming of DNA methylation to regain the underlying totipotency in PGCs and prepare for the subsequent germ cell-specific developmental process. Therefore, it is also important to understand the reprogramming processes of DNA methylation during human germ cell development. However, the studies about DNA methylation in human germ cells are very limited (Almstrup et al., 2010; Gkountela et al., 2013; Wermann et al., 2010). In order to establish a definitive timescale of DNA methylation reprogramming in human germ cells, more

investigations have been performed in the study here. The investigation of dynamic changes of 5mC has been expanded from 6wga to 37-years old human ovaries by immunohistochemistry and immunofluorescence. Meanwhile, TETs and 5hmC were also explored in human gonads across these different stages.

4.2 *Results*

4.2.1 **Distinct distribution of 5mC and 5hmC in mouse ESCs**

5hmC is one of the oxidized derivatives of 5mC; the antibodies against 5mC and 5hmC are easy to cross-reacting. In order to discriminate 5mC and 5hmC, the antibodies against 5mC and 5hmC were detected in the NBF fixed mouse ESCs before being performed in the human tissues (Fig 4.1). Different distributions of 5mC and 5hmC have been observed in some mouse ESCs, in which the chromocenters are intense for 5mC but absent of 5hmC staining (Fig 4.1, white arrow). The different distribution of 5mC and 5hmC in mouse ESCs indicates that the 5mC antibody has no detectable cross-reactivity to 5hmC.

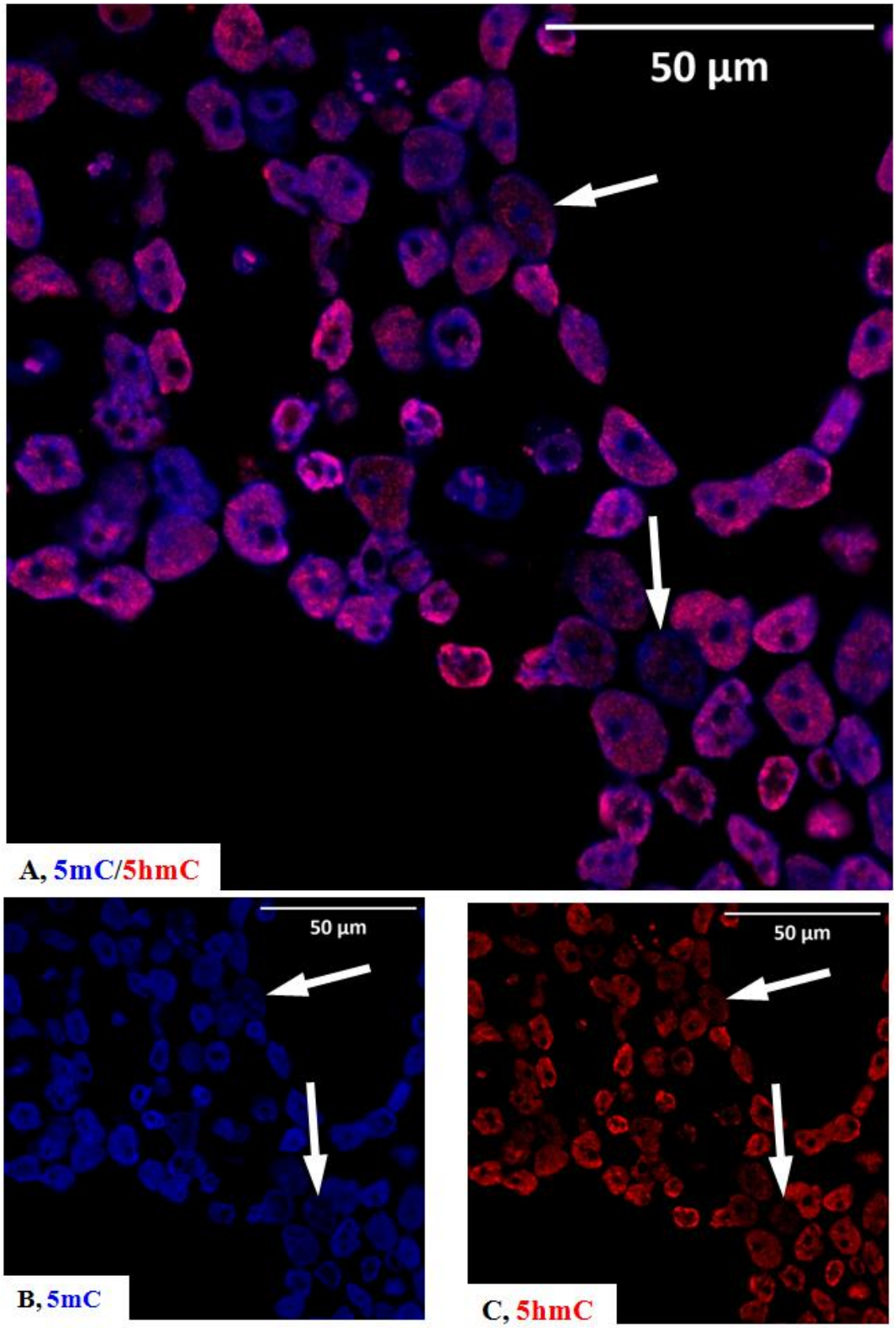

Figure4.1. Distribution of 5mC and 5hmC in NBF fixed mouse ESCs. A, The merged image for 5mC and 5hmC； **B**, 5mC； **C**, 5hmC; the staining of 5mC is shown in blue while the staining of 5hmC is shown in red. White arrows represent the mouse ESCs, in which the chromocenters were positive for 5mC but negative for 5hmC. The scale bars equal to 50µm in all panels.

4.2.2 Dynamic changes of 5mC in human fetal and adult ovaries

As the limitation of taking early human embryo sample, only one 6wga human female embryo has been detected. At around 6wga in human, some of the migrating PGCs have reached the genital ridge and started to colonize the gonads (Francavilla et al., 1990; Fujimoto et al., 1977) (Fig 4.2A). The H&E staining of this 6wga human female embryo is showed in Fig 4.2B, in which the dashed box indicates the region of genital ridges (Fig 4.2B).

In this Bouins fixed 6wga human female embryo, double immunofluorescence was used to detect the distribution of 5mC (Fig 4.3). In order to label the PGCs, an anti-OCT4 antibody was used in this 6wga human embryo (Fig 4.3, Green). The inserted panel in Fig 4.3A shows the whole 6wga embryo, in which nearly all the cells are 5mC-positive (Fig 4.3A, inserted panel). Fig 4.3A is a higher resolution image, in which the migrating PGCs are clearly labeled by OCT4 antibody (Fig 4.3A, Green). Fig 4.3B is a much higher resolution image, in which nearly all OCT4-negative somatic cells were 5mC-positive at this 6wga human embryo (Fig 4.3B). Meanwhile, in this 6wga human embryo, the staining of 5mC was clearly observed in the OCT4-positive PGCs (Fig 4.3 B, Red). However, compared with the surrounding somatic cells, the 5mC staining in the PGCs is less intense, suggesting that DNA was hypomethylated in PGCs when compared to that in somatic cells at 6wga (Fig 4.3 B).

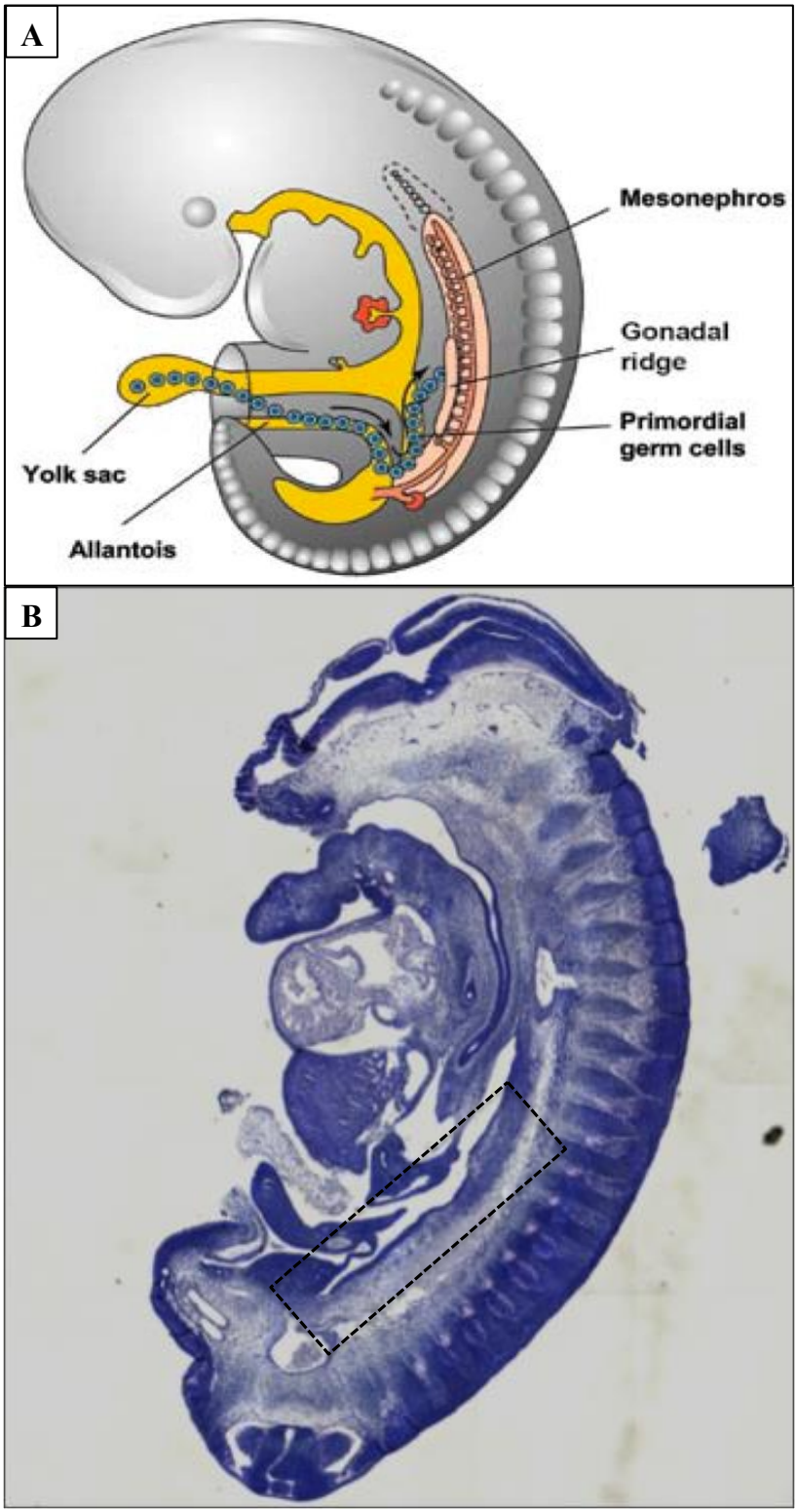

Figure 4.2 Schematic diagram and H&E staining of Bouins fixed 6wga human female embryo. A, A schematic diagram of 6wga human embryo showing the migrating PGCs and genital ridge. **B**, H&E staining of 6wga human female embryo. The head of this embryo had been removed for SRY detection. The dashed box represents the regions of genital ridge in the embryo. Panel A is reproduced from (Kousta et al., 2010)

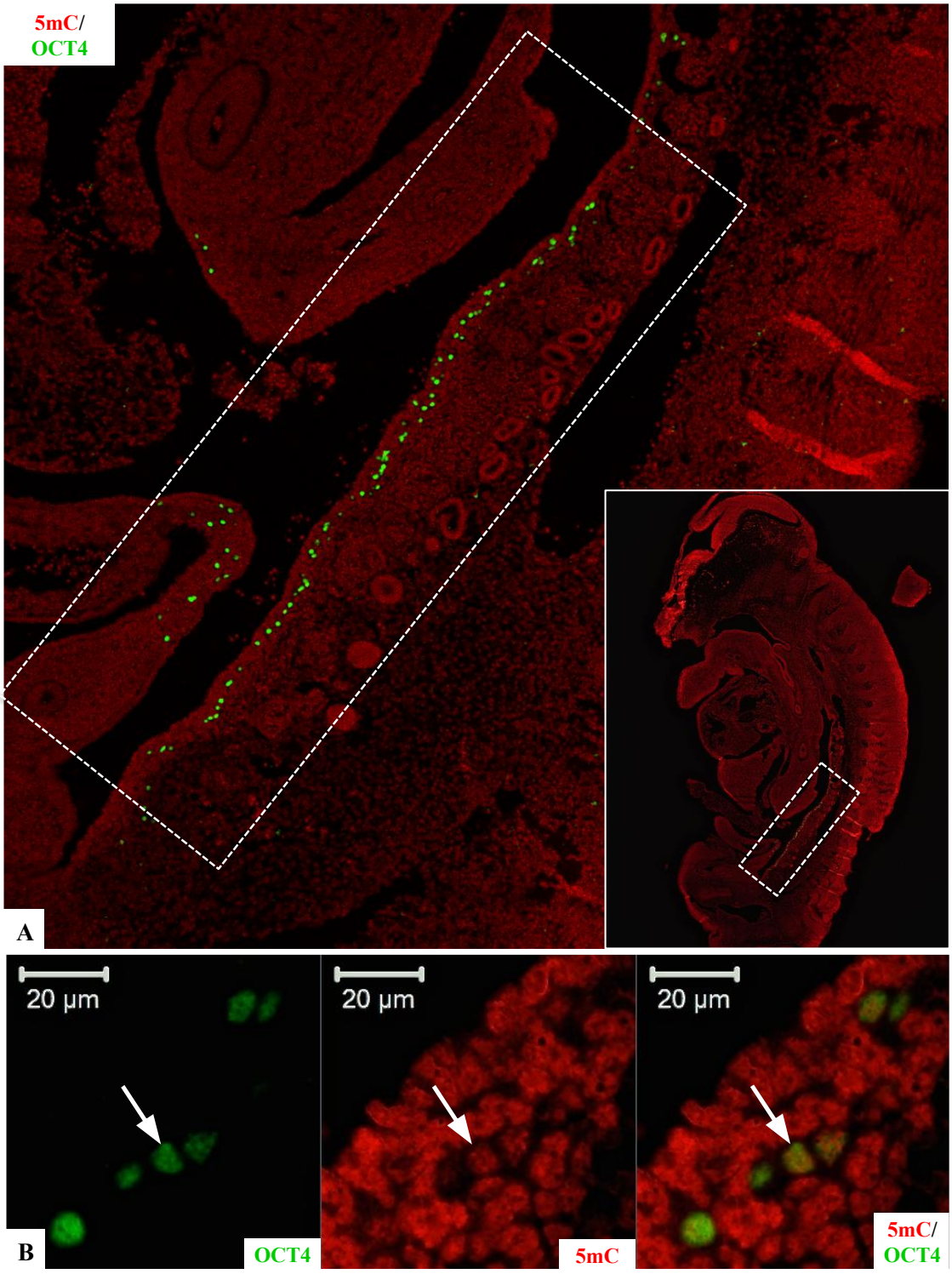

Figure 4.3 Distribution of 5mC in Bouins fixed 6wga human female embryo. A, low resolution image of the 6wga human embryo, the dashed box shows migrating PGCs in this 6wga human embryo; the inserted image in **A** is the lower resolution image, which shows the staining of the whole embryo; **B,** a higher resolution image of the 6wga human embryo. The staining of OCT4 is shown in green, while the staining of 5mC is shown in red. White arrow represents the PGCs which were positive for both OCT4 and 5mC. The scale bars equal to 20µm in B panel.

The distribution of 5mC was also detected in human post-migratory fetal and adult ovaries by DAB immunohistochemistry.

Different from the 6wga human female PGCs, which was positive for 5mC staining, most of the human ovarian PGCs were 5mC-negative at 8wga (Fig 4.4 A, White arrow), even though a few of them displayed weak 5mC staining (Fig 4.4 A, Black arrow). From 14wga onwards, 5mC was below the level of detection at all stages of fetal ovarian germ cell development (Fig 4.4 B and C, White arrow). This observation implied that global deletion of 5mC has been initiated by 8wga and completely by early 2nd trimester in human fetal ovarian germ cells.

The levels of 5mC in the human fetal ovarian somatic cells were relatively stable and displayed intense 5mC staining from 8 to 18wga (Fig 4.4 A-C, Black arrowhead). The negative control is shown in Fig 4.4 D.

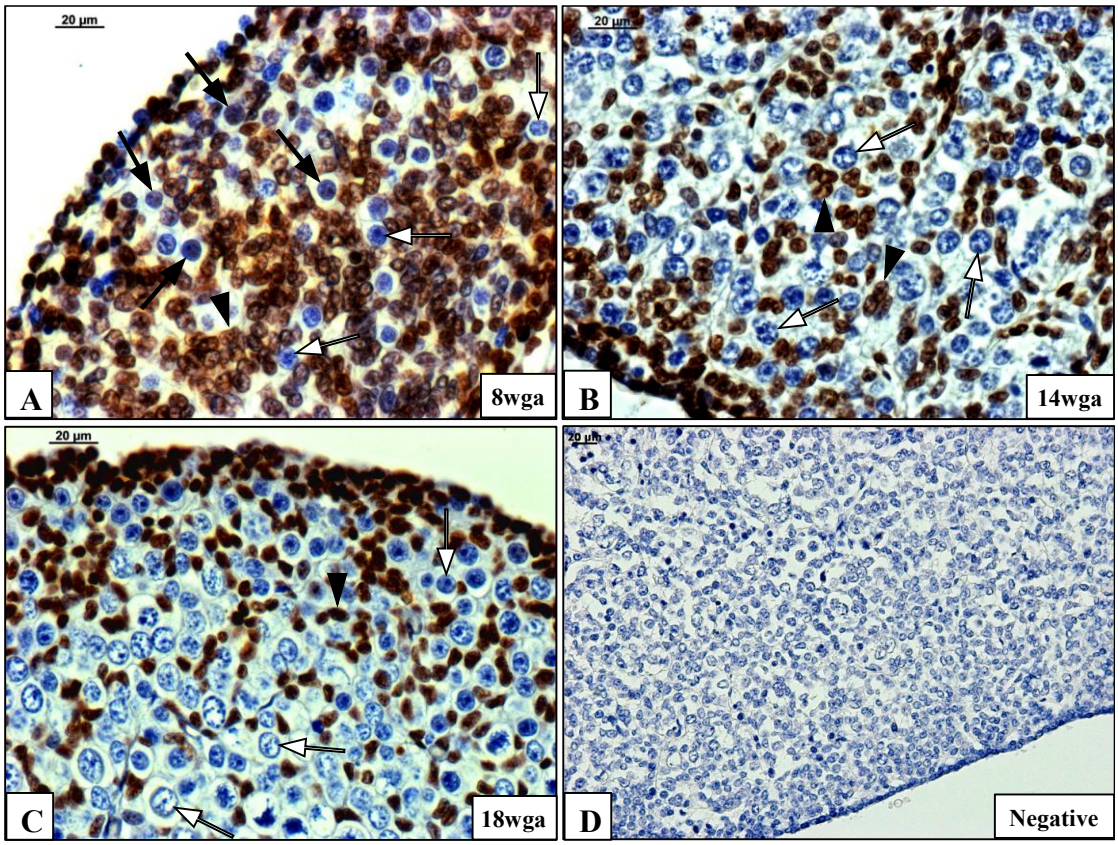

Figure 4.4 Distribution of 5mC in Bouins fixed human post-migratory fetal ovaries. A. 8wga human fetal ovary; **B**, 14wga human fetal ovary; **C**, 18wga human fetal ovary; **D**, negative control; Black and white arrows represent 5mC-positive and negative germ cells, respectively. While black arrowheads represent 5mC-positive somatic cells. The scale bars equal to 20µm in all panels.

Notably, 5mC was regained in human postnatal oocytes (Fig 4.5), although a few of them remained 5mC-negative (Fig 4.5 E). In the 5mC-positive oocytes, most of the

nucleolus were 5mC-positive (Fig 4.5 A, B and C), while some of them were 5mC-negative (Fig 4.5 D and F). These findings indicated that DNA de novo methylation has been initiated in human ovarian germ cells after birth.

The somatic cells in human postnatal ovaries are not all positive for 5mC. In human postnatal ovaries, most of the granulosa cells were 5mC-positive (Fig 4.5, Black arrowhead), while some of the mesenchymal somatic cells are clearly 5mC-negative (Fig 4.5, White arrowhead).

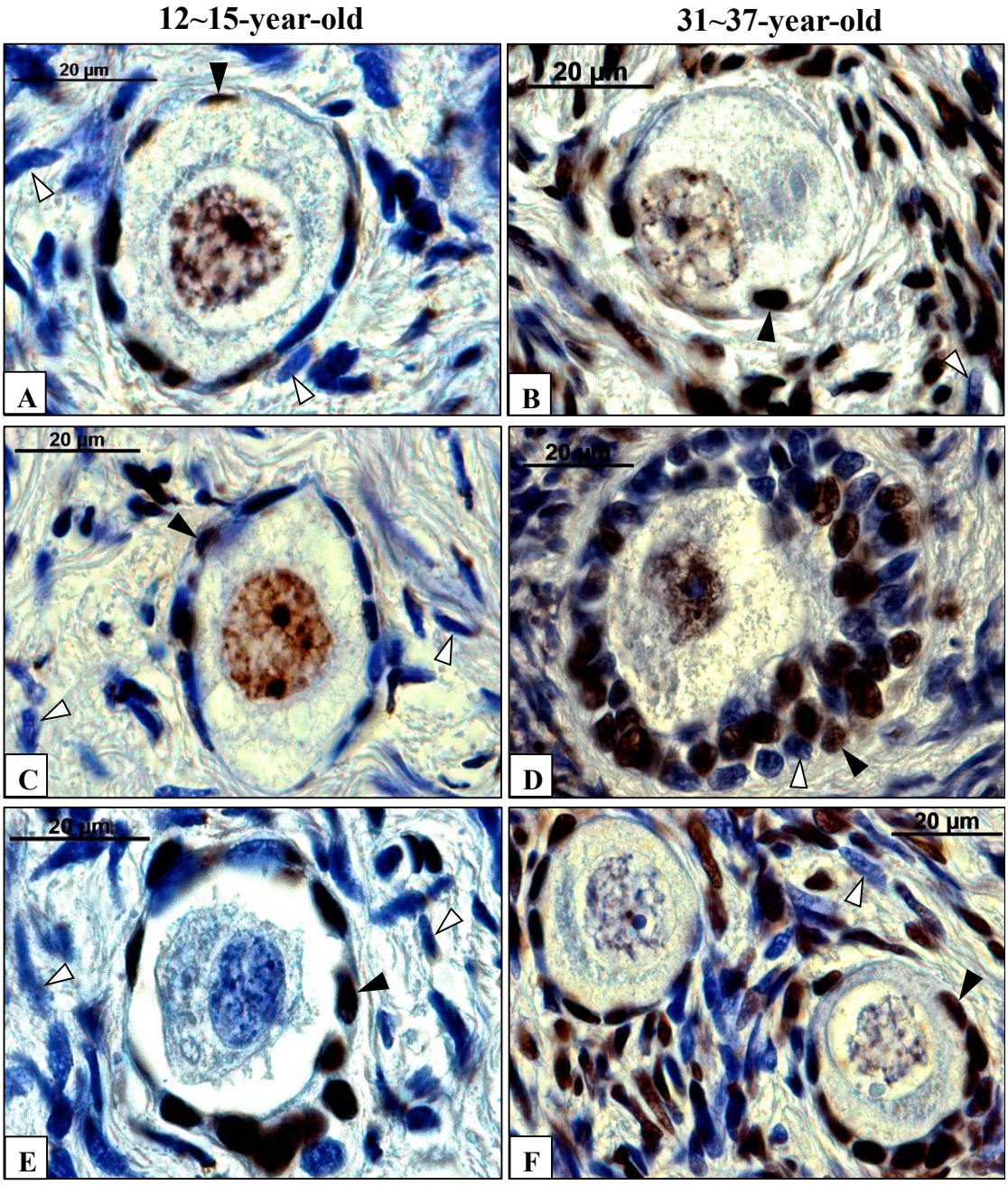

Figure 4.5 Distribution of 5mC in NBF fixed human postnatal ovaries. A, C and **E:** primary follicles in 12~15-year old human ovaries; **B, D** and **F:** primary follicles in 31~37-year old human ovaries. Black and white arrowheads represent 5mC-positive and negative somatic cells, respectively. The scale bars equal to 20µm in all panels.

4.2.3 Dynamic changes of 5mC in human fetal testis

In Bouins fixed human fetal testes, 5mC was undetectable in germ cells at both 8wga and 14wga (Fig 4.6 A and B, White arrow). At 18wga, most of the testicular germ cells remained 5mC-negative (Fig 4.6 C and D, White arrow). Meanwhile, some testicular germ cells stated to display 5mC staining at this stage (Fig 4.6 C and D, Black arrow). A similar distribution of 5mC was also observed in 19wga human testis (Fig 4.6 E). The negative control is shown in Fig 4.6 F.

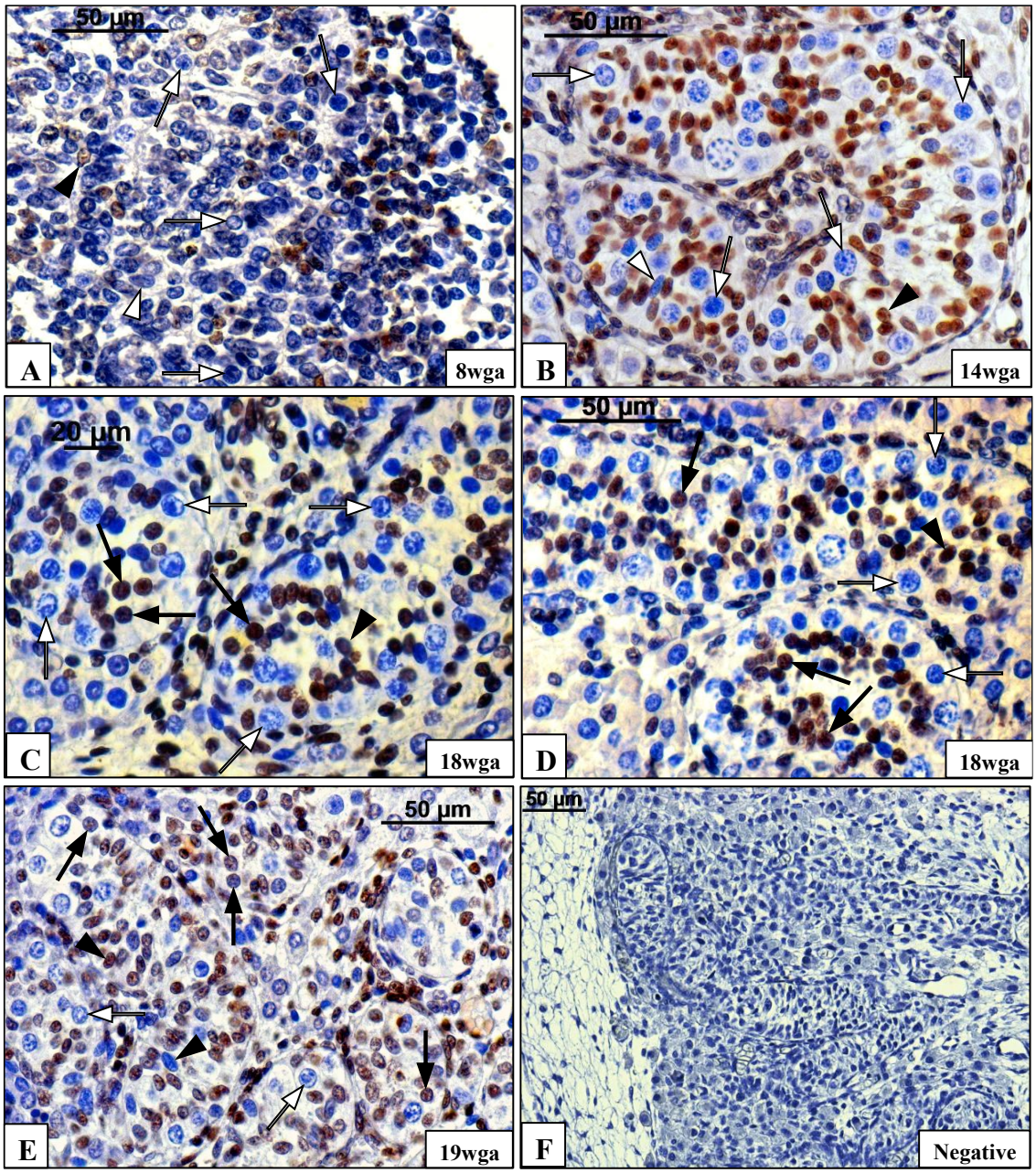

Figure 4.6 Distribution of 5mC in Bouins fixed human fetal testes. A, 8wga; **B,** 14wga; **C** and **D,** 18wga; **E,** 19wga; **F,** Negative control**;** Black and white arrows represent 5mC-positive and negative germ cells, respectively. While black arrowheads represent 5mC-positive somatic cells. The scale bars equal to 20µm in C panel，50µm in A,B,D,E and F panels.

4.2.4 Dynamic changes of 5hmC in human fetal and adult ovaries

In Bouin fixed 6wga human fetamle embryo, 5hmC, the oxidized derivative of 5mC, was also detected by double immunofluorescence. In this 6wga human female embryo, PGCs were marked by OCT4 antibody (Fig 4.7, Green). High resolution images are shown in Fig 4.7 B. Most of the OCT4-positive human PGCs displayed 5hmC staining (Fig 4.7 B, White arrow). However, OCT4-positive and 5hmC-negative/weak PGCs were also detected in the 6wga human embryo (Fig 4.7 B, White arrowhead). Nearly all the OCT4-negative somatic cells were positive for 5hmC in this 6wga human embryo (Fig 4.7).

The distribution of 5hmC was examined by DAB immunohistochemistry in both fetal and adult ovaries (Fig 4.8 and 4.9). Most of the Bouin fixed human fetal ovarian germ cells did not displayed 5hmC staining from 8 to 18wga (Fig 4.8, A-C, White arrow), apart from very few ovarian germ cells which displayed weak 5mC staining at 8wga (Fig 4.8 A, Black arrow). Interestingly, most of the oocytes in the NBF fixed human postnatal ovaries were 5hmC-positive (Fig 4.9). Some of the nucleolus in the 5hmC-positive oocytes were 5hmC-positive (Fig 4.9, A and B), while some of them were 5mC-negative (Fig 4.9, B-D).

The ovarian somatic cells displayed strong 5hmC staining throughout all the fetal gestations that we examined (Fig 4.8, Black arrowhead). Different from the human fetal ovaries, some ovarian somatic cells in human postnatal ovaries are 5hmC-negative (Fig 4.9, White arrowhead). However, the granulosa cells in human postnatal ovaries were mostly 5hmC-positive (Fig 4.9, Black arrowhead).
A negative control was shown in Fig 4.8D.

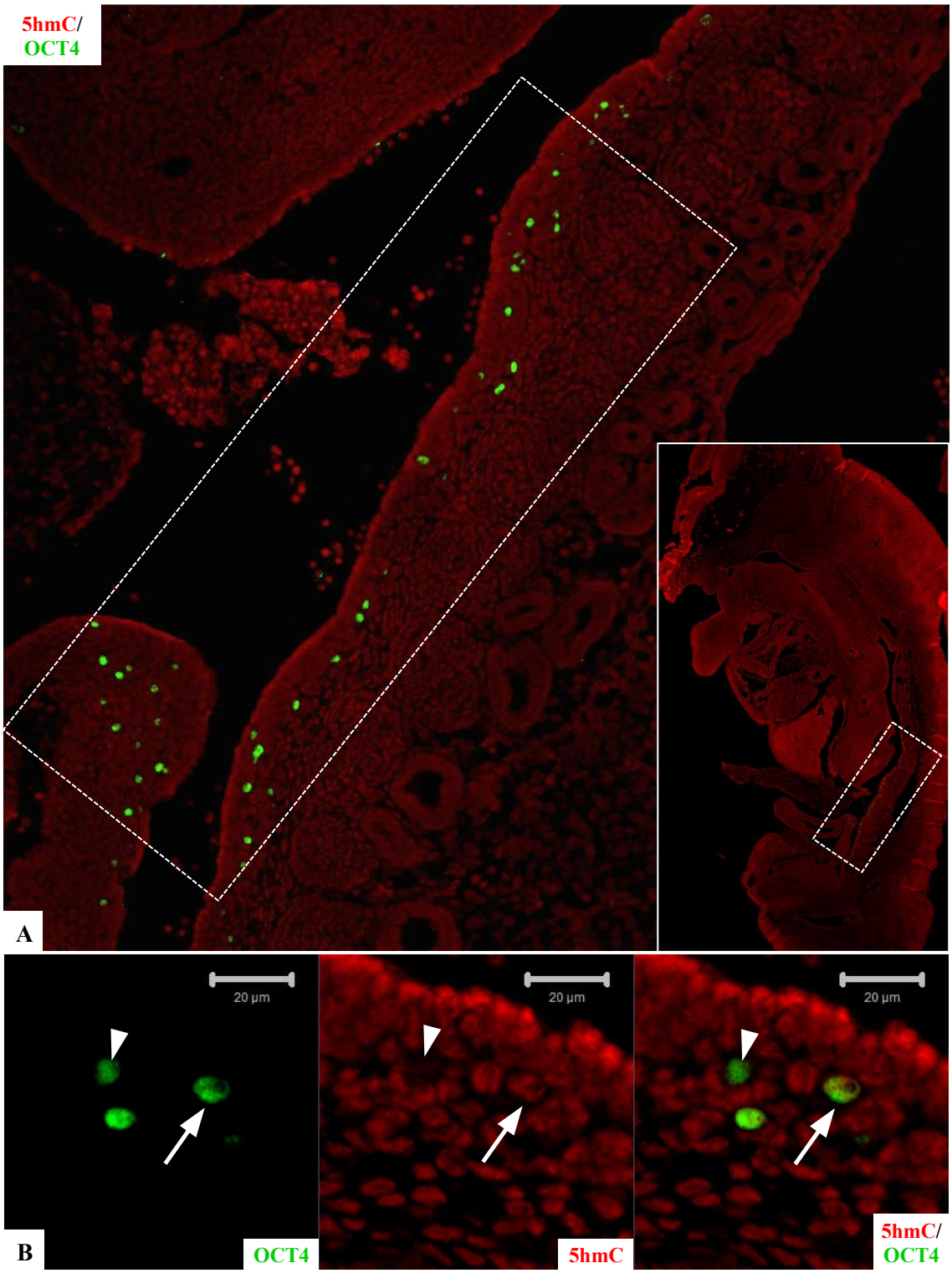

Figure 4.7 Distribution of 5hmC in Bouins fixed 6wga human female embryo. A, low resolution image of the 6wga human embryo; the dashed box shows the migrating PGCs in this 6wga human embryo; the insert photo in **A** is the lower resolution image of A; **B,** high resolution images of the 6wga human embryo. White arrow represents PGC which were positive for both OCT4 and 5hmC, while the white arrowhead shows a PGC which was positive for OCT4 but negative for 5hmC. The scale bars equal to 20µm in panel B.

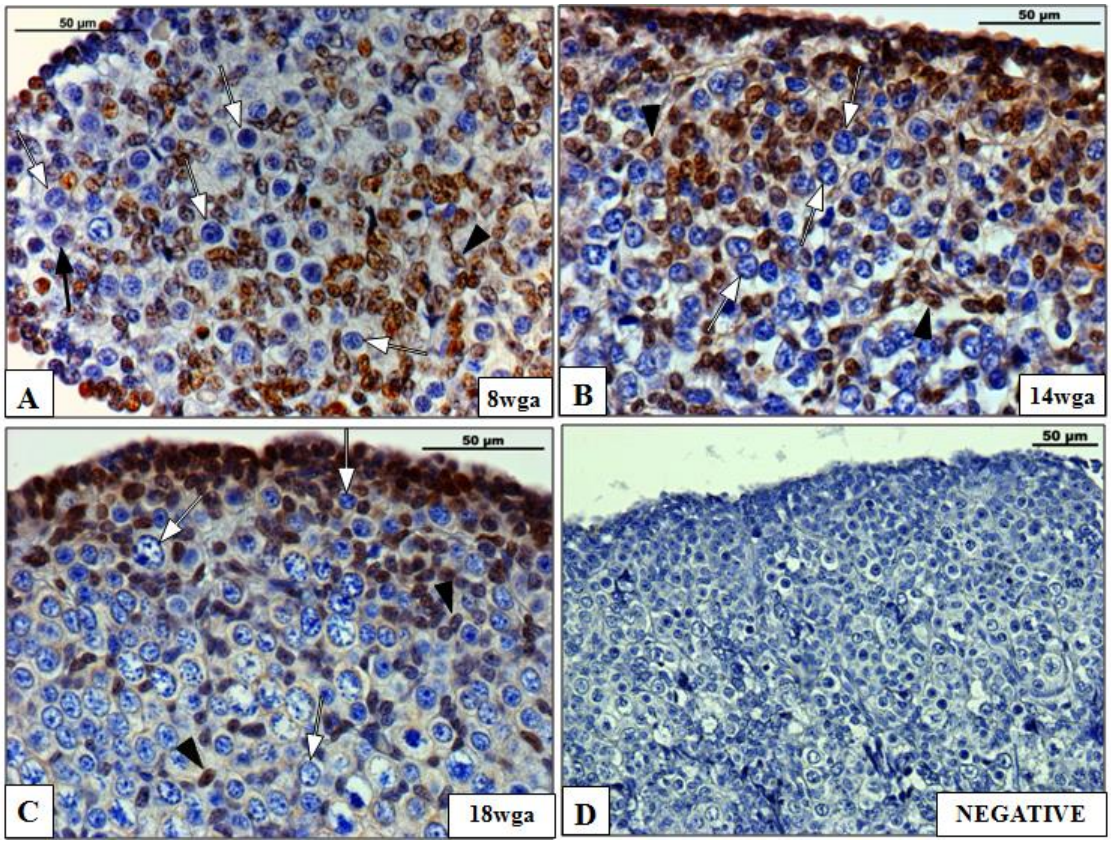

Figure 4.8 Distribution of 5hmC in Bouins fixed human fetal ovaries. A-C: human fetal ovaries from 8wga to 18wga; **D**, Negative control. Black and white arrows represent 5hmC-positive and negative germ cells, respectively. While black arrowheads represent 5hmC-positive somatic cells. The scale bars equal to 50µm in all panels.

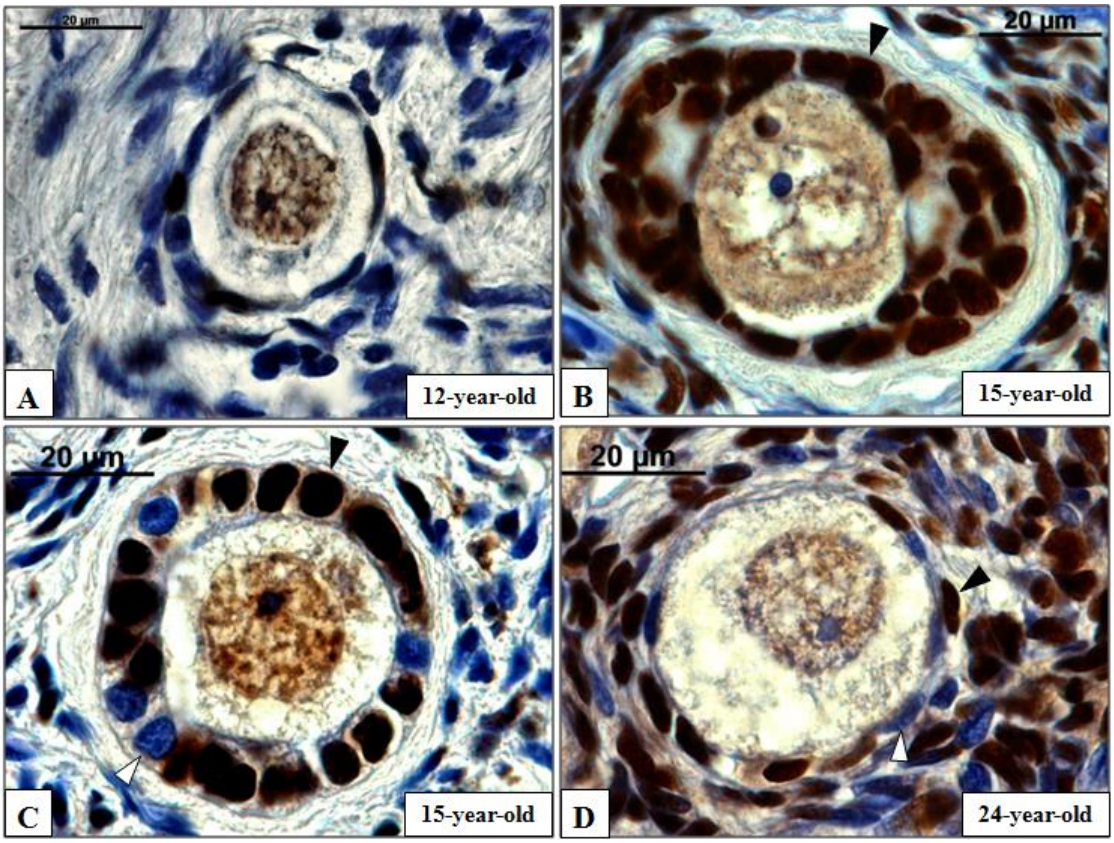

Figure 4.9 Distribution of 5hmC in NBF fixed human postnatal ovaries (12~24-year old human ovaries). A, 12-year-old; **B** and **C**, 15-year-old; **D**, 24-year-old; the nucleuses of the oocytes were all 5hmC positive. Black and white arrowheads represent 5hmC-positive and negative somatic cells, respectively. The scale bars equa tol 20µm in all panels.

4.2.5 The distribution of 5hmC in human fetal testes

In human fetal testes, the majority of testicular germ cells were 5hmC-negative from 8-18wga (Fig 4.10 A, B and C, White arrow). However, a few strongly 5hmC-positive fetal testicular germ cells were observed throughout these gestations (Fig 4.10 A, B and C, Black arrow).

The testicular somatic cells were 5hmC-positive at 8wga (Fig 4.10 A, Black arrowhead), however, from 14wga onwards, some Sertoli cells displayed only weak 5hmC staining, whilst peritubular cells surrounding cords were intensely 5hmC-positive (Fig 4.10 B and C). The negative control is shown in the Fig 4.10 D.

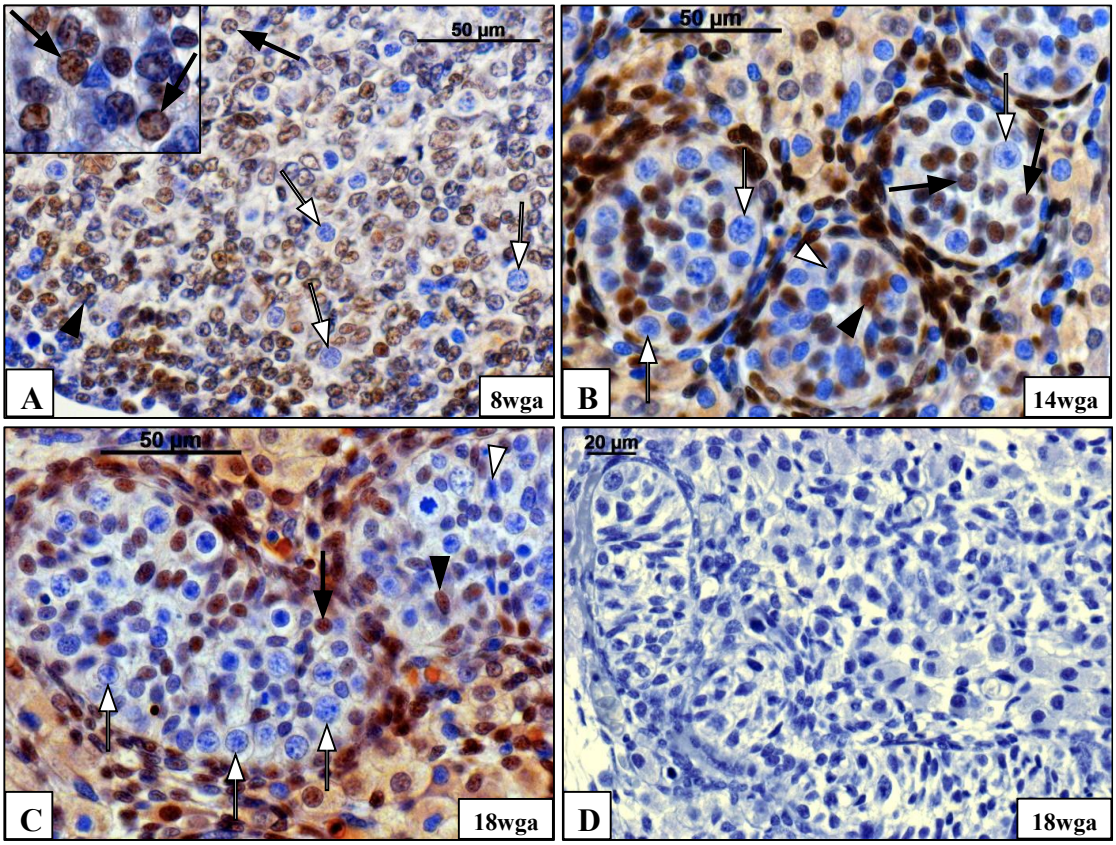

Figure 4.10 Distribution of 5hmC in Bouins fixed human post-migratory fetal testes. Black and white arrows represent 5mC-positive and negative germ cells, respectively, while black and white arrowheads represent 5hmC-positive and negative somatic cells, respectively. The scale bars equal to 50µm in A, B and C panels, 20µm in D panel.

4.2.6 Global changes in *TET1, 2* and *3* mRNA levels in human fetal gonads

To determine the mRNA levels of *TET1, 2* and *3* during human fetal ovarian and testicular development, QRT-PCR was performed for *TET1, 2* and *3* across different gestations (Fig 4.11 and 4.12). Human fetal gonads were grouped into three gestational stages, 1st trimester (8-11wga), early 2nd trimester (13-16wga), and late 2nd trimester (17-20wga). Statistical analysis was performed using GraphPad Prism 5 software (La Jolla, CA, USA).

In human fetal ovaries, the mRNA levels of *TET1, TET2* and *TET3* all significantly decreased with increasing gestations (Fig 4.11, data were analyzed using one-way ANOVA analysis of variance with linear trend post-hoc test for statistical significance, $P < 0.05$). In human fetal ovaries, the mRNA levels of *TET1, TET2* and *TET3* all significantly decreased in early and late 2nd trimester when compared to 1st trimester. There is no significant difference between early and late 2nd trimester for the expression of *TET1, TET2* and *TET3* in human fetal ovaries (Fig 4.11, data were analyzed using one-way ANOVA analysis of variance with Newman-Keuls Multiple Comparison post-test to determine significant changes between gestational values, $P < 0.05$).

In human fetal testes, the mRNA levels of *TET1* and *TET3* all fell significantly with increasing gestations. However, the mRNA level of *TET2* did not significantly change across the examined gestations in fetal testes (Fig 4.12, data were analyzed using one-way ANOVA with linear trend post-hoc test for statistical significance, $P < 0.05$). In human fetal testes, the expression of *TET1* and *TET3* all significantly decreased in early and late 2nd trimester when compared to 1st trimester. There is no significant difference between early and late 2nd trimester for the expression of *TET1* and *TET3* in human fetal testes (Fig 4.12, data were analyzed using one-way ANOVA with Newman-Keuls Multiple Comparison post-test to determine significant changes between gestational values, $P < 0.05$).

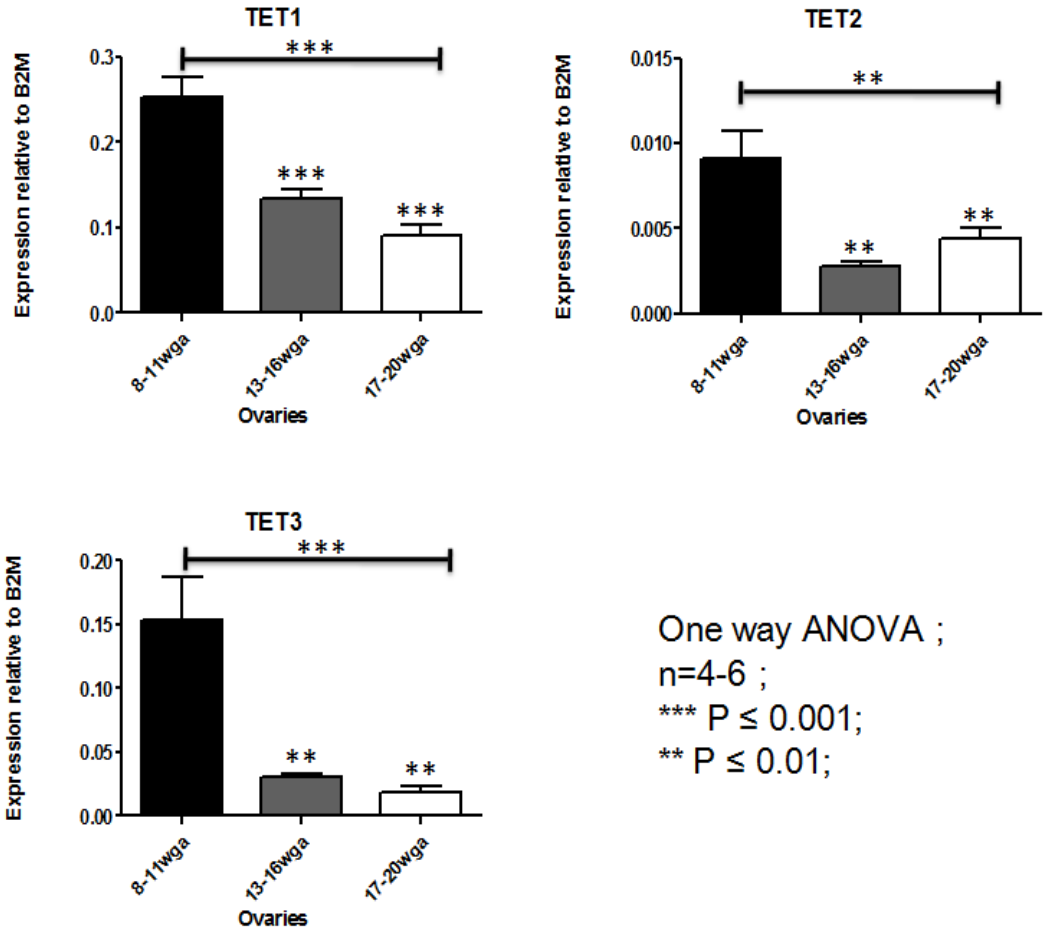

Figure 4.11 mRNA levels of *TET1*, *2* and *3* in human fetal ovaries across different gestations. The expression of *TET1, 2* and *3* was analyzed by QRT-PCR across different gestations and split into three age groups: 8-11wga, 13-16wga and 17-20wga. The sample number was between 4-6 ovaries from individual fetuses per gestational group. Error bars in histograms represent ±SEM. In order to allow quantitative comparisons, the expression of *TET1, 2* and *3* was normalized to that of the housekeeping gene *B2M*, which remained stable across gestation. Data were analyzed utilizing the One-way ANOVA with Newman-Keuls Multiple Comparison post-test to determine significant changes between gestational values. One-way ANOVA with linear trend post-test was also used to determine significant changes across gestations.

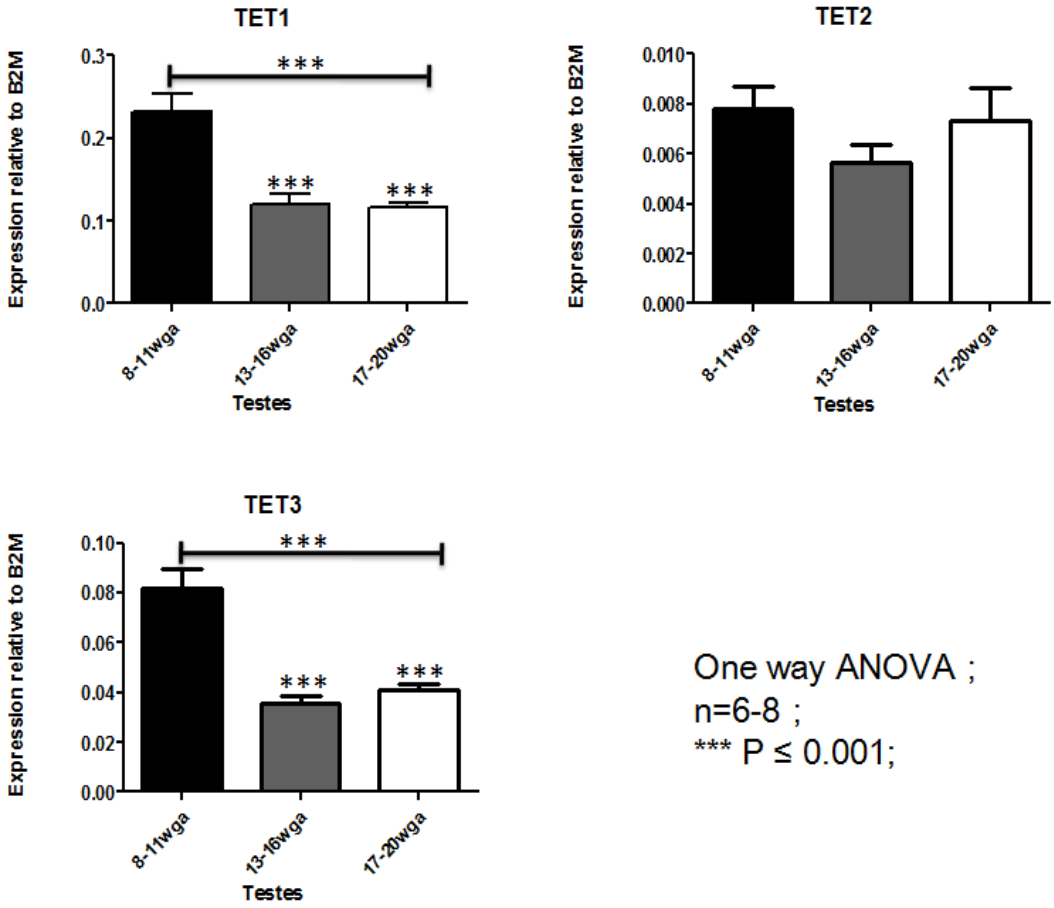

Figure 4.12 mRNA levels of *TET1*, *2* and *3* in human fetal teses across different gestations. The expression of *TET1, 2* and *3* was analyzed by QRT-PCR across different gestations and split into three age groups: 8-11wga, 13-16wga and 17-20wga. The sample number was between 6-8 testes from individual fetuses per gestational group. Error bars in histograms represent ±SEM. In order to allow quantitative comparisons, the expression of *TET1, 2* and *3* was normalized to that of the housekeeping gene *B2M*, which remained stable across gestation. Data were analyzed utilizing the One-way ANOVA with Newman-Keuls Multiple Comparison post-test to determine significant changes between gestational values. One-way ANOVA with linear trend post-test was also used to determine significant changes across gestations.

4.3 *Discussion*

4.3.1 Global 5mC changes dynamically in human germ cells

As elucidated earlier, it has been found that in the case of mouse PGCs they cause sequential epigenetic changes and genome-wide DNA demethylation to change the

epigenome for totipotency (Hajkova et al., 2002; Seisenberger et al., 2012; Yamaguchi et al., 2013). This provides one of the potential mechanistic bases to understand the global changes of 5mC in human germ cells (Hackett et al., 2013).

In previous studies, by immunohistochemistry (Wermann et al., 2010) and immunofluorescence (Gkountela et al., 2013), 5mC was undetectable in the human fetal ovarian germ cells from 6 to 19wga; 5mC was also not detected even in human postnatal oocytes (Wermann et al., 2010). In Gkountela *et al*'s study, human testicular germ cells were also 5mC-negative from 6wga to 19wga (Gkountela et al., 2013). Similar to these previous reports, my investigation showed that nearly all of the human post-migratory ovarian and testicular germ cells were 5mC-negative. However in contrast to these previous reports, PGCs in a 6wga human female fetus did display 5mC staining, postnatal human oocytes were shown to regain 5mC staining and fetal testicular germ cells also regained 5mC staining from 18 to 19wga (Fig 4.13). In previous studies, 5mC detection by immunohistochemistry (Wermann et al., 2010) and immunofluorescence (Gkountela et al., 2013) was performed without permeabilization and DNA denaturization. As 5mC is localized in the 5-position of DNA cytosine, it is difficult to detect with antibodies; permeabilization and DNA denaturization can improve binding affinity of the 5mC antibodies. The undetectable 5mC in 6wga human ovarian germ cells (Gkountela et al., 2013), postnatal oocytes (Wermann et al., 2010) and later fetal testicular germ cells (Gkountela et al., 2013), may be associated with the absence of permeabilization and DNA denaturization during 5mC detection.

The findings here on the global changes of 5mC in human germ cells were consistent with what has been reported in mouse germ cells (Abe et al., 2011; Hajkova et al., 2010; Seki et al., 2005), suggesting that the reprogramming of global DNA methylation is conserved between human and mouse germ cells.

The DNA of human PGCs appears to be methylated at 6wga. During this early stage, almost all the human PGCs are positive for the pluripotent marker OCT4 and negative for the post-migratory germ cell markers VASA and DAZL (Anderson et al., 2007). In the post-migratory human fetal ovarian and testicular germ cells, global DNA demethylation is initiated after germ cell migration in human. From 13wga, the expression of VASA significantly increased in both ovarian and testicular germ cells (Anderson et al., 2007). The genome-wide erasure of DNA methylation, which is associated with gene repression (Deaton and Bird, 2011; Meissner et al., 2008), may be associated with the upregulation of post-migratory germ cell markers in human post-migratory fetal germ cells.

DNA de novo methylation was initiated asynchronously in human male and female germ cells. 5mC was detected again in the later fetal testicular germ cells but regained in the human oocytes after birth. After 11wga, the expression of the meiosis-associated gene *DAZL* was significantly increased in the human ovaries and some human oogonia start to enter into meiosis (Anderson et al., 2007; He et al., 2013). The expression of

DAZL has been found to be activated by DNA demethylation in mammalian germ cells (Linher et al., 2009; Maatouk et al., 2006a). Human fetal ovarian germ cells maintained a demethylated state until birth, which may be associated with the further upregulation of *DAZL* and the meiotic process in human fetal ovarian germ cells. DNA remethylation was initiated in the later human fetal testicular germ cells, which undergo mitotic arrest rather than meiosis. In a word, the delay of DNA remethylation in human ovarian germ cells may be associated with the expression of meiotic genes in human fetal ovary.

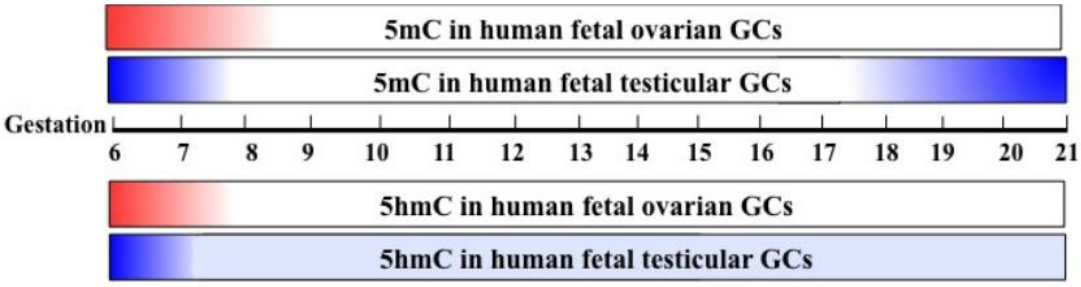

Figure 4.13 Dynamic changes of 5mC and 5hmC in human fetal germ cells from 6wga to 20wga. Red bars represent the expression of 5mC or 5hmC in ovarian germ cells (GCs), while blue bars represent the expression of 5mC or 5hmC in testicular germ cells.

4.3.2 Global 5hmC changes dynamically in human germ cells

In the research that was undertaken here, it was found that the presence of 5hmC in the OCT4-positive PGCs at 6wga was consistent with previous findings, in which 5hmC was detectable in OCT4A-positive ovarian and testicular PGCs at 7wga (Gkountela et al., 2013). In later fetal gestations, 5hmC was undetectable in human fetal ovarian germ cells by immunohistochemistry, which is different from what was found in Gkountela et al's study, in which 5hmC was detectable in the OCT4A-positive ovarian PGCs from 7-19wga by immunofluorescence (Gkountela et al., 2013). The lack of detection of 5hmC in here in post-migratory human fetal ovarian germ cells may be associated with the sensitivity of the immunohistochemistry used here. In human fetal testes, 5hmC was also detectable in OCT4-positive testicular PGCs, which showed 5hmC staining at 8 and 17wga, but were negative for 5hmC at 13.5-16wga (Gkountela et al., 2013). But here, 5hmC was detectable in throughout all these gestations. This may be because Gkountela *et al*. only used OCT4A to mark human fetal PGCs (Gkountela et al., 2013), however, in the later gestation, some mature germ cells are OCTA-negative, and whether they displayed 5hmC or not would not be detected in that study.

5hmC is the oxidative derivative of 5mC, and the generation of 5hmC depends on the pre-existence of 5mC. This conversion is initiated by the TET1 protein (Ito et al., 2011). It was observed that both 5mC and 5hmC were present in human 6wga female PGCs. From 8 to 18wga, both 5mC and 5hmC were erased in human fetal ovarian germ cells. In these stages, the female germ cells show low methyalted and low

hydroxymethylated levels, suggesting that 5hmC may be further processed to 5fC or 5caC, or even unmodified cytosine in these post-migratory fetal ovarian germ cells. The loss of 5hmC appeared rapid in human post-migratory fetal ovarian germ cells. Postnatal human oocytes, which regained 5mC, also displayed 5hmC staining.

Post-migratory human testicular germ cells displayed low DNA methylated levels by 18wga. However, some testicular germ cells still displayed intense 5hmC staining throughout these gestations, indicating that the excision of 5hmC in human fetal testicular germ cells was slower or less complete than in ovarian germ cells. At later gestations, both 5mC and 5hmC were detectable in some testicular germ cells.

From the findings above, the existence of 5mC and 5hmC in human germ cells were synchronous rather than alternate, the presence or the erasure of 5hmC followed closely that of 5mC. All these findings suggest that rather than playing an important role in DNA demethylation, 5hmC may play other unknown role in human fetal germ cell development, which need further investigation.

4.3.3 Global changes of *TETs* in human fetal gonads

In Gkountela *et al*'s study, *TET1, 2* and *3* were expressed in C-KIT-positive human PGCs at 16-16.5wga by RNA-Sequencing (Gkountela et al., 2013). In the study here detected by qPCR, *TET1, 2* and *3* were also expressed in the human fetal gonads across different gestations, including 16-16.5wga.

In human fetal ovaries, the mRNA levels of *TET1*, *TET2* and *TET3* all significantly decreased with increasing gestations. Compared to the ovaries in 1st trimester, the mRNA levels of these three *TETs* all significantly decreased in early and late 2nd trimester. During these stages, the decrease in *TETs* may be associated with the global loss of 5hmC in human fetal ovarian germ cells, which were negative for 5hmC at these stages. Tet1 has been found to be involved in the mouse meiosis, as deficiency in *Tet1* led to loss of meiotic genes in mouse ovarian germ cells (Yamaguchi et al., 2012). The decrease of *TET1* in human fetal ovaries was coincident with the initiation of meiosis. However, whether the decrease of TET1 was restrict to the ovarian germ cells or not was unknown. So the relationship of TET1 and meiosis in ovarian germ cells still need further investigation.

In human fetal testes, the mRNA levels of *TET1* and *TET3* all significantly decreased with increasing gestations. Compared to the testes in 1st trimester, the mRNA levels of *TET1* and *TET3* all significantly decreased in early and late 2nd trimester. During these stages, the decrease in *TET1* and *TET3* may be associated with the global loss of 5hmC in human fetal testicular germ cells, most of which were negative for 5hmC at these stages. Notably, the mRNA level of *TET2* did not change across gestation in human fetal testes, suggesting that TET2 may play a less important role in the human fetal testes.

Chapter5. The impact of chemical DNA demethylation in the expression of germ cell-specific genes and meiotic genes in human

5.1 *Introduction*

Germ cells have a unique ability to undergo meiosis, which generates haploid gametes. In mammals, the timing of meiotic entry is different between male and female germ cells. The mouse ovarian germ cells enter into meiotic prophase I prenatally, while the testicular germ cells do not enter into meiosis until puberty (Hilscher et al., 1974; McLaren and Southee, 1997). The extrinsic signaling molecule RA, derived from the adjacent mesonephros, is critically required for meiotic initiation in the developing mouse fetal ovary (Anderson et al., 2008; Bowles et al., 2006; Koubova et al., 2006). In addition to extrinsic signals, Dazl has been identified as an intrinsic factor for germ cells to acquire the competence to respond to RA signals (Lin et al., 2008; Lin and Page, 2005; Seligman and Page, 1998). However, in the mouse fetal testis, RA is degraded by Cyp26b1 and the mouse fetal testicular germ cells enter mitotic arrest for the remaining embryonic period (Bowles et al., 2006; Koubova et al., 2006; Menke and Page, 2002; Western et al., 2008).

In the human fetal ovary, at around 11wga, some central localized oogonia start to enter into meiotic prophase I while the fetal testicular germ cells undergo mitotic arrest (Gondos et al., 1986; Le Bouffant et al., 2010). Gonad-derived RA has been found to contribute to the initiation of meiosis in the human fetal ovarian germ cell (Childs et al., 2011; Le Bouffant et al., 2010). The RA-responsive gene, *STRA8*, is significantly increased in human fetal ovaries at around the onset of meiosis; on the other hand, *STRA8* is present in a very low level across all gestations in human fetal testes (Childs et al., 2011; Le Bouffant et al., 2010). From 2nd trimester, the expression of *DAZL* was increased in human fetal ovaries and DAZL protein was trans-located from the nucleus to the cytoplasm in pre-meiotic human fetal oogonias (Anderson et al., 2007). Low expression of *DAZL* was detected in human fetal testes across all gestations (Anderson et al., 2007).

The observations above indicate that RA is required for germ cells meiosis in both mice and human. During mouse embryo development, RA is distributed widely in many embryonic tissues (Mark et al., 2009), however, only germ cells respond to RA by entering meiosis. This leads to the question as to what makes germ cells become competent to upregulate *Stra8* and enter into meiosis in response to RA. Some particular epigenetic mechanisms have been suggested that may be associated with germ cell meiotic competence to respond to RA (Bowles and Koopman, 2010).

Global DNA demethylation is initiated in migrating mice PGCs, and completed by E13.5, after which PGCs enter meiosis in females and mitotic arrest in males (Hackett et al., 2012; Hajkova et al., 2002; Seki et al., 2005). At around the onset of meiosis,

global methylation levels are significantly lower in female germ cells than in male (Popp et al., 2010). DNA demethylation loosens the chromatin conformation and increases chromatin accessibility, and may be associated with the establishment of meiotic competence in mice fetal germ cells (Popp et al., 2010). During mouse fetal germ cell development, DNA demethylation has been found to regulate the temporal expression of germ cell-specific genes and meiotic genes (Maatouk et al., 2006a). Even though global DNA demethylation has occurred in mouse fetal germ cells upon entry into the gonad, postmigratory germ cell-specific genes and meiotic genes, such as *Mvh*, *Dazl* and *Sycp3*, remained DNA methylated (Maatouk et al., 2006a). In the later gestation, the promoters of these genes undergo DNA demethylation and these genes become highly expressed. The delayed DNA demethylation in these genes may be associated with the appropriate activation timing for these genes (Maatouk et al., 2006a). In the *Dnmt1* deficient mice embryos, in which global genomic DNA methylation is lost, the expression of *Mvh*, *Dazl* and *Sycp3* increases much earlier than normal, indicating that the activation timing of these genes is controlled by DNA methylation (Maatouk et al., 2006a). Thus, although RA is a key regulator of meiosis, the appropriate DNA methylation status in the developing germ cells is also essential for the meiosis initiation and early progression of meiosis.

According to the studies described in chapter 4, postmigratory human fetal germ cells all undergo global DNA demethylation. This leads to a question as to whether DNA demethylation also regulates the expression of postmigratory germ cell-specific genes and meiotic genes in human. In order to answer this question, TCam-2 cells, an *in-vitro* PGC model, were chemically demethylated by 5-azacytidine, which prevents further DNA methylation in living cells by forming a covalent adduct with DNA methyltransferases (Jones and Taylor, 1980). After that, the expression of postmigratory germ cell-specific genes and meiotic genes was quantified in the DNA demethylated TCam-2 cells. In order to further identify whether DNA demethylation is associated with the RA responsiveness in human fetal germ cells, chemical DNA demethylated TCam-2 cells were further treated with RA and the expression of meiotic genes were examined. *Ex-vivo* studies in human fetal gonads were also performed.

5.2 *Results*

5.2.1 The expression of postmigratory germ cell-specific genes and meiotic genes in chemical DNA demethylated TCam-2 cells

In order to detect whether DNA demethylation regulates the expression of postmigratory germ cell-specific genes and meiotic genes in human, TCam-2 cells were used as an *in-vitro* PGC model. Chemical DNA demethylation in TCam-2 cells was performed by treatment with different doses of 5-azacytidine for 5 days; meanwhile, control TCam-2 cells were incubated with DMSO respectively.
After 5μM of 5-azacytidine treatment for 5 days, the morphology of the TCam-2 cells appeared normal and the number of floating cells was similar to the control TCam-2 cells (Fig 5.1 A-D), suggesting that 5μM of 5-azacytidine is below the toxic dosage for TCam-2 cells.

The levels of 5mC were investigated in TCam-2 cells as a test of the effect of treatment. The control TCam-2 cells, incubated with DMSO, displayed high levels of 5mC (Fig 5.1E). However, after the treatment with 5μM of 5-azacytidine for 5 days, 5mC was barely detectable in the TCam-2 cells (Fig 5.1F), indicating that most of the TCam-2 cells have been globally DNA demethylated after 5 days 5μM 5-azacytidine treatments.

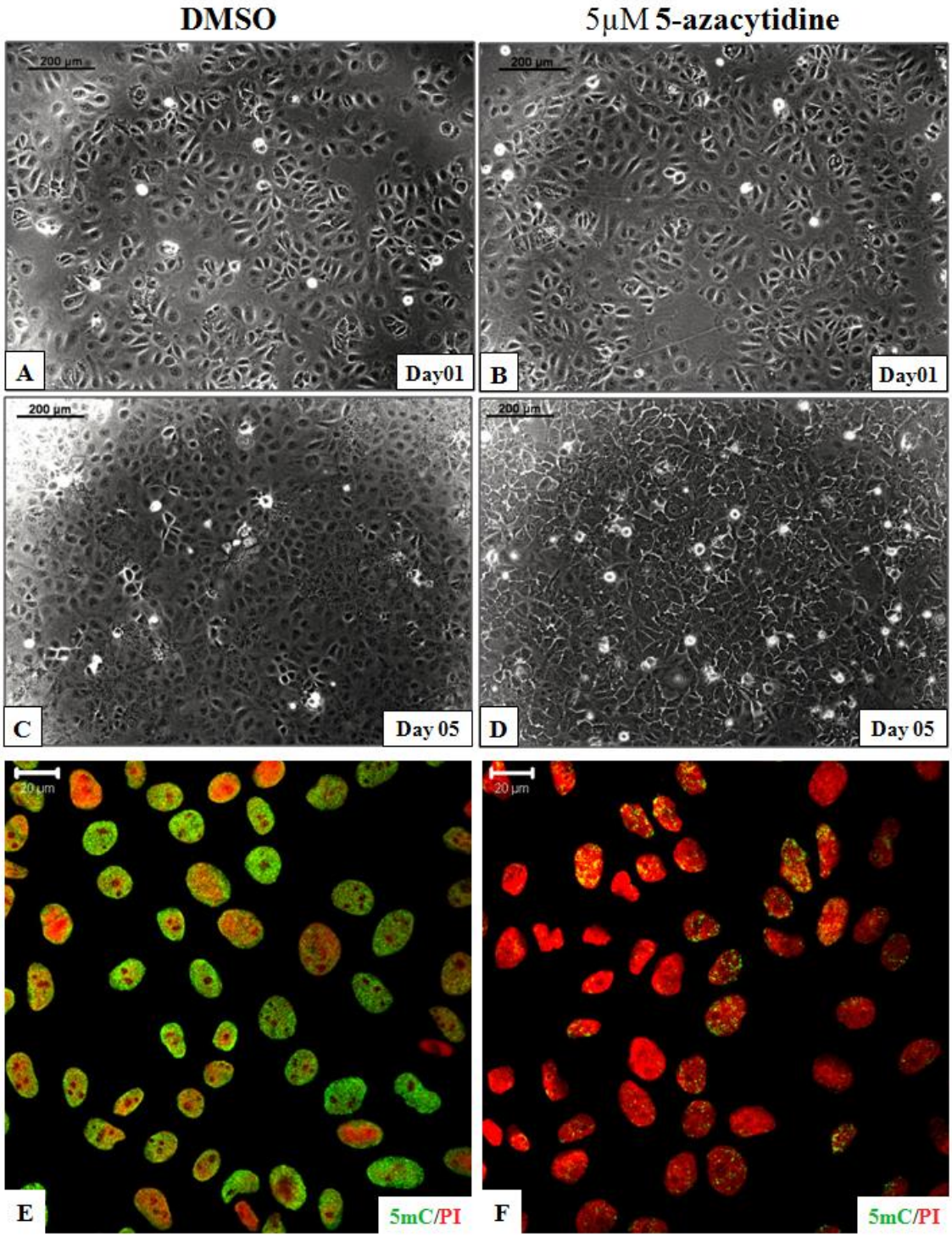

Figure5.1. Live photos and the staining of 5mC in TCam-2 cells, which were cultured respectively with DMSO and 5-azacytidine for 5 days. A and **B**, the live photos of TCam-2 cells cultured respectively with DMSO and 5-azacytidine on Day01; **C** and **D**, the live photos of TCam-2 cells cultured respectively with DMSO and 5-azacytidine on Day05; **E** and **F**, the staining of 5mC in the TCam-2 cells cultured respectively with DMSO and 5-azacytidine for 5 days. The staining of 5mC is shown in green; the PI nuclear counterstaining is shown in red. The scale bars equal to 200μm in A, B, C and D panels; 20μm in E and F panels.

After cultured with different dosages of 5-azacytidine, DAZL, a germ cell-intrinsic meiotic competence factor, was detected in TCam-2 cells (Fig 5.2).

The mRNA levels of *DAZL* in TCam-2 cells were detected by qRT-PCR. In the control TCam-2 cells, which were incubated with DMSO for 5days, the mRNA of *DAZL* was below the detectable levels. However, after chemical DNA demethylation by 5-azacytidine, the mRNA levels of *DAZL* increased significantly in the 5-azacytidin (doses of 2μM，3μM, 4μM and 5μM) treated TCam-2 cells, when compared to the control TCam-2 cells (Fig 5.2A, data were analyzed using Paired T-test to determine significant changes between control cells and the 5-azacytidine treated cells, all the results were compared with the 0μM TCam-2 cells, $P < 0.05$). Interestingly, the mRNA levels of *DAZL* significantly increased with the increasing dose of 5-azacytidine in TCam-2 cells (Fig 5.2A, data were analyzed using one-way ANOVA with linear trend post-test to determine significant changes in TCam-2 cells across different dosages of 5-azacytidine treatment, $P < 0.05$).

Detecting by Western Blot, the expression of DAZL proteins were undetectable in the control TCam-2 cells. However, after the treatment by 3μM, 4μM and 5μM 5-azacytidine, respectively, the expression of DAZL proteins became detectable in the chemical DNA demethylated TCam-2 cells (Fig 5.2 B). Among these DNA demethylated TCam-2 cells, which were incubated with different doses of 5-azacytidine, the 5μM treated TCam-2 cells expressed the highest level of DAZL proteins (Fig 5.2 B).

From the results above, the mRNA and protein levels of DAZL were increased in a dose response pattern in the 5-azacytidine treated TCam-2 cells, and the most effective dosage for TCam-2 cells is 5μM (Fig 5.2).

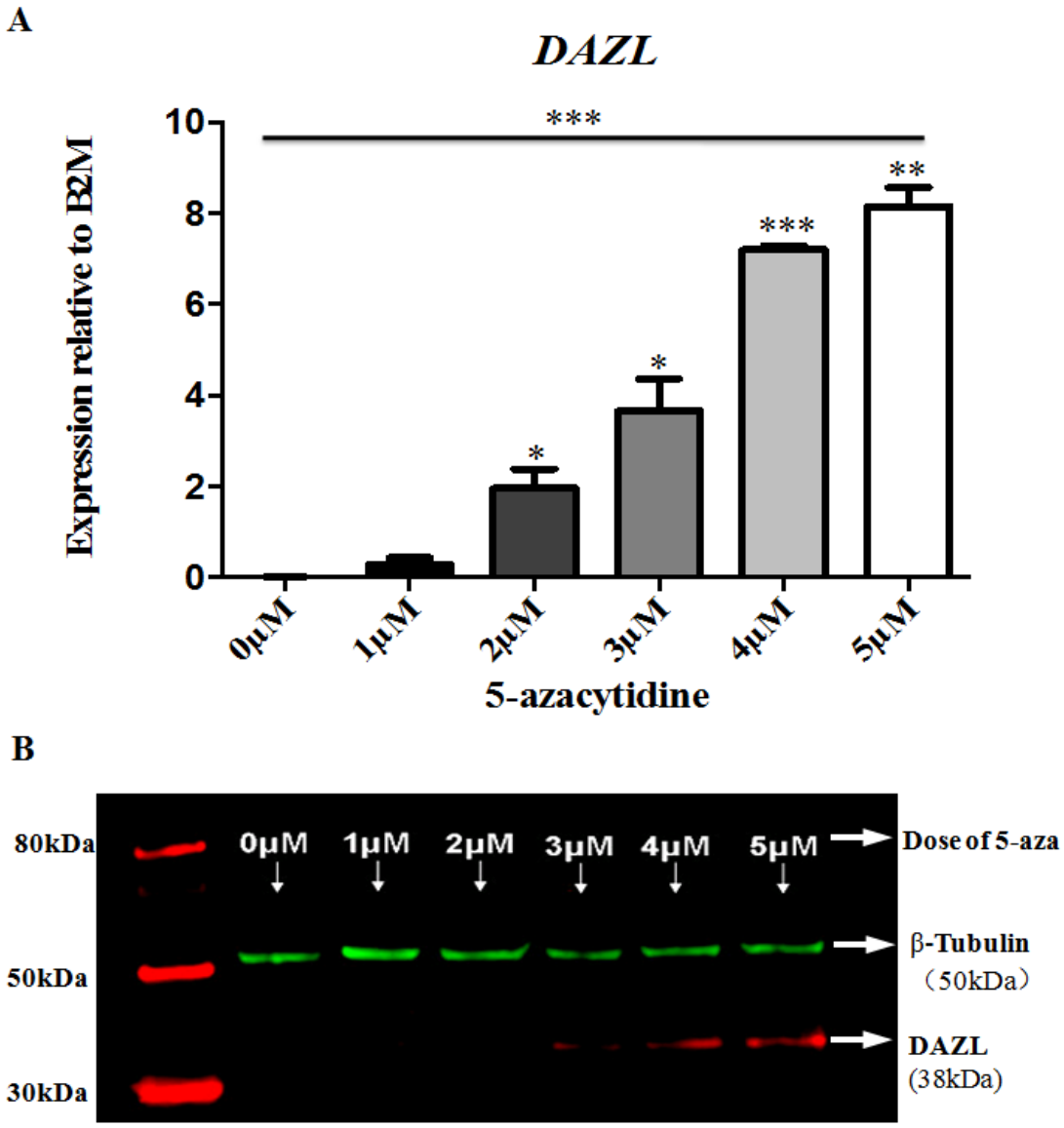

Figure5.2. mRNA and protein levels of DAZL in TCam-2 cells treated with different doses of 5-azacytidine for 5 days. A. The mRNA levels of *DAZL* in TCam-2 cells were detected by qRT-PCR. Error bars in histograms represent ±SEM. The expression of *DAZL* was normalized to that of the housekeeping gene *B2M*, which remained stable between treatments. Data were analyzed using Paired T-test to determine significant changes between control cells and the 5-azacytidine treated cells; all the results were compared with the 0μM TCam-2 cells. Data were also analyzed using one-way ANOVA with linear trend post-test to determine significant changes in TCam-2 cells across different dosage of 5-azacytidine treatments. The expression of *DAZL* was increased in a dose response pattern; the maximum increase was observed in the TCam-2 cells treated with 5μM of 5-azacytidine. n=3; * $P \leq 0.05$; ** $P \leq 0.01$; *** $P \leq 0.001$. **B.** By Western Blot, the DAZL proteins were undetectable in the control TCam-2 cells, the 1μM and 2μM 5-azacytidine treated TCam-2 cells; and became detectable in the TCam-2 cells treated with 3μM, 4μM and 5μM of 5-azacytidine; the 5μM treated TCam-2 cells expressed the highest level of DAZL protein.

In control TCam-2 cells, the expression of postmigratory germ cell-specific genes and meiotic genes, *STRA8*, *VASA*, *SYCP3*, *SYCP1* and *BOLL*; were present in a low level or barely detectable *(*Fig 5.3). However, after chemical DNA demethylation by 5-azacytidine, the mRNA levels of *STRA8*, *VASA*, *SYCP3* and *BOLL* increased significantly in the 5-azacytidin (2μM，3μM, 4μM and 5μM) treated TCam-2 cells, when compared to the control TCam-2 cells (Fig 5.3A, B, C and E, data were analyzed using Paired T-test to determine significant changes between control cells and the 5-azacytidine treated cells, all the results were compared with the 0μM TCam-2 cells, $P < 0.05$). Similar to *DAZL*, the expression of *STRA8*, *VASA*, *SYCP3* and *BOLL* were increased in a dose response pattern in the 5-azacytidine treated TCam-2 cells (Fig 5.3A, B, C and E). After treated with different dosages of 5-azacytidine, the expression of *STRA8*, *VASA*, *SYCP3* and *BOLL* were significantly upregulated with the increasing dose of 5-azacytidine in TCam-2 cells (Fig 5.3A, B, C and E, data were analyzed using one-way ANOVA with linear trend post-test to determine significant changes in TCam-2 cells across different dosage of 5-azacytidine treatment, $P < 0.05$). The expression of *SYCP1* only increased significantly after treated with 4μM 5-azacytidine and did not change significantly in a dose pattern in TCam-2 cells (Fig5.3 D).

The results above indicated that the expression of postmigratory germ cell-specific genes and meiotic genes *DAZL*, *STRA8*, *VASA*, *SYCP3* and *BOLL* were all upregulated by DNA demethylated agent 5-azacytidine in TCam-2 cells (Fig 5.2 and Fig 5.3).

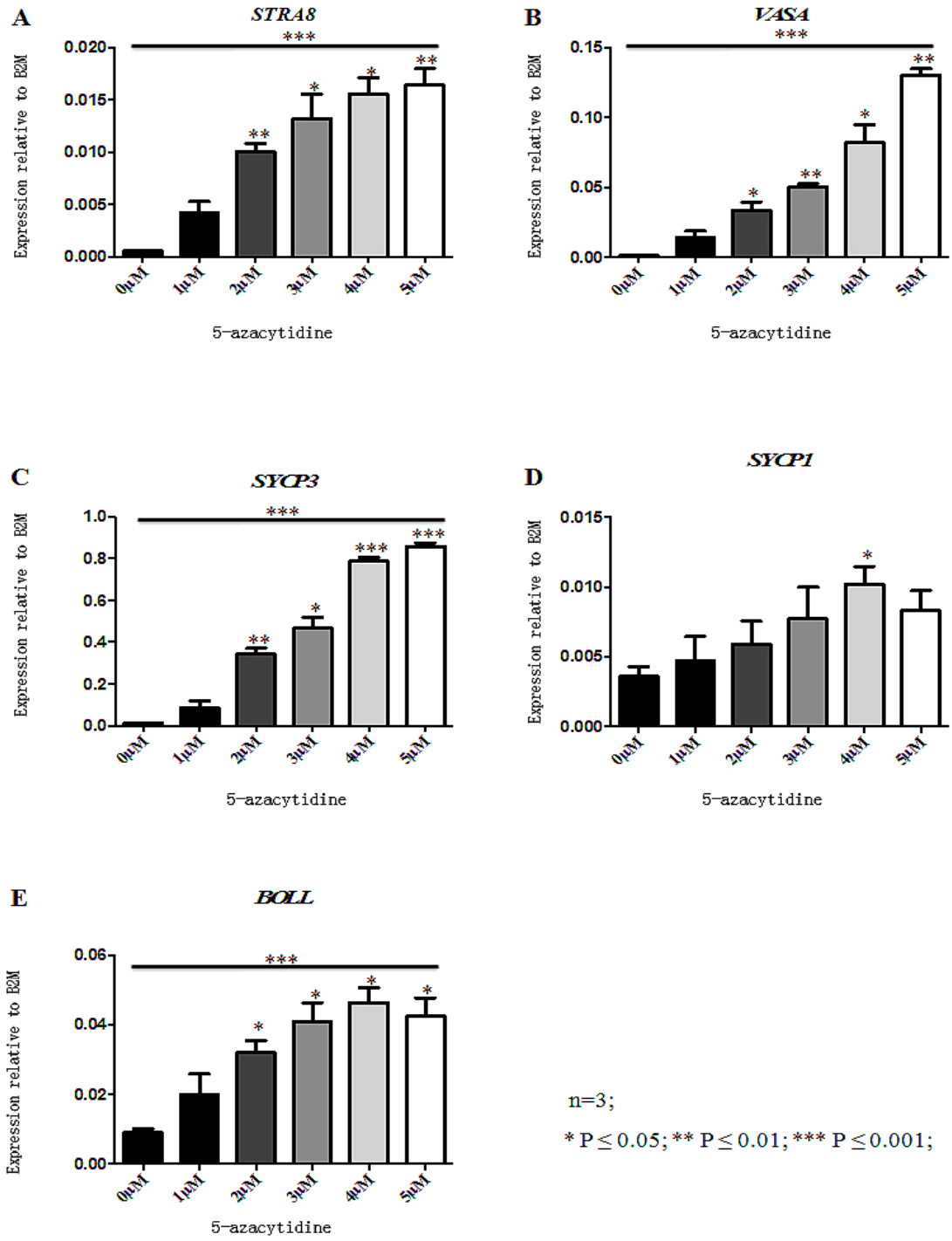

Figure 5.3 mRNA levels of postmigratory germ cell-specific genes and meiotic genes in the TCam-2 cells treated with different doses of 5-azacytidine for 5 days. A, *STRA8;* ***B,*** *VASA;* ***C,*** *SYCP3;* ***D,*** *SYCP1;* ***E,*** *BOLL;* mRNA levels of these genes were detected by qRT-PCR in TCam-2 cells. Error bars in histograms represent ±SEM. The expressions of these genes were normalized to that of the housekeeping gene *B2M*. Data were analyzed using Paired T-test to determine significant changes between control cells and the 5-azacytidine treated cells; all the results were compared with the 0μM TCam-2 cells. Data were also analyzed using one-way ANOVA with linear trend post-test to determine significant changes in

TCam-2 cells across different dosage of 5-azacytidine treatments. The expressions of *STRA8, VASA*, *SYCP3* and *BOLL* were increased in a dose response pattern.

Nevertheless, the data above leads to the question whether Chemical DNA demethylation in TCam-2 cells increases the expression of all the genes or just upregulates some specific genes. In order to answer this question, other types of genes were also investigated in the 5-azacytidine treated TCam-2 cells. The pluripotency-associated genes *OCT4* and *NANOG* (Fig5.4 A and B) and epigenetic genes *TET1*, *2* and *3* (Fig5.4 C, D and E) were detected in TCam-2 cells. In TCam-2 cells, the mRNA of these genes was present in a high level. After treated with 5-azacytidine, the expression of these genes did not significantly change (Fig5.4). The human AFP (Alpha-fetoprotein) gene, which encodes a major plasma protein produced by the yolk sac and liver during fetal development (Mizejewski, 2001), was also detected (Fig5.4 F). As a positive control, high levels of AFP were detected in the human fetal liver; however, AFP remained undetectable in the TCam-2 cells no matter treated with or without 5-azacytidine (Fig5.4 F).

The findings above indicated that chemical DNA demethylation by 5-azacytidine specifically increased the expression of postmigratory germ cell-specific genes and meiotic genes in TCam-2 cells rather than increasing the expression of all genes.

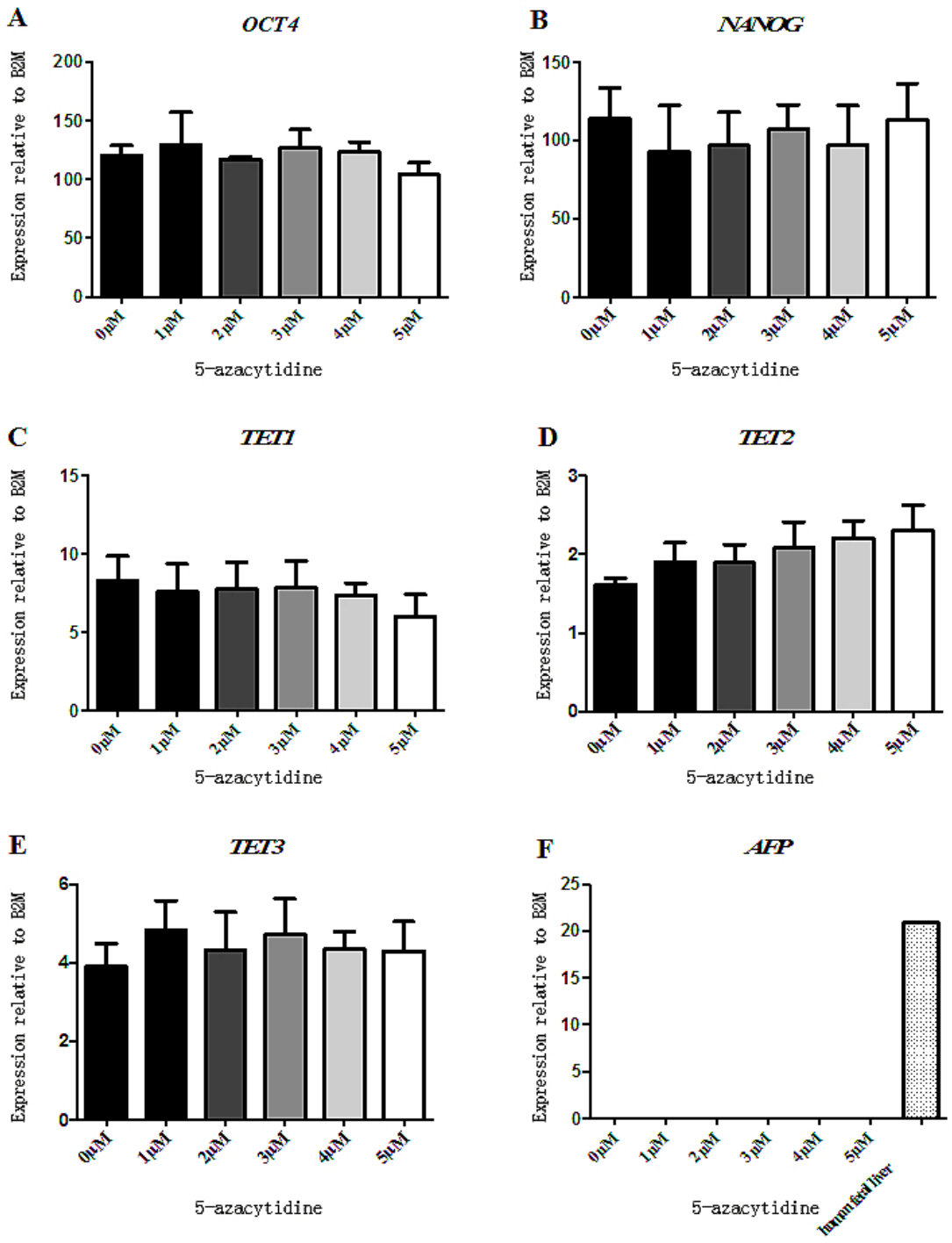

Figure 5.4 mRNA levels of *OCT4*, *NANOG*, *TET1, TET2, TET3* and *AFP* in the TCam-2 cells treated with different doses of 5-azacytidine for 5 days. A,*OCT4*; **B**,*NANOG*; **C**,*TET1*; **D**,*TET2* ; **E,***TET3*; **F,** *AFP*; mRNA levels of these genes were detected by qRT-PCR in TCam-2 cells. Error bars in histograms represent ±SEM. The expressions of these genes were normalized to that of the housekeeping gene *B2M*. The expression of *OCT4*, *NANOG, TET1, TET2* and *TET3* did not significant change in TCam-2 cells after 5-azacytidine treatment. *AFP* was present in a high level in the human fetal liver, but was undetectable in the TCam-2 cells even after 5-azacytidine treatment.

5.2.2 The correlation between chemical DNA demethylation and RA responsiveness in TCam-2 cells

According to the results above, 5-azacytidine specifically increased the expression of postmigratory germ cell-specific genes and meiotic genes in TCam-2 cells. However, whether chemical DNA demethylation associated with RA responsiveness and further upregulated the expression of meiotic genes in human fetal germ cells was still unknown.

In order to investigate this, further RA treatment was performed in the chemical DNA demethylated TCam-2 cells. The control TCam-2 cells were incubated with DMSO for 3 days firstly; afterwards, all these control TCam-2 cells were treated with different doses of RA (0, 0.1 and 1nM) for 2 days. Meanwhile, the treated TCam-2 cells were incubated with 5μM of 5-azacytidine for 3days to erase the methylated DNA; afterwards, all these DNA demethylated TCam-2 cells were treated with different doses of RA (0, 0.1 and 1nM) for 2 days. After all the incubations, the live photos on Day05 showed that the morphology of all the TCam-2 cells, including the control and treated TCam-2 cells, appeared normal; and the number of floating dead cells was similar between the control and treated TCam-2 cells (Fig 5.5), indicating that RA treatment used in these studies was below the toxic dosage for the TCam-2 cells.

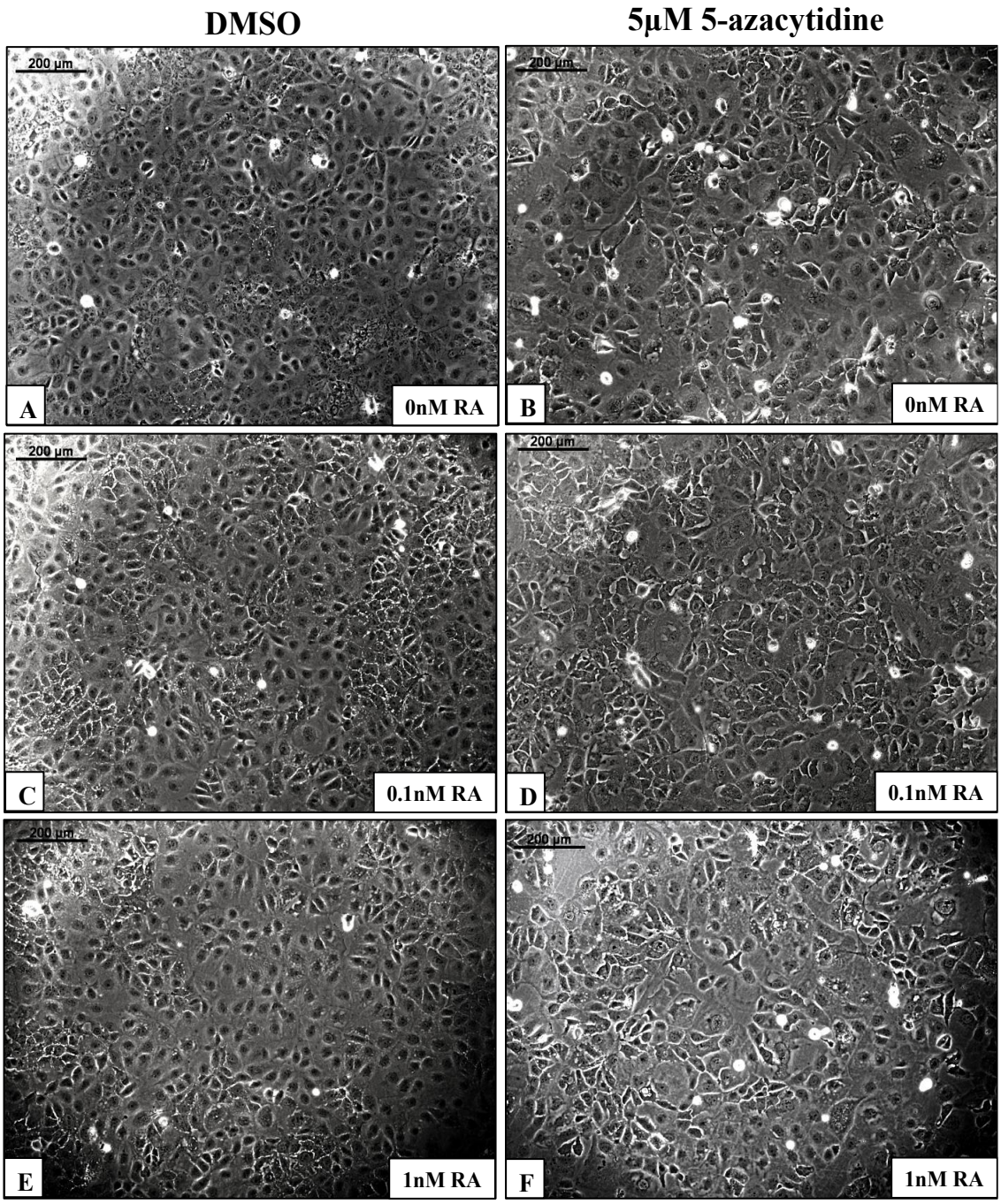

Figure 5.5 Live photos of the control and DNA demethylated TCam-2 cells, which were treated with different doses of RA for 2days. A, C and **E,** the live photos of TCam-2 cells which were incubated with DMSO for 3 days and then with 0, 0.1 and 1nM of RA for 2days; **B, D** and **F,** the live photos of TCam-2 cells which were cultured with 5-azacytidine for 3 days and then with 0, 0.1 and 1nM of RA for 2 days. The scale bars equal to 200μm in all panels.

After RA treatment, the mRNA levels of germ cell-specific genes and meiotic genes *DAZL, VASA, STRA8, SYCP3, SYCP1, DMC1* and *BOLL* were all detected in the control and DNA demethylated TCam-2 cells (Fig 5.6 and Fig 5.7). The mRNA levels of these genes were detected by qRT-PCR in TCam-2 cells. The expressions of these genes were normalized to that of the housekeeping gene B2M.

In the control TCam-2 cells, RA treatment did not significantly change the expression of these germ cell-specific genes and meiotic genes (Fig 5.6, data were analyzed using Paired T-test to determine significant changes between the TCam-2 cells treated with and without RA, all the results were compared to the 0nM RA TCam-2 cells).

In the DNA demethylated TCam-2 cells, which were cultured with 5-azacytidine firstly, RA treatment significantly increased the mRNA levels of pre-meiotic gene *STRA8* and further increased its putative targets *SYCP3* and *VASA.* However, other germ cell-specific genes and meiotic genes, such as *DAZL, SYCP1, DMC1* and *BOLL*, did not significantly change after different doses of RA treatment (Fig 5.7, data were analyzed using Paired T-test to determine significant changes between the TCam-2 cells treated with and without RA, all the results were compared to the 0nM RA TCam-2 cells).

Among the DNA demethylated TCam-2 cells, the cells treated with 0.1nM RA all significantly increased the expression of *VASA, STRA8* and *SYCP3;* however, the cells treated with 1nM RA only significantly increased the expression of *VASA* and *STRA8,* but not *SYCP3* (Fig 5.7 B, C and D). These results suggested that 0.1nM RA was a more effective dose for the treatment in TCam-2 cells.

Intriguingly, the expression of *RAR-β* significantly increased after RA treatment in both of the DMSO and 5-azacytidine treated TCam-2 cells (Fig 5.6 H and Fig 5.7 H), suggesting that all these cells were receiving and transducing RA signals.

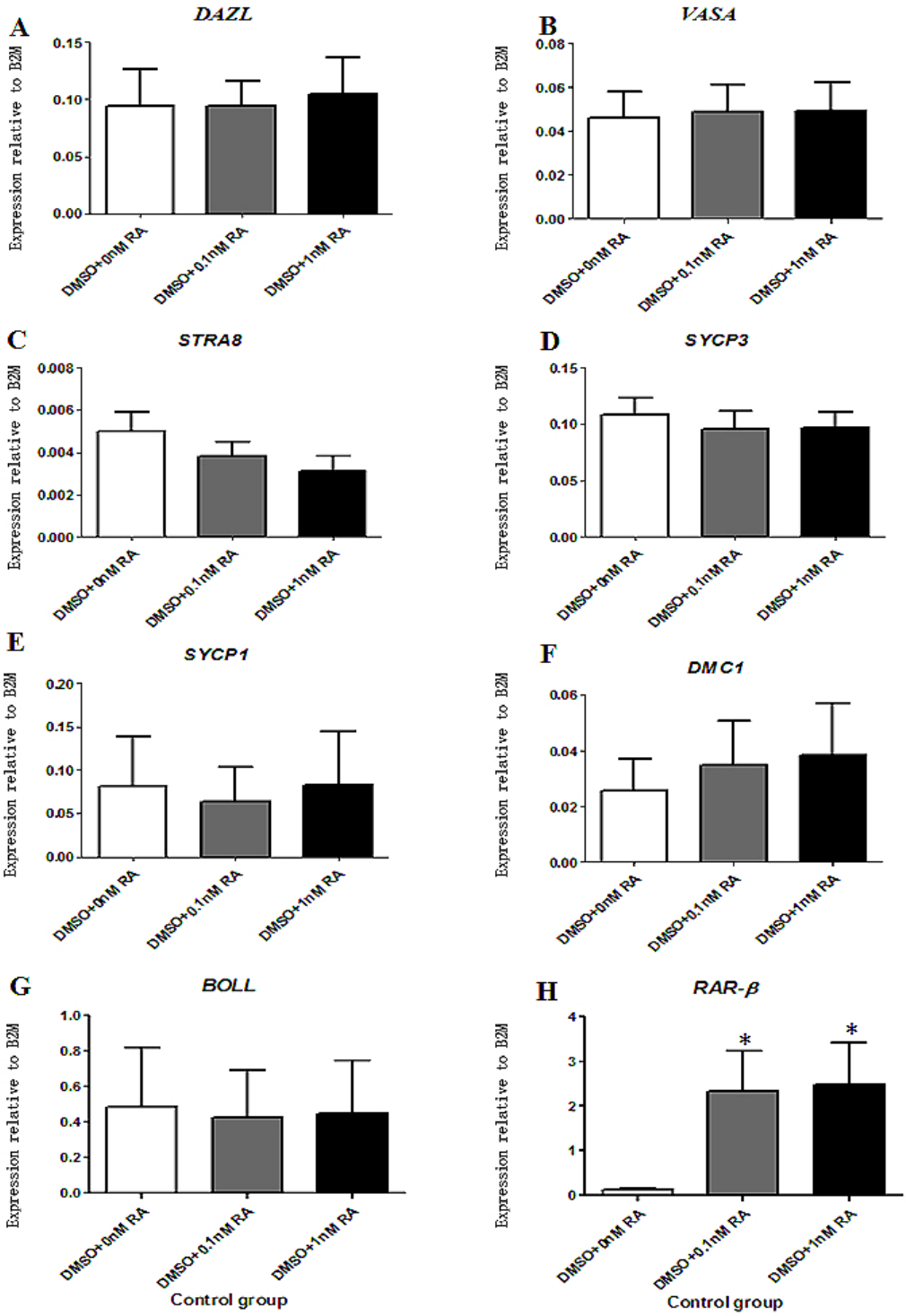

Figure 5.6 mRNA levels of *DAZL*, *VASA*, *STRA8*, *SYCP3*, *SYCP1*, *DMC1*, *BOLL* and *RAR-β* in the control TCam-2 cells, which were cultured with DMSO firstly and then treated with different doses of RA for 2 days. A, *DAZL*; ***B***, *VASA;* **C**, *STRA8; **D**, SYCP3; **E**, SYCP1; **F**, DMC1; **G**, BOLL; **H**, RAR-β;* error bars in histograms represent ±SEM. Data were analyzed using Paired T-test to determine significant changes between the cells treated with and without RA; all the results were compared with the 0nM RA TCam-2 cells.

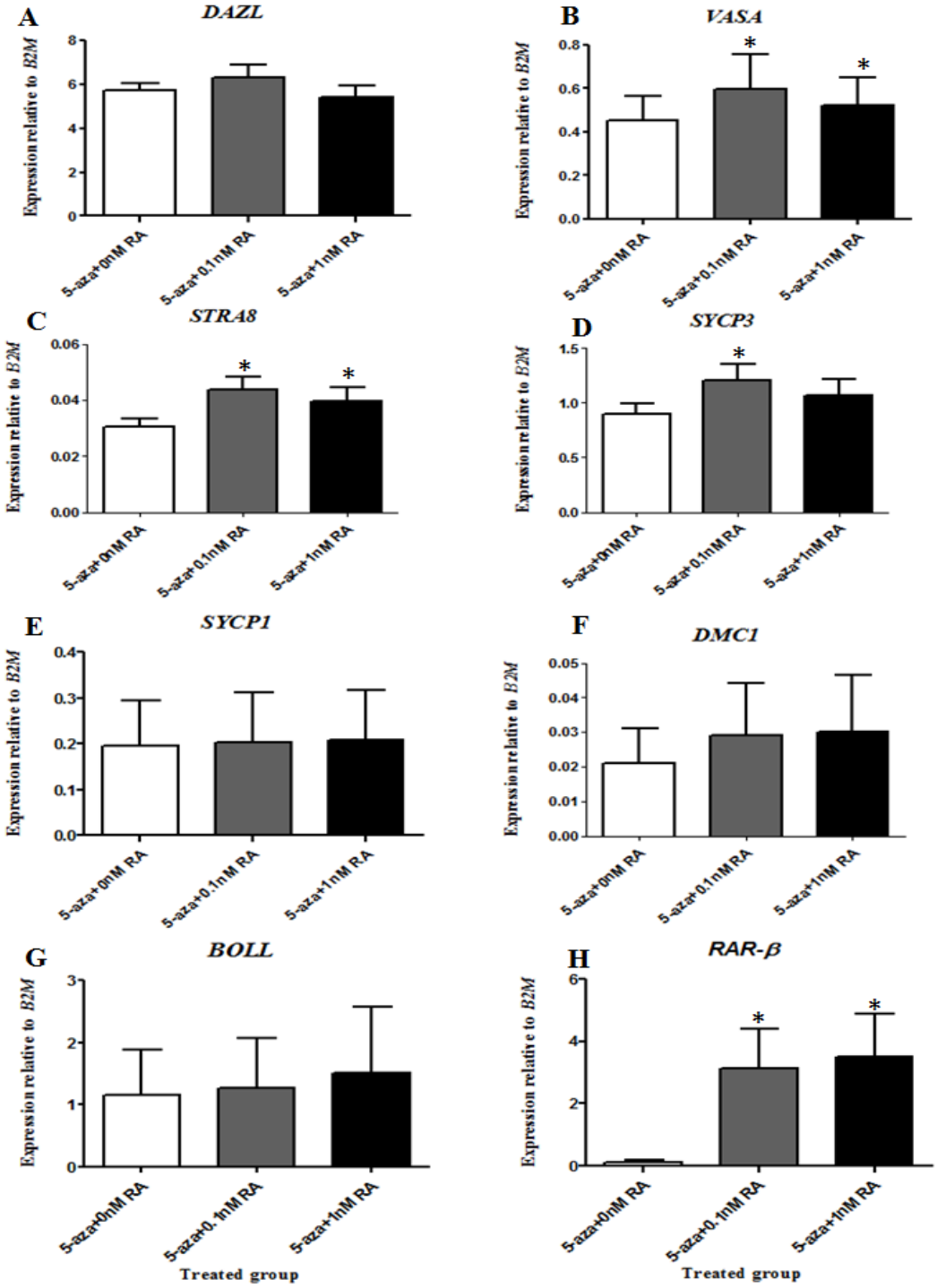

Figure 5.7 mRNA levels of *DAZL*, *VASA*, *STRA8*, *SYCP3*, *SYCP1*, *DMC1*, *BOLL* and *RAR-β* in the DNA demethylated TCam-2 cells, which were cultured with 5-azacytidine firstly and then treated with different doses of RA for 2 days. A, *DAZL*; ***B**, VASA;* **C**, *STRA8;* ***D**, SYCP3;* ***E**, SYCP1;* ***F**, DMC1;* ***G**, BOLL;* ***H**, RAR-β;* error bars in histograms represent ±SEM. Data were analyzed using Paired T-test to determine significant changes between the cells treated with and without RA; all the results were compared with the 0nM RA TCam-2 cells.

The expression of DAZL and SYCP3 proteins were also detected in the control and chemical DNA demethylated TCam-2 cells, which were treated with different doses of RA afterwards (Fig 5.8 and 5.9).

In the control TCam-2 cells, which were incubated with DMSO firstly, DAZL protein was undetectable even after RA treatment (Fig 5.8 A, C and E). However, the DAZL protein was detectable in the DNA demethylated TCam-2 cells, indicating that DNA demethylation is required for the expression of DAZL in the TCam-2 cells (Fig 5.8 B, D and F). In the DNA demethylated TCam-2 cells, which were treated with 0nM RA afterwards, most of the DAZL staining was restricted to the nucleus of the cells (Fig 5.8 B). However, in the DNA demethylated TCam-2 cells, which were treated with 0.1nM and 1nM RA afterwards, most of the DAZL staining was restricted to the cytoplasm of the cells (Fig 5.8 D and F).

The expression of SYCP3 was detectable in the control and DNA demethylated TCam-2 cells treated with or without RA (Fig 5.9). In the control TCam-2 cells, which were incubated with DMSO firstly, most of the SYCP3 staining was localized in the cytoplasm (Fig 5.9 A, C and E). However, in the DNA demethylated TCam-2 cells, treated with or without RA treatment, most of the SYCP3 staining were localized in both nucleus and cytoplasm (Fig 5.9 B, D and F).

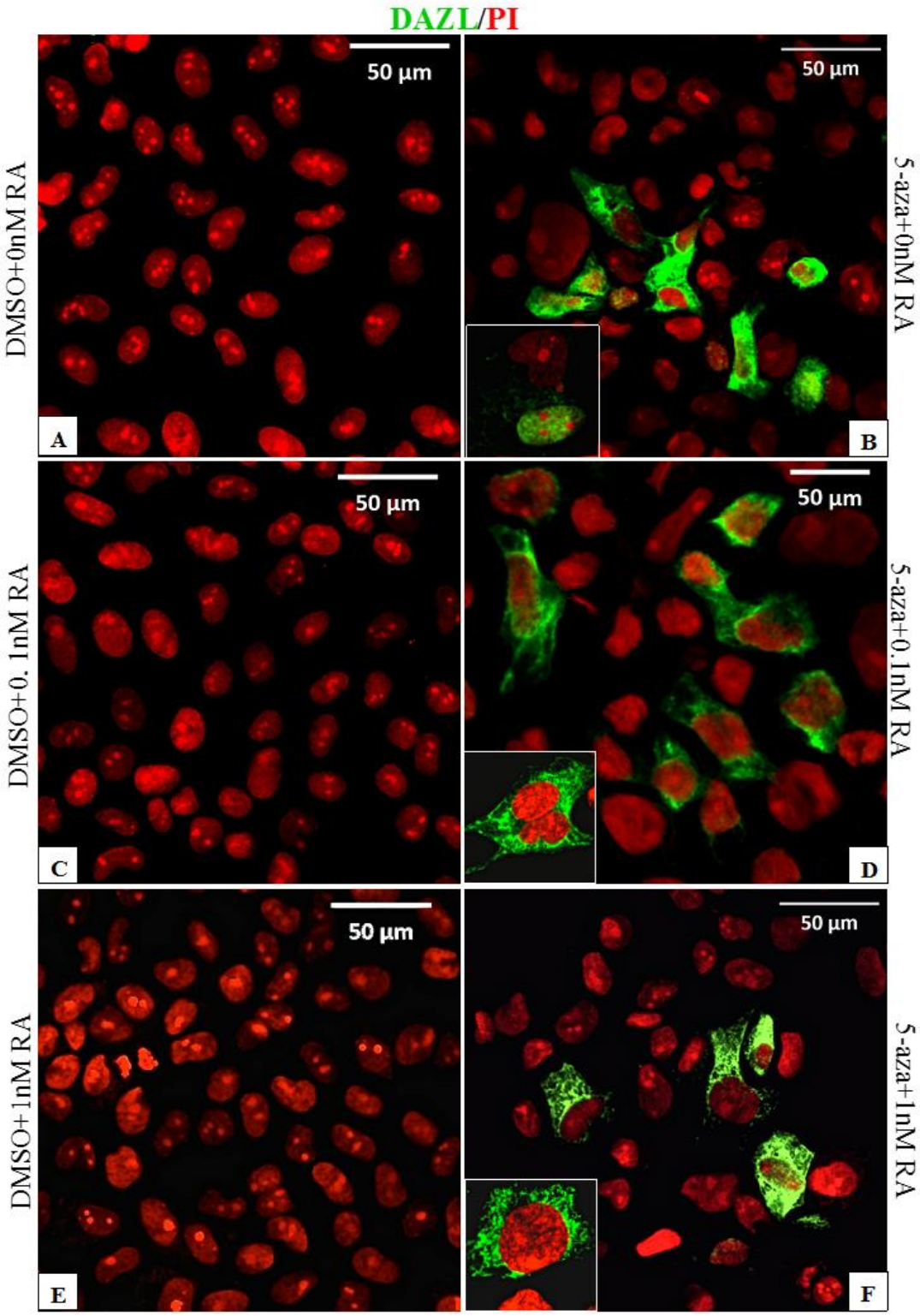

Figure 5.8. Distribution of DAZL in the control and DNA demethylated TCam-2 cells, which were treated with different doses of RA afterwards. The staining of DAZL is shown in green; the PI nuclear counterstaining is shown in red. The scale bars equal to 50μm in A, B, C, D，E and F panels.

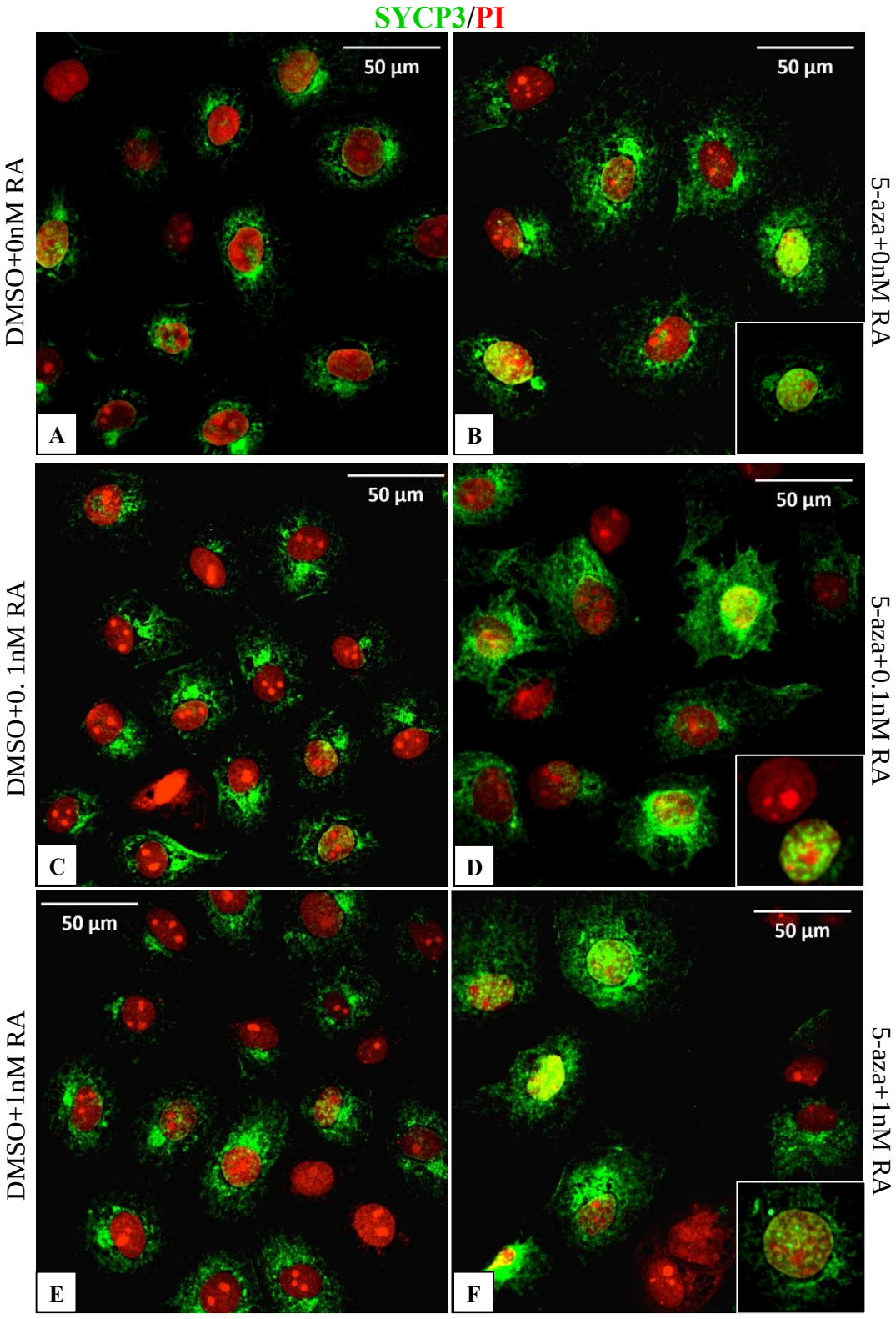

Figure 5.9. Distribution of SYCP3 in the control and DNA demethylated TCam-2 cells, which were treated with different doses of RA afterwards. The staining of SYCP3 is shown in green; the PI nuclear counterstaining is shown in red. The scale bars equal to 50µm in A, B, C, D, E and F panels.

5.2.3 *mStra8* transfection in TCam-2 cells

The results above indicate that the pre-meiotic gene *STRA8* did not respond to RA and the expression of meiotic genes was not upregulated in the TCam-2 cells without chemical DNA demethylation; however, *STRA8* and its putative targets *SYCP3* and *VASA* were further increased by RA in the TCam-2 cells with chemical DNA demethylation. This leads to a question that whether the further upregulation of *SYCP3* and *VASA* was affected by the increasing *STRA8* or directly by RA in the DNA demethylated TCam-2 cells.

In order to identify this, *stra8* vector was transfected into TCam-2 cells, and then the expression of its putative targets *SYCP3* and *VASA*, and other meiotic genes were detected. The previous research by Miyamoto (Miyamoto et al., 2002) compared the amino acid sequences between human *STRA8* and mouse *Stra8* and identified that human STRA8 protein has some homology to mouse stra8 (55% identity overall). As there is lacking of human *STRA8* vector, and the homology between human *STRA8* and mouse *Stra8* is 55%, a mouse pEGFP-C1-*Stra8* vector was transfected into TCam-2 for 3 days.

In the control TCam-2 cells, which were transfected with an empty vector (pCMV6-Entry), *mStra8* was not detectable. However, in the TCam-2 cells, which were transfected with mouse *Stra8* vector (pEGFP-C1-*Stra8)*, *mStra8* was highly expressed (Fig 5.10 A, data were analyzed using Paired T-test to determine significant changes between the control and *mStra8* transfected TCam-2 cells, all the results were compared to the pCMV6-Entry transfected TCam-2 cells). The live photos taken by fluorescent microscopy showed that mStra8 protein was present both in the nucleus and cytoplasm of pEGFP-C1-*Stra8* transfected TCam-2 cells (Fig 5.10 B), suggesting that mStra8 has been transfected into TCam-2 cells successfully.

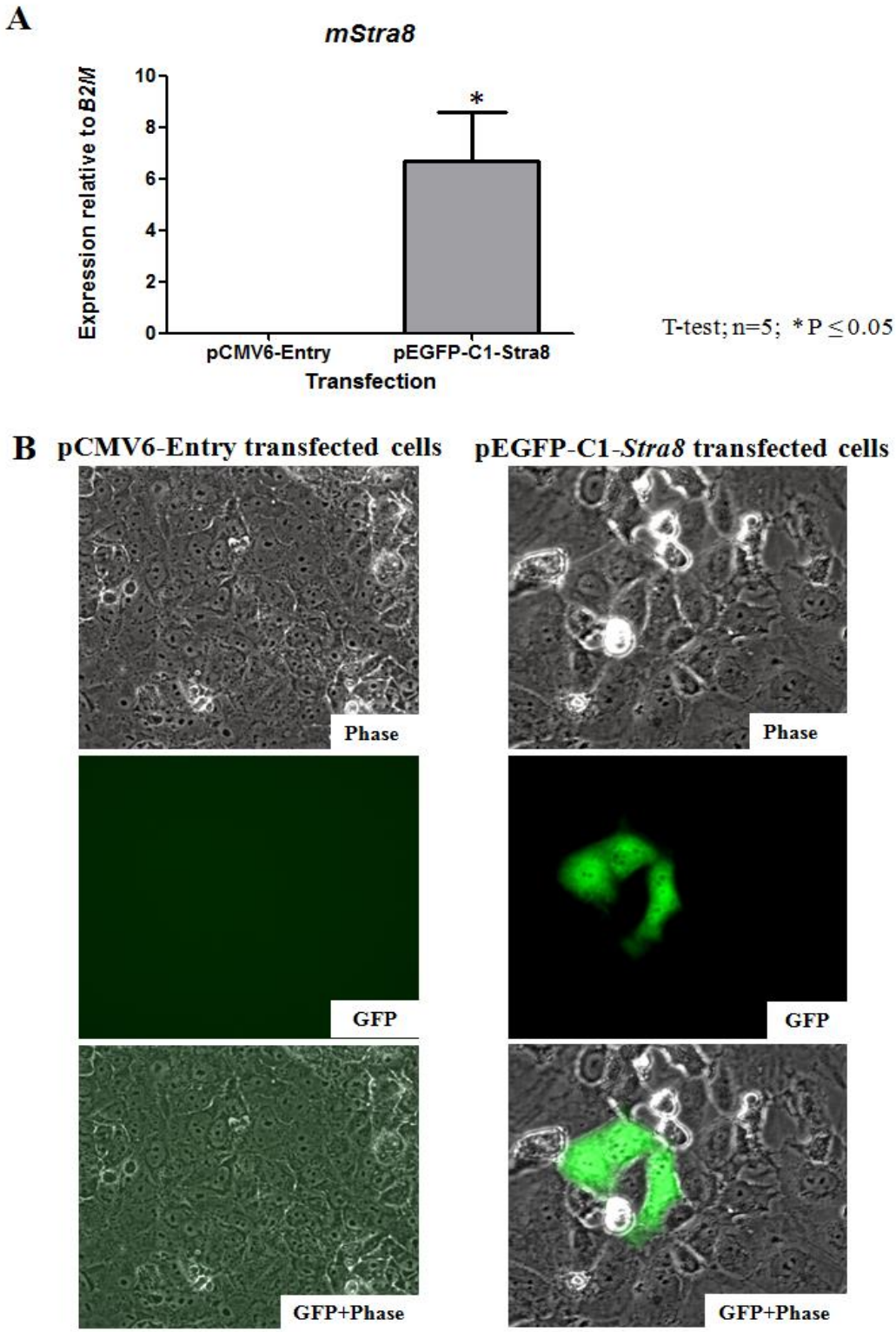

Figure 5.10 TCam-2 cells transfected with pCMV6-Entry and mouse pEGFP-C1-*Stra8* vectors for 3days. A, the mRNA levels of *mStra8* in TCam-2 cells after pCMV6-Entry and mouse pEGFP-C1-*Stra8* vectors transfection; error bars in histograms represent ±SEM; the expressions of *mstra8* were normalized to that of the housekeeping gene *B2M*; **B,** live photos of the transfected TCam-2 cells detected by the fluorescent microscopy.

The expression of meiotic and pluripotency-associated genes was detected in the control and mouse pEGFP-C1-*Stra8* transfected TCam-2 cells by QRT-PCR. Compared with the control TCam-2 cells, expression of *SYCP3* and *DAZL* were significantly increased after *mStra8* transfection, however, the mRNA levels of *SYCP1*, *DMC1*, *VASA* and *OCT4* did not significantly change (Fig 5.11, data were analyzed using Paired T-test to determine significant changes between the control and *mStra8* transfected TCam-2 cells, all the results were compared to the pCMV6-Entry transfected TCam-2 cells). The results above indicated that mouse stra8, which has 55% homology of human *STRA8*, can upregulated the expression of *STRA8*'s putative targets *SYCP3* and *DAZL*, but cannot increase all the meiotic genes.

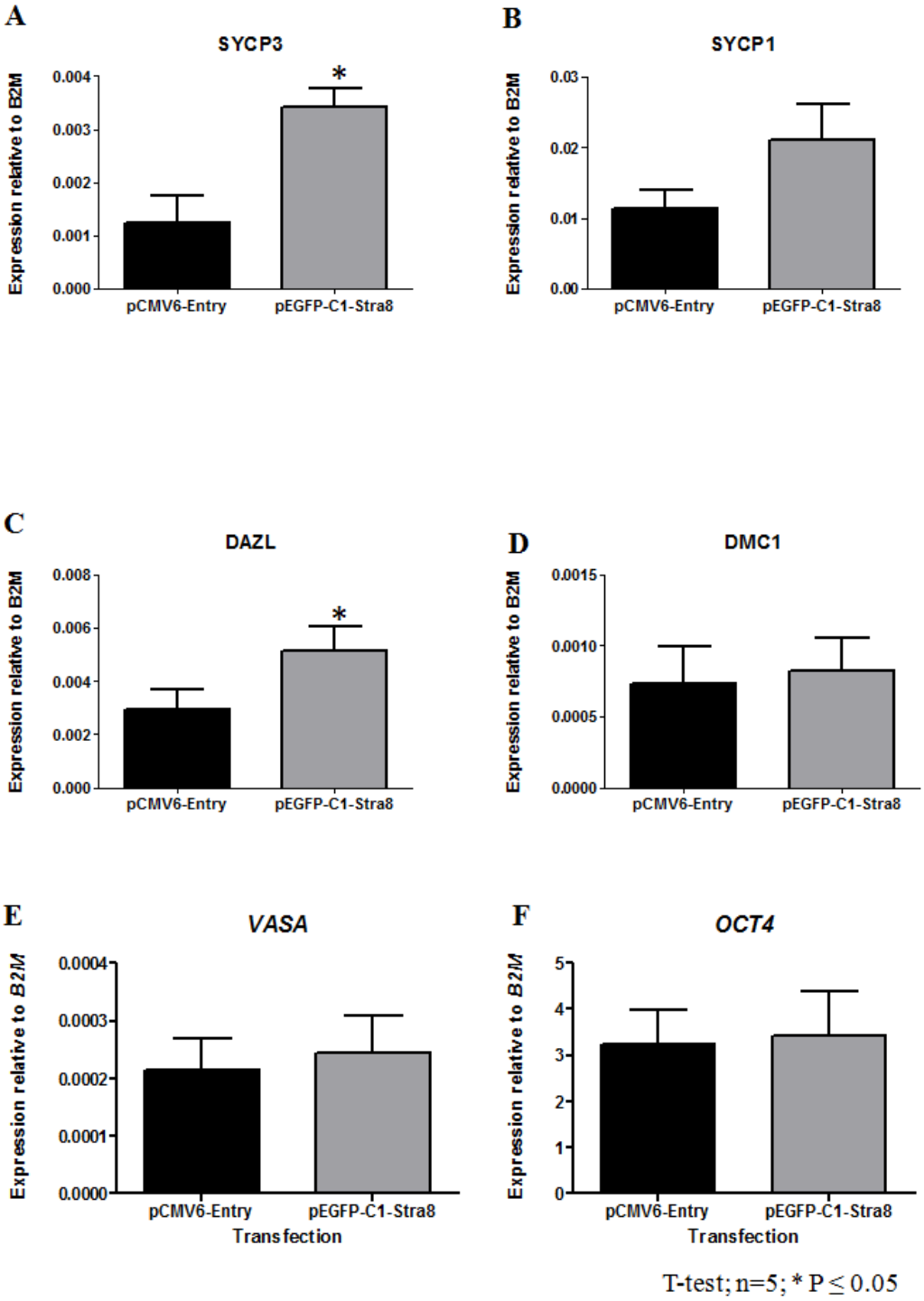

Figure 5.11 expression of meiotic and pluripotency-associated genes in the TCam-2 cells after pCMV6-Entry and mouse pEGFP-C1-*Stra8* transfection. A, *SYCP3*; **B**, *SYCP1*; **C**, *DAZL*; **D**, *DMC1*; **E**, *VASA;* and **F,** *OCT4;* error bars in histograms represent ±SEM; the expressions of these genes were normalized to that of the housekeeping gene *B2M;* data were analyzed using Paired T-test to determine significant changes between the control and *mStra8* transfected TCam-2 cells, all the results were compared to the pCMV6-Entry transfected TCam-2 cells

5.2.4 The expression of postmigratory germ cell-specific genes and meiotic genes in the DNA demethylated human fetal gonads

The *in-vitro* studies mentioned above showed that chemical DNA demethylation specifically increased the expression of postmigratory germ cell-specific genes and meiotic genes in TCam-2 cells. However, whether chemical DNA demethylation regulates the expression of these genes in human fetal gonads or not was unknown. In order to answer this question, human fetal gonads were incubated in 5μM of 5-azacytidine for 4 days.

The mRNA levels of *DAZL*, *STRA8*, *SYCP3*, *SYCP1*, *DMC1*, *VASA* and *OCT4* were detected in the human 1st trimester fetal ovaries by QRT-PCR. During the 1st trimester, the expression of postmigratory germ cell-specific genes and meiotic genes was present at very low levels in the control ovaries, which were incubated with DMSO. Compared with the control 1st trimester ovaries, the mRNA levels of *DAZL*, *SYCP3* and *VASA* were all significantly increased in the 5-azacytidine treated 1st trimester ovaries (Fig 5.12, data were analyzed using Paired T-test to determine significant changes between the control and 5-azacytidine treated human 1st trimester fetal ovaries, all the results were compared to the DMSO incubated ovaries). However, in the human 2nd trimester ovaries, in which some germ cells have already entered into meiosis, the expression of these genes were already in high levels. After being treated with 5-azacytidine, the expression of these genes did not significantly change in the human 2nd trimester ovaries (Fig 5.13). All these results suggested that the expression of *DAZL*, *SYCP3* and *VASA* were all repressed by DNA methylation in 1st trimester human fetal ovaries. Surprisingly, the pluripotency-associated gene *OCT4*, which was already present in a high level in human 1st trimester fetal ovaries, was also further upregulated by chemical DNA demethylation (Fig 5.12 G). However, during 2nd trimester, expression of *OCT4*, which has already decreased in human fetal ovaries, was not affected by DNA demethylation (Fig 5.13 G).

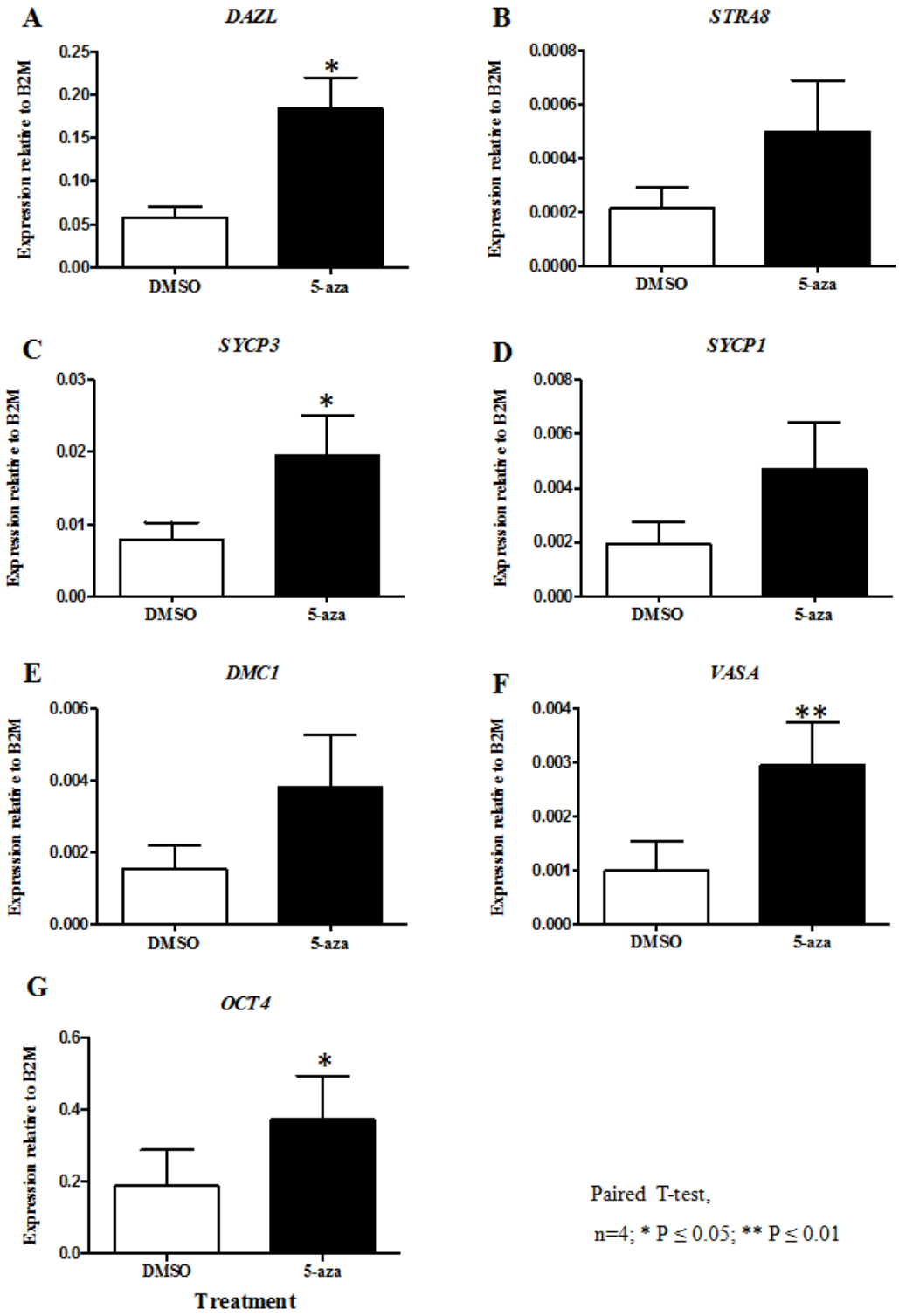

Figure 5.12. mRNA levels of postmigratory germ cell-specific genes, meiotic genes and pluripotent gene in human 1st trimester ovaries (9-10wga), which were incubated with DMSO and 5μM of 5-azacytidine, respectively, for 4 days. **A**, *DAZL*; **B**, *STRA8*; **C**, *SYCP3*; **D**, *SYCP1*; **E**, *DMC1*; **F**, *VASA and* **G**, *OCT4*; error bars in histograms represent ±SEM; the expressions of these genes were normalized to that of the housekeeping gene *B2M*

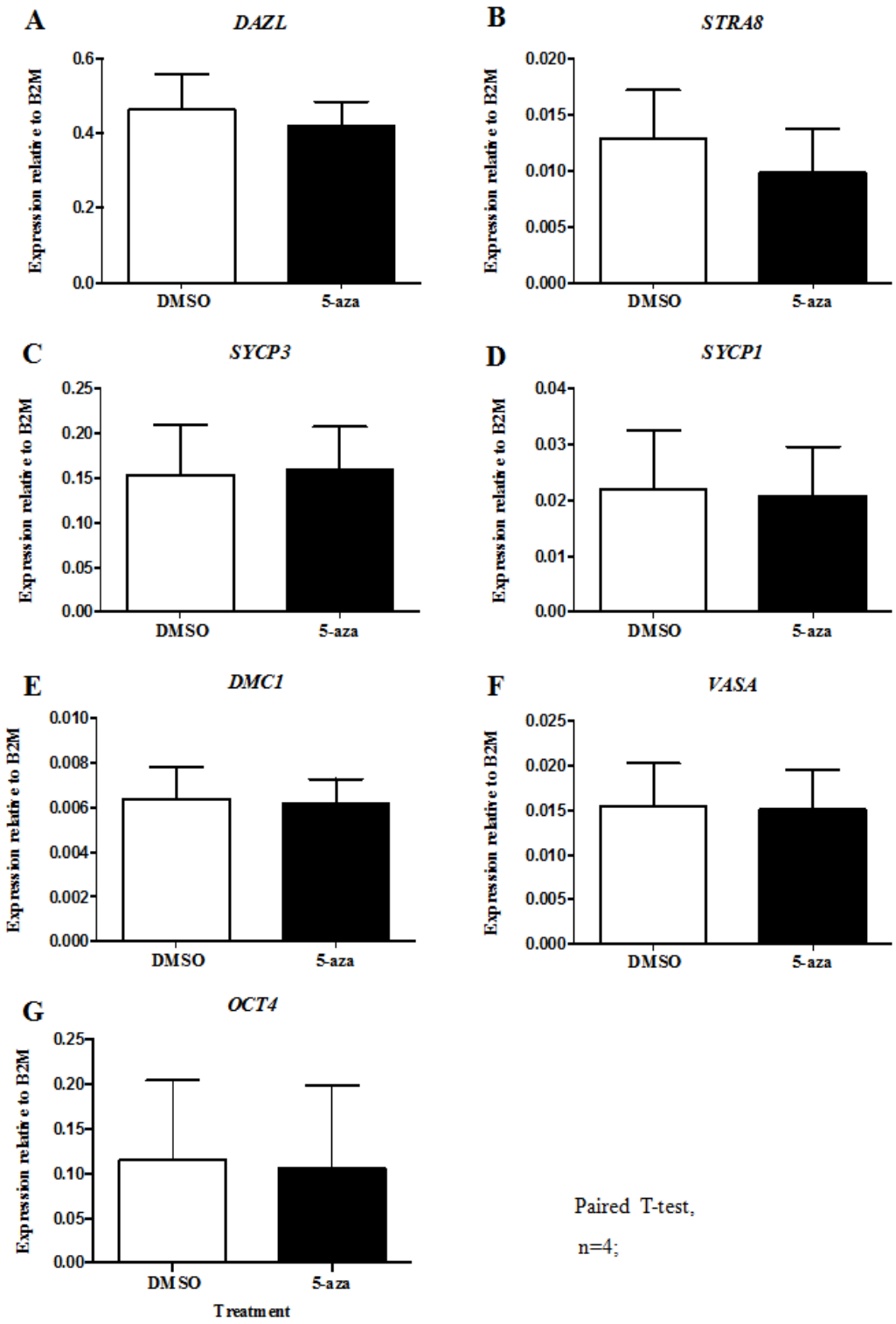

Figure 5.13. mRNA levels of postmigratory germ cell-specific genes, meiotic genes and pluripotent gene in human 2nd trimester ovaries (13-15wga), which were incubated with DMSO and 5μM of 5-azacytidine, respectively, for 4 days. **A**, *DAZL*; **B**, *STRA8*; **C**, *SYCP3*; **D**, *SYCP1*; **E**, *DMC1*; **F**, *VASA and* **G**, *OCT4*; error bars in histograms represent ±SEM; the expressions of these genes were normalized to that of the housekeeping gene *B2M*

After incubated in 5μM of 5-azacytidine for 4 days, the mRNA levels of *DAZL, STRA8, SYCP3, SYCP1, DMC1, VASA* and *OCT4* were also detected in the human 1st trimester fetal testes by QRT-PCR (Fig 5.14).

During the 1st trimester, the expression of postmigratory germ cell-specific genes and meiotic genes was present at very low levels in the control testes, which were incubated with DMSO. After being treated with 5-azacytidine, the mRNA levels of *DAZL* and *SYCP3* were significantly increased in the 1st trimester testes (Fig 5.14, data were analyzed using Paired T-test to determine significant changes between the control and 5-azacytidine treated human 1st trimester fetal testes, all the results were compared to the DMSO incubated testes).

The expression of DAZL and SYCP3 proteins were detected in the DMSO and 5-azacytidine treated 9wga human fetal testis (Fig 5.15). The staining of DAZL protein was detected in the germ cell nucleus of control testis, which was incubated with DMSO for 4days (Fig 5.15 A). In the 5-azacytidine treated 9wga human fetal testis, the staining of DAZL became much stronger, and most of the DAZL staining remained restricted to the germ cell nucleus (Fig 5.15 B), suggesting that DNA demethylation increased the expression DAZL but did not change the distribution of DAZL in the 9wga human fetal testis. However, SYCP3 was undetectable in the 9wga human fetal testis no matter with or without 5-azacytidine treatments (Fig 5.15 C and D), suggesting that the expression of meiotic protein SYCP3 was not activated by DNA demethylation in the 9wga human fetal testis.

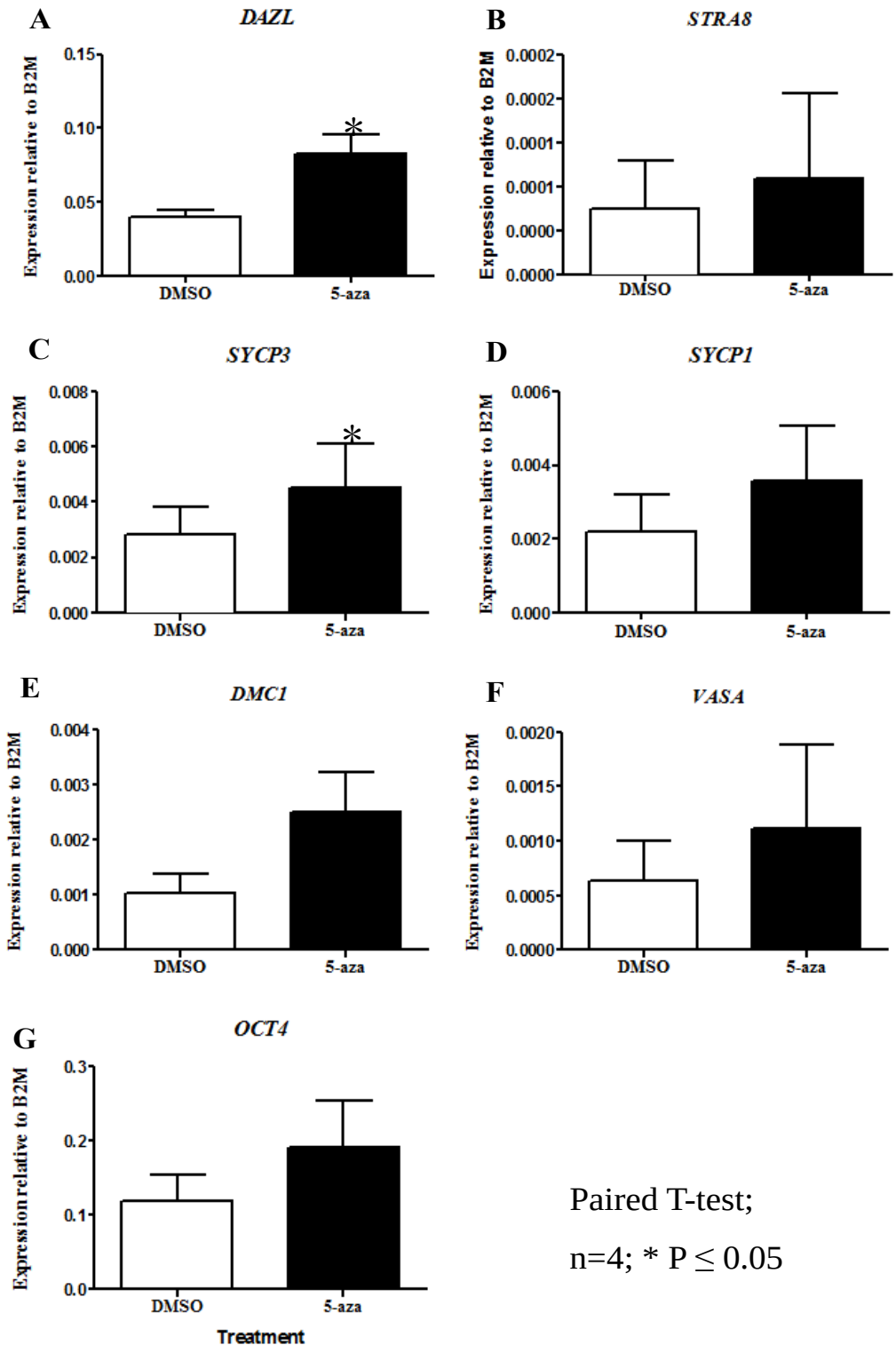

Figure 5.14. mRNA levels of postmigratory germ cell-specific genes, meiotic genes and pluripotent gene in human 1st trimester testes (8-9wga), which were incubated with DMSO and 5μM of 5-azacytidine, respectively, for 4 days. **A**, *DAZL*; **B**, *STRA8*; **C**, *SYCP3*; **D**, *SYCP1*; **E**, *DMC1*; **F**, *VASA and* **G**, *OCT4*; error bars in histograms represent ±SEM; the expressions of these genes were normalized to that of the housekeeping gene *B2M*

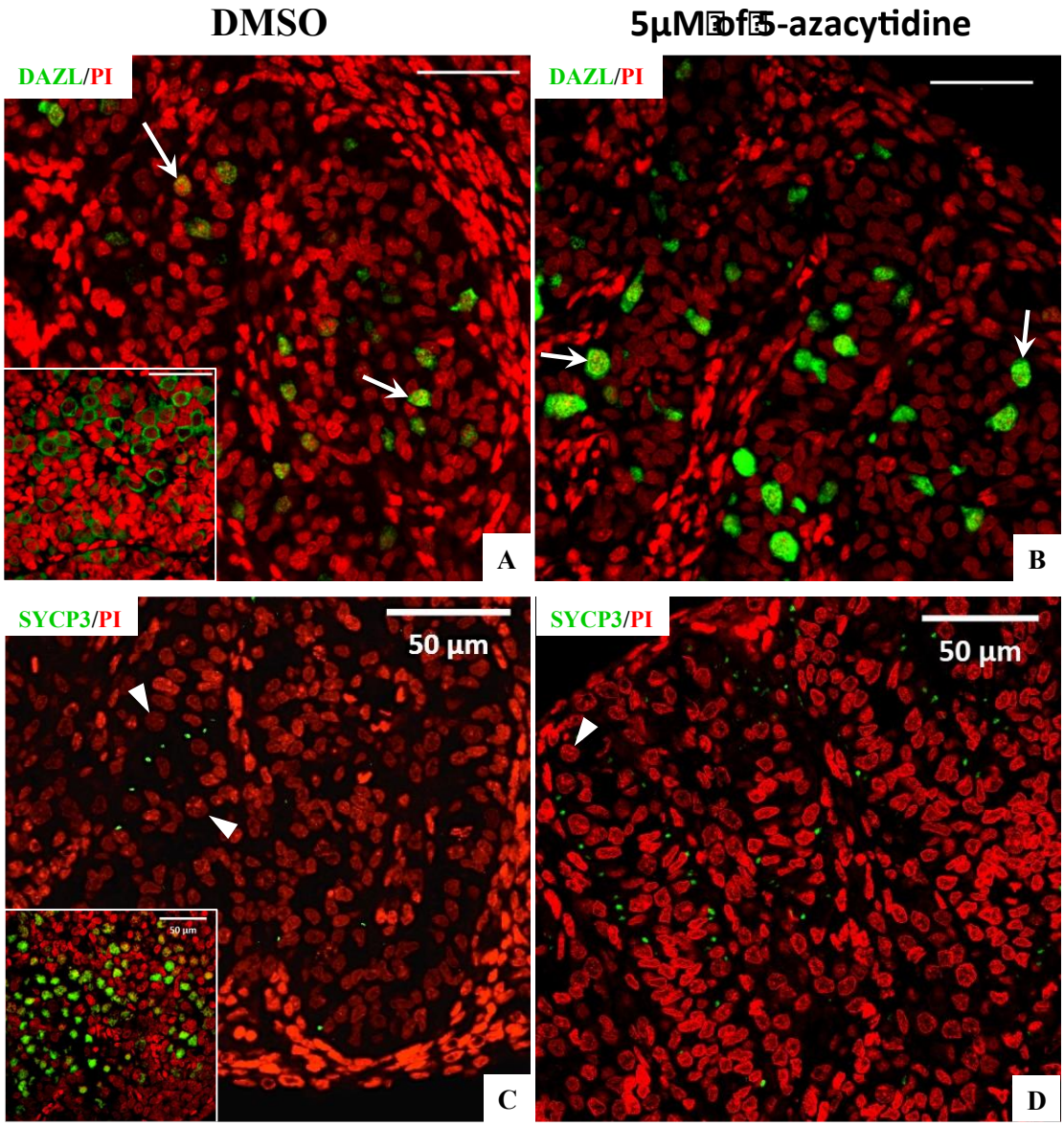

Figure 5.15. Expression of DAZL and SYCP3 proteins in the 9wga human fetal testis; which was incubated with DMSO and 5µM of 5-azacytidine, respectively, for 4 days; The insert panel in A shows the expression of DAZL in 14wga human fetal ovaries, which represents a positive control of DAZL. The insert panel in C shows the expression of SYCP3 in 18wga human fetal ovaries, which was used as a positive control. The staining of DAZL/SYCP3 is shown in green, the PI nuclear counterstaining is shown in red. The arrows in A and B represent the DAZL-positive testicular germ cells, while the arrowheads in C and D represents the SYCP3-negative testicular germ cells. The scale bars equal to 50µm in A, B, C and D panels.

5.2.5 The correlation between chemical DNA demethylation and RA responsiveness in human 1st trimester fetal gonads

The *in-vitro* studies in TCam-2 cells showed that expression of meiotic genes (*STRA8 SYCP3* and *VASA*,) were further upregulated by RA in the chemical DNA demethylated TCam-2 cells. In addition, the *ex-vivo* studies in human 1st trimester gonads showed that most of the postmigratory germ cell-specific genes and meiotic genes (*DAZL*, *SYCP3* and *VASA*) were specifically upregulated by DNA demethylation. However, whether chemical DNA demethylation associated with RA responsiveness and further upregulated the expression of meiotic genes in human fetal gonads or not was still unknown.

In order to answer this question, the 1st trimester human fetal gonads were separated into 4 pieces and cultured with different treatments. Two of them were used as controls, which were incubated with DMSO for 4 days and then treated with or without 1nM RA for another 2 days. The other two pieces were incubated with 5μM of 5-azacytidine for 4 days and then treated with or without 1nM RA for another 2 days. The mRNA levels of *DAZL, STRA8, SYCP3, SYCP1, DMC1, VASA* and *OCT4* were also detected in the human 1st trimester fetal ovaries and testes by QRT-PCR (Fig 5.16-5.19).

In the control 1st trimester gonads, which were incubated with DMSO firstly, the expression of DAZL and SYCP3 were increased by RA in ovaries and testes, respectively (Fig 5.16 and 5.18, data were analyzed using Paired T-test to determine significant changes between the control and RA treated human 1st trimester fetal gonads, all the results were compared to the 0nM incubated gonads). In the DNA demethylated 1st trimester gonads, which were incubated with 5-azacytine firstly, the expression of postmigratory germ cell-specific genes and meiotic genes did not significantly change by RA treatment (Fig 5.17 and 5.19).

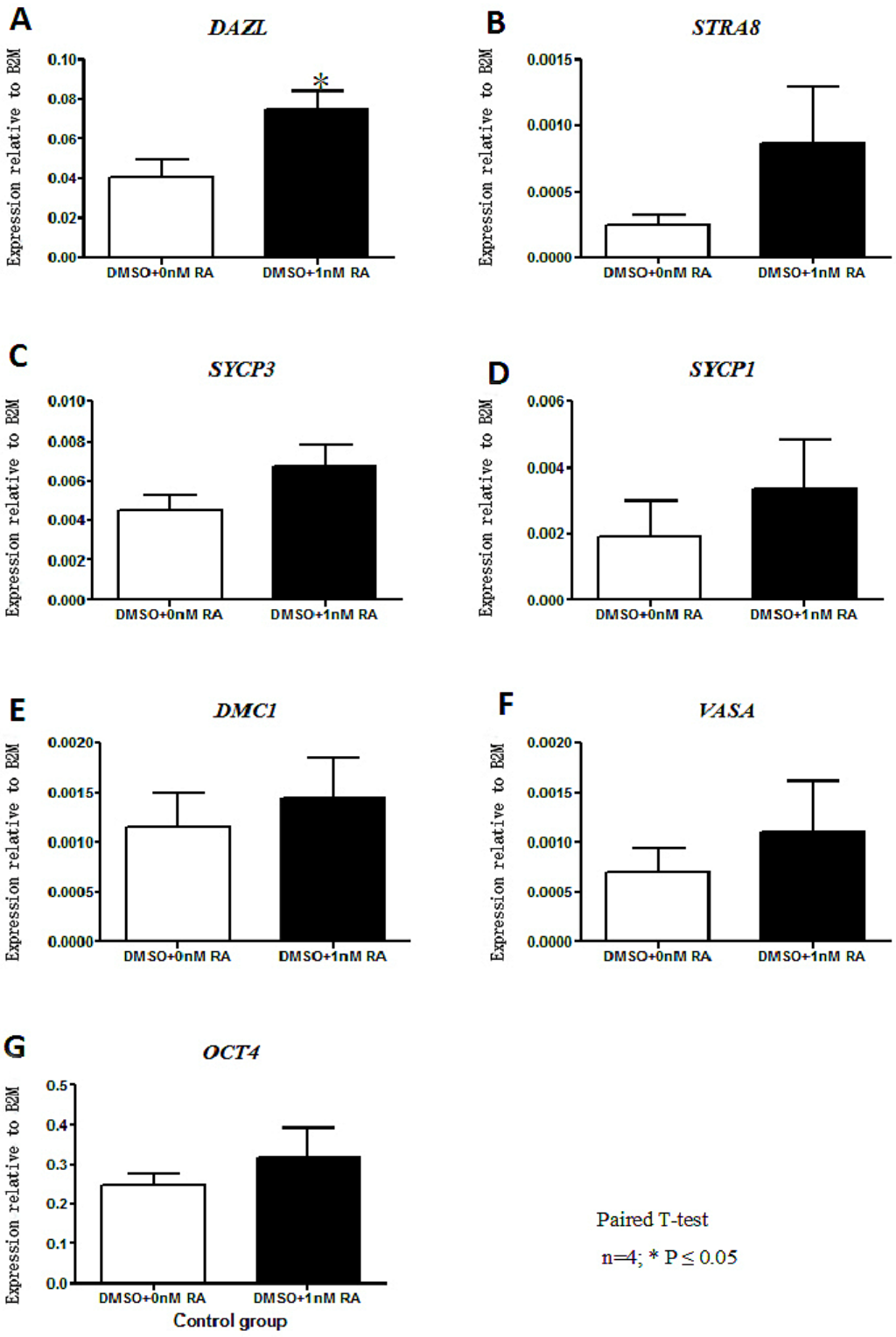

Figure 5.16. mRNA levels of postmigratory germ cell-specific genes, meiotic genes and pluripotent gene in human 1st trimester ovaries (8-10wga), which were incubated with DMSO for 4 days, and then treated with or without RA. A, *DAZL*; **B**, *STRA8*; **C**, *SYCP3*; **D**, *SYCP1*; **E**, *DMC1*; **F**, *VASA and* **G**, *OCT4*; error bars in histograms represent ±SEM; the expressions of these genes were normalized to that of the housekeeping gene *B2M*

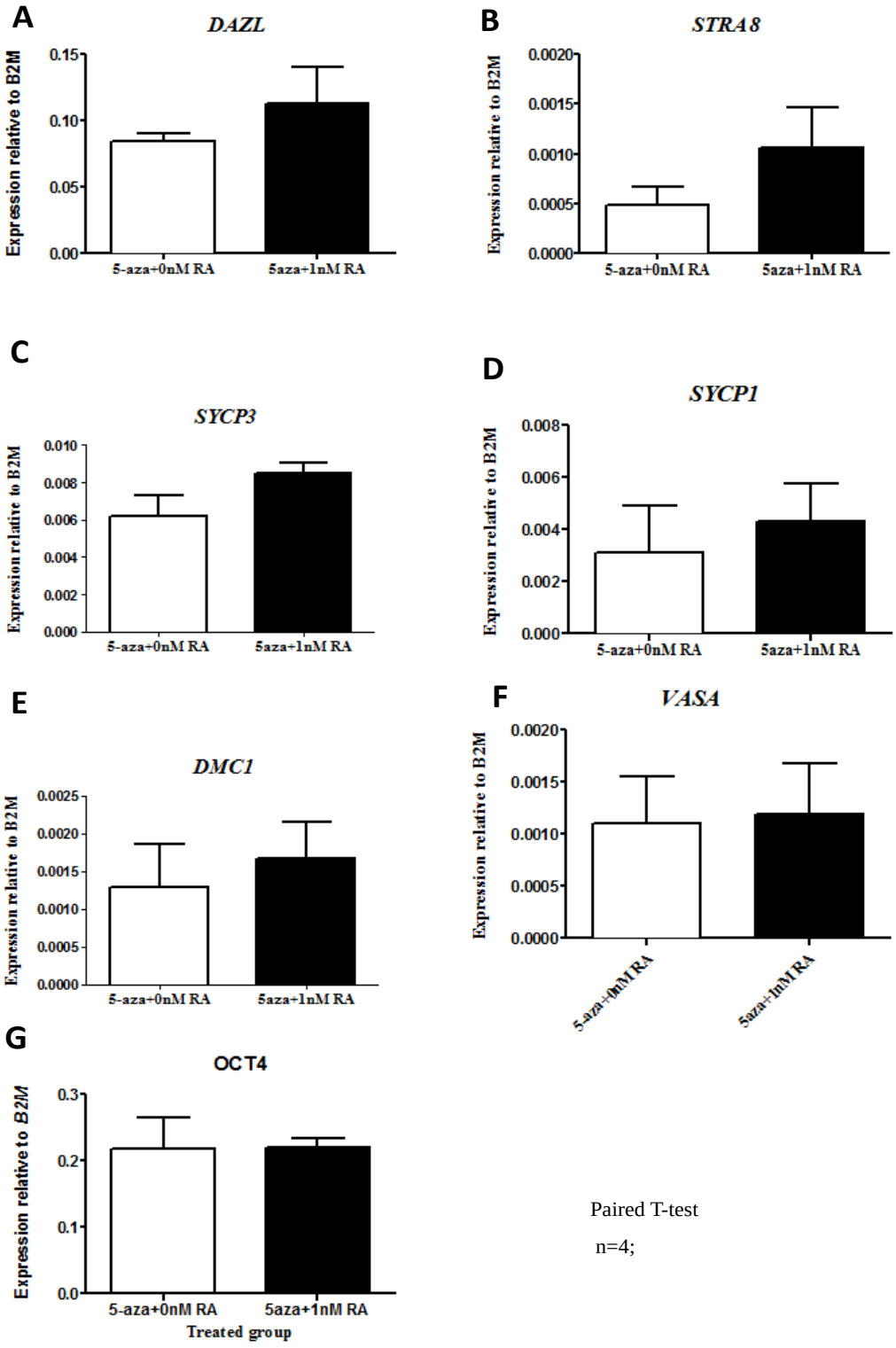

Figure 5.17 mRNA levels of postmigratory germ cell-specific genes, meiotic genes and pluripotent gene in human 1st trimester ovaries (8-10wga), which were incubated with 5-azacytidien for 4 days, and then treated with or without RA. A, *DAZL*; **B**, *STRA8*; **C**, *SYCP3*; **D**, *SYCP1*; **E**, *DMC1*; **F**, *VASA and* **G**, *OCT4*; error bars in histograms represent ±SEM; the expressions of these genes were normalized to that of the housekeeping gene *B2M*

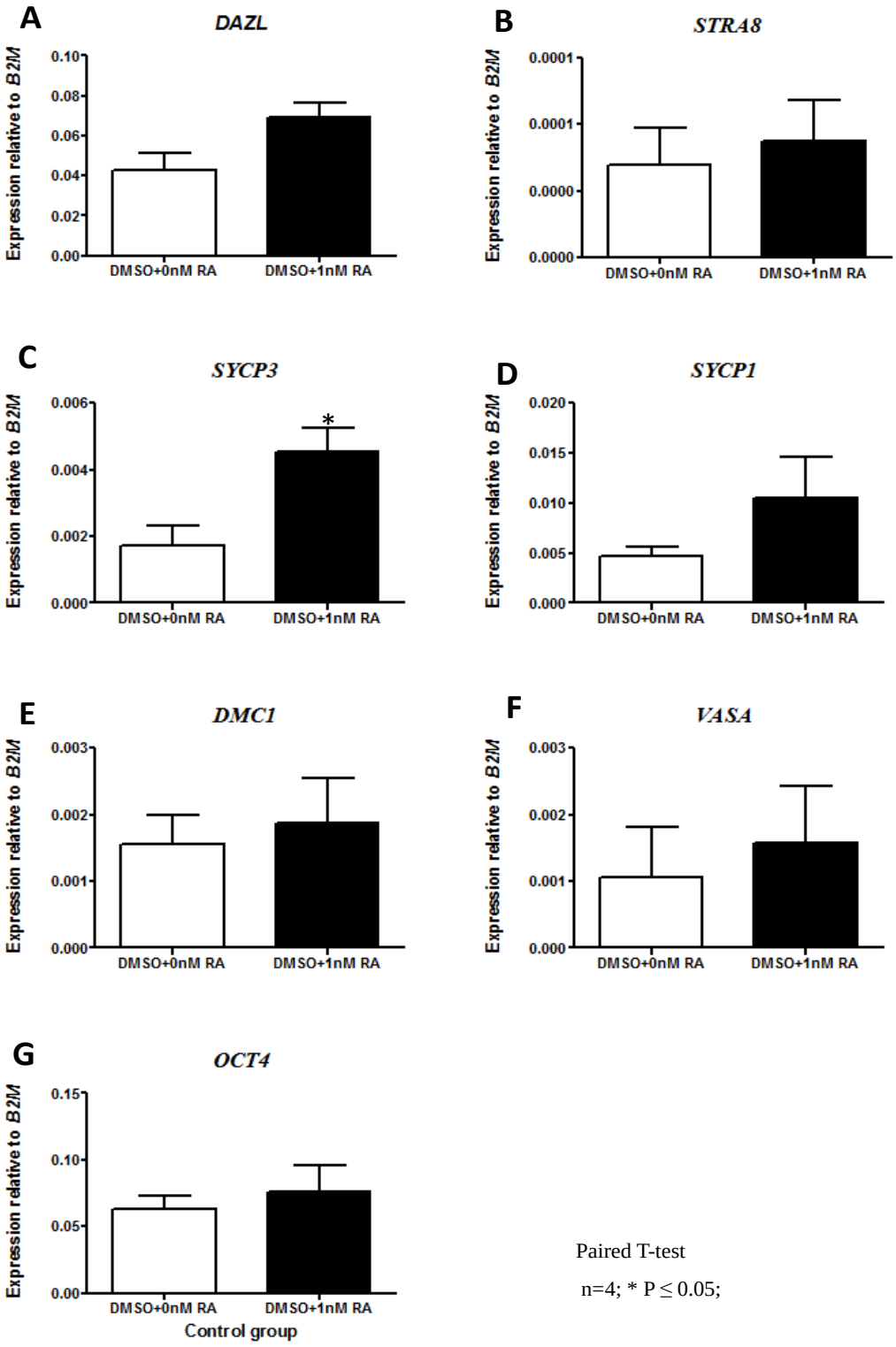

Figure 5.18 mRNA levels of postmigratory germ cell-specific genes, meiotic genes and pluripotent gene in human 1st trimester testes (8-9wga), which were incubated with DMSO for 4 days, and then treated with or without RA. A, *DAZL*; **B**, *STRA8*; **C**, *SYCP3*; **D**, *SYCP1*; **E**, *DMC1*; **F**, *VASA and* **G**, *OCT4*; error bars in histograms represent ±SEM; the expressions of these genes were normalized to that of the housekeeping gene *B2M*

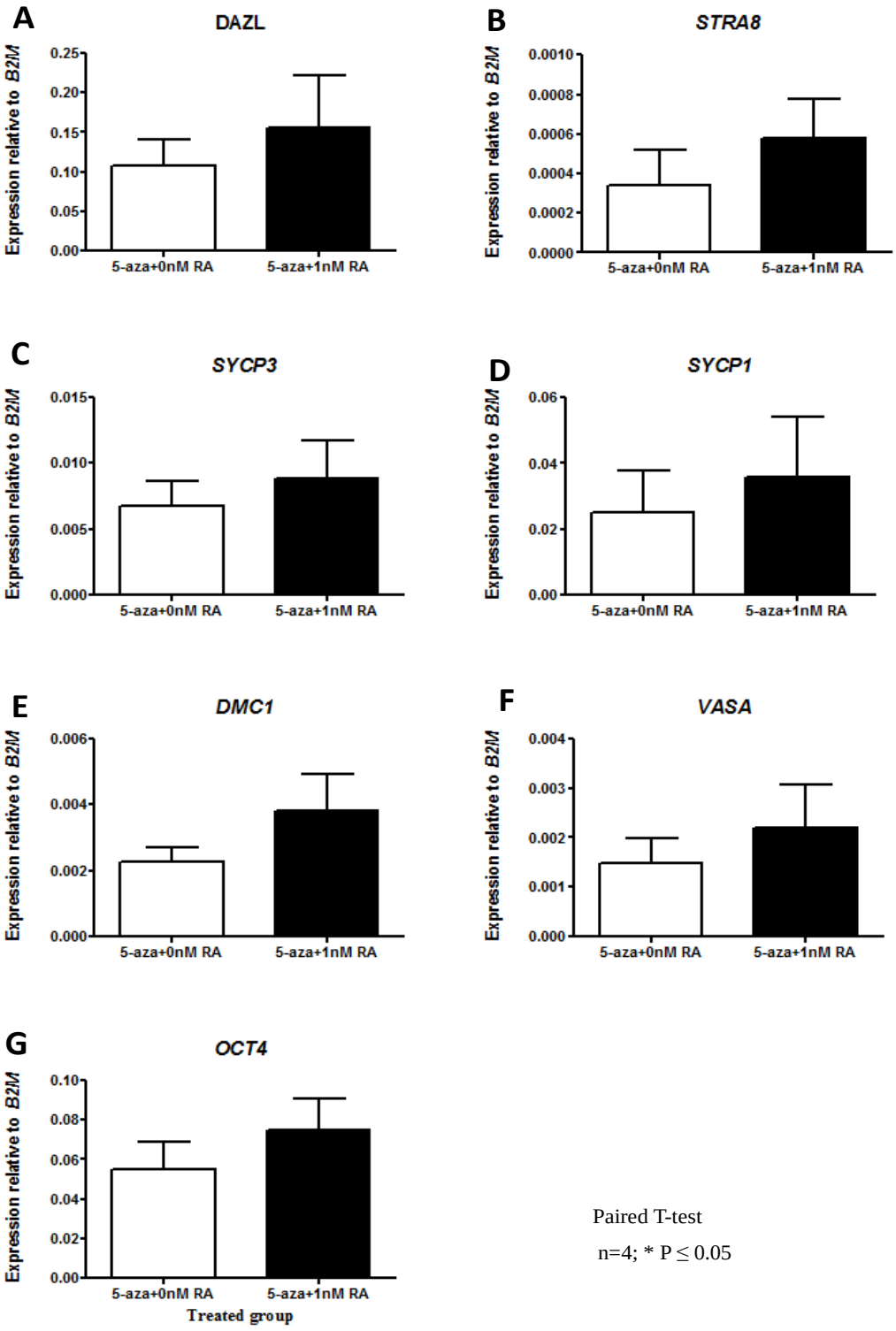

Figure 5.19 mRNA levels of postmigratory germ cell-specific genes, meiotic genes and pluripotent gene in human 1st trimester testes (8-9wga), which were incubated with 5-azacytidien for 4 days, and then treated with or without RA. A, *DAZL*; **B**, *STRA8*; **C**, *SYCP3*; **D**, *SYCP1*; **E**, *DMC1*; **F**, *VASA and* **G**, *OCT4*; error bars in histograms represent ±SEM; the expressions of these genes were normalized to that of the housekeeping gene *B2M*

5.3 *Discussion*

5.3.1 Chemical DNA demethylation specifically upregulated the expression of postmigratory germ cell-specific genes and meiotic genes; and also increased RA responsiveness in TCam-2 cells

These *in-vitro* studies in TCam-2 cells revealed that 5-azacytidine significantly increased the expression of germ cell-specific genes and meiotic genes (*DAZL, STRA8, SYCP3, VASA* and *BOLL*). Chemical DNA demethylation also has been found to increase the RA responsiveness and further upregulate the expression of *STRA8, SYCP3* and *VASA* in TCam-2 cells.

In previous studies, *Dazl* has been found to be repressed by DNA methylation in early mice PGCs, and become demethylated when it is expressed in the later germ cells (Maatouk et al., 2006a). Other findings by Linher *et al* (Linher et al., 2009) also demonstrated that *Dazl* promoter activity is regulated by DNA demethylation in porcine PGCs. The *in-vitro* study here revealed that DAZl, which was undetectable in TCam-2 cells, was significantly increased by DNA demethylating agent 5-azacytidine at both mRNA and protein levels. This finding demonstrated that the activation of *DAZL* was regulated by DNA methylation in TCam-2 cells, which is consistent with the previous findings. However, *DAZL* was not further upregulated by RA in either the DMSO or 5-azacytidine treated TCam-2 cells, suggesting that *DAZL* is not a RA-regulated gene in TCam-2 cells. Without DNA demethylation, RA neither increased the DAZL expression nor affected the DAZL distribution of DAZL in the control TCam-2 cells. However, in the DNA demethylated TCam-2 cells, RA affected the distribution of DAZL by transferring DAZL from nucleus to cytoplasm in some DNA demethylated TCam-2 cells. The cytoplasmic location of DAZL has been identified as an essential factor for meiotic entry (Anderson et al., 2007; Reijo et al., 2000), suggesting that chemical DNA demethylation increase the RA responsiveness and facilitate the meiotic entry in this human TCam-2 cell model.

Stra8 was first identified as a RA responsive gene in mouse P19 embryonic carcinoma cells (Bouillet et al., 1995; Oulad-Abdelghani et al., 1996). Stra8 has been demonstrated to be required for pre-meiotic DNA replication and subsequent meiotic progression in both spermatogenesis and oogenesis (Anderson et al., 2008; Baltus et al., 2006; Mark et al., 2008). *In-vitro* studies in TCam-2 cells here have shown that *STRA8* is also increased by DNA demethylation. In TCam-2 cells, *STRA8* was barely detectable; however, the mRNA levels of *STRA8* were significantly increased by 5-azacytidine treatments. *STRA8* was not upregulated by RA in control TCam-2 cells. However, in TCam-2 cells incubated with 5-azacytidine, *STRA8* expression, which has already increased by DNA demethylation, was further upregulated by RA. All these results suggested indicate the indispensable role of DNA demethylation for *STRA8* induction and RA responsiveness in TCam-2 cells.

During mice germ cell meiosis, Sycp3 and Sycp1 are required for synaptonemal complex assembly (de Vries et al., 2005; Yuan et al., 2000), and Dmc1 is critical for meiotic DSB repair (Pittman et al., 1998; Yoshida et al., 1998). VASA also has been identified as a key factor to induce human meiotic progression *in-vitro* (Medrano et al., 2012). BOLL, a member of DAZ-family proteins, is expressed in human oocytes during mid-to-late meiotic prophase I (He et al., 2013). In TCam-2 cells, the mRNA levels of *SYCP3*, *VASA* and *BOLL* were extremely low. After DNA demethylation, the expression of these meiotic genes were all significantly upregulated in TCam-2 cells, suggesting that DNA methylation is associated with repression of these genes in TCam-2 cells. RA did not significantly change the expression of *VASA*, *SYCP3*, *SYCP1*, *DMC1* and *BOLL* in the control TCam-2 cells. However, in the DNA demethylated TCam-2 cells, RA further increased the expression of *SYCP3* and *VASA.*

*SYC*P3, a synaptonemal complex protein (Moens and Spyropoulos, 1995), was also detected in TCam-2 cells. No significant change in SYCP3 was observed in TCam-2 cells after DNA demethylation, but the distribution of this protein was changed: cytoplasmic SYCP3-positive cells were decreased while the nuclear and cytoplasmic SYCP3-positive cells were increased. In human fetal oocytes, SYCP3 is specifically expressed in typical nuclear patterns from pre-meiosis to diplotene (Roig et al., 2004). However, the nucleus-localized *SYCP3* protein was undetectable in the DNA demethylated TCam-2 cells after RA treatment. In the DNA demethylated TCam-2 cell, only *VASA* and *SYCP3* were upregulated by RA, other meiotic genes *SYCP1*, *DMC1* and *BOLL* were all remained at low levels. Meanwhile, the nucleus-localized *SYCP3* protein was undetectable in the DNA demethylated TCam-2 cells after RA treatment. All the data above suggest that DNA demethylation may increase the RA responsiveness, but not enough to initiate robust meiotic entry in this TCam-2 cell *model.* This may need longer treatment here, which needs further investigation.

In the *mStra8* transfected TCam-2 cells, the expression of *STRA8*'s putative targets *SYCP3* and *DAZL* were upregulated, but other detected meiotic genes did not significantly change, suggesting that the upregulation of *SYCP3* in the DNA demethylated TCam-2 cells after RA treatment, may be associated with the increasing *STRA8.*

RAR and RXR have been demonstrated to be necessary for the induction of *Stra8* and the initiation of meiosis in mice (Boulogne et al., 1999; Bowles et al., 2006; Dufour and Kim, 1999; Koubova et al., 2006). RA induces the expression of *Stra8* by binding to two nuclear receptors, RAR and RXR, which are bound to RAREs in the *Stra8* promoters (Duester, 2008). Intriguingly, the expression of *RAR-β* was significantly increased by 0.1nM RA in both the DMSO and 5-azacytidine treated TCam-2 cells, confirming that all these cells were receiving and transducing RA signals, and that this was not dependent on DNA demethylation.

5.3.2 DNA demethylation specifically upregulated the expression of postmigratory germ cell-specific genes and meiotic genes in human 1st trimester gonads

The mRNA levels of *DAZL*, *SYCP3* and *VASA* were very low in 1st trimester human fetal ovaries, but was markedly increased in the 2nd trimester human fetal ovaries, which initiate the meiotic entry (Anderson et al., 2007; Childs et al., 2011; Le Bouffant et al., 2010). In *ex-vivo* studies here, the low expression of *DAZL*, *SYCP3* and *VASA* were significantly increased by DNA demethylating agent 5-azacytidine in 1st trimester ovaries. However, in the 2nd trimester ovaries, no significant change in these genes was observed after 5-azacytidine treatments. These findings indicate that DNA methylation contributes to the repression of these genes in the 1st trimester human ovaries; and DNA demethylation is associated with the up-regulation of these genes in the 2nd trimester ovaries. This observation is consistent with previous findings in mice ovarian germ cells, in which the activation of *Dazl*, *Sycp3* and *Mvh* was also regulated by DNA demethylation (Maatouk et al., 2006a). All these findings lead to a conclusion that DNA demethylation controls the activation of these post-migratory germ cell-specific genes and meiotic genes and this is conserved in human and mouse fetal ovary.

The expression of *DAZL* and *SYCP3* remained low in both 1st and 2nd trimester testis with no significant difference between gestations (Anderson et al., 2007; Childs et al., 2011; Le Bouffant et al., 2010). In *ex-vivo* studies here, the low expression of *DAZL*, *SYCP3* were all upregulated by DNA demethylation in human 1st trimester testes. Among them, *DAZL* increased nearly 2-fold, which is much less marked than that seen in 1st trimester ovaries. The expression of DAZL and SYCP3 proteins were detected in the DMSO and 5-azacytidine treated 9wga human fetal testis. DNA demethylation increased the expression of DAZL but did not change the nuclear localization of DAZL in the 9wga human fetal testis. The expression of meiosis-related protein SYCP3 was not activated by DNA demethylation in the 9wga human fetal testis. Testicular germ cells do not enter into meiosis during fetal life, and the pre-meiotic gene *STRA8* was nearly undetectable in human fetal testis (Childs et al., 2011; Le Bouffant et al., 2010). The lower responsiveness to DNA demethylation in human 1st trimester testes may be associated with an unknown mechanism in the testis environment, which is antagonistic to meiosis initiation and was not affected by DNA demethylation. All the data above suggested that DNA demethylation did not confer meiosis component to testicular germ cells in this *ex-vivo* model.

Surprisingly, the pluripotency-associated gene *OCT4*, which was already present at a high level in human 1st trimester fetal ovaries, was also further up-regulated by chemical DNA demethylation, suggesting that part of the *OCT4* promoter is still suppressed by DNA methylation at this stage. Previous studies in mice ESCs also indicate that the expression of *Oct4* is regulated by DNA methylation (Gu et al., 2006; Hattori et al., 2007; Hattori et al., 2004; Sato et al., 2006). The observation in human

1st trimester fetal ovaries confirmed the essential role of DNA demethylation in *OCT4* activation in early human PGCs. However, during 2nd trimester, expression of *OCT4*, which was slightly deceased in human fetal ovaries, did not markedly change with DNA demethylation. The observation in 2nd trimester ovaries suggested that the *OCT4* promoter has already undergone complete DNA demethylation, and the decrease of *OCT4* in 2nd trimester ovaries is regulated by other unknown mechanisms.

In the 1st trimester ovaries or testes with or without DNA demethylation, nearly all the detected post-migratory genes and meiotic genes were not significantly changed by RA treatment, suggesting that DNA demethylation did not increase the RA responsiveness and further facilitate meiotic entry in in this experimental model.

From the studies above, chemical DNA demethylation has been found to be associated with expression of postmigratory germ cell-specific genes and meiotic genes in both of the TCam-2 cells and 1st trimester human fetal ovaries. However, chemical DNA demethylation only increase the RA responsiveness in the TCam-2 cell model, but not in the *ex-vivo* cultured human fetal gonads model. Other mechanisms, like Tet1 (Yamaguchi et al., 2012) and histone acetylation (Wang and Tilly, 2010) have been found to regulation germ cell meiosis in mice, are worthy to be explored in human as well.

Chapter 6. General Discussion

6.1 *Introduction*

In mammals, epigenetic modifications are involved in the regulation of germ cell development and aberrancies may lead to aberrant germ cell development and apoptosis (Stringer et al., 2013). Therefore, understanding the accurate epigenetic modifications in human germ cells is important for the further investigation on the germ cell tumors, fertility problems and the epigenetic origin of reproductive disorders.

Among known epigenetic modifications, DNA methylation and histone modification are the most significant (Berger et al., 2009). Gene expression can be either activated or repressed by histone modifications. For example, some modifications of histone, H3K4me3 (Barski et al., 2007) and H3K9ac (Nishida et al., 2006), up-regulate the expression of genes through transcriptional activation. On the other hand, other histone modifications such as H3K27me3 (Boyer et al., 2006), H3K9me2 (Rice et al., 2003) and H3K9me3 (Lachner et al., 2001), can act as crucial histone marks for the transcriptional repression. Expression of genes can also be repressed through methylating cytosine to 5mC (Deaton and Bird, 2011; Meissner et al., 2008). Another modified cytosine variant, 5hmC, and the enzymes responsible for it, members of the TETs family, may be involved in the process of DNA demethylation (Ito et al., 2010; Tahiliani et al., 2009).

In mouse fetal germ cells, dynamic and extensive epigenetic reprogramming, which includes histone modifications and DNA methylation, has been investigated (Hajkova et al., 2008; Hajkova et al., 2010; Popp et al., 2010; Seisenberger et al., 2012; Seki et al., 2005). In addition, the appropriate DNA methylation status in the developing germ cells has also been found to be essential for meiotic progression in mice (Maatouk et al., 2006a). In line with epigenetic reprogramming in mouse fetal germ cells, human fetal germ cells may also undergo global reprogramming of histone marks and DNA methylation. However, observations about these epigenetic modifications in human fetal germ cells are limited (Almstrup et al., 2010; Bartkova et al., 2010; Gkountela et al., 2013; Wermann et al., 2010).

In order to establish a more accurate timeline of epigenetic reprograming in human germ cells, I have characterized a definitive trend of 5 important histone marks (H3K9me2, H3K9me3, H3K27me3, H3K4me3, H3K9ac) in human fetal germ cells. The accurate time of DNA demethylation and DNA remethyaltion in human germ cells have also been detected. Furthermore, the relationship between DNA demethylation and human germ cell meiosis has been investigated *in vitro* and *ex vivo*.

6.2 *General Discussion*

6.2.1 Dynamic histone modifications in human germ cell development

The *in-vivo* studies were conducted to understand about the genome wide posttranslational histone modifications in human fetal germ cells. In human fetal ovarian and testicular germ cells, the levels of permissive histone mark H3K4me3 and repressive histone mark H3K27me3 were progressively reduced with maturation of human fetal gonads. In later gestation, H3K4me3 and H3K27me3 were restricted to the smaller and undifferentiating human fetal germ cells. In this work, repressive histone mark H3K9me2 and H3K9me3 displayed distinct and sex-specific distributions in human fetal germ cells. At approximate 14wga, shortly after the onset of meiotic germ cell differentiation, H3K9me2 was transiently peaked in the human fetal ovarian germ cells. At other detected gestations, the fetal ovarian germ cells displayed low levels of H3K9me2. On the other hand, H3K9me2 was undetectable in testicular germ cells at all detected gestations. For the case of H3K9me3, similar trend are found in human fetal testicular germ cells at all detected stages. However, H3K9me3 was present at a low level in human ovarian germ cells at early gestations, and then increased and accumulated to the more mature ovarian germ cells at later gestations. The histone modifications mentioned above were strikingly different from those reported in mouse fetal germ cells (Hajkova et al., 2008; Seki et al., 2005), and hence suggesting the existence of species differences in histone modifications between human and mouse, which further emphasize the importance of human study.

Previous studies in undifferentiated human ESCs have shown that H3K4me3 is associated with the maintenance of pluripotency (Pan et al., 2007), while H3K27me3 contributes to the repression of developmental genes (Boyer et al., 2006; Lee et al., 2006). Inferring from this knowledge, the restriction of H3K4me3 and H3K27me3 in the smaller and undifferentiating human fetal germ cells may be associated with the expression of pluripotency-related genes and the repression of developmental genes, respectively.

In the differentiating murine ESCs, H3K9me2 is associated with the suppression of pluripotency-associated gene *Oct3/4* (Feldman et al., 2006). Moreover, H3K9 dimethylatransferase, G9a, plays an important role in meiotic prophase of mouse (Tachibana et al., 2007). According to the previous findings and the observation of H3K9me2 here, the specific upregulation of H3K9me2 in the early 2nd trimester human ovarian germ cell may be associated with the suppression of the pluripotency-associated genes and the initiation of meiosis.

In mice, H3K9 trimethyltransferase Suv39h and its modified chromatin H3K9me3 are critical for germ cell meiosis (Peters et al., 2001). Double deletions of *Suv39h1* and *Suv39h2* in mice cause the absence of H3K9me3 and aberration of meiosis in both male and female (Peters et al., 2001). On the basis of the previous findings in mice and the observation here, the accumulation of H3K9me3 in mature human fetal ovarian

germ cells may be associated with the onset of germ cells differentiation and /or meiosis in humans.

It should be noted that, with different types of fixation, the distribution of H3K9ac in human fetal ovaries was different. Consequently, the results of H3K9ac here were unreliable and further investigation is required.

6.2.2 Reprogramming of DNA methylation in human germ cell development

The studies of DNA methylation in human in this work revealed that global reprogramming of DNA methylation is largely conserved between human and mouse. Before mouse germ cell specification, the DNA methylated features are similar in the pluripotent epiblast cells and PGC precursor cells (Hajkova et al., 2002; Saitou et al., 2002). In order to avoid somatic fate and generate germ cell potency, the novel mouse PGCs begin to lose genome-wide DNA methylation (Hajkova et al., 2002; Saitou et al., 2002). In 6wga human ovary, the DNA of migrating PGCs was hypomethylated compared with neighboring somatic cells, suggesting that PGCs at this stage started to lose 5mC to adopt the germ cell fate. DNA methylation has been found to be associated with the repression of pluripotent gene *Pou5f1* in mouse ESCs (Gu et al., 2006; Hattori et al., 2007; Hattori et al., 2004; Sato et al., 2006). The low methylated levels in 6wga PGCs may also be associated with the activation of the pluripotency genes in human. My research based on only one 6wga human embryo sample due to the limited availability of such tissue. More samples are required to confirm the global levels of 5mC in migrating human PGCs in the future studies.

In mice, DNA demethylation has been found to regulate the temporal expression of postmigratory germ cell-specific genes such as *Mvh* (Maatouk et al., 2006a). In human, the mature germ cell-specific gene *VASA* was almost undetectable in early PGCs, and significantly increased in both ovarian and testicular germ cells at later gestational ages (Anderson et al., 2007). Moreover, the studies for human in this work revealed that 5mC was barely detected in the postmigratory human fetal germ cell. All these observations suggested that genome-wide erasure of DNA methylation in the postmigratory human fetal germ cells may be associated with the upregulation of mature germ cell-specific gene expression in human.

In mice, the expression of meiosis-related genes *Dazl* and *Sycp3* are also regulated by DNA methylation (Maatouk et al., 2006a). In human, the mRNA of *DAZL* and *SYCP3* were up-regulated in the late-gestational fetal ovaries (Anderson et al., 2007; He et al., 2013; Houmard et al., 2009), but remained low in the late-gestational fetal testes (Anderson et al., 2007; He et al., 2013; Houmard et al., 2009). The DNA methylation studies in human here showed that 5mC was redetected in some of the later fetal testicular germ cells, but remained undetectable in the fetal ovarian germ cells across all the detected gestations. Thus, the delay of DNA de novo methylation in human

ovarian germ cells may correlate with further upregulation of *DAZL* and the activation of meiotic genes in human fetal ovary.

5hmC is generated through oxidation of 5mC by Tets enzymes (Ficz et al., 2011; Szwagierczak et al., 2010). Genome-wide mapping in mouse and human ESCs reveals that 5hmC mainly gatheres around euchromatic regions, and may be positively correlated to transcriptional activity (Ficz et al., 2011; Pastor et al., 2011; Williams et al., 2011; Wu et al., 2011; Xu et al., 2011; Yildirim et al., 2011). However, the exact function of 5hmC is still not fully elucidated. One hypothesis raised from mouse studies indicates that 5hmC may serve as an intermediate in the process of DNA demethylation (Guo et al., 2011; He et al., 2011; Inoue and Zhang, 2011; Iqbal et al., 2011; Ito et al., 2011; Wossidlo et al., 2011; Wu and Zhang, 2010; Xu et al., 2011). Different from the findings in mouse PGCs (Hackett et al., 2013; Yamaguchi et al., 2013), the studies in human adult liver show that 5hmC tends to co-localize with 5mC in the hepatocyte nucleus (Ivanov et al., 2013). The genomic study in mammalian cells also indicates that 5mC and 5hmC often coexist at the same cytosine in the cells with a steady state (Yu et al., 2012).

The studies in human germ cells here demonstrated that the existence of 5mC and 5hmC were synchronous rather than alternate. At 6wga, 5hmC was also present in the OCT4-positive human PGCs. In human ovary, 5hmC was undetectable in most of the postmigratory fetal ovarian germ cells, and was regained after birth. In human testis, 5hmC was detected only in a few of fetal testicular germ cells. According to the previous studies and the finding in human germ cells of this work, the synchronous presence of 5hmC and 5mC in human germ cells suggests that rather than being involved in DNA demethylation, 5hmC may play an important role in the development of germ cell with its unique epigenetic regulatory functions, which need further investigation.

In mammal, Tets enzymes mediate the conversion of 5mC to 5hmC, and may be associated with DNA demethylation (Ito et al., 2010; Ito et al., 2011; Ko et al., 2010; Tahiliani et al., 2009). During mouse PGC development, Tet1 and 2 have been found to be involved in oxidizing 5mC to 5hmC (Hackett et al., 2013; Yamaguchi et al., 2013).

In the 1st trimester human fetal gonads, mRNA levels of *TET1, 2* and *3* were all at a very high level, which may be associated with the erasure of 5mC. Notably, the level of *TET2* is much lower than *TET1* and *TET3* across all the gestation; therefore, TET2 may play a less important role in human fetal gonads. In human fetal testes, *TET2* did not change across gestations. Notably, *TET1* and *TET3* fell significantly in the early 2nd trimester and remained stable thereafter. The significant fall in *TET1* and *TET3* may be associated with the global erasure of 5hmC in most of the human testicular germ cells. With increasing gestational age, the expression of these three *TETs* genes decreased in the postmigratory human fetal ovaries, which may be related to the loss

of 5hmC in the postmigratory human fetal ovarian germ cells. Tet1 has been found to be involved in the mouse meiosis, as deficiency in *Tet1* led to loss of meiotic genes in mouse ovarian germ cells (Yamaguchi et al., 2012). In human fetal ovaries, the mRNA levels of *TET1* decreased coincident with meiotic initiation. However, whether the decrease of TET1 protein was restrict to the ovarian germ cells or not was unknown. So the relationship of TET1 and meiosis in ovarian germ cells still need further investigation.

6.2.3 Chemical DNA demethylation regulate the expression of postmigratory germ cell-specific and meiotic genes in human

In PGC-like cells derived from mouse ESCs, DNA demethylation caused by *Dnmt1* deficiency up-regulates the expression of PGC-related genes (Mochizuki et al., 2012). In mouse ESCs, DNA demethylation is associated with the activation of pluripotent genes Pou5f1 and Nanog (Gu et al., 2006; Hattori et al., 2007; Hattori et al., 2004; Sato et al., 2006). DNA demethylation also has been found to be associated with the high expression of postmigratory germ cell-specific and meiotic genes *Mvh, Dazl* and *Sycp3* in mouse fetal germ cells (Maatouk et al., 2006a).

In-vitro studies in TCam-2 cells here revealed that the silenced postmigratory germ cell-specific and meiotic genes were specifically up-regulated by DNA demethylating agent 5-azacytidine. Chemical DNA demethylation also has been found to increase the RA responsiveness by further facilitating RA to increase the mRNA levels of *STRA8, SYCP3* and *VASA,* and also the cytoplasmic localization of DAZL in TCam-2 cells.

In human fetal ovaries, the expression of *DAZL*, *STRA8*, *SYCP3*, *SYCP1*, *DMC1* and *VASA* was low at 1st trimester *and* was significantly increased at 2nd trimester. In the *ex-vivo* study here, most of these low-expressing genes (*DAZL*, *SYCP3* and *VASA*) were all significantly increased by DNA demethylating agent 5-azacytidine in the 1st trimester ovaries. However, the expression of these genes was not significantly changed by DNA demethylation in the 2nd trimester ovaries, in which the expression of these genes has already been increased. The responsiveness to DNA demethylation was much more lower in human 1st trimester testes, in which testicular germ cells do not enter into meiosis during fetal life, and the pre-meiotic gene *STRA8* was nearly undetectable in human fetal testis (Bendsen et al., 2003; Gaskell et al., 2004). DNA demethylation did not further facilitate RA to increase meiotic genes in 1st trimester human fetal ovaries and testes.

From the studies above, chemical DNA demethylation has been found to be associated with expression of postmigratory germ cell-specific genes and meiotic genes in both of the TCam-2 cells and 1st trimester human fetal ovaries. However, chemical DNA demethylation only increase the RA responsiveness in the TCam-2 cell model, but not in the *ex-vivo* cultured human fetal gonads model. Other mechanisms, like Tet1 (Yamaguchi et al., 2012) and histone acetylation (Wang and Tilly, 2010) have been

found to regulation germ cell meiosis in mice, are worthy to be explored in human as well.

6.2.4 Link between histone modification and DNA methylation in human fetal germ cells

In mice, DNA demethylation have been found to associate with the activation of pluripotent genes, the high expression of postmigratory germ cell-specific and meiotic genes in mouse fetal germ cells (Gu et al., 2006; Hattori et al., 2007; Hattori et al., 2004; Maatouk et al., 2006a; Mochizuki et al., 2012; Sato et al., 2006). The studies in human fetal gonads here showed that the undifferentiated human PGCs displayed high levels of H3K4me3 and H3K27me3 and low levels of 5mC, which may be associated with the expression of pluripotency-related genes. In human, the mature fetal ovarian germ cells displayed high levels of H3K9me3 and were 5mC-negative, which may be associated with the onset of germ cells differentiation and /or meiosis in humans. Histone modification is associated with short-term modifications and is reversible, while DNA methylation is associated with stable long-term repression (Ng, and Adrian, 1999). Histone modifications and DNA methylation are inextricably linked as the regulation of transcriptional control depends significantly on DNA methylation as well as on histone modifications (Kouzarides, 2007; Lande-Diner et al., 2007). As explained by Cedar *et al.* (Cedar and Bergman, 2009), the DNA methylation pattern is established with the contribution of some histone modifications, while the maintenance of some histone modifications patterns requires DNA methylation.

In mice, a correlation has been established between high levels of DNA methylation as well as H3K9 trimethylation and pericentric heterochromatin (Lehnertz et al., 2003; Lewis et al., 1992; Peters et al., 2001). Furthermore, Esteve *et al.* (Esteve et al., 2006) demonstrated that there is a direct interaction between the H3K9me2-specific methyltransferase G9a-Glp complex and Dnmt1, while Dong *et al.* (2008) reported that this complex is also necessary for the de novo DNA methylation of retrotransposons in ESCs. Several researchers highlighted the anti-correlation between genome wide H3K4 methylation and DNA methylation (Erfurth et al., 2008; Ooi et al., 2007). The unmethylated CpG sequences in CpG islands are bound by the H3K4 methyltransferase MLL, which can also oppose DNA methylation in the binding location (Erfurth et al., 2008). The researches in cancer cells and ESCs indicated that the correlation of DNA methylation and H3K27 methylation depends on cell type (Vire et al., 2006) (Kondo et al., 2008; Mendenhall et al., 2010; Mohn et al., 2008).

Therefore, the dynamic histone modifications and reprogramming of DNA methylations in human fetal germ cells are all related to each other, and the mechanism of this link need further investigation.

6.3 *Conclusions*

This thesis revealed that dynamic histone modifications occurring during human fetal germ cells development are strikingly different from those reported in mouse fetal germ cells (Hajkova et al., 2008; Seki et al., 2005). Dynamic reprogramming of global DNA methylation in human germ cells was consistent with that in mouse germ cells (Abe et al., 2011; Hajkova et al., 2010; Seki et al., 2005). The *in-vitro* and *ex-vivo* culture studies in TCam-2 cells and human fetal gonads indicated that treatment with known DNA demethylating agents is also associated with the activation of the postmigratory germ cell-specific and meiotic genes in human.

6.4 *Future Directions*

Although this thesis has identified the dynamic histone modifications and DNA methylation reprogramming during the development of human fetal germ cell, further work is required to fully understand the mechanisms and overall function of these epigenetic modifications in human fetal germ cell, which are shown as follows:

6.4.1 **The biological significance of H3K4me3, H3K27me3, H3K9me2 and H3K9me3 in human fetal germ cells**

The studies in human fetal germ cells here showed that histone marks underwent dynamic modifications. However, the biological significance of these histone modifications still needs further investigation.

The studies here suggested that H3K4me3 and H3K27me3 might be associated with the undifferentiated status in human fetal germ cells. To investigate whether H3K4me3 is associated with the expression of pluripotency-related genes in human fetal germ cells, double immunofluorescence analysis for H3K4me3 and pluripotent markers (Such as OCT4) can be carried out in human fetal gonads across different gestations. Triple immunofluorescence analysis for H3K27me3, pluripotent markers and mature germ cell markers (Such as VASA, DAZL) can be performed to determine whether H3K27me3 is associated with the repression of developmental genes in human fetal germ cells.

The studies in human here revealed that H3K9me2 and H3K9me3 might be associated with the suppression of pluripotency-associated genes, onset of differentiation and initiation of meiosis in human ovarian germ cells. The role of H3K9me2 and H3K9me3 in human fetal germ cell can be further explored by performing the double or triple immunofluorescence with pluripotent markers, mature germ cell markers or meiotic markers (Such as SYCP3).

6.4.2 **Dynamic change of H3K9ac during human fetal germ cell development**

It is worth noting that H3K9ac distributed differently in Bouins and NBF fixed human ovaries at comparable gestational ages. During 2nd trimester, most of Bouins fixed

human fetal ovarian germ cells were negative for H3K9ac; only the smaller, undifferentiated PGC-like cells displayed this histone mark. Contrarily, nearly all of the NBF fixed human fetal ovarian germ cells displayed H3K9ac-staining at these later gestational ages.

The results of H3K9ac here were unreliable, and needed further investigation. Human fetal gonads can be disaggregated into a single-cell suspension by mechanical and enzymatic dispersion (Childs et al., 2010; Coutts et al., 2008). The cell suspension, which consists of both gonadal somatic and germ cells, can be fluorescently labeled with PGC marker OCT4 and mature germ cell marker VASA. The OCT4 or VASA-labeled human fetal germ cells can be sorted from the unlabeled somatic cells by Fluorescence-Activated Cell Sorting (FACS) (Mozdziak et al., 2005; Woods and Tilly, 2013). The isolated human fetal germ cells can be collected for protein extraction; and western blotting can be performed to determine the levels of H3K9ac in these isolated fetal germ cells. These detections can be performed in human fetal gonads across different gestations, and then the dynamic changes of H3K9ac in human fetal germ cells can be identified reliably.

6.4.3 Role of 5hmC in human germ cell development

The studies here suggested that 5hmC may not be involved in DNA demethylation during human germ cell development, and may play an important role in germ cell development with its unique epigenetic regulatory functions. The genome-wide mapping of 5hmC can be further investigated in human germ cells by sodium and oxidative bisulfite sequencing to identify the epigenetic regulatory functions of 5hmC in human germ cells (Booth et al., 2013).

The studies in mouse PGCs showed that 5hmC is enriched in the promoter of *Dazl* gene (Hackett et al., 2013), which is activated by promoter DNA demethylation (Hackett et al., 2012; Maatouk et al., 2006b). However, global 5hmC is present in the early migrating PGCs and erased in the postmigratory human germ cells, suggesting that 5hmC may not be involved in the activation of *DAZL* in human. The distribution of 5hmC at the promoters of *DAZL*, PGC genes and other postmigratory germ cell-specific genes can be detected by hmeDIP-Sequencing and glucosyltransferase-quantitative polymerase chain reaction (Glu-qPCR) (Hackett et al., 2013) to identify whether the presence of 5hmC in human germ cells facilitate the activation of these genes or not.

6.4.4 The relationship between DNA demethylation and meiotic prophase I in human fetal ovaries

In the DNA demethylated TCam-2 cell, only *STRA8*, *VASA* and *SYCP3* were further upregulated by RA, other meiosis-related genes *SYCP1*, *DMC1* and *BOLL* did not respond to RA induction. In the DNA demethylated 1st trimester human fetal ovaries and testes, only *STRA8* was further upregulated by RA, other meiosis-related genes

did not respond to RA induction. The *in-vitro and ex-vivo* findings above suggested that DNA demethylation may increase the RA responsiveness, but not enough to facilitate germ cells to enter into meiosis in response to RA, in this experimental model. These findings led to a question that whether the incubating time of RA is associated with the initiation of meiosis in DNA demethylated human fetal gonads. In the future studies, the DNA demethylated human fetal gonads can be cultured with RA for a longer period and the expression of meiotic genes can be further detected, which can lead to a conclusion of whether DNA demethylation is associated with meiotic prophase I in human fetal ovaries.

6.4.5 Other epigenetic mechanisms in prophase I in human fetal ovaries

Other mechanisms, like Tet1 (Yamaguchi et al., 2012) and histone acetylation (Wang and Tilly, 2010), which also have been found to regulate germ cell meiosis in mice, are worthy to be explored in human as well.

The role of TETs in human germ cell meiosis can be demonstrated by *TETs*-knockout studies in human fetal ovaries via RNA interference. After that, the DNA methylation status and the expression of meiotic genes can be further detected in the *TETs*-deficiency human fetal ovaries.

In addition, the human fetal ovaries can be cultured with the histone deacetylase inhibitor TSA to identify the role of histone acetylation in human germ cell meiosis as well.

References

Abcam. H3K9ac. Anti-Histone H3 (acetyl K9) antibody - ChIP Grade (ab10812).

Abcam. H3K9me2. Anti-Histone H3 (di methyl K9) antibody [mAbcam 1220] - ChIP Grade (ab1220).

Abcam. H3K9me3. Anti-Histone H3 (tri methyl K9) antibody - ChIP Grade (ab8898).

Abe, M., S.Y. Tsai, S.G. Jin, G.P. Pfeifer, and P.E. Szabo. 2011. Sex-specific dynamics of global chromatin changes in fetal mouse germ cells. *PloS one*. 6:e23848.

Adams, I.R., and A. McLaren. 2002. Sexually dimorphic development of mouse primordial germ cells: switching from oogenesis to spermatogenesis. *Development*. 129:1155-1164.

Alberts, B. 2008. Molecular biology of the cell. Garland Science, New York.

Aletta, J.M., T.R. Cimato, and M.J. Ettinger. 1998. Protein methylation: a signal event in post-translational modification. *Trends in biochemical sciences*. 23:89-91.

Allegrucci, C., A. Thurston, E. Lucas, and L. Young. 2005. Epigenetics and the germline. *Reproduction*. 129:137-149.

Allfrey, V.G., and A.E. Mirsky. 1964. Structural Modifications of Histones and their Possible Role in the Regulation of RNA Synthesis. *Science*. 144:559.

Almstrup, K., J.E. Nielsen, O. Mlynarska, M.T. Jansen, A. Jorgensen, N.E. Skakkebaek, and E. Rajpert-De Meyts. 2010. Carcinoma in situ testis displays permissive chromatin modifications similar to immature foetal germ cells. *British journal of cancer*. 103:1269-1276.

Anderson, E.L., A.E. Baltus, H.L. Roepers-Gajadien, T.J. Hassold, D.G. de Rooij, A.M. van Pelt, and D.C. Page. 2008. Stra8 and its inducer, retinoic acid, regulate meiotic initiation in both spermatogenesis and oogenesis in mice. *Proceedings of the National Academy of Sciences of the United States of America*. 105:14976-14980.

Anderson, R., T.K. Copeland, H. Scholer, J. Heasman, and C. Wylie. 2000. The onset of germ cell migration in the mouse embryo. *Mechanisms of development*. 91:61-68.

Anderson, R.A., N. Fulton, G. Cowan, S. Coutts, and P.T. Saunders. 2007. Conserved and divergent patterns of expression of DAZL, VASA and OCT4 in the germ cells of the human fetal ovary and testis. *BMC developmental biology*. 7:136.

Arents, G., and E.N. Moudrianakis. 1993. Topography of the histone octamer surface: repeating structural motifs utilized in the docking of nucleosomal DNA. *Proceedings of the National Academy of Sciences of the United States of America*. 90:10489-10493.

Arents, G., and E.N. Moudrianakis. 1995. The histone fold: a ubiquitous architectural motif utilized in DNA compaction and protein dimerization.

Proceedings of the National Academy of Sciences of the United States of America. 92:11170-11174.

Baker, T.G. 1963. A Quantitative and Cytological Study of Germ Cells in Human Ovaries. *Proceedings of the Royal Society of London. Series B, Containing papers of a Biological character. Royal Society*. 158:417-433.

Baltus, A.E., D.B. Menke, Y.C. Hu, M.L. Goodheart, A.E. Carpenter, D.G. de Rooij, and D.C. Page. 2006. In germ cells of mouse embryonic ovaries, the decision to enter meiosis precedes premeiotic DNA replication. *Nature genetics*. 38:1430-1434.

Bannister, A.J., R. Schneider, and T. Kouzarides. 2002. Histone methylation: dynamic or static? *Cell*. 109:801-806.

Bannister, A.J., P. Zegerman, J.F. Partridge, E.A. Miska, J.O. Thomas, R.C. Allshire, and T. Kouzarides. 2001. Selective recognition of methylated lysine 9 on histone H3 by the HP1 chromo domain. *Nature*. 410:120-124.

Barrionuevo, F., S. Bagheri-Fam, J. Klattig, R. Kist, M.M. Taketo, C. Englert, and G. Scherer. 2006. Homozygous inactivation of Sox9 causes complete XY sex reversal in mice. *Biology of reproduction*. 74:195-201.

Barski, A., S. Cuddapah, K. Cui, T.Y. Roh, D.E. Schones, Z. Wang, G. Wei, I. Chepelev, and K. Zhao. 2007. High-resolution profiling of histone methylations in the human genome. *Cell*. 129:823-837.

Bartkova, J., P. Moudry, Z. Hodny, J. Lukas, E. Rajpert-De Meyts, and J. Bartek. 2010. Heterochromatin marks HP1 gamma, HP1 alpha and H3K9me3, and DNA damage response activation in human testis development and germ cell tumours. *International journal of andrology*. 34:E103-E113.

Baudat, F., K. Manova, J.P. Yuen, M. Jasin, and S. Keeney. 2000. Chromosome synapsis defects and sexually dimorphic meiotic progression in mice lacking Spo11. *Molecular cell*. 6:989-998.

Bayne, R.A., S.L. Eddie, C.S. Collins, A.J. Childs, H.N. Jabbour, and R.A. Anderson. 2009. Prostaglandin E2 as a regulator of germ cells during ovarian development. *The Journal of clinical endocrinology and metabolism*. 94:4053-4060.

Beisel, C., A. Imhof, J. Greene, E. Kremmer, and F. Sauer. 2002. Histone methylation by the Drosophila epigenetic transcriptional regulator Ash1. *Nature*. 419:857-862.

Bendsen, E., A.G. Byskov, C.Y. Andersen, and L.G. Westergaard. 2006. Number of germ cells and somatic cells in human fetal ovaries during the first weeks after sex differentiation. *Human reproduction*. 21:30-35.

Bendsen, E., A.G. Byskov, S.B. Laursen, H.P. Larsen, C.Y. Andersen, and L.G. Westergaard. 2003. Number of germ cells and somatic cells in human fetal testes during the first weeks after sex differentiation. *Human reproduction*. 18:13-18.

Berger, S.L. 2001. An embarrassment of niches: the many covalent modifications of histones in transcriptional regulation. *Oncogene*. 20:3007-3013.

Berger, S.L. 2007. The complex language of chromatin regulation during transcription. *Nature*. 447:407-412.

Berger, S.L., T. Kouzarides, R. Shiekhattar, and A. Shilatifard. 2009. An operational definition of epigenetics. *Genes Dev*. 23:781-783.

Bernstein, B.E., M. Kamal, K. Lindblad-Toh, S. Bekiranov, D.K. Bailey, D.J. Huebert, S. McMahon, E.K. Karlsson, E.J. Kulbokas, 3rd, T.R. Gingeras, S.L. Schreiber, and E.S. Lander. 2005. Genomic maps and comparative analysis of histone modifications in human and mouse. *Cell*. 120:169-181.

Bernstein, B.E., T.S. Mikkelsen, X. Xie, M. Kamal, D.J. Huebert, J. Cuff, B. Fry, A. Meissner, M. Wernig, K. Plath, R. Jaenisch, A. Wagschal, R. Feil, S.L. Schreiber, and E.S. Lander. 2006. A bivalent chromatin structure marks key developmental genes in embryonic stem cells. *Cell*. 125:315-326.

Bird, A. 2002. DNA methylation patterns and epigenetic memory. *Genes Dev*. 16:6-21.

Bird, A. 2007. Perceptions of epigenetics. *Nature*. 447:396-398.

Bird, A.P. 1980. DNA methylation and the frequency of CpG in animal DNA. *Nucleic Acids Res*. 8:1499-1504.

Bird, A.P. 1984. DNA methylation--how important in gene control? *Nature*. 307:503-504.

Bird, A.P. 1986. CpG-rich islands and the function of DNA methylation. *Nature*. 321:209-213.

Bird, A.P., and A.P. Wolffe. 1999. Methylation-induced repression--belts, braces, and chromatin. *Cell*. 99:451-454.

Booth, M.J., T.W. Ost, D. Beraldi, N.M. Bell, M.R. Branco, W. Reik, and S. Balasubramanian. 2013. Oxidative bisulfite sequencing of 5-methylcytosine and 5-hydroxymethylcytosine. *Nature protocols*. 8:1841-1851.

Borgel, J., S. Guibert, Y. Li, H. Chiba, D. Schubeler, H. Sasaki, T. Forne, and M. Weber. 2010. Targets and dynamics of promoter DNA methylation during early mouse development. *Nature genetics*. 42:1093-1100.

Borum, K. 1961. Oogenesis in the mouse. A study of the meiotic prophase. *Experimental cell research*. 24:495-507.

Bostick, M., J.K. Kim, P.O. Esteve, A. Clark, S. Pradhan, and S.E. Jacobsen. 2007. UHRF1 plays a role in maintaining DNA methylation in mammalian cells. *Science*. 317:1760-1764.

Bouillet, P., M. Oulad-Abdelghani, S. Vicaire, J.M. Garnier, B. Schuhbaur, P. Dolle, and P. Chambon. 1995. Efficient cloning of cDNAs of retinoic acid-responsive genes in P19 embryonal carcinoma cells and characterization of a novel mouse gene, Stra1 (mouse LERK-2/Eplg2). *Developmental biology*. 170:420-433.

Boulogne, B., C. Levacher, P. Durand, and R. Habert. 1999. Retinoic acid receptors and retinoid X receptors in the rat testis during fetal and postnatal

development: immunolocalization and implication in the control of the number of gonocytes. *Biology of reproduction*. 61:1548-1557.

Bowles, J., D. Knight, C. Smith, D. Wilhelm, J. Richman, S. Mamiya, K. Yashiro, K. Chawengsaksophak, M.J. Wilson, J. Rossant, H. Hamada, and P. Koopman. 2006. Retinoid signaling determines germ cell fate in mice. *Science*. 312:596-600.

Bowles, J., and P. Koopman. 2007. Retinoic acid, meiosis and germ cell fate in mammals. *Development*. 134:3401-3411.

Bowles, J., and P. Koopman. 2010. Sex determination in mammalian germ cells: extrinsic versus intrinsic factors. *Reproduction*. 139:943-958.

Boyer, L.A., K. Plath, J. Zeitlinger, T. Brambrink, L.A. Medeiros, T.I. Lee, S.S. Levine, M. Wernig, A. Tajonar, M.K. Ray, G.W. Bell, A.P. Otte, M. Vidal, D.K. Gifford, R.A. Young, and R. Jaenisch. 2006. Polycomb complexes repress developmental regulators in murine embryonic stem cells. *Nature*. 441:349-353.

Bracken, A.P., N. Dietrich, D. Pasini, K.H. Hansen, and K. Helin. 2006. Genome-wide mapping of Polycomb target genes unravels their roles in cell fate transitions. *Genes Dev*. 20:1123-1136.

Branciamore, S., Z.X. Chen, A.D. Riggs, and S.N. Rodin. 2010. CpG island clusters and pro-epigenetic selection for CpGs in protein-coding exons of HOX and other transcription factors. *Proceedings of the National Academy of Sciences of the United States of America*. 107:15485-15490.

Branco, M.R., G. Ficz, and W. Reik. 2012. Uncovering the role of 5-hydroxymethylcytosine in the epigenome. *Nature reviews. Genetics*. 13:7-13.

Briggs, S.D., T. Xiao, Z.W. Sun, J.A. Caldwell, J. Shabanowitz, D.F. Hunt, C.D. Allis, and B.D. Strahl. 2002. Gene silencing: trans-histone regulatory pathway in chromatin. *Nature*. 418:498.

Bullejos, M., and P. Koopman. 2004. Germ cells enter meiosis in a rostro-caudal wave during development of the mouse ovary. *Molecular reproduction and development*. 68:422-428.

Bullejos, M., and P. Koopman. 2005. Delayed Sry and Sox9 expression in developing mouse gonads underlies B6-Y(DOM) sex reversal. *Developmental biology*. 278:473-481.

Byskov, A.G. 1986. Differentiation of mammalian embryonic gonad. *Physiological reviews*. 66:71-117.

Cao, R., L. Wang, H. Wang, L. Xia, H. Erdjument-Bromage, P. Tempst, R.S. Jones, and Y. Zhang. 2002. Role of histone H3 lysine 27 methylation in Polycomb-group silencing. *Science*. 298:1039-1043.

Castrillon, D.H., B.J. Quade, T.Y. Wang, C. Quigley, and C.P. Crum. 2000. The human VASA gene is specifically expressed in the germ cell lineage. *Proceedings of the National Academy of Sciences of the United States of America*. 97:9585-9590.

Cedar, H., and Y. Bergman. 2009. Linking DNA methylation and histone modification: patterns and paradigms. *Nature reviews. Genetics*. 10:295-304.

CellSignaling. H3K4me3. Tri-Methyl-Histone H3 (Lys4) Antibody #9727.

CellSignaling. H3K27me3. Tri-Methyl-Histone H3 (Lys27) (C36B11) Rabbit mAb #9733.

Chamberlain, S.J., D. Yee, and T. Magnuson. 2008. Polycomb repressive complex 2 is dispensable for maintenance of embryonic stem cell pluripotency. *Stem cells*. 26:1496-1505.

Chedin, F., M.R. Lieber, and C.L. Hsieh. 2002. The DNA methyltransferase-like protein DNMT3L stimulates de novo methylation by Dnmt3a. *Proceedings of the National Academy of Sciences of the United States of America*. 99:16916-16921.

Chen, T., and E. Li. 2006. Establishment and maintenance of DNA methylation patterns in mammals. *Current topics in microbiology and immunology*. 301:179-201.

Cheung, P., C.D. Allis, and P. Sassone-Corsi. 2000. Signaling to chromatin through histone modifications. *Cell*. 103:263-271.

Chi, P., C.D. Allis, and G.G. Wang. 2010. Covalent histone modifications--miswritten, misinterpreted and mis-erased in human cancers. *Nature reviews. Cancer*. 10:457-469.

Childs, A.J., R.A. Bayne, A.A. Murray, S.J. Martins Da Silva, C.S. Collins, N. Spears, and R.A. Anderson. 2010. Differential expression and regulation by activin of the neurotrophins BDNF and NT4 during human and mouse ovarian development. *Developmental dynamics : an official publication of the American Association of Anatomists*. 239:1211-1219.

Childs, A.J., G. Cowan, H.L. Kinnell, R.A. Anderson, and P.T. Saunders. 2011. Retinoic Acid signalling and the control of meiotic entry in the human fetal gonad. *PloS one*. 6:e20249.

Childs, A.J., H.L. Kinnell, J. He, and R.A. Anderson. 2012. LIN28 is selectively expressed by primordial and pre-meiotic germ cells in the human fetal ovary. *Stem cells and development*. 21:2343-2349.

Chuma, S., and N. Nakatsuji. 2001. Autonomous transition into meiosis of mouse fetal germ cells in vitro and its inhibition by gp130-mediated signaling. *Developmental biology*. 229:468-479.

Clark, A.T., M.S. Bodnar, M. Fox, R.T. Rodriquez, M.J. Abeyta, M.T. Firpo, and R.A. Pera. 2004. Spontaneous differentiation of germ cells from human embryonic stem cells in vitro. *Human molecular genetics*. 13:727-739.

Cortellino, S., J. Xu, M. Sannai, R. Moore, E. Caretti, A. Cigliano, M. Le Coz, K. Devarajan, A. Wessels, D. Soprano, L.K. Abramowitz, M.S. Bartolomei, F. Rambow, M.R. Bassi, T. Bruno, M. Fanciulli, C. Renner, A.J. Klein-Szanto, Y. Matsumoto, D. Kobi, I. Davidson, C. Alberti, L. Larue, and A. Bellacosa. 2011.

Thymine DNA glycosylase is essential for active DNA demethylation by linked deamination-base excision repair. *Cell*. 146:67-79.

Coutts, S.M., A.J. Childs, N. Fulton, C. Collins, R.A. Bayne, A.S. McNeilly, and R.A. Anderson. 2008. Activin signals via SMAD2/3 between germ and somatic cells in the human fetal ovary and regulates kit ligand expression. *Developmental biology*. 314:189-199.

Czermin, B., G. Schotta, B.B. Hulsmann, A. Brehm, P.B. Becker, G. Reuter, and A. Imhof. 2001. Physical and functional association of SU(VAR)3-9 and HDAC1 in Drosophila. *EMBO reports*. 2:915-919.

Damelin, M., and T.H. Bestor. 2007. Biological functions of DNA methyltransferase 1 require its methyltransferase activity. *Molecular and cellular biology*. 27:3891-3899.

Davis, T.L., G.J. Yang, J.R. McCarrey, and M.S. Bartolomei. 2000. The H19 methylation imprint is erased and re-established differentially on the parental alleles during male germ cell development. *Human molecular genetics*. 9:2885-2894.

De Felici, M., S. Dolci, and M. Pesce. 1992. Cellular and molecular aspects of mouse primordial germ cell migration and proliferation in culture. *Int J Dev Biol*. 36:205-213.

de Jong, J., H. Stoop, A.J. Gillis, R. Hersmus, R.J. van Gurp, G.J. van de Geijn, E. van Drunen, H.B. Beverloo, D.T. Schneider, J.K. Sherlock, J. Baeten, S. Kitazawa, E.J. van Zoelen, K. van Roozendaal, J.W. Oosterhuis, and L.H. Looijenga. 2008. Further characterization of the first seminoma cell line TCam-2. *Genes, chromosomes & cancer*. 47:185-196.

De Pol, A., F. Vaccina, A. Forabosco, E. Cavazzuti, and L. Marzona. 1997. Apoptosis of germ cells during human prenatal oogenesis. *Human reproduction*. 12:2235-2241.

de Ruijter, A.J., A.H. van Gennip, H.N. Caron, S. Kemp, and A.B. van Kuilenburg. 2003. Histone deacetylases (HDACs): characterization of the classical HDAC family. *The Biochemical journal*. 370:737-749.

de Vries, F.A.T., E. de Boer, M. van den Bosch, W.M. Baarends, M. Ooms, L. Yuan, J.G. Liu, A.A. van Zeeland, C. Heyting, and A. Pastink. 2005. Mouse Sycp1 functions in synaptonemal complex assembly, meiotic recombination., and XY body formation. *Gene Dev*. 19:1376-1389.

Deaton, A.M., and A. Bird. 2011. CpG islands and the regulation of transcription. *Genes Dev*. 25:1010-1022.

DeFalco, T., S. Takahashi, and B. Capel. 2011. Two distinct origins for Leydig cell progenitors in the fetal testis. *Developmental biology*. 352:14-26.

Dillon, N. 2004. Heterochromatin structure and function. *Biology of the cell / under the auspices of the European Cell Biology Organization*. 96:631-637.

Dorfman, D.M., D.R. Genest, and R.A. Reijo Pera. 1999. Human DAZL1 encodes a candidate fertility factor in women that localizes to the prenatal and postnatal germ cells. *Human reproduction*. 14:2531-2536.

Duester, G. 2008. Retinoic acid synthesis and signaling during early organogenesis. *Cell*. 134:921-931.

Dufour, J.M., and K.H. Kim. 1999. Cellular and subcellular localization of six retinoid receptors in rat testis during postnatal development: identification of potential heterodimeric receptors. *Biology of reproduction*. 61:1300-1308.

Eckert, D., K. Biermann, D. Nettersheim, A.J. Gillis, K. Steger, H.M. Jack, A.M. Muller, L.H. Looijenga, and H. Schorle. 2008. Expression of BLIMP1/PRMT5 and concurrent histone H2A/H4 arginine 3 dimethylation in fetal germ cells, CIS/IGCNU and germ cell tumors. *BMC developmental biology*. 8:106.

Eddie, S.L. 2011. Novel regulators of human gonadal development.

Egger, G., G. Liang, A. Aparicio, and P.A. Jones. 2004. Epigenetics in human disease and prospects for epigenetic therapy. *Nature*. 429:457-463.

Eijpe, M., H. Offenberg, R. Jessberger, E. Revenkova, and C. Heyting. 2003. Meiotic cohesin REC8 marks the axial elements of rat synaptonemal complexes before cohesins SMC1 beta and SMC3. *Journal of Cell Biology*. 160:657-670.

Eram, M.S., S.P. Bustos, E. Lima-Fernandes, A. Siarheyeva, G. Senisterra, T. Hajian, I. Chau, S. Duan, H. Wu, L. Dombrovski, M. Schapira, C.H. Arrowsmith, and M. Vedadi. 2014. Trimethylation of histone H3 lysine 36 by human methyltransferase PRDM9 protein. *The Journal of biological chemistry*. 289:12177-12188.

Erfurth, F.E., R. Popovic, J. Grembecka, T. Cierpicki, C. Theisler, Z.B. Xia, T. Stuart, M.O. Diaz, J.H. Bushweller, and N.J. Zeleznik-Le. 2008. MLL protects CpG clusters from methylation within the Hoxa9 gene, maintaining transcript expression. *Proceedings of the National Academy of Sciences of the United States of America*. 105:7517-7522.

Esteve, P.O., H.G. Chin, A. Smallwood, G.R. Feehery, O. Gangisetty, A.R. Karpf, M.F. Carey, and S. Pradhan. 2006. Direct interaction between DNMT1 and G9a coordinates DNA and histone methylation during replication. *Genes Dev*. 20:3089-3103.

Falin, L.I. 1969. The development of genital glands and the origin of germ cells in human embryogenesis. *Acta anatomica*. 72:195-232.

Feldman, N., A. Gerson, J. Fang, E. Li, Y. Zhang, Y. Shinkai, H. Cedar, and Y. Bergman. 2006. G9a-mediated irreversible epigenetic inactivation of Oct-3/4 during early embryogenesis. *Nature cell biology*. 8:188-194.

Ficz, G., M.R. Branco, S. Seisenberger, F. Santos, F. Krueger, T.A. Hore, C.J. Marques, S. Andrews, and W. Reik. 2011. Dynamic regulation of 5-hydroxymethylcytosine in mouse ES cells and during differentiation. *Nature*. 473:398-U589.

Flanagan, J.F., L.Z. Mi, M. Chruszcz, M. Cymborowski, K.L. Clines, Y. Kim, W. Minor, F. Rastinejad, and S. Khorasanizadeh. 2005. Double chromodomains cooperate to recognize the methylated histone H3 tail. *Nature*. 438:1181-1185.

Francavilla, S., G. Cordeschi, G. Properzi, N. Concordia, F. Cappa, and V. Pozzi. 1990. Ultrastructure of Fetal Human Gonad before Sexual-Differentiation and during Early Testicular and Ovarian Development. *J Submicr Cytol Path*. 22:389-400.

Fujimoto, T., Y. Miyayama, and M. Fuyuta. 1977. The origin, migration and fine morphology of human primordial germ cells. *The Anatomical record*. 188:315-330.

Fulton, N., S.J. Martins da Silva, R.A. Bayne, and R.A. Anderson. 2005. Germ cell proliferation and apoptosis in the developing human ovary. *The Journal of clinical endocrinology and metabolism*. 90:4664-4670.

Fuss, A. 1912. Über die Geschlechtszellen des Menschen und der Säugetiere. *Archiv für mikroskopische Anatomie*. 81:a1-a23.

Gallinari, P., S. Di Marco, P. Jones, M. Pallaoro, and C. Steinkuhler. 2007. HDACs, histone deacetylation and gene transcription: from molecular biology to cancer therapeutics. *Cell research*. 17:195-211.

Gaskell, T.L., A. Esnal, L.L. Robinson, R.A. Anderson, and P.T. Saunders. 2004. Immunohistochemical profiling of germ cells within the human fetal testis: identification of three subpopulations. *Biology of reproduction*. 71:2012-2021.

Ghyselinck, N.B., N. Vernet, C. Dennefeld, N. Giese, H. Nau, P. Chambon, S. Viville, and M. Mark. 2006. Retinoids and spermatogenesis: lessons from mutant mice lacking the plasma retinol binding protein. *Developmental dynamics : an official publication of the American Association of Anatomists*. 235:1608-1622.

Gkountela, S., Z.W. Li, J.J. Vincent, K.X. Zhang, A. Chen, M. Pellegrini, and A.T. Clark. 2013. The ontogeny of cKIT(+) human primordial germ cells proves to be a resource for human germ line reprogramming, imprint erasure and in vitro differentiation. *Nature cell biology*. 15:113-U247.

Goldberg, A.D., C.D. Allis, and E. Bernstein. 2007. Epigenetics: a landscape takes shape. *Cell*. 128:635-638.

Gondos, B., L. Westergaard, and A.G. Byskov. 1986. Initiation of oogenesis in the human fetal ovary: ultrastructural and squash preparation study. *American journal of obstetrics and gynecology*. 155:189-195.

Gondos, B., and L. Zamboni. 1969. Ovarian development: the functional importance of germ cell interconnections. *Fertility and sterility*. 20:176-189.

Gowher, H., K. Liebert, A. Hermann, G. Xu, and A. Jeltsch. 2005. Mechanism of stimulation of catalytic activity of Dnmt3A and Dnmt3B DNA-(cytosine-C5)-methyltransferases by Dnmt3L. *The Journal of biological chemistry*. 280:13341-13348.

Grewal, S.I., and S. Jia. 2007. Heterochromatin revisited. *Nature reviews. Genetics*. 8:35-46.

Griswold, M.D., C.A. Hogarth, J. Bowles, and P. Koopman. 2012. Initiating meiosis: the case for retinoic acid. *Biology of reproduction*. 86:35.

Gu, P., D. Le Menuet, A.C. Chung, and A.J. Cooney. 2006. Differential recruitment of methylated CpG binding domains by the orphan receptor GCNF initiates the repression and silencing of Oct4 expression. *Molecular and cellular biology*. 26:9471-9483.

Gu, T.P., F. Guo, H. Yang, H.P. Wu, G.F. Xu, W. Liu, Z.G. Xie, L.Y. Shi, X.Y. He, S.G. Jin, K. Iqbal, Y.J.G. Shi, Z.X. Deng, P.E. Szabo, G.P. Pfeifer, J.S. Li, and G.L. Xu. 2011. The role of Tet3 DNA dioxygenase in epigenetic reprogramming by oocytes. *Nature*. 477:606-U136.

Guerrero, R., and P.E. Florez. 1969. The duration of pregnancy. *Lancet*. 2:268-269.

Guibert, S., T. Forne, and M. Weber. 2012. Global profiling of DNA methylation erasure in mouse primordial germ cells. *Genome research*. 22:633-641.

Guo, J.U., Y. Su, C. Zhong, G.L. Ming, and H. Song. 2011. Hydroxylation of 5-methylcytosine by TET1 promotes active DNA demethylation in the adult brain. *Cell*. 145:423-434.

Hacker, A., B. Capel, P. Goodfellow, and R. Lovell-Badge. 1995. Expression of Sry, the mouse sex determining gene. *Development*. 121:1603-1614.

Hackett, J.A., J.P. Reddington, C.E. Nestor, D.S. Dunican, M.R. Branco, J. Reichmann, W. Reik, M.A. Surani, I.R. Adams, and R.R. Meehan. 2012. Promoter DNA methylation couples genome-defence mechanisms to epigenetic reprogramming in the mouse germline. *Development*. 139:3623-3632.

Hackett, J.A., R. Sengupta, J.J. Zylicz, K. Murakami, C. Lee, T.A. Down, and M.A. Surani. 2013. Germline DNA Demethylation Dynamics and Imprint Erasure Through 5-Hydroxymethylcytosine. *Science*. 339:448-452.

Hajkova, P., K. Ancelin, T. Waldmann, N. Lacoste, U.C. Lange, F. Cesari, C. Lee, G. Almouzni, R. Schneider, and M.A. Surani. 2008. Chromatin dynamics during epigenetic reprogramming in the mouse germ line. *Nature*. 452:877-881.

Hajkova, P., S. Erhardt, N. Lane, T. Haaf, O. El-Maarri, W. Reik, J. Walter, and M.A. Surani. 2002. Epigenetic reprogramming in mouse primordial germ cells. *Mechanisms of development*. 117:15-23.

Hajkova, P., S.J. Jeffries, C. Lee, N. Miller, S.P. Jackson, and M.A. Surani. 2010. Genome-wide reprogramming in the mouse germ line entails the base excision repair pathway. *Science*. 329:78-82.

Hanley, N.A., D.M. Hagan, M. Clement-Jones, S.G. Ball, T. Strachan, L. Salas-Cortes, K. McElreavey, S. Lindsay, S. Robson, P. Bullen, H. Ostrer, and D.I. Wilson. 2000. SRY, SOX9, and DAX1 expression patterns during human sex determination and gonadal development. *Mechanisms of development*. 91:403-407.

Hartley, P.S., R.A. Bayne, L.L. Robinson, N. Fulton, and R.A. Anderson. 2002. Developmental changes in expression of myeloid cell leukemia-1 in human germ cells during oogenesis and early folliculogenesis. *The Journal of clinical endocrinology and metabolism*. 87:3417-3427.

Hashimoto, H., S. Hong, A.S. Bhagwat, X. Zhang, and X. Cheng. 2012. Excision of 5-hydroxymethyluracil and 5-carboxylcytosine by the thymine DNA glycosylase domain: its structural basis and implications for active DNA demethylation. *Nucleic Acids Res*. 40:10203-10214.

Hassan, A.H., P. Prochasson, K.E. Neely, S.C. Galasinski, M. Chandy, M.J. Carrozza, and J.L. Workman. 2002. Function and selectivity of bromodomains in anchoring chromatin-modifying complexes to promoter nucleosomes. *Cell*. 111:369-379.

Hattori, N., Y. Imao, K. Nishino, N. Hattori, J. Ohgane, S. Yagi, S. Tanaka, and K. Shiota. 2007. Epigenetic regulation of Nanog gene in embryonic stem and trophoblast stem cells. *Genes to cells : devoted to molecular & cellular mechanisms*. 12:387-396.

Hattori, N., K. Nishino, Y.G. Ko, N. Hattori, J. Ohgane, S. Tanaka, and K. Shiota. 2004. Epigenetic control of mouse Oct-4 gene expression in embryonic stem cells and trophoblast stem cells. *The Journal of biological chemistry*. 279:17063-17069.

Hayashi, K., S.M. de Sousa Lopes, and M.A. Surani. 2007. Germ cell specification in mice. *Science*. 316:394-396.

Hayashi, K., and Y. Matsui. 2006. Meisetz, a novel histone tri-methyltransferase, regulates meiosis-specific epigenesis. *Cell cycle*. 5:615-620.

Hayashi, K., K. Yoshida, and Y. Matsui. 2005. A histone H3 methyltransferase controls epigenetic events required for meiotic prophase. *Nature*. 438:374-378.

He, J., K. Stewart, H.L. Kinnell, R.A. Anderson, and A.J. Childs. 2013. A Developmental Stage-Specific Switch from DAZL to BOLL Occurs during Fetal Oogenesis in Humans, but Not Mice. *PloS one*. 8.

He, Y.F., B.Z. Li, Z. Li, P. Liu, Y. Wang, Q. Tang, J. Ding, Y. Jia, Z. Chen, L. Li, Y. Sun, X. Li, Q. Dai, C.X. Song, K. Zhang, C. He, and G.L. Xu. 2011. Tet-mediated formation of 5-carboxylcytosine and its excision by TDG in mammalian DNA. *Science*. 333:1303-1307.

Hebbes, T.R., A.W. Thorne, and C. Crane-Robinson. 1988. A direct link between core histone acetylation and transcriptionally active chromatin. *The EMBO journal*. 7:1395-1402.

Heintzman, N.D., R.K. Stuart, G. Hon, Y. Fu, C.W. Ching, R.D. Hawkins, L.O. Barrera, S. Van Calcar, C. Qu, K.A. Ching, W. Wang, Z. Weng, R.D. Green, G.E. Crawford, and B. Ren. 2007. Distinct and predictive chromatin signatures of transcriptional promoters and enhancers in the human genome. *Nature genetics*. 39:311-318.

Heyn, R., S. Makabe, and P.M. Motta. 2001. Ultrastructural morphodynamics of human Sertoli cells during testicular differentiation. *Italian journal of anatomy and embryology = Archivio italiano di anatomia ed embriologia*. 106:163-171.

Hilscher, B., W. Hilscher, B. Bulthoff-Ohnolz, U. Kramer, A. Birke, H. Pelzer, and G. Gauss. 1974. Kinetics of gametogenesis. I. Comparative histological and autoradiographic studies of oocytes and transitional prospermatogonia during oogenesis and prespermatogenesis. *Cell and tissue research*. 154:443-470.

Holliday, R., and J.E. Pugh. 1975. DNA modification mechanisms and gene activity during development. *Science*. 187:226-232.

Houmard, B., C. Small, L. Yang, T. Naluai-Cecchini, E. Cheng, T. Hassold, and M. Griswold. 2009. Global gene expression in the human fetal testis and ovary. *Biology of reproduction*. 81:438-443.

Hublitz, P., M. Albert, and A.H. Peters. 2009. Mechanisms of transcriptional repression by histone lysine methylation. *Int J Dev Biol*. 53:335-354.

Hunt, P.A., and T.J. Hassold. 2008. Human female meiosis: what makes a good egg go bad? *Trends in genetics : TIG*. 24:86-93.

Inoue, A., L. Shen, Q. Dai, C. He, and Y. Zhang. 2011. Generation and replication-dependent dilution of 5fC and 5caC during mouse preimplantation development. *Cell research*. 21:1670-1676.

Inoue, A., and Y. Zhang. 2011. Replication-Dependent Loss of 5-Hydroxymethylcytosine in Mouse Preimplantation Embryos. *Science*. 334:194-194.

Ioshikhes, I.P., and M.Q. Zhang. 2000. Large-scale human promoter mapping using CpG islands. *Nature genetics*. 26:61-63.

Iqbal, K., S.G. Jin, G.P. Pfeifer, and P.E. Szabo. 2011. Reprogramming of the paternal genome upon fertilization involves genome-wide oxidation of 5-methylcytosine. *Proceedings of the National Academy of Sciences of the United States of America*. 108:3642-3647.

Ito, S., A.C. D'Alessio, O.V. Taranova, K. Hong, L.C. Sowers, and Y. Zhang. 2010. Role of Tet proteins in 5mC to 5hmC conversion, ES-cell self-renewal and inner cell mass specification. *Nature*. 466:1129-1133.

Ito, S., L. Shen, Q. Dai, S.C. Wu, L.B. Collins, J.A. Swenberg, C. He, and Y. Zhang. 2011. Tet Proteins Can Convert 5-Methylcytosine to 5-Formylcytosine and 5-Carboxylcytosine. *Science*. 333:1300-1303.

Ivanov, M., M. Kals, M. Kacevska, I. Barragan, K. Kasuga, A. Rane, A. Metspalu, L. Milani, and M. Ingelman-Sundberg. 2013. Ontogeny, distribution and potential roles of 5-hydroxymethylcytosine in human liver function. *Genome biology*. 14:R83.

Jenuwein, T., and C.D. Allis. 2001. Translating the histone code. *Science*. 293:1074-1080.

Jeske, Y.W., J. Bowles, A. Greenfield, and P. Koopman. 1995. Expression of a linear Sry transcript in the mouse genital ridge. *Nature genetics*. 10:480-482.

Jia, D., R.Z. Jurkowska, X. Zhang, A. Jeltsch, and X. Cheng. 2007. Structure of Dnmt3a bound to Dnmt3L suggests a model for de novo DNA methylation. *Nature*. 449:248-251.

John Polkinghorne. 1989. Review of the Guidance on the Research Use of Fetuses and Fetal Material. Stationery Office Books, London.

Jones, P.A., and G.N. Liang. 2009. OPINION Rethinking how DNA methylation patterns are maintained. *Nature Reviews Genetics*. 10:805-811.

Jones, P.A., and S.M. Taylor. 1980. Cellular-Differentiation, Cytidine Analogs and DNA Methylation. *Cell*. 20:85-93.

Jorgensen, A., J.E. Nielsen, M. Blomberg Jensen, N. Graem, and E. Rajpert-De Meyts. 2012. Analysis of meiosis regulators in human gonads: a sexually dimorphic spatio-temporal expression pattern suggests involvement of DMRT1 in meiotic entry. *Molecular human reproduction*. 18:523-534.

Kagiwada, S., K. Kurimoto, T. Hirota, M. Yamaji, and M. Saitou. 2013. Replication-coupled passive DNA demethylation for the erasure of genome imprints in mice. *The EMBO journal*. 32:340-353.

Kastner, P., M. Mark, N. Ghyselinck, W. Krezel, V. Dupe, J.M. Grondona, and P. Chambon. 1997. Genetic evidence that the retinoid signal is transduced by heterodimeric RXR/RAR functional units during mouse development. *Development*. 124:313-326.

Kee, K., V.T. Angeles, M. Flores, H.N. Nguyen, and R.A. Reijo Pera. 2009. Human DAZL, DAZ and BOULE genes modulate primordial germ-cell and haploid gamete formation. *Nature*. 462:222-225.

Kee, K., J.M. Gonsalves, A.T. Clark, and R.A. Pera. 2006. Bone morphogenetic proteins induce germ cell differentiation from human embryonic stem cells. *Stem cells and development*. 15:831-837.

Kerr, C.L., C.M. Hill, P.D. Blumenthal, and J.D. Gearhart. 2008a. Expression of pluripotent stem cell markers in the human fetal ovary. *Human reproduction*. 23:589-599.

Kerr, C.L., C.M. Hill, P.D. Blumenthal, and J.D. Gearhart. 2008b. Expression of pluripotent stem cell markers in the human fetal testis. *Stem cells*. 26:412-421.

Klose, R.J., E.M. Kallin, and Y. Zhang. 2006. JmjC-domain-containing proteins and histone demethylation. *Nature reviews. Genetics*. 7:715-727.

Ko, M., Y. Huang, A.M. Jankowska, U.J. Pape, M. Tahiliani, H.S. Bandukwala, J. An, E.D. Lamperti, K.P. Koh, R. Ganetzky, X.S. Liu, L. Aravind, S. Agarwal, J.P. Maciejewski, and A. Rao. 2010. Impaired hydroxylation of 5-methylcytosine in myeloid cancers with mutant TET2. *Nature*. 468:839-843.

Kohli, R.M., and Y. Zhang. 2013. TET enzymes, TDG and the dynamics of DNA demethylation. *Nature*. 502:472-479.

Kondo, Y., L. Shen, A.S. Cheng, S. Ahmed, Y. Boumber, C. Charo, T. Yamochi, T. Urano, K. Furukawa, B. Kwabi-Addo, D.L. Gold, Y. Sekido, T.H. Huang, and J.P. Issa. 2008. Gene silencing in cancer by histone H3 lysine 27 trimethylation independent of promoter DNA methylation. *Nature genetics*. 40:741-750.

Koopman, P., J. Gubbay, N. Vivian, P. Goodfellow, and R. Lovell-Badge. 1991. Male development of chromosomally female mice transgenic for Sry. *Nature*. 351:117-121.

Kornberg, R.D. 1974. Chromatin structure: a repeating unit of histones and DNA. *Science*. 184:868-871.

Kornberg, R.D. 1977. Structure of chromatin. *Annual review of biochemistry*. 46:931-954.

Kota, S.K., and R. Feil. 2010. Epigenetic transitions in germ cell development and meiosis. *Developmental cell*. 19:675-686.

Koubova, J., D.B. Menke, Q. Zhou, B. Capel, M.D. Griswold, and D.C. Page. 2006. Retinoic acid regulates sex-specific timing of meiotic initiation in mice. *Proceedings of the National Academy of Sciences of the United States of America*. 103:2474-2479.

Kousta, E., A. Papathanasiou, and N. Skordis. 2010. Sex determination and disorders of sex development according to the revised nomenclature and classification in 46,XX individuals. *Hormones*. 9:218-131.

Kouzarides, T. 2007. Chromatin modifications and their function. *Cell*. 128:693-705.

Krejci, J., R. Uhlirova, G. Galiova, S. Kozubek, J. Smigova, and E. Bartova. 2009. Genome-wide reduction in H3K9 acetylation during human embryonic stem cell differentiation. *Journal of cellular physiology*. 219:677-687.

Kriaucionis, S., and N. Heintz. 2009. The Nuclear DNA Base 5-Hydroxymethylcytosine Is Present in Purkinje Neurons and the Brain. *Science*. 324:929-930.

Kristensen, D.M., S.B. Sonne, A.M. Ottesen, R.M. Perrett, J.E. Nielsen, K. Almstrup, N.E. Skakkebaek, H. Leffers, and E. Rajpert-De Meyts. 2008. Origin of pluripotent germ cell tumours: the role of microenvironment during embryonic development. *Molecular and cellular endocrinology*. 288:111-118.

Kumar, S., C. Chatzi, T. Brade, T.J. Cunningham, X.L. Zhao, and G. Duester. 2011. Sex-specific timing of meiotic initiation is regulated by Cyp26b1 independent of retinoic acid signalling. *Nat Commun*. 2.

Kuo, M.H., and C.D. Allis. 1998. Roles of histone acetyltransferases and deacetylases in gene regulation. *BioEssays : news and reviews in molecular, cellular and developmental biology*. 20:615-626.

Kurimoto, K., Y. Yabuta, Y. Ohinata, M. Shigeta, K. Yamanaka, and M. Saitou. 2008. Complex genome-wide transcription dynamics orchestrated by Blimp1 for the specification of the germ cell lineage in mice. *Genes Dev*. 22:1617-1635.

Kuzmichev, A., K. Nishioka, H. Erdjument-Bromage, P. Tempst, and D. Reinberg. 2002. Histone methyltransferase activity associated with a human multiprotein complex containing the Enhancer of Zeste protein. *Genes Dev*. 16:2893-2905.

Kuzmichev, A., and D. Reinberg. 2001. Role of histone deacetylase complexes in the regulation of chromatin metabolism. *Current topics in microbiology and immunology*. 254:35-58.

Lachner, M., and T. Jenuwein. 2002. The many faces of histone lysine methylation. *Current opinion in cell biology*. 14:286-298.

Lachner, M., D. O'Carroll, S. Rea, K. Mechtler, and T. Jenuwein. 2001. Methylation of histone H3 lysine 9 creates a binding site for HP1 proteins. *Nature*. 410:116-120.

Lande-Diner, L., J. Zhang, I. Ben-Porath, N. Amariglio, I. Keshet, M. Hecht, V. Azuara, A.G. Fisher, G. Rechavi, and H. Cedar. 2007. Role of DNA methylation in stable gene repression. *The Journal of biological chemistry*. 282:12194-12200.

Lanman, J.T., and L. Seidman. 1977. Length of gestation in mice under a 21-hour day. *Biology of reproduction*. 17:224-227.

Lasko, P.F., and M. Ashburner. 1988. The product of the Drosophila gene vasa is very similar to eukaryotic initiation factor-4A. *Nature*. 335:611-617.

Lawson, K.A., N.R. Dunn, B.A.J. Roelen, L.M. Zeinstra, A.M. Davis, C.V.E. Wright, J.P.W.F.M. Korving, and B.L.M. Hogan. 1999. Bmp4 is required for the generation of primordial germ cells in the mouse embryo. *Gene Dev*. 13:424-436.

Lawson, K.A., and W.J. Hage. 1994. Clonal analysis of the origin of primordial germ cells in the mouse. *Ciba Foundation symposium*. 182:68-84; discussion 84-91.

Le Bouffant, R., M.J. Guerquin, C. Duquenne, N. Frydman, H. Coffigny, V. Rouiller-Fabre, R. Frydman, R. Habert, and G. Livera. 2010. Meiosis initiation in the human ovary requires intrinsic retinoic acid synthesis. *Human reproduction*. 25:2579-2590.

Lee, J., T. Iwai, T. Yokota, and M. Yamashita. 2003. Temporally and spatially selective loss of Rec8 protein from meiotic chromosomes during mammalian meiosis. *Journal of cell science*. 116:2781-2790.

Lee, T.I., R.G. Jenner, L.A. Boyer, M.G. Guenther, S.S. Levine, R.M. Kumar, B. Chevalier, S.E. Johnstone, M.F. Cole, K. Isono, H. Koseki, T. Fuchikami, K. Abe, H.L. Murray, J.P. Zucker, B. Yuan, G.W. Bell, E. Herbolsheimer, N.M. Hannett, K. Sun, D.T. Odom, A.P. Otte, T.L. Volkert, D.P. Bartel, D.A. Melton, D.K. Gifford, R. Jaenisch, and R.A. Young. 2006. Control of developmental regulators by Polycomb in human embryonic stem cells. *Cell*. 125:301-313.

Lehnertz, B., Y. Ueda, A.A.H.A. Derijck, U. Braunschweig, L. Perez-Burgos, S. Kubicek, T.P. Chen, E. Li, T. Jenuwein, and A.H.F.M. Peters. 2003. Suv39h-mediated histone H3 lysine 9 methylation directs DNA methylation to major satellite repeats at pericentric heterochromatin. *Current Biology*. 13:1192-1200.

Lewis, J.D., R.R. Meehan, W.J. Henzel, I. Maurer-Fogy, P. Jeppesen, F. Klein, and A. Bird. 1992. Purification, sequence, and cellular localization of a novel chromosomal protein that binds to methylated DNA. *Cell*. 69:905-914.

Li, H., and M. Clagett-Dame. 2009. Vitamin A deficiency blocks the initiation of meiosis of germ cells in the developing rat ovary in vivo. *Biology of reproduction*. 81:996-1001.

Li, H., S. Ilin, W. Wang, E.M. Duncan, J. Wysocka, C.D. Allis, and D.J. Patel. 2006. Molecular basis for site-specific read-out of histone H3K4me3 by the BPTF PHD finger of NURF. *Nature*. 442:91-95.

Li, H., K. Palczewski, W. Baehr, and M. Clagett-Dame. 2011. Vitamin A deficiency results in meiotic failure and accumulation of undifferentiated spermatogonia in prepubertal mouse testis. *Biology of reproduction*. 84:336-341.

Liang, G.G., M.F. Chan, Y. Tomigahara, Y.C. Tsai, F.A. Gonzales, E. Li, P.W. Laird, and P.A. Jones. 2002. Cooperativity between DNA methyltransferases in the maintenance methylation of repetitive elements. *Molecular and cellular biology*. 22:480-491.

Lin, I.Y., F.L. Chiu, C.H. Yeang, H.F. Chen, C.Y. Chuang, S.Y. Yang, P.S. Hou, N. Sintupisut, H.N. Ho, H.C. Kuo, and K.I. Lin. 2014. Suppression of the SOX2 Neural Effector Gene by PRDM1 Promotes Human Germ Cell Fate in Embryonic Stem Cells. *Stem cell reports*. 2:189-204.

Lin, Y., M.E. Gill, J. Koubova, and D.C. Page. 2008. Germ cell-intrinsic and -extrinsic factors govern meiotic initiation in mouse embryos. *Science*. 322:1685-1687.

Lin, Y., and D.C. Page. 2005. Dazl deficiency leads to embryonic arrest of germ cell development in XY C57BL/6 mice. *Developmental biology*. 288:309-316.

Linher, K., Q. Cheung, P. Baker, G. Bedecarrats, K. Shiota, and J. Li. 2009. An epigenetic mechanism regulates germ cell-specific expression of the porcine Deleted in Azoospermia-Like (DAZL) gene. *Differentiation; research in biological diversity*. 77:335-349.

Luger, K., T.J. Rechsteiner, A.J. Flaus, M.M. Waye, and T.J. Richmond. 1997. Characterization of nucleosome core particles containing histone proteins made in bacteria. *Journal of molecular biology*. 272:301-311.

Luger, K., and T.J. Richmond. 1998. The histone tails of the nucleosome. *Current opinion in genetics & development*. 8:140-146.

Lynch, C.D., and J. Zhang. 2007. The research implications of the selection of a gestational age estimation method. *Paediatric and perinatal epidemiology*. 21 Suppl 2:86-96.

Maatouk, D.M., L.D. Kellam, M.R. Mann, H. Lei, E. Li, M.S. Bartolomei, and J.L. Resnick. 2006a. DNA methylation is a primary mechanism for silencing postmigratory primordial germ cell genes in both germ cell and somatic cell lineages. *Development*. 133:3411-3418.

Maatouk, D.M., L.D. Kellam, M.R.W. Mann, H. Lei, E. Li, M.S. Bartolomei, and J.L. Resnick. 2006b. DNA methylation is a primary mechanism for silencing postmigratory primordial germ cell genes in both germ cell and somatic cell lineages. *Development*. 133:3411-3418.

MacLean, G., S. Abu-Abed, P. Dolle, A. Tahayato, P. Chambon, and M. Petkovich. 2001. Cloning of a novel retinoic-acid metabolizing cytochrome P450, Cyp26B1, and comparative expression analysis with Cyp26A1 during early murine development. *Mechanisms of development*. 107:195-201.

MacLean, G., H. Li, D. Metzger, P. Chambon, and M. Petkovich. 2007. Apoptotic extinction of germ cells in testes of Cyp26b1 knockout mice. *Endocrinology*. 148:4560-4567.

Maeda, I., D. Okamura, Y. Tokitake, M. Ikeda, H. Kawaguchi, N. Mise, K. Abe, T. Noce, A. Okuda, and Y. Matsui. 2013. Max is a repressor of germ cell-related gene expression in mouse embryonic stem cells. *Nat Commun*. 4.

Mahadevaiah, S.K., J.M. Turner, F. Baudat, E.P. Rogakou, P. de Boer, J. Blanco-Rodriguez, M. Jasin, S. Keeney, W.M. Bonner, and P.S. Burgoyne. 2001. Recombinational DNA double-strand breaks in mice precede synapsis. *Nature genetics*. 27:271-276.

Mamsen, L.S., M.C. Lutterodt, E.W. Andersen, A.G. Byskov, and C.Y. Andersen. 2011. Germ cell numbers in human embryonic and fetal gonads during the first two trimesters of pregnancy: analysis of six published studies. *Human reproduction*. 26:2140-2145.

Mansour, A.A., O. Gafni, L. Weinberger, A. Zviran, M. Ayyash, Y. Rais, V. Krupalnik, M. Zerbib, D. Amann-Zalcenstein, I. Maza, S. Geula, S. Viukov, L. Holtzman, A. Pribluda, E. Canaani, S. Horn-Saban, I. Amit, N. Novershtern, and J.H. Hanna. 2012. The H3K27 demethylase Utx regulates somatic and germ cell epigenetic reprogramming. *Nature*. 488:409-413.

Margueron, R., and D. Reinberg. 2011. The Polycomb complex PRC2 and its mark in life. *Nature*. 469:343-349.

Mark, M., N.B. Ghyselinck, and P. Chambon. 2009. Function of retinoic acid receptors during embryonic development. *Nuclear receptor signaling*. 7:e002.

Mark, M., H. Jacobs, M. Oulad-Abdelghani, C. Dennefeld, B. Feret, N. Vernet, C.A. Codreanu, P. Chambon, and N.B. Ghyselinck. 2008. STRA8-deficient spermatocytes initiate, but fail to complete, meiosis and undergo premature chromosome condensation. *Journal of cell science*. 121:3233-3242.

McLaren, A., and D. Southee. 1997. Entry of mouse embryonic germ cells into meiosis. *Developmental biology*. 187:107-113.

Medrano, J.V., C. Ramathal, H.N. Nguyen, C. Simon, and R.A. Reijo Pera. 2012. Divergent RNA-binding proteins, DAZL and VASA, induce meiotic progression in human germ cells derived in vitro. *Stem cells*. 30:441-451.

Meissner, A., T.S. Mikkelsen, H. Gu, M. Wernig, J. Hanna, A. Sivachenko, X. Zhang, B.E. Bernstein, C. Nusbaum, D.B. Jaffe, A. Gnirke, R. Jaenisch, and E.S. Lander. 2008. Genome-scale DNA methylation maps of pluripotent and differentiated cells. *Nature*. 454:766-770.

Mendenhall, E.M., R.P. Koche, T. Truong, V.W. Zhou, B. Issac, A.S. Chi, M. Ku, and B.E. Bernstein. 2010. GC-rich sequence elements recruit PRC2 in mammalian ES cells. *PLoS genetics*. 6:e1001244.

Menke, D.B., J. Koubova, and D.C. Page. 2003. Sexual differentiation of germ cells in XX mouse gonads occurs in an anterior-to-posterior wave. *Developmental biology*. 262:303-312.

Menke, D.B., and D.C. Page. 2002. Sexually dimorphic gene expression in the developing mouse gonad. *Gene expression patterns : GEP*. 2:359-367.

Messerschmidt, D.M., B.B. Knowles, and D. Solter. 2014. DNA methylation dynamics during epigenetic reprogramming in the germline and preimplantation embryos. *Genes Dev*. 28:812-828.

Mikkelsen, T.S., M. Ku, D.B. Jaffe, B. Issac, E. Lieberman, G. Giannoukos, P. Alvarez, W. Brockman, T.K. Kim, R.P. Koche, W. Lee, E. Mendenhall, A. O'Donovan, A. Presser, C. Russ, X. Xie, A. Meissner, M. Wernig, R. Jaenisch, C. Nusbaum, E.S. Lander, and B.E. Bernstein. 2007. Genome-wide maps of chromatin state in pluripotent and lineage-committed cells. *Nature*. 448:553-560.

Milne, T.A., S.D. Briggs, H.W. Brock, M.E. Martin, D. Gibbs, C.D. Allis, and J.L. Hess. 2002. MLL targets SET domain methyltransferase activity to Hox gene promoters. *Molecular cell*. 10:1107-1117.

Miyamoto, T., K. Sengoku, N. Takuma, S. Hasuike, H. Hayashi, T. Yamauchi, T. Yamashita, and M. Ishikawa. 2002. Isolation and expression analysis of the testis-specific gene, STRA8, stimulated by retinoic acid gene 8. *Journal of assisted reproduction and genetics*. 19:531-535.

Mizejewski, G.J. 2001. Alpha-fetoprotein structure and function: relevance to isoforms, epitopes, and conformational variants. *Experimental biology and medicine*. 226:377-408.

Mizuno, Y., A. Gotoh, S. Kamidono, and S. Kitazawa. 1993. [Establishment and characterization of a new human testicular germ cell tumor cell line (TCam-2)]. *Nihon Hinyokika Gakkai zasshi. The japanese journal of urology*. 84:1211-1218.

Mochizuki, K., and Y. Matsui. 2010. Epigenetic profiles in primordial germ cells: global modulation and fine tuning of the epigenome for acquisition of totipotency. *Development, growth & differentiation*. 52:517-525.

Mochizuki, K., M. Tachibana, M. Saitou, Y. Tokitake, and Y. Matsui. 2012. Implication of DNA demethylation and bivalent histone modification for selective gene regulation in mouse primordial germ cells. *PloS one*. 7:e46036.

Moens, P.B., and B. Spyropoulos. 1995. Immunocytology of Chiasmata and Chromosomal Disjunction at Mouse Meiosis. *Chromosoma*. 104:175-182.

Mohn, F., M. Weber, M. Rebhan, T.C. Roloff, J. Richter, M.B. Stadler, M. Bibel, and D. Schubeler. 2008. Lineage-specific polycomb targets and de novo DNA methylation define restriction and potential of neuronal progenitors. *Molecular cell*. 30:755-766.

Molyneaux, K.A., J. Stallock, K. Schaible, and C. Wylie. 2001. Time-lapse analysis of living mouse germ cell migration. *Developmental biology*. 240:488-498.

Moore, K.L. 1967. Sex determination, sexual differentiation and intersex development. *Canadian Medical Association journal*. 97:292-295.

Morgan, H.D., F. Santos, K. Green, W. Dean, and W. Reik. 2005. Epigenetic reprogramming in mammals. *Human molecular genetics*. 14 Spec No 1:R47-58.

Mozdziak, P.E., J. Angerman-Stewart, B. Rushton, S.L. Pardue, and J.N. Petitte. 2005. Isolation of chicken primordial germ cells using fluorescence-activated cell sorting. *Poultry science*. 84:594-600.

Mu, X., J. Wen, M. Guo, J. Wang, G. Li, Z. Wang, Y. Wang, Z. Teng, Y. Cui, and G. Xia. 2013. Retinoic acid derived from the fetal ovary initiates meiosis in mouse germ cells. *Journal of cellular physiology*. 228:627-639.

Muller, J., C.M. Hart, N.J. Francis, M.L. Vargas, A. Sengupta, B. Wild, E.L. Miller, M.B. O'Connor, R.E. Kingston, and J.A. Simon. 2002. Histone methyltransferase activity of a Drosophila Polycomb group repressor complex. *Cell*. 111:197-208.

Murray, T.J., P.A. Fowler, D.R. Abramovich, N. Haites, and R.G. Lea. 2000. Human fetal testis: second trimester proliferative and steroidogenic capacities. *The Journal of clinical endocrinology and metabolism*. 85:4812-4817.

Nabel, C.S., H. Jia, Y. Ye, L. Shen, H.L. Goldschmidt, J.T. Stivers, Y. Zhang, and R.M. Kohli. 2012. AID/APOBEC deaminases disfavor modified cytosines implicated in DNA demethylation. *Nature chemical biology*. 8:751-758.

Nakanishi, S., B.W. Sanderson, K.M. Delventhal, W.D. Bradford, K. Staehling-Hampton, and A. Shilatifard. 2008. A comprehensive library of histone mutants identifies nucleosomal residues required for H3K4 methylation. *Nature structural & molecular biology*. 15:881-888.

Nakatsuji, N., and S. Chuma. 2001. Differentiation of mouse primordial germ cells into female or male germ cells. *Int J Dev Biol*. 45:541-548.

Nakayama, J., J.C. Rice, B.D. Strahl, C.D. Allis, and S.I. Grewal. 2001. Role of histone H3 lysine 9 methylation in epigenetic control of heterochromatin assembly. *Science*. 292:110-113.

Nicholson, J.M., and C.M. Wood. 2006. Chromatin structure and function, 2006. Transworld Research Network, Kerala, India. 152 p. pp.

Nielsen, S.J., R. Schneider, U.M. Bauer, A.J. Bannister, A. Morrison, D. O'Carroll, R. Firestein, M. Cleary, T. Jenuwein, R.E. Herrera, and T. Kouzarides. 2001. Rb targets histone H3 methylation and HP1 to promoters. *Nature*. 412:561-565.

Nishida, H., T. Suzuki, S. Kondo, H. Miura, Y. Fujimura, and Y. Hayashizaki. 2006. Histone H3 acetylated at lysine 9 in promoter is associated with low nucleosome density in the vicinity of transcription start site in human cell. *Chromosome research : an international journal on the molecular, supramolecular and evolutionary aspects of chromosome biology*. 14:203-211.

Nishioka, K., S. Chuikov, K. Sarma, H. Erdjument-Bromage, C.D. Allis, P. Tempst, and D. Reinberg. 2002. Set9, a novel histone H3 methyltransferase that facilitates transcription by precluding histone tail modifications required for heterochromatin formation. *Genes Dev*. 16:479-489.

Ohinata, Y., B. Payer, D. O'Carroll, K. Ancelin, Y. Ono, M. Sano, S.C. Barton, T. Obukhanych, M. Nussenzweig, A. Tarakhovsky, M. Saitou, and M.A. Surani. 2005. Blimp1 is a critical determinant of the germ cell lineage in mice. *Nature*. 436:207-213.

Ohno, R., M. Nakayama, C. Naruse, N. Okashita, O. Takano, M. Tachibana, M. Asano, M. Saitou, and Y. Seki. 2013. A replication-dependent passive mechanism modulates DNA demethylation in mouse primordial germ cells. *Development*. 140:2892-2903.

Ohta, K., Y.L. Lin, N. Hogg, M. Yamamoto, and Y. Yamazaki. 2010. Direct Effects of Retinoic Acid on Entry of Fetal Male Germ Cells into Meiosis in Mice. *Biology of reproduction*. 83:1056-1063.

Okano, M., D.W. Bell, D.A. Haber, and E. Li. 1999. DNA methyltransferases Dnmt3a and Dnmt3b are essential for de novo methylation and mammalian development. *Cell*. 99:247-257.

Ooi, S.K., and T.H. Bestor. 2008. The colorful history of active DNA demethylation. *Cell*. 133:1145-1148.

Ooi, S.K., C. Qiu, E. Bernstein, K. Li, D. Jia, Z. Yang, H. Erdjument-Bromage, P. Tempst, S.P. Lin, C.D. Allis, X. Cheng, and T.H. Bestor. 2007. DNMT3L connects unmethylated lysine 4 of histone H3 to de novo methylation of DNA. *Nature*. 448:714-717.

Oulad-Abdelghani, M., P. Bouillet, D. Decimo, A. Gansmuller, S. Heyberger, P. Dolle, S. Bronner, Y. Lutz, and P. Chambon. 1996. Characterization of a premeiotic germ cell-specific cytoplasmic protein encoded by Stra8, a novel retinoic acid-responsive gene. *The Journal of cell biology*. 135:469-477.

Palmer, S.J., and P.S. Burgoyne. 1991. In situ analysis of fetal, prepuberal and adult XX----XY chimaeric mouse testes: Sertoli cells are predominantly, but not exclusively, XY. *Development*. 112:265-268.

Pan, G., S. Tian, J. Nie, C. Yang, V. Ruotti, H. Wei, G.A. Jonsdottir, R. Stewart, and J.A. Thomson. 2007. Whole-genome analysis of histone H3 lysine 4 and lysine 27 methylation in human embryonic stem cells. *Cell stem cell*. 1:299-312.

Panula, S., J.V. Medrano, K. Kee, R. Bergstrom, H.N. Nguyen, B. Byers, K.D. Wilson, J.C. Wu, C. Simon, O. Hovatta, and R.A. Reijo Pera. 2011. Human germ cell

differentiation from fetal- and adult-derived induced pluripotent stem cells. *Human molecular genetics*. 20:752-762.

Pastor, W.A., U.J. Pape, Y. Huang, H.R. Henderson, R. Lister, M. Ko, E.M. McLoughlin, Y. Brudno, S. Mahapatra, P. Kapranov, M. Tahiliani, G.Q. Daley, X.S. Liu, J.R. Ecker, P.M. Milos, S. Agarwal, and A. Rao. 2011. Genome-wide mapping of 5-hydroxymethylcytosine in embryonic stem cells. *Nature*. 473:394-397.

Pelliniemi, L.F., K. Patanko, J. 1993. Embryological and prenatal development and function of Sertoli cells. Cache River Press, Illinois.

Pesce, M., X. Wang, D.J. Wolgemuth, and H. Scholer. 1998. Differential expression of the Oct-4 transcription factor during mouse germ cell differentiation. *Mechanisms of development*. 71:89-98.

Peters, A.H., S. Kubicek, K. Mechtler, R.J. O'Sullivan, A.A. Derijck, L. Perez-Burgos, A. Kohlmaier, S. Opravil, M. Tachibana, Y. Shinkai, J.H. Martens, and T. Jenuwein. 2003. Partitioning and plasticity of repressive histone methylation states in mammalian chromatin. *Molecular cell*. 12:1577-1589.

Peters, A.H., D. O'Carroll, H. Scherthan, K. Mechtler, S. Sauer, C. Schofer, K. Weipoltshammer, M. Pagani, M. Lachner, A. Kohlmaier, S. Opravil, M. Doyle, M. Sibilia, and T. Jenuwein. 2001. Loss of the Suv39h histone methyltransferases impairs mammalian heterochromatin and genome stability. *Cell*. 107:323-337.

Pittman, D.L., J. Cobb, K.J. Schimenti, L.A. Wilson, D.M. Cooper, E. Brignull, M.A. Handel, and J.C. Schimenti. 1998. Meiotic prophase arrest with failure of chromosome synapsis in mice deficient for Dmc1, a germline-specific RecA homolog. *Molecular cell*. 1:697-705.

Popp, C., W. Dean, S. Feng, S.J. Cokus, S. Andrews, M. Pellegrini, S.E. Jacobsen, and W. Reik. 2010. Genome-wide erasure of DNA methylation in mouse primordial germ cells is affected by AID deficiency. *Nature*. 463:1101-1105.

Prieto, I., C. Tease, N. Pezzi, J.M. Buesa, S. Ortega, L. Kremer, A. Martinez, A.C. Martinez, M.A. Hulten, and J.L. Barbero. 2004. Cohesin component dynamics during meiotic prophase I in mammalian oocytes. *Chromosome research : an international journal on the molecular, supramolecular and evolutionary aspects of chromosome biology*. 12:197-213.

Rea, S., F. Eisenhaber, D. O'Carroll, B.D. Strahl, Z.W. Sun, M. Schmid, S. Opravil, K. Mechtler, C.P. Ponting, C.D. Allis, and T. Jenuwein. 2000. Regulation of chromatin structure by site-specific histone H3 methyltransferases. *Nature*. 406:593-599.

Reijo, R.A., D.M. Dorfman, R. Slee, A.A. Renshaw, K.R. Loughlin, H. Cooke, and D.C. Page. 2000. DAZ family proteins exist throughout male germ cell development and transit from nucleus to cytoplasm at meiosis in humans and mice. *Biology of reproduction*. 63:1490-1496.

Reik, W. 2007. Stability and flexibility of epigenetic gene regulation in mammalian development. *Nature*. 447:425-432.

Reynolds, N., B. Collier, V. Bingham, N.K. Gray, and H.J. Cooke. 2007. Translation of the synaptonemal complex component Sycp3 is enhanced in vivo by the germ cell specific regulator Dazl. *Rna*. 13:974-981.

Rice, J.C., S.D. Briggs, B. Ueberheide, C.M. Barber, J. Shabanowitz, D.F. Hunt, Y. Shinkai, and C.D. Allis. 2003. Histone methyltransferases direct different degrees of methylation to define distinct chromatin domains. *Molecular cell*. 12:1591-1598.

Riggs, A.D. 1975. X inactivation, differentiation, and DNA methylation. *Cytogenetics and cell genetics*. 14:9-25.

Robert, M.F., S. Morin, N. Beaulieu, F. Gauthier, I.C. Chute, A. Barsalou, and A.R. MacLeod. 2003. DNMT1 is required to maintain CpG methylation and aberrant gene silencing in human cancer cells. *Nature genetics*. 33:61-65.

Rogakou, E.P., D.R. Pilch, A.H. Orr, V.S. Ivanova, and W.M. Bonner. 1998. DNA double-stranded breaks induce histone H2AX phosphorylation on serine 139. *The Journal of biological chemistry*. 273:5858-5868.

Roh, T.Y., S. Cuddapah, and K. Zhao. 2005. Active chromatin domains are defined by acetylation islands revealed by genome-wide mapping. *Genes Dev*. 19:542-552.

Roig, I., B. Liebe, J. Egozcue, L. Cabero, M. Garcia, and H. Scherthan. 2004. Female-specific features of recombinational double-stranded DNA repair in relation to synapsis and telomere dynamics in human oocytes. *Chromosoma*. 113:22-33.

Romanienko, P.J., and R.D. Camerini-Otero. 2000. The mouse Spo11 gene is required for meiotic chromosome synapsis. *Molecular cell*. 6:975-987.

Roth, S.Y., J.M. Denu, and C.D. Allis. 2001. Histone acetyltransferases. *Annual review of biochemistry*. 70:81-120.

Ruggiu, M., R. Speed, M. Taggart, S.J. McKay, F. Kilanowski, P. Saunders, J. Dorin, and H.J. Cooke. 1997. The mouse Dazla gene encodes a cytoplasmic protein essential for gametogenesis. *Nature*. 389:73-77.

Saba, R., Q. Wu, and Y. Saga. 2014. CYP26B1 promotes male germ cell differentiation by suppressing STRA8-dependent meiotic and STRA8-independent mitotic pathways. *Developmental biology*. 389:173-181.

Saitou, M. 2009. Specification of the germ cell lineage in mice. *Frontiers in bioscience*. 14:1068-1087.

Saitou, M., S.C. Barton, and M.A. Surani. 2002. A molecular programme for the specification of germ cell fate in mice. *Nature*. 418:293-300.

Saitou, M., S. Kagiwada, and K. Kurimoto. 2012. Epigenetic reprogramming in mouse pre-implantation development and primordial germ cells. *Development*. 139:15-31.

Saitou, M., and M. Yamaji. 2012. Primordial germ cells in mice. *Cold Spring Harbor perspectives in biology*. 4.

Santos-Rosa, H., R. Schneider, A.J. Bannister, J. Sherriff, B.E. Bernstein, N.C.T. Emre, S.L. Schreiber, J. Mellor, and T. Kouzarides. 2002. Active genes are tri-methylated at K4 of histone H3. *Nature*. 419:407-411.

Sasaki, H., and Y. Matsui. 2008. Epigenetic events in mammalian germ-cell development: reprogramming and beyond. *Nature reviews. Genetics*. 9:129-140.

Sato, M., T. Kimura, K. Kurokawa, Y. Fujita, K. Abe, M. Masuhara, T. Yasunaga, A. Ryo, M. Yamamoto, and T. Nakano. 2002. Identification of PGC7, a new gene expressed specifically in preimplantation embryos and germ cells. *Mechanisms of development*. 113:91-94.

Sato, N., M. Kondo, and K. Arai. 2006. The orphan nuclear receptor GCNF recruits DNA methyltransferase for Oct-3/4 silencing. *Biochemical and biophysical research communications*. 344:845-851.

Saunders, P.T.K., J.M.A. Turner, M. Ruggiu, M. Taggart, P.S. Burgoyne, D. Elliott, and H.J. Cooke. 2003. Absence of mDazl produces a final block on germ cell development at meiosis. *Reproduction*. 126:589-597.

Schneider, R., A.J. Bannister, F.A. Myers, A.W. Thorne, C. Crane-Robinson, and T. Kouzarides. 2004. Histone H3 lysine 4 methylation patterns in higher eukaryotic genes. *Nature cell biology*. 6:73-77.

Schwartz, Y.B., and V. Pirrotta. 2007. Polycomb silencing mechanisms and the management of genomic programmes. *Nature reviews. Genetics*. 8:9-22.

Seboun, E., S. Barbaux, T. Bourgeron, S. Nishi, A. Agulnik, M. Egashira, N. Nikkawa, C. Bishop, M. Fellous, K. McElreavey, and M. Kasahara. 1997. Gene sequence, localization, and evolutionary conservation of DAZLA, a candidate male sterility gene. *Genomics*. 41:227-235.

Seisenberger, S., S. Andrews, F. Krueger, J. Arand, J. Walter, F. Santos, C. Popp, B. Thienpont, W. Dean, and W. Reik. 2012. The dynamics of genome-wide DNA methylation reprogramming in mouse primordial germ cells. *Molecular cell*. 48:849-862.

Seki, Y., K. Hayashi, K. Itoh, M. Mizugaki, M. Saitou, and Y. Matsui. 2005. Extensive and orderly reprogramming of genome-wide chromatin modifications associated with specification and early development of germ cells in mice. *Developmental biology*. 278:440-458.

Seki, Y., M. Yamaji, Y. Yabuta, M. Sano, M. Shigeta, Y. Matsui, Y. Saga, M. Tachibana, Y. Shinkai, and M. Saitou. 2007. Cellular dynamics associated with the genome-wide epigenetic reprogramming in migrating primordial germ cells in mice. *Development*. 134:2627-2638.

Sekido, R., I. Bar, V. Narvaez, G. Penny, and R. Lovell-Badge. 2004. SOX9 is up-regulated by the transient expression of SRY specifically in Sertoli cell precursors. *Developmental biology*. 274:271-279.

Seligman, J., and D.C. Page. 1998. The Dazh gene is expressed in male and female embryonic gonads before germ cell sex differentiation. *Biochemical and biophysical research communications*. 245:878-882.

Shen, L., Y. Kondo, Y. Guo, J. Zhang, L. Zhang, S. Ahmed, J. Shu, X. Chen, R.A. Waterland, and J.P. Issa. 2007. Genome-wide profiling of DNA methylation reveals a class of normally methylated CpG island promoters. *PLoS genetics*. 3:2023-2036.

Shen, X., Y. Liu, Y.J. Hsu, Y. Fujiwara, J. Kim, X. Mao, G.C. Yuan, and S.H. Orkin. 2008. EZH1 mediates methylation on histone H3 lysine 27 and complements EZH2 in maintaining stem cell identity and executing pluripotency. *Molecular cell*. 32:491-502.

Siedlecki, P., and P. Zielenkiewicz. 2006. Mammalian DNA methyltransferases. *Acta biochimica Polonica*. 53:245-256.

Smallwood, A., P.O. Esteve, S. Pradhan, and M. Carey. 2007. Functional cooperation between HP1 and DNMT1 mediates gene silencing. *Genes Dev*. 21:1169-1178.

Smith, Z.D., M.M. Chan, T.S. Mikkelsen, H. Gu, A. Gnirke, A. Regev, and A. Meissner. 2012. A unique regulatory phase of DNA methylation in the early mammalian embryo. *Nature*. 484:339-344.

Speed, R.M. 1982. Meiosis in the foetal mouse ovary. I. An analysis at the light microscope level using surface-spreading. *Chromosoma*. 85:427-437.

Stoop, H., F. Honecker, M. Cools, R. de Krijger, C. Bokemeyer, and L.H. Looijenga. 2005. Differentiation and development of human female germ cells during prenatal gonadogenesis: an immunohistochemical study. *Human reproduction*. 20:1466-1476.

Strahl, B.D., and C.D. Allis. 2000. The language of covalent histone modifications. *Nature*. 403:41-45.

Stringer, J.M., S. Barrand, and P. Western. 2013. Fine-tuning evolution: germ-line epigenetics and inheritance. *Reproduction*. 146:R37-48.

Struhl, K. 1998. Histone acetylation and transcriptional regulatory mechanisms. *Genes Dev*. 12:599-606.

Su, Z., L. Han, and Z. Zhao. 2011. Conservation and divergence of DNA methylation in eukaryotes: new insights from single base-resolution DNA methylomes. *Epigenetics : official journal of the DNA Methylation Society*. 6:134-140.

Suganuma, T., and J.L. Workman. 2008. Crosstalk among Histone Modifications. *Cell*. 135:604-607.

Surani, M.A., K. Hayashi, and P. Hajkova. 2007. Genetic and epigenetic regulators of pluripotency. *Cell*. 128:747-762.

Szwagierczak, A., S. Bultmann, C.S. Schmidt, F. Spada, and H. Leonhardt. 2010. Sensitive enzymatic quantification of 5-hydroxymethylcytosine in genomic DNA. *Nucleic Acids Res*. 38:e181.

Tachibana, M., M. Nozaki, N. Takeda, and Y. Shinkai. 2007. Functional dynamics of H3K9 methylation during meiotic prophase progression. *The EMBO journal*. 26:3346-3359.

Tachibana, M., J. Ueda, M. Fukuda, N. Takeda, T. Ohta, H. Iwanari, T. Sakihama, T. Kodama, T. Hamakubo, and Y. Shinkai. 2005. Histone methyltransferases G9a and GLP form heteromeric complexes and are both crucial for methylation of euchromatin at H3-K9. *Gene Dev*. 19:815-826.

Tahiliani, M., K.P. Koh, Y.H. Shen, W.A. Pastor, H. Bandukwala, Y. Brudno, S. Agarwal, L.M. Iyer, D.R. Liu, L. Aravind, and A. Rao. 2009. Conversion of 5-Methylcytosine to 5-Hydroxymethylcytosine in Mammalian DNA by MLL Partner TET1. *Science*. 324:930-935.

Tam, P.P.L., and M.H.L. Snow. 1981. Proliferation and Migration of Primordial Germ-Cells during Compensatory Growth in Mouse Embryos. *J Embryol Exp Morph*. 64:133-147.

Tanaka, S.S., and Y. Matsui. 2002. Developmentally regulated expression of mil-1 and mil-2, mouse interferon-induced transmembrane protein like genes, during formation and differentiation of primordial germ cells. *Mechanisms of development*. 119 Suppl 1:S261-267.

Tilgner, K., S.P. Atkinson, A. Golebiewska, M. Stojkovic, M. Lako, and L. Armstrong. 2008. Isolation of primordial germ cells from differentiating human embryonic stem cells. *Stem cells*. 26:3075-3085.

Tingen, C., A. Kim, and T.K. Woodruff. 2009. The primordial pool of follicles and nest breakdown in mammalian ovaries. *Molecular human reproduction*. 15:795-803.

Toyooka, Y., N. Tsunekawa, Y. Takahashi, Y. Matsui, M. Satoh, and T. Noce. 2000. Expression and intracellular localization of mouse Vasa-homologue protein during germ cell development. *Mechanisms of development*. 93:139-149.

Trautmann, E., M.J. Guerquin, C. Duquenne, J.B. Lahaye, R. Habert, and G. Livera. 2008. Retinoic acid prevents germ cell mitotic arrest in mouse fetal testes. *Cell cycle*. 7:656-664.

Tung, J.Y., M.P. Rosen, L.M. Nelson, P.J. Turek, J.S. Witte, D.W. Cramer, M.I. Cedars, and R.A. Reijo-Pera. 2006. Novel missense mutations of the Deleted-in-AZoospermia-Like (DAZL) gene in infertile women and men. *Reproductive biology and endocrinology : RB&E*. 4:40.

Turner, B.M. 2000. Histone acetylation and an epigenetic code. *BioEssays : news and reviews in molecular, cellular and developmental biology*. 22:836-845.

Turner, B.M. 2005. Reading signals on the nucleosome with a new nomenclature for modified histones. *Nature structural & molecular biology*. 12:110-112.

Turner, B.M. 2007. Defining an epigenetic code. *Nature cell biology*. 9:2-6.

Valinluck, V., and L.C. Sowers. 2007. Endogenous cytosine damage products alter the site selectivity of human DNA maintenance methyltransferase DNMT1. *Cancer research*. 67:946-950.

Van Holde, K.E. 1989. Chromatin. Springer-Verlag, New York. xii, 497 p. pp.

Vaskivuo, T.E., M. Anttonen, R. Herva, H. Billig, M. Dorland, E.R. te Velde, F. Stenback, M. Heikinheimo, and J.S. Tapanainen. 2001. Survival of human ovarian follicles from fetal to adult life: apoptosis, apoptosis-related proteins, and transcription factor GATA-4. *The Journal of clinical endocrinology and metabolism*. 86:3421-3429.

Vaute, O., E. Nicolas, L. Vandel, and D. Trouche. 2002. Functional and physical interaction between the histone methyl transferase Suv39H1 and histone deacetylases. *Nucleic Acids Res*. 30:475-481.

Vermeulen, M., and H.T. Timmers. 2010. Grasping trimethylation of histone H3 at lysine 4. *Epigenomics*. 2:395-406.

Vincent, J.J., Y. Huang, P.Y. Chen, S. Feng, J.H. Calvopina, K. Nee, S.A. Lee, T. Le, A.J. Yoon, K. Faull, G. Fan, A. Rao, S.E. Jacobsen, M. Pellegrini, and A.T. Clark. 2013. Stage-specific roles for tet1 and tet2 in DNA demethylation in primordial germ cells. *Cell stem cell*. 12:470-478.

Vincent, S.D., N.R. Dunn, R. Sciammas, M. Shapiro-Shalef, M.M. Davis, K. Calame, E.K. Bikoff, and E.J. Robertson. 2005. The zinc finger transcriptional repressor Blimp1/Prdm1 is dispensable for early axis formation but is required for specification of primordial germ cells in the mouse. *Development*. 132:1315-1325.

Vire, E., C. Brenner, R. Deplus, L. Blanchon, M. Fraga, C. Didelot, L. Morey, A. Van Eynde, D. Bernard, J.M. Vanderwinden, M. Bollen, M. Esteller, L. Di Croce, Y. de Launoit, and F. Fuks. 2006. The Polycomb group protein EZH2 directly controls DNA methylation. *Nature*. 439:871-874.

Wang, H., R. Cao, L. Xia, H. Erdjument-Bromage, C. Borchers, P. Tempst, and Y. Zhang. 2001. Purification and functional characterization of a histone H3-lysine 4-specific methyltransferase. *Molecular cell*. 8:1207-1217.

Wang, N., and J.L. Tilly. 2010. Epigenetic status determines germ cell meiotic commitment in embryonic and postnatal mammalian gonads. *Cell cycle*. 9:339-349.

Wang, Z., C. Zang, J.A. Rosenfeld, D.E. Schones, A. Barski, S. Cuddapah, K. Cui, T.Y. Roh, W. Peng, M.Q. Zhang, and K. Zhao. 2008. Combinatorial patterns of histone acetylations and methylations in the human genome. *Nature genetics*. 40:897-903.

Wartenberg, H. 1981. Differentiation and development of the testes. Raven Press, New York.

Wartenberg, H. 1982. Development of the early human ovary and role of the mesonephros in the differentiation of the cortex. *Anatomy and embryology*. 165:253-280.

Weber, M., I. Hellmann, M.B. Stadler, L. Ramos, S. Paabo, M. Rebhan, and D. Schubeler. 2007. Distribution, silencing potential and evolutionary impact of promoter DNA methylation in the human genome. *Nature genetics*. 39:457-466.

Wermann, H., H. Stoop, A.J. Gillis, F. Honecker, R.J. van Gurp, O. Ammerpohl, J. Richter, J.W. Oosterhuis, C. Bokemeyer, and L.H. Looijenga. 2010. Global DNA methylation in fetal human germ cells and germ cell tumours: association with differentiation and cisplatin resistance. *The Journal of pathology*. 221:433-442.

Western, P.S., D.C. Miles, J.A. van den Bergen, M. Burton, and A.H. Sinclair. 2008. Dynamic regulation of mitotic arrest in fetal male germ cells. *Stem cells*. 26:339-347.

Wilhelm, D., F. Martinson, S. Bradford, M.J. Wilson, A.N. Combes, A. Beverdam, J. Bowles, H. Mizusaki, and P. Koopman. 2005. Sertoli cell differentiation is induced both cell-autonomously and through prostaglandin signaling during mammalian sex determination. *Developmental biology*. 287:111-124.

Wilhelm, D., S. Palmer, and P. Koopman. 2007. Sex determination and gonadal development in mammals. *Physiological reviews*. 87:1-28.

Williams, K., J. Christensen, M.T. Pedersen, J.V. Johansen, P.A. Cloos, J. Rappsilber, and K. Helin. 2011. TET1 and hydroxymethylcytosine in transcription and DNA methylation fidelity. *Nature*. 473:343-348.

Witschi, E. 1948. Migration of the germ cells of human embryos from the yolk sac to the primitive gonadal folds. *In* Contributions to Embryology. Vol. 32.

Wolffe, A.P., and J.J. Hayes. 1999. Chromatin disruption and modification. *Nucleic Acids Res*. 27:711-720.

Wolffe, A.P., and M.A. Matzke. 1999. Epigenetics: regulation through repression. *Science*. 286:481-486.

Woods, D.C., and J.L. Tilly. 2013. Isolation, characterization and propagation of mitotically active germ cells from adult mouse and human ovaries. *Nature protocols*. 8:966-988.

Wossidlo, M., T. Nakamura, K. Lepikhov, C.J. Marques, V. Zakhartchenko, M. Boiani, J. Arand, T. Nakano, W. Reik, and J. Walter. 2011. 5-Hydroxymethylcytosine in the mammalian zygote is linked with epigenetic reprogramming. *Nat Commun*. 2.

Wu, H., A.C. D'Alessio, S. Ito, Z. Wang, K. Cui, K. Zhao, Y.E. Sun, and Y. Zhang. 2011. Genome-wide analysis of 5-hydroxymethylcytosine distribution reveals its dual function in transcriptional regulation in mouse embryonic stem cells. *Genes Dev*. 25:679-684.

Wu, J., and M. Grunstein. 2000. 25 years after the nucleosome model: chromatin modifications. *Trends in biochemical sciences*. 25:619-623.

Wu, S.C., and Y. Zhang. 2010. Active DNA demethylation: many roads lead to Rome. *Nature reviews. Molecular cell biology*. 11:607-620.

Xu, Y., F. Wu, L. Tan, L. Kong, L. Xiong, J. Deng, A.J. Barbera, L. Zheng, H. Zhang, S. Huang, J. Min, T. Nicholson, T. Chen, G. Xu, Y. Shi, K. Zhang, and Y.G. Shi. 2011. Genome-wide regulation of 5hmC, 5mC, and gene expression by

Tet1 hydroxylase in mouse embryonic stem cells. *Molecular cell*. 42:451-464.

Yabuta, Y., K. Kurimoto, Y. Hinata, Y. Seki, and M. Saitou. 2006. Gene expression dynamics during germline specification in mice identified by quantitative single-cell gene expression profiling. *Biology of reproduction*. 75:705-716.

Yamaguchi, S., K. Hong, R. Liu, A. Inoue, L. Shen, K. Zhang, and Y. Zhang. 2013. Dynamics of 5-methylcytosine and 5-hydroxymethylcytosine during germ cell reprogramming. *Cell research*. 23:329-339.

Yamaguchi, S., K. Hong, R. Liu, L. Shen, A. Inoue, D. Diep, K. Zhang, and Y. Zhang. 2012. Tet1 controls meiosis by regulating meiotic gene expression. *Nature*. 492:443-447.

Yamaji, M., Y. Seki, K. Kurimoto, Y. Yabuta, M. Yuasa, M. Shigeta, K. Yamanaka, Y. Ohinata, and M. Saitou. 2008. Critical function of Prdm14 for the establishment of the germ cell lineage in mice. *Nature genetics*. 40:1016-1022.

Yang, X.J. 2004. Lysine acetylation and the bromodomain: a new partnership for signaling. *BioEssays : news and reviews in molecular, cellular and developmental biology*. 26:1076-1087.

Yao, H.H., L. DiNapoli, and B. Capel. 2003. Meiotic germ cells antagonize mesonephric cell migration and testis cord formation in mouse gonads. *Development*. 130:5895-5902.

Yashiro, K., X. Zhao, M. Uehara, K. Yamashita, M. Nishijima, J. Nishino, Y. Saijoh, Y. Sakai, and H. Hamada. 2004. Regulation of retinoic acid distribution is required for proximodistal patterning and outgrowth of the developing mouse limb. *Developmental cell*. 6:411-422.

Yen, P.H., N.N. Chai, and E.C. Salido. 1996. The human autosomal gene DAZLA: testis specificity and a candidate for male infertility. *Human molecular genetics*. 5:2013-2017.

Yildirim, O., R. Li, J.H. Hung, P.B. Chen, X. Dong, L.S. Ee, Z. Weng, O.J. Rando, and T.G. Fazzio. 2011. Mbd3/NURD complex regulates expression of 5-hydroxymethylcytosine marked genes in embryonic stem cells. *Cell*. 147:1498-1510.

Ying, Y., X.M. Liu, A. Marble, K.A. Lawson, and G.Q. Zhao. 2000. Requirement of Bmp8b for the generation of primordial germ cells in the mouse. *Molecular endocrinology*. 14:1053-1063.

Ying, Y., X. Qi, and G.Q. Zhao. 2001. Induction of primordial germ cells from murine epiblasts by synergistic action of BMP4 and BMP8B signaling pathways. *Proceedings of the National Academy of Sciences of the United States of America*. 98:7858-7862.

Ying, Y., and G.Q. Zhao. 2001. Cooperation of endoderm-derived BMP2 and extraembryonic ectoderm-derived BMP4 in primordial germ cell generation in the mouse. *Developmental biology*. 232:484-492.

Yokoyama, A., Z. Wang, J. Wysocka, M. Sanyal, D.J. Aufiero, I. Kitabayashi, W. Herr, and M.L. Cleary. 2004. Leukemia proto-oncoprotein MLL forms a SET1-like histone methyltransferase complex with menin to regulate Hox gene expression. *Molecular and cellular biology*. 24:5639-5649.

Yoshida, K., G. Kondoh, Y. Matsuda, T. Habu, Y. Nishimune, and T. Morita. 1998. The mouse RecA-like gene Dmc1 is required for homologous chromosome synapsis during meiosis. *Molecular cell*. 1:707-718.

Yu, M., G.C. Hon, K.E. Szulwach, C.X. Song, L. Zhang, A. Kim, X. Li, Q. Dai, Y. Shen, B. Park, J.H. Min, P. Jin, B. Ren, and C. He. 2012. Base-resolution analysis of 5-hydroxymethylcytosine in the mammalian genome. *Cell*. 149:1368-1380.

Yuan, L., J.G. Liu, J. Zhao, E. Brundell, B. Daneholt, and C. Hoog. 2000. The murine SCP3 gene is required for synaptonemal complex assembly, chromosome synapsis, and male fertility. *Molecular cell*. 5:73-83.

Zayed, A.E., M.M. Abd-Elnaeim, S. Abd-Elghaffar, A. Hild, R. Brehm, and K. Steger. 2007. Prenatal development of murine gonads with special reference to germ cell differentiation: a morphological and immunohistochemical study. *Andrologia*. 39:93-100.

Zegerman, P., B. Canas, D. Pappin, and T. Kouzarides. 2002. Histone H3 lysine 4 methylation disrupts binding of nucleosome remodeling and deacetylase (NuRD) repressor complex. *The Journal of biological chemistry*. 277:11621-11624.

Zhang, C.L., T.A. McKinsey, and E.N. Olson. 2002. Association of class II histone deacetylases with heterochromatin protein 1: potential role for histone methylation in control of muscle differentiation. *Molecular and cellular biology*. 22:7302-7312.

Zhang, Y., R. Cao, L. Wang, and R.S. Jones. 2004. Mechanism of Polycomb group gene silencing. *Cold Spring Harbor symposia on quantitative biology*. 69:309-317.

Zhang, Y., and D. Reinberg. 2001. Transcription regulation by histone methylation: interplay between different covalent modifications of the core histone tails. *Genes Dev*. 15:2343-2360.

Zheng, P., M.D. Griswold, T.J. Hassold, P.A. Hunt, C.L. Small, and P. Ye. 2010. Predicting meiotic pathways in human fetal oogenesis. *Biology of reproduction*. 82:543-551.

Zhou, Q., Y. Li, R. Nie, P. Friel, D. Mitchell, R.M. Evanoff, D. Pouchnik, B. Banasik, J.R. McCarrey, C. Small, and M.D. Griswold. 2008. Expression of stimulated by retinoic acid gene 8 (Stra8) and maturation of murine gonocytes and spermatogonia induced by retinoic acid in vitro. *Biology of reproduction*. 78:537-545.